OPTIMISATION OF MONOPILES SUPPORTING OFFSHORE WIND TURBINES THROUGH ADVANCED NUMERICAL MODELLING OF CYCLIC LOADING

Louis-Marin Lapastoure

Submitted in fulfilment of the requirements for the degree of
Doctor of Philosophy

Department of Civil, Structural and Environmental Engineering
School of Engineering
Trinity College Dublin, the University of Dublin
2024

(intentionally left blank)

I declare that this thesis has not been submitted as an exercise for a degree at this or any other university and it is entirely my own work. This thesis contains published work and/or work prepared for publication, some of which have been co-authored.

I agree to deposit this thesis in the University's open access institutional repository or allow the Library to do so on my behalf, subject to Irish Copyright Legislation and Trinity College Library conditions of use and acknowledgement.

I consent to the examiner retaining a copy of the thesis beyond the examining period, should they so wish.

(intentionally left blank)

Abstract

The European Union (EU) has established ambitious renewable energy targets in order to de-carbonise the energy sector. In Ireland, it is estimated that 2.3GW of offshore wind capacity will be installed by 2030 at an estimated cost of €6 billion. The foundations for offshore wind turbines (OWTs) can represent up to 30% of the overall cost of development. Among all components of an OWT structure, the foundations offer the greatest scope for optimisation. Monopile foundations, which are large diameter (typically 4 – 8m) steel tubes driven into the ground, represent around 80% of all offshore wind turbine foundations installed to date and will continue to be the most common foundation solution for offshore wind for at least the next 15 years. As larger wind turbines are being developed, XL monopiles from 8 – 12m in diameter are needed to support these. These larger diameter piles typically have a lower slenderness (length to diameter ratio) than standard monopiles and are therefore significantly more susceptible to the effects of cyclic loading. Because of an inadequate understanding of the effects of cyclic loading, XL monopiles are currently over-designed, causing excessive manufacturing, transportation, and installation costs. This project aims to improve design methods for cyclic loading effects on XL monopiles through state-of-the-art numerical modelling and calibration against new field test data and will lead to significant advances in scientific knowledge and improvements in the design efficiency of OWTs. Specifically, this will build upon recent advances in the state of the art in numerical modelling of monopiles and will be validated against recent and new monopile field test data. The ultimate goal is to reduce cost and improve the viability of offshore energy, leading to a more rapid reduction in carbon emissions and reliance on fossil fuels.

(intentionally left blank)

Authorship declaration

This thesis contains work that has been published or submitted for application. The bibliographic details and the contribution of the candidate are stated below for all papers.

Reference	**Location in thesis**	**Candidate contribution**
Published as: Lapastoure, L.-M. and Igoe, D. (2022). Review of cyclic models for the design of monopiles supporting offshore wind turbines. Geotechnical Society of Ireland Conference 2022, Portlaoise, Ireland.	Chapter 1 Section 3.3	Conceptualisation, Writing – Original draft
Published as: Lapastoure, L. M., Diambra, A., Jalilvand, S., and Igoe, D. (2023). Assessment of cyclic superposition approaches for the cyclic design of monopiles supporting offshore wind turbines. Ocean Engineering, 287, 115759.	Chapter 2	Conceptualisation, Methodology, Software, Validation, Formal analysis, Visualisation, Writing – Original draft
Submitted to Geotechnique as: Igoe, D. and Lapastoure, L.-M. (2024). Field lateral load tests on monopiles in dense sand at Blessington - Part 1 - Monotonic Loading.	Chapter 3	Investigation, Software, Validation, Formal analysis, Visualisation, Writing – Original draft
Submitted to Geotechnique as: Igoe, D. and Lapastoure, L.-M. (2024). Field lateral load tests on monopiles in dense sand at Blessington - Part 2 - Cyclic Loading	Chapter 4	Investigation, Software, Validation, Formal analysis, Visualisation, Writing – Original draft

Soon to be submitted for publication as: Lapastoure, L.-M. and Igoe, D. (2024) Validation of a contour diagram based model for monopile cyclic design in sand and clay.	Chapter 5	Conceptualisation, Methodology, Software, Validation, Formal analysis, Visualisation, Writing – Original draft
Published as: Lapastoure, L.-M. and David, Igoe (2022). A comparison of soil lateral reaction models for monopile design in clay. 20th International Conference on Soil Mechanics and Geotechnical Engineering (ICSMGE), Sydney, Australia.	Appendix A	Conceptualisation, Formal analysis, Visualisation, Writing – Original draft
Published as: Lapastoure, L.-M. and Igoe, D. (2022). Implementation of PISA numerical framework for offshore wind foundation design. Civil Engineering Research in Ireland (CERI) conference, Dublin, Ireland	Appendix B	Conceptualisation, Methodology, Software, Validation, Formal analysis, Visualisation, Writing – Original draft
Published as: Lapastoure, L.-M. and Igoe, D. (2022). 3D FE derivation of CPT based soil reaction curves for monopile lateral static design in sand. 5th International Symposium on Cone Penetration Testing (CPT'22), Bologna, Italy.	Appendix C	Conceptualisation, Methodology, Software, Formal analysis, Visualisation, Writing – Original draft
Published as: Lapastoure, L.-M., Diambra, A., Thusyanthan, I. Jalilvand, S. and Igoe, D. (2023). Overview of a new cyclic methodology for the geotechnical design of monopiles supporting offshore wind turbines in sand. 9th International SUT OSIG Conference, London, UK.	Appendix D	Conceptualisation, Methodology, Software, Formal analysis, Visualisation, Writing – Original draft
Published as: Lapastoure, L.-M. and Igoe, D. (2023). Exploring the use of machine learning for the geotechnical design of monopiles supporting offshore wind turbines, ISMLG conference, Cork, Ireland.	Appendix E	Conceptualisation, Methodology, Software, Validation, Formal analysis, Visualisation, Writing – Original draft

Submitted as: Lapastoure, L.-M. and Igoe, D. (2024). Prediction of short piles response to lateral monotonic load in dense sand at Blessington. XVIII European Conference on Soil Mechanics and Geotechnical Engineering, Lisbon, Portugal.	Appendix F	Conceptualisation, Methodology, Software, Investigation, Validation, Formal analysis, Visualisation, Writing – Original draft

(intentionally left blank)

Acknowledgements

First and foremost, I would like to thank my supervisor, Prof. David Igoe, for his support and guidance throughout the project. I would also like to acknowledge the constructive comments of my examiners, Prof. Breiffni Fitzgerald and Prof. Richard Jardine.

The research presented in this thesis was funded by the Irish Research Council under the employment-based postgraduate program under grant EBPPG/2019/4. The research was carried out in collaboration with the Department of Civil, Structural and Environmental Engineering at Trinity College Dublin and with Gavin and Doherty Geosolutions. Thanks to Roadstone, In-situ SI, Terradrive piling, Lloyds datum group and J.W. Carnegie for their help with the experimental field tests.

I would also like to thank my fellow PhD students, post-docs and technicians in the Department of Civil, Structural and Environmental Engineering at Trinity College Dublin for their help with setting up and carrying out the experimental field tests.

I would also like to thank my colleagues at Gavin and Doherty Geosolutions for the valuable industry experience.

Finally, thanks to my family and friends for the support during these years.

(intentionally left blank)

Table of Contents

List of Figures

List of Tables

Chapter 1: Overview, motivation, and background

1.1 INTRODUCTION

One of the main ways of reducing costs for the offshore wind sector is through optimising the foundation design. The foundation design has the highest degree of uncertainty in the engineering design process, due to the variability and complex behaviour of soils. The high costs of the foundations (up to 30% of the overall structure; Arany et al., 2017) are a result of not only the high volumes of steel required but also the cost of hiring specialist equipment (piling hammers) and jack-up vessels to install the foundations, which can cost up to €500,000 per day to mobilise. Reducing the size of the piles required to support OWTs leads to cost savings in both the materials and time required to install the piles.

The size of the piles required to support an OWT is typically determined by a geotechnical engineer using semi-empirical calculations to estimate the pile response, based on the strength and stiffness of the soil at the location. While significant progress has been made on the design of monopiles for static loading ultimate capacity, the understanding and modelling of cyclic loading is still developing. As pile diameters increase due to larger turbines and deeper water depths, the cyclic loading considerations become the primary design driver. Traditional design practice for estimating the response of offshore piles under cyclic loading was based on old American Petroleum Institute (API) standards which were developed for the oil and gas industry with an emphasis on safety and conservatism, rather than an optimised design. The API approach for cyclic loading involves effectively downrating the stiffness and ultimate capacity, which is appropriate for long slender piles used in the oil and gas industry but not monopiles. Alternative approaches for cyclic loading of monopiles have been developed, making use of small laboratory scale model pile tests to provide relationships between pile mudline deflection and cycle no. These semi-empirical approaches lack rigorous description of the fundamental behaviour of the soil-pile response and do not account for changes in pile capacity, stiffness or damping and are difficult to adapt for load packets of different amplitude. As a result, these approaches are applied under the conservative assumption of linear cumulative damage leading to significant and costly

over-designs. The main aim of this research is to build upon the state of the art in numerical modelling and develop a new approach for estimating the cyclic response of monopile foundations.

1.2 OFFSHORE WIND

1.2.1 Offshore wind market trends

The offshore wind market has been growing quickly over the past decade with more and more capacity installed every year to reach a total of about 22.5 GW in Europe (see Figure 1-1). The European Commission has set targets of 60 GW installed by 2030 and 300 GW by 2050 (European Commission, 2020). This leads to estimated investments of 800 billion euros until 2050. In Ireland, no offshore wind turbine has been installed since the first wind farm in Arklow Bank commissioned in 2004 (25 MW). However, the market in Ireland is undergoing a significant transition with momentum being triggered by improvements in consenting, subsidy and grid connection with the government fixing a target of 7 GW commissioned by 2030 (CAP, 2021).

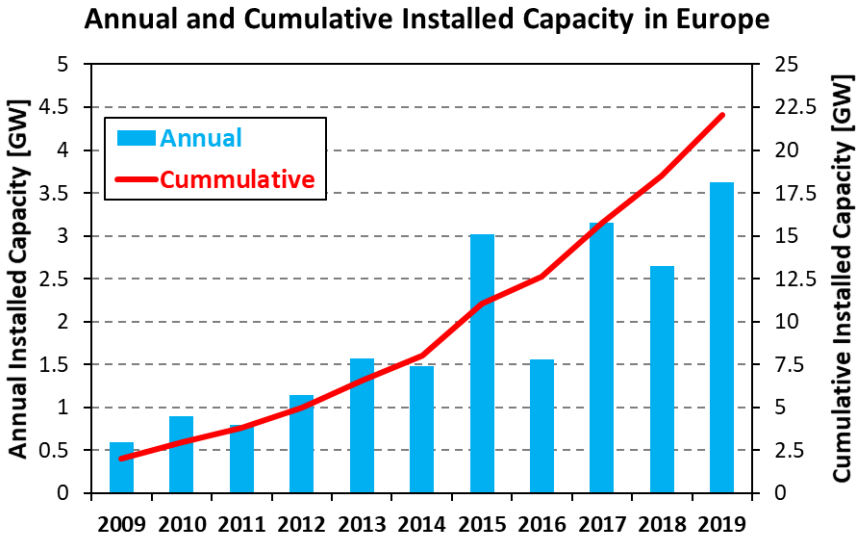

Figure 1-1. Installed offshore wind capacity installed in Europe to date (Wind Europe, 2020)

As the offshore wind market is gaining in maturity, the average installed turbine capacity has been consistently increasing over the past decade. The left-hand side of Figure 1-2 shows an average 16% increase every year since 2014. This is expected to keep increasing over the next decade with future turbines with rated capacity over 10 MW being developed (GE Haliade-X up to 14 MW or MySE 16 MW). At the same time, the average water depth at which offshore wind farms are being installed is increasing as well (right-hand side Figure 1-2). Hence, foundations need to undertake considerably larger loads while

the cost needs to be minimised in order to ensure offshore wind is cost-competitive with fossil energy.

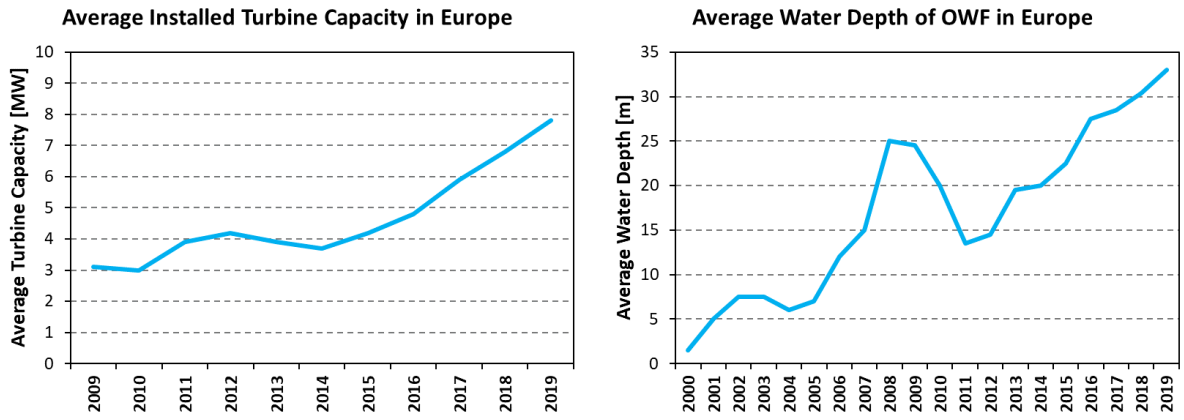

Figure 1-2: Evolution of average turbine capacity and water depth (Wind Europe, 2020).

There are a variety of foundation types able to support offshore wind turbines. The main foundation types are presented in the next section. The choice of the foundation type is mostly driven by the water depth at which the turbine is installed. As wind farms are moving in deeper water, jacket foundations and floating wind are becoming more popular. However, monopiles have always been and are still the most popular foundation type (see Figure 1-3). Monopiles represented 70% of the newly installed foundations in 2019 and 80% of all foundations installed by end 2019 in Europe. With the recent development in monopile design approaches and the maturity of the supply chain, these are becoming cost-competitive in increasing larger water depths and are likely to remain the main foundation type for the next decade (Smith, 2018).

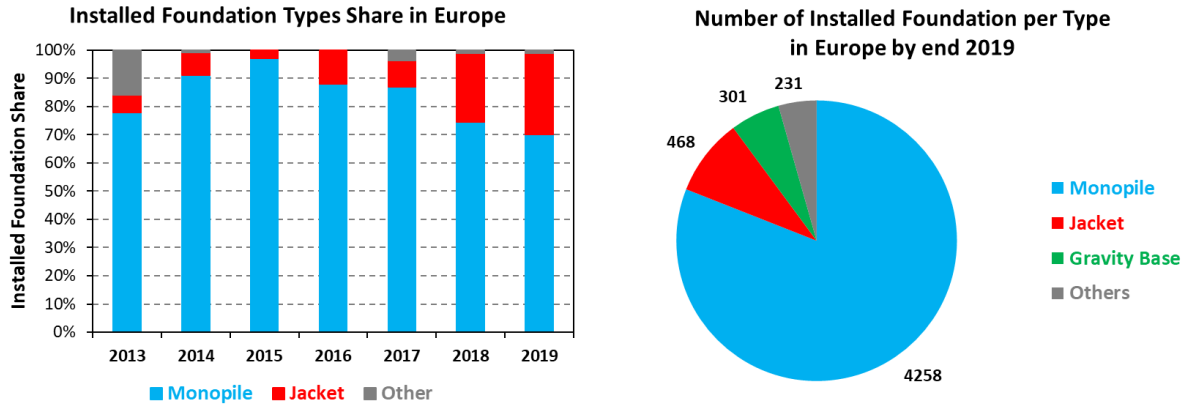

Figure 1-3: Foundation types share (Wind Europe, 2020)

1.2.2 Foundation types

The main foundation types supporting offshore wind turbines are presented in Figure 1-4. The choice of the foundation type is mostly driven by the water depth at which the turbine

is installed but may also be dictated by the strength of the soil. Each foundation type is discussed below.

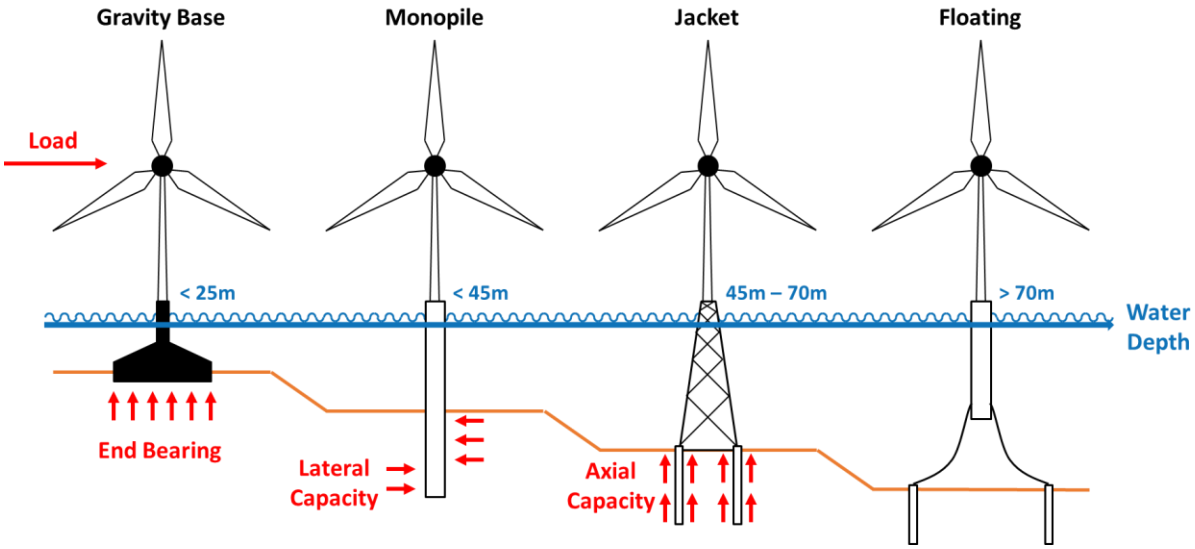

Figure 1-4: Main foundation types supporting offshore wind turbine.

Gravity-base foundations are support structures relying on their self-weight to withstand the overturning moment and sliding shear force generated by wind, waves, and current acting on the turbine structure. Gravity-base foundations are generally made of reinforced concrete and are installed to rest on the seabed. The geometry, size and weight are varied to meet project-specific requirements. Gravity-based foundations benefit from the small cost and wide availability of concrete compared to steel. If no seabed preparation is required, it also benefits from a simple installation procedure with no driving required. It can also be conveniently ballasted and tugged to the site to avoid costly installation vessels. The major drawback of gravity-base foundations is that they rely on the end bearing capacity of the shallow seabed deposits making it only suitable for shallow water depth (about less than 25 m). Indeed, large overturning moments require prohibitively large foundation sizes. Gravity-based foundations may even not be suitable at all if the soil is too soft. Lastly, limited design tools are available to address technical issues around differential displacements and rotations.

Monopiles are by far the most popular foundation type, representing 80% of the foundations installed to date in Europe (Wind Europe, 2020). Monopiles are large-diameter diameter open-ended still piles driven into the seabed. They rely on the soil lateral resistance to overcome overturning moment and lateral shear force generated by the turbine structure. Monopiles are made of a single element, making them simple and quick to fabricate and install. Being the most popular foundation types, they benefit from the experience from thousands of monopiles already installed offshore. Extensive research is still ongoing to

produce efficient design tools and continue to optimise their design. However, monopiles are subjected to high and very variable steel costs which may be a risk to the project development. They require specialist equipment and suppliers for the fabrication and installation which are not available everywhere or at any time. Also, there is growing concern about the environmental impact of the noise generated by pilling. Monopiles are suitable until water depths of about 45 m but may be used in deeper waters with the development of new design methods and tools. The suitability of monopile may also be limited by the presence of shallow bedrock making pile driving impossible.

Jacket structures are much stiffer than monopiles and thus can be installed in deeper water. Jacket structures can be founded on long and slender piles (most popular) which take advantage of the axial capacity of deep strata or on suction caissons (larger diameter but very short penetration) which rely on the strength of shallow soil deposits. Jacket structures are made of multiple small elements which are easier to fabricate and transport but the final assembly may be costly and time-consuming. Jacket structures benefit from the massive experience of the oil and gas industry. However, jacket structures have the same drawback as monopiles concerning steel cost and pile driving. They are typically heavier and more expensive than monopiles and are only used when monopiles are not suitable (water depth is too large).

Floating wind is a major research topic and is regarded as having the most potential for the future of offshore wind development in deeper waters. However, this technology is not yet mature and significantly more costly than current fixed-base offshore wind with many different designs being considered. The main challenges for floating wind do not really concern the geotechnical capacity of the foundation but the design of the mooring line and the floating system. Hence, this is not discussed further here.

1.3 MONOPILES DESIGN PRACTICES

Soils exhibit a very complex behaviour with severe non-linearities, anisotropy, vertical and lateral variability, etc. Additionally, soil brittleness and sensitivity are a particular concern for a safe foundation design. The following is not intended to address the challenges of modern soil mechanics but rather provided an overview of current monopile design practices. It should be noted that most of the current design approaches are calibrated against onfshore experimental tests: medium scale field tests, small scale lab tests, full scale centrifuge tests. When unsaturated or partially saturated, these onshore experimental tests might not be fully representative of the offshore conditions (fully saturated). Experimental tests onshore often exhibit soil cracks and gapping which might not happened offshore. Yet,

those experiments are the best source of information due to the prohibitive cost of offshore testing at full scale.

1.3.1 Design criteria

Monopiles are the most popular foundation type for offshore wind turbines due to their relatively simple design. Monopiles below ground level are a simple cylinder shape and therefore there are three parameters to optimise:

1. The outer diameter (D): the diameter of the monopile is typically designed to provide sufficient stiffness to the tower so as to avoid resonance between the natural frequency of the entire structure and the forcing frequencies (wind and wave loads, rotor and blade passing frequencies) as required in DNV (2021). The diameter is mainly governed by water depth and turbine capacity. The soil profile and the effect of cyclic loading influence the foundation stiffness which in turn influences the natural frequency of the structure. In order to reduce hydrodynamic loads, a conical section can be introduced between the mudline and the tower interface level. A transition piece is also often used to mount the secondary steel (ladders, boat landing etc.) and to attach to the wind turbine tower.
2. The wall thickness (t): the thickness of the monopile is typically governed by structural considerations to avoid buckling and minimise fatigue as required in DNV (2021). The wall thickness is not constant but varies along the length of the monopile. The soil response to lateral loading is a key input to the optimisation of the wall thickness profile as it influences the shear force and bending moment diagrams. The cyclic loading should be taken into account as it usually causes the depth and the magnitude of the maximum bending moment to increase.
3. The monopile embedded length (L): the embedded length is typically governed by geotechnical considerations. The pile embedded length should be sufficient to provide enough lateral capacity to sustain the design loads in the ultimate limit states. Cyclic loading might reduce the ultimate capacity of the monopile. In addition, DNV (2021) requires the designer to ensure the accumulation of permanent pile deflection at mudline does not become excessive as a result of cyclic loading.

It is clear from the above design criteria required by DNV (2021) that an accurate representation of the pile-soil interactions is critical for both monopile geotechnical and

structural design. Cyclic loading influences every aspect of the design. Any optimisation of the pile diameter, wall thickness or penetration does not only reduce the fabrication costs, but also transportation and installation. Hence, the following presents the current approaches to model both monotonic and cyclic monopile lateral response.

1.3.2 Monotonic modelling

1.3.2.1 API

The traditional industry approach consists of modelling the embedded part of the monopile using discrete Euler-Bernoulli beam elements as shown in Figure 1-5. Soil lateral reactions are modelled as a series of independent non-linear springs. These curves, called 'p-y' curves, give the lateral reaction force p pushing against the pile as a result of the pile lateral displacement y. This approach is directly taken from the oil and gas industry (API, 2014) and is recommended in the main offshore wind standards (DNV, 2014). The equations for the 'p-y' curves are provided in the standards.

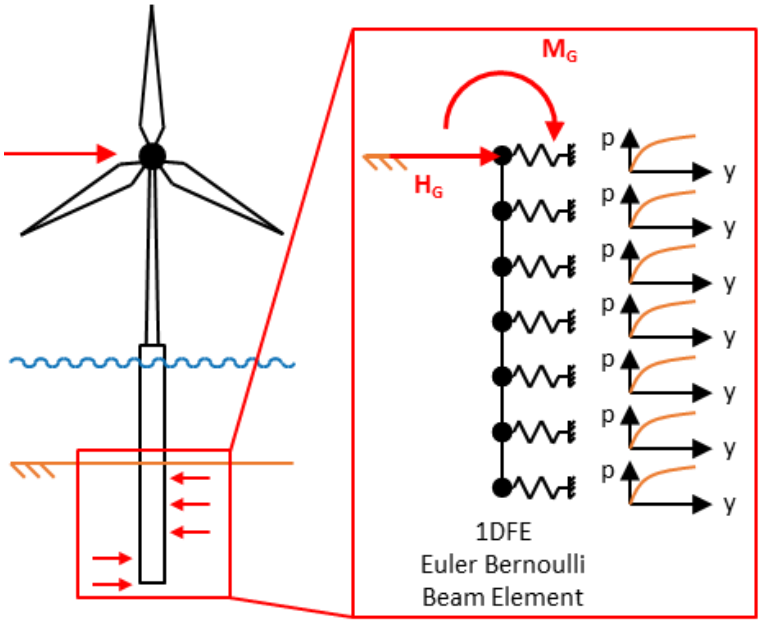

Figure 1-5: Representation of the API 'p-y' approach.

For example, in soft clay, API (2014) recommends curves based on the work of Matlock (1970) as below:

$$\frac{p}{p_u} = \frac{1}{2}\left(\frac{y}{y_c}\right)^{\frac{1}{3}} \leq 1 \tag{1.1}$$

Where p_u is the ultimate lateral reaction calculated from the undrained shear strength (s_u), the depth (z), the effective unit weight (γ'), the pile diameter (D) and an empirical dimensionless constant (J) in the range of 0.25 to 0.5 as per:

$$p_u = (3s_u + z\gamma')D + Js_u z \leq 9s_u D$$

And y_c is the reference displacement at which 50% of the ultimate capacity is mobilized. It is directly scaled from the strain at one-half of the maximum stress in an undrained tri-axial compression test (ε_{50}) as per:

$$y_c = 2.5\varepsilon_{50}D \tag{1.2}$$

In sands, it takes the form of a hyperbolic tangent as shown below:

$$p = Ap_u \tanh\left(\frac{kz}{Ap_u}y\right) \tag{1.3}$$

Where:

- $A = \left(3 - 0.8\frac{z}{D}\right) \geq 0.9$ for monotonic loading or 0.9 for cyclic loading
- p_u is the ultimate lateral resistance at depth z.
- k is the rate of increase with depth of initial modulus of subgrade reaction at depth z.
- y is the lateral pile deflection at depth z.
- z is the depth below ground level.

The interested reader is invited to refer to API (2014) section 8.5.6 for additional information, including the basis for the calculation of p_u and k.

The API 'p-y' approach has been used in the oil and gas industry for decades and was used at the early stage of the offshore wind industry. However, it is now widely acknowledged that this approach is unsuitable for monopile design due to significant differences in pile geometries used in the two industries. The API p-y approach has only been validated against a small database of field tests on long and slender piles with diameter up to about 1 m. In contrast, monopiles are relatively short with a diameter larger than 5 m, and length to diameter ratios between 2 and 6. DNV-ST-0126 clause 7.6.2.6 acknowledges the unsuitability of the traditional API p-y approach and now recommends validating the use of p-y curves for monopiles by means of finite element analysis (DNV, 2021).

The upcoming revision of the API is expected to address these limitations. Especially in clay, the next API revision is expected to recommend building the soil reaction curves after a framework based on the concept of similarity between DSS and p-y curves proposed by Jeanjean et al. (2017). The approaches expected to be recommended in the next revision of the API are not discussed further as it has not been published yet.

1.3.2.2 PISA

Due to the shortcomings of the API 'p-y' approach, the recently completed PISA project aimed at developing a state-of-the-art design methodology for monopiles. One of the key

differences is the addition of other soil reaction components such as distributed moment, base shear and base moment (see Figure 1-6). Upon lateral loading, monopiles not only mobilise soil lateral reactions but also vertical tractions as a result of their rotation due to their large diameter. Also, monopiles typically behave rigidly (due to their low slenderness ratio) and show significant toe displacement mobilising base shear force and base resisting moment. Similar to the API 'p-y' approach, these four soil reaction components are integrated into 1D finite element. However, the PISA project recommended to use of Timoshenko beam elements instead of Euler-Bernoulli in order to take into account shear deformations which may be more significant for low slenderness piles. Byrne et al. (2015) compared monopile load-displacement curves at mudline obtained from 3D and 1D finite element modelling. The response considering 'p-y' curves only was found to be significantly softer. The PISA project showed that adding these additional soil reactions makes the response stiffer and in better agreement with 3D FE. It was also shown that their contributions become more significant as pile diameter increases and pile slenderness decreases.

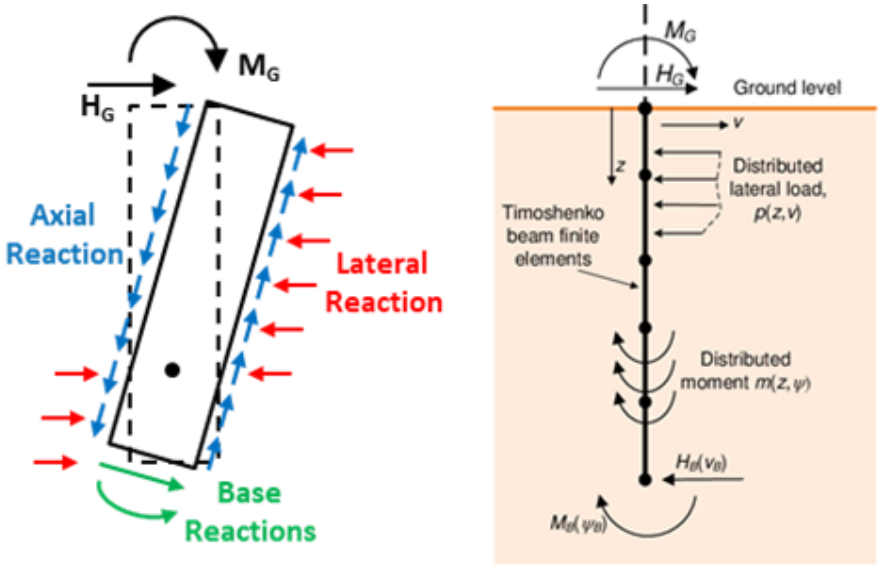

Figure 1-6: Representation of the PISA approach (modified after Burd et al., 2020).

In the PISA framework, the soil reaction curves are normalised. Figure 1-7 shows a 'p-y' curve in clay as an example. The lateral reaction p is normalised over the pile diameter (D) and the undrained shear strength (s_u) while the displacement y is normalised by the ratio of shear modulus at small strain (G_0) over the pile diameter and undrained shear strength. In sand, the undrained shear strength is replaced by the vertical effective stress (σ'_v). Then, the curves are parameterised according to a conic function with 4 parameters (x_u, k, n, y_u) to be fitted. Each of them relates to a particular aspect of the curve as shown in Figure 1-7.

$$-n\left(\frac{\bar{y}}{\bar{y}_u}-\frac{x}{\bar{x}_u}\right)^2+(1-n)\left(\frac{\bar{y}}{\bar{y}_u}-\frac{xk}{\bar{y}_u}\right)\left(\frac{\bar{y}}{\bar{y}_u}-1\right)=0 \quad (1.4)$$

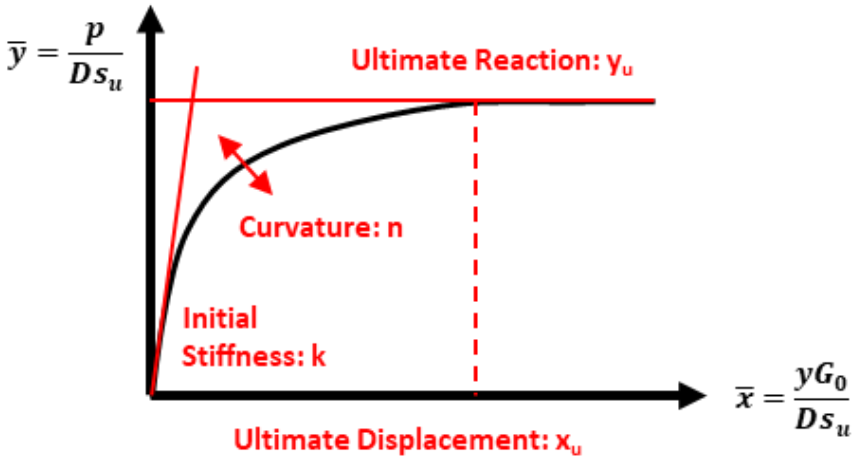

Figure 1-7: Example of PISA normalisation and parameterisation.

Normalisation of each component in both sand and clay is reported in Table 1-1 after Byrne et al. (2020) and Burd et al. (2020).

Table 1-1. Soil reaction curves normalisation after Byrne et al. (2020) and Burd et al. (2020).

Normalised Variable	Dimensionless form	
	in SAND	in CLAY
Lateral displacement, $\bar{v}$	$\frac{vG_0}{D\sigma'_v}$	$\frac{vG_0}{Ds_u}$
Pile cross-section rotation, $\bar{\psi}$	$\frac{\psi G_0}{\sigma'_v}$	$\frac{\psi G_0}{s_u}$
Distributed lateral load, $\bar{p}$	$\frac{p}{D\sigma'_v}$	$\frac{p}{Ds_u}$
Distributed moment, $\bar{m}$	$\frac{m}{D\lvert p\rvert}$	$\frac{m}{D^2 s_u}$
Base horizontal load, $\bar{H}_B$	$\frac{H_B}{D^2\sigma'_V}$	$\frac{H_B}{D^2 s_u}$
Base moment, $\bar{M}_B$	$\frac{M_B}{D^3\sigma'_v}$	$\frac{M_B}{D^3 s_u}$

The PISA project developed two approaches: the 'rule-based' approach and the 'numerical-based' approach. These are discussed in the following sections.

1.3.2.2.1 PISA rule-based approach

In the PISA rule-based approach, generic depth variation functions give profiles of these 4 parameters with depth for each soil reaction component, giving a total of 16 depth variation functions. Table 1-2 reports the depth variation functions that were calibrated for the still Cowden till (Byrne et al., 2020) and for the medium dense to dense Dunkirk sand (Burd et al., 2020) for a wide range of pile geometry examined during the PISA project. At the

monopile concept design stage, these could be used in any similar clay and/or sand units. Only a limited number of soil input parameters are required (undrained shear strength, s_u, and small strain shear modulus, $G_{0,}$ in clay; vertical effective stress, σ'_v, small strain shear modulus, $G_{0,}$ and relative density, RD, in sand) to de-normalise the soil reaction curves. Monopile mudline response under any loads can then be quickly estimated in a 1D finite element solver.

Table 1-2: Depth variation functions calibrated in Cowden till (Byrne et al., 2020) and Dunkirk sand (Burd et al., 2020).

Soil reaction component	**Parameter**	**Depth variation functions in clay**	**Depth variation functions in sand**
Distributed lateral load, p	x_u	241.4	146.1 – 92.11 * RD
	k	10.60 – 1.650 * Z/D	8.731 – 0.6982 * RD - 0.9178 * Z/D
	n	0.9390 – 0.03345 * Z/D	0.917 + 0.06193 * RD
	y_u	10.70 – 7.101 * exp(-0.3085 * Z/D)	0.3667 + 25.89 * RD – (0.3375 – 8.9)*Z/L
Distributed moment, m	x_u	Given by y_u/k	Given by y_u/k
	k	1.420 – 0.09643 * Z/D	17
	n	0	0
	y_u	0.2899 – 0.04775 * Z/D	0.2605 + (-0.1989 + 0.2019 * RD) * Z/L
Base shear, H_b	x_u	235.7	0.515 + 2.883 * RD + (0.1695 – 0.7018 * RD) * L/D
	k	2.717 – 0.3575 * L/D	6.505 - 2.985 * RD + (-0.007969 + 0.7974 * RD) * L/D
	n	0.8793 – 0.03150 * L/D	0.09978 + 0.7974 * RD + (0.004994 – 0.7005 * RD) * Z/L
	y_u	0.4038 + 0.04812 * L/D	0.09952 + 0.7996 * RD + (0.03988 – 0.1606 * RD) * Z/L
Base Moment, M_b	x_u	173.1	44.86
	k	0.2146 – 0.002132 * L/D	0.3515
	n	1.079 – 0.1087 * L/D	0.3 + 0.4986 * RD
	y_u	0.8192 – 0.08588 * L/D	0.09981 + 0.371 * RD + (0.01988 – 0.09041 * RD) * Z/L

1.3.2.2.2 PISA numerical-based approach

The PISA framework also offers the possibility to develop site-specific soil reaction curves. This approach involves running numerous advanced 3D finite element models for a range of pile geometries. For each geometry, the soil reaction curves are extracted, normalised, and parameterised, giving site-specific fitting parameters (x_u, k, n, y_u). The 16 depth variation functions are then fitted to the site-specific fitting parameters. Figure 1-8 shows an example of such fitting for the normalized ultimate lateral distributed load in Cowden till (Byrne et al., 2020). Dots show fitting parameters from different pile geometries while the lines show successive fitting attempts.

This is not a straightforward process as most 3D FE software will not provide soil reaction curves directly. This approach is implemented in the commercially available Plaxis Monopile Designer software (Panagoulias, 2018) which can automatically extract the soil reaction curves and fit the depth variation functions. However, it is shown that Monopile Designer is missing a key component: the '2nd stage optimisation'. Lapastoure and Igoe (2022) showed how this might lead to inaccurate calibration and have suggested improved implementation using the PYTHON API of PLAXIS 3D (see Appendix B).

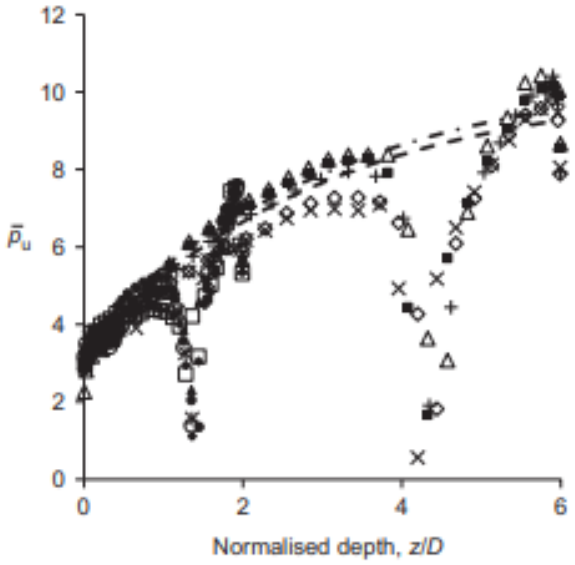

Figure 1-8: Example of depth variation function fitted to normalised ultimate lateral distributed load in Cowden till (Byrne et al., 2018)

The PISA numerical based approach is now widely used in the industry when sufficient site-specific data are available. The accuracy of the calibrated soil reaction curves depends on the accuracy of the 3D FE analyses. The soil constitutive models and their input parameters required careful calibration.

1.3.3 Cyclic modelling

Abadie (2016) distinguishes three main categories of models used in practice to predict the static response of laterally loaded piles (see Figure 1-9). The same categorization applies to cyclic loading. The models are classified depending on their complexity: three-dimensional finite element analyses (1), Winkler-type approaches (2) and macro-element models (3).

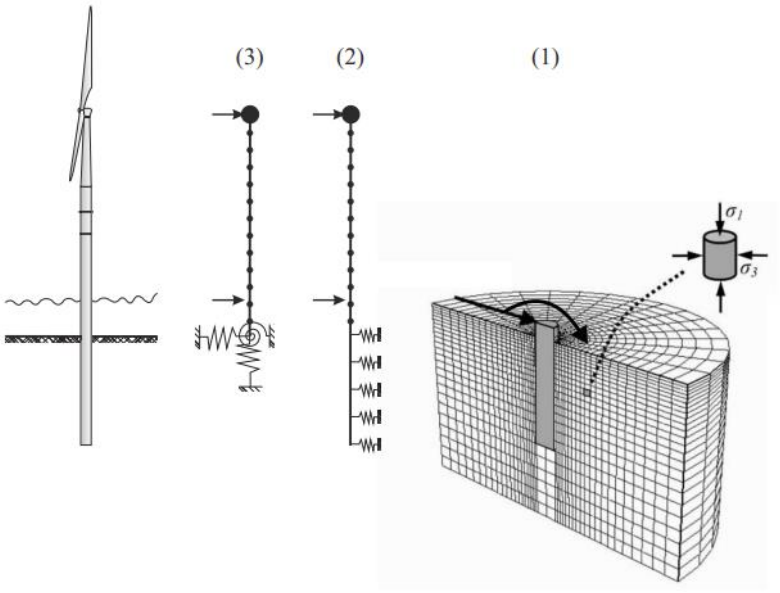

Figure 1-9. Monopile-soil interaction modelling methodologies after Abadie (2016).

1.3.3.1 Three-dimensional finite element analyses

Three-dimensional finite element analyses model the soil surrounding the pile as a continuum. It allows inspection of stress and strain distributions within the soil in addition to pile deflections and internal forces. Such approaches require advanced soil constitutive models and numerous input parameters. Once, properly calibrated they are regarded as the most accurate approaches but require large computation time. In recent years, undertaking 3DFE as part of the engineering design process for an offshore wind farm has become relatively routine (e.g. PISA numerical framework, Byrne et al., 2015). Optimisation of the foundation design for an entire wind farm requires analyses at numerous locations for varying load conditions, foundation dimensions and soil properties, often requiring thousands of analysis cases. For this reason, relying solely on 3D FEA would be too computationally expensive.

Most constitutive models available in commercial 3DFE software are unable to capture the cyclic ratcheting behaviour of soils. One exception is the SANISAND-MS soil model (Liu et al., 2019), which was specifically tailored to model the cyclic ratcheting behaviour of sands. This model is an enhancement of SANISAND04 (Dafalias & Manzari, 2014) with the addition of a memory surface accounting for the fabric effects during cyclic loading. The

memory surface only requires 3 additional parameters to the standard 13. The predicting capabilities of the SANISAND-MS soil model were demonstrated by comparison with drained (Liu et al., 2019) and undrained (Liu et al., 2020) soil element cyclic tests. Liu et al. (2021) investigated the sensitivity of monopile cyclic response to sand relative density and loading conditions using SANISAND-MS in Opensees. Both one-way, partial one-way and partial two-way loading were considered with peak load ranging from 0.125% to 50% of pile ultimate capacity. The results were qualitatively compared to the 1-g laboratory experiments by Leblanc et al. (2010) and Richards et al. (2020) to showcase the suitability of the approach. However, no quantitative comparison of the predicted monopile accumulated rotation was made. Only 100 cycles were considered and yet it required 49 hours to compute. Such advanced implicit constitutive soil models are very valuable for research purposes to investigate complex soil-structure interactions such as the sand densification upon lateral cyclic loading as shown in Figure 1-10. However, they cannot yet be realistically applied in day-to-day engineering.

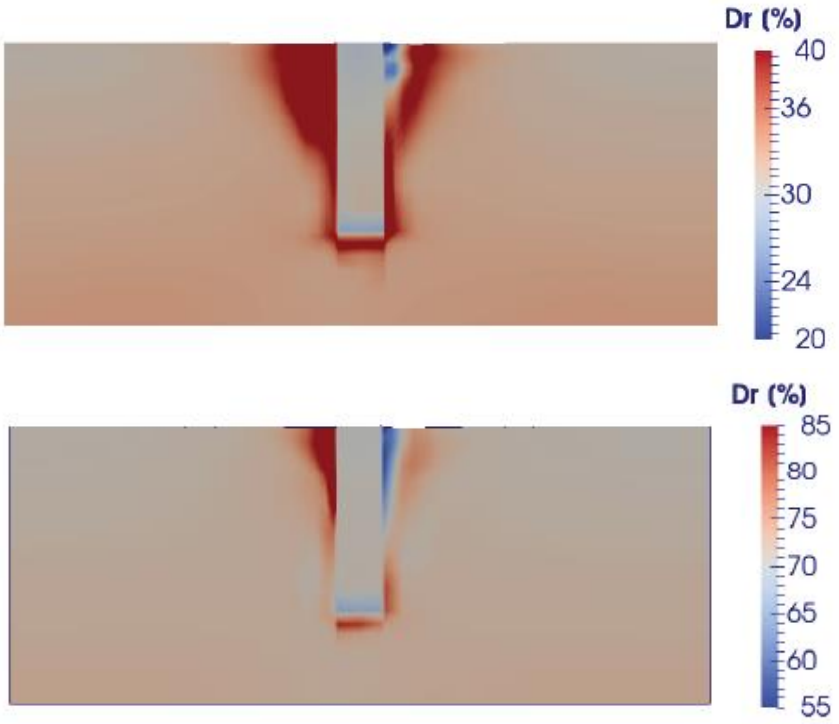

Figure 1-10. Densification of sand after 100 load cycles investigated with SANISAND-MS soil model in Opensees (modified after Liu, 2020). (top) $D_R^{initial}$ = 30%. (bottom) $D_R^{initial}$ = 70%.

Another constitutive model developed to capture cyclic ratcheting behaviour is the High Cycle Accumulation (HCA) model from Niemunis et al. (2005), which was developed for the accumulation of strain in sand. It can be regarded as a trade-off between implicit and explicit procedures. In implicit procedures (such as SANISAND-MS), small strain increments after each load cycle are summed to obtain the final accumulated strains. The

applicability of such procedures is limited by the number of cycles. Computation time can be prohibitive and small inaccuracies, inherent in finite element analysis, may accumulate and lead to large errors. Explicit procedures where the accumulated strain is directly calculated as a function of the cycle number are more robust and time-efficient. However, they are often less accurate due to simplifications required to obtain such explicit formulation. Niemunis et al. (2005) proposed to calculate implicitly the first few load cycles using an extended hypoplasticity model (Niemunis & Herle, 1997). The rate of strain accumulation is then explicitly extrapolated for a large number of cycles, drastically reducing computation time (see Figure 1-11). The explicit accumulation procedure can be occasionally interrupted to implicitly calculate so-called 'control cycles' to update the rate of accumulation and test the admissibility of the stress state. At the soil element scale, the HCA model was validated against cyclic triaxial texts by Wichtmann (2016). Settlement measurements during the full-scale test of a gravity base foundation for offshore wind turbines were compared to the HCA prediction made by Zachert et al. (2015), validating the approach at the foundation scale. Page et al. (2021) applied the HCA model to a monopile foundation showing a good match with centrifuge cyclic tests reported by Bayton et al. (2018). Although such a hybrid implicit-explicit approach is expected to be computationally less expensive than implicit formulation, no computation time were reported. In addition, HCA is not available in any 3D FEA commercial software. Finally, HCA requires numerous parameters that may not be easily calibrated from standard element tests.

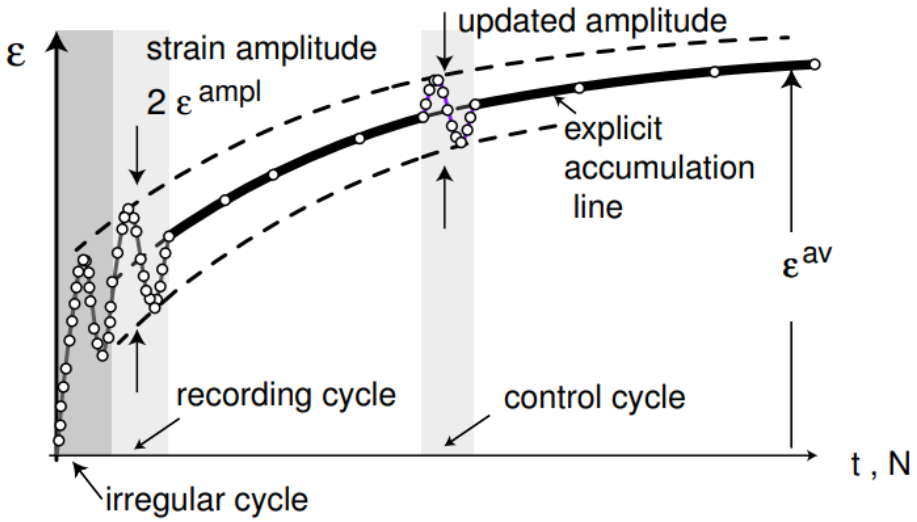

Figure 1-11. Rationale of the High Cyclic Accumulation model explicit formulation (Niemunis et al., 2005).

Building on their experience with soil cyclic contour diagrams, NGI (Norwegian Geotechnical Institute) developed monopile design procedures under cyclic loading applicable in finite element analysis. UDCAM (Undrained Cyclic Accumulation Model) and PDCAM (Partially Drained Cyclic Accumulation Model) were both implemented as user-

defined soil models in the commercial finite element software PLAXIS 3D (Page et al., 2013). 3D contour diagrams from cyclic and monotonic triaxial and DSS tests constitute the main inputs enabling the modelling of the non-linear average and cyclic stress-strain relationship. UDCAM is applicable to clays where undrained behaviour is considered for both the average and the cyclic loads. On the contrary, PDCAM is applicable to sands where effective stress analysis (partly drained) is considered for the average load. In addition to the accumulation of shear strain, PDCAM considers the accumulation of volume deformations and pore pressures. The latter requires an additional pore pressure contour diagram. These two models are built upon the strain accumulation principle developed by NGI (Andersen, 1976). The different cyclic load packets, each of constant amplitude, are explicitly accounted for to define an equivalent number of cycles (N_{eq}) varying along and around the pile (see Figure 1-12). The larger N_{eq}, the more severe the soil degradation due to cyclic loading. Jostad et al. (2014) applied UDCAM to offshore foundation design. Good predicting capabilities were demonstrated by comparison with gravity-based foundation tests reported by Dyvik et al. (1989). It is also shown that UDCAM is well suited for monopile cyclic modelling by comparison with results based on the API 'p-y' approach. UDCAM predict displacements in the ULS and SLS 50% smaller than that predicted by API. It is suggested by the authors that such procedure is much more time-efficient and robust than models following each cycle, especially when a large number of cycles is considered. A simplified version of UDCAM is now available to anyone in PLAXIS (Plaxis, 2022).

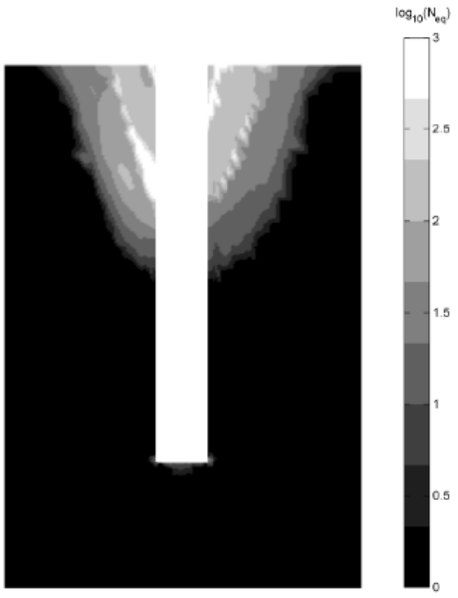

Figure 1-12. UDCAM prediction of Neq in the soil surrounding cyclically laterally loaded monopile (Jostad et al., 2014).

1.3.3.2 Winkler-type approaches

Winkler-type approaches are often regarded as a satisfactory compromise between accuracy and computation time. They involve modelling the pile embedment by means of one-dimensional elastic beam elements. The pile-soil interactions are captured by nonlinear soil reaction curves such as 'p-y' curves, predicting the soil reaction, p, as a function of the pile lateral displacement, y. Winkler-type approaches allow for inspection of deflection and internal forces along the entire pile embedment but give no indication of the stress and strain distribution in the soil continuum surrounding the pile. The accuracy of such approaches relies on the calibration of the soil reaction curves considered. Cyclic soil reaction curves are typically obtained by degradation of the static curves. It is unclear how these can be translated into the new PISA framework for monopile design when considering the additional soil reaction components: distributed moment, base shear, and base moment.

The API cyclic approach for laterally loaded piles in sands (API, 2014) consists of significantly reducing ultimate soil reaction at shallow depths. No modification to the initial stiffness of the curves is considered. The magnitude of the cyclic degradation does not account for the number of cycles applied nor the magnitude of the cyclic loading. This simplistic approach has been successfully applied for decades in the oil and gas industry for which the focus is on conservative design against structural failure. However, monopile design optimisation requires accurate prediction of accumulated permanent rotation as a function of the cycle number.

The work carried out by SOLCYP (Puech & Garnier, 2017), including an extensive review of the literature and numerous centrifuge cyclic lateral pile tests, resulted in a more elaborate degradation of the 'p-y' curves. The results from this program suggested a reduction of ultimate soil reaction with the number of cycles at shallow depth while deeper reactions are less affected (Figure 1-13). Hence, the proposed approach, termed SOLCYP-L, accounts for both the number of cycles and the load magnitude, with respect to the capacity of the pile. The degradation varies with depth and no degradation is considered below a depth of 5 times the pile diameter. The degradation parameters are applied as a p-multiplier, affecting both the ultimate capacity and initial stiffness of the curves. However, the static soil reaction curves were computed according to NF P 94-262 (AFNOR, 1997), considering only 'p-y' curves. The tests were carried out on rather slender flexible piles with a slenderness ratio (L/D) over 15. No special consideration for the load eccentricity was made, although this is a key characteristic of the lateral loading experienced by monopiles. Hence, there is no evidence of direct applicability of the SOLCYP-L for monopile design.

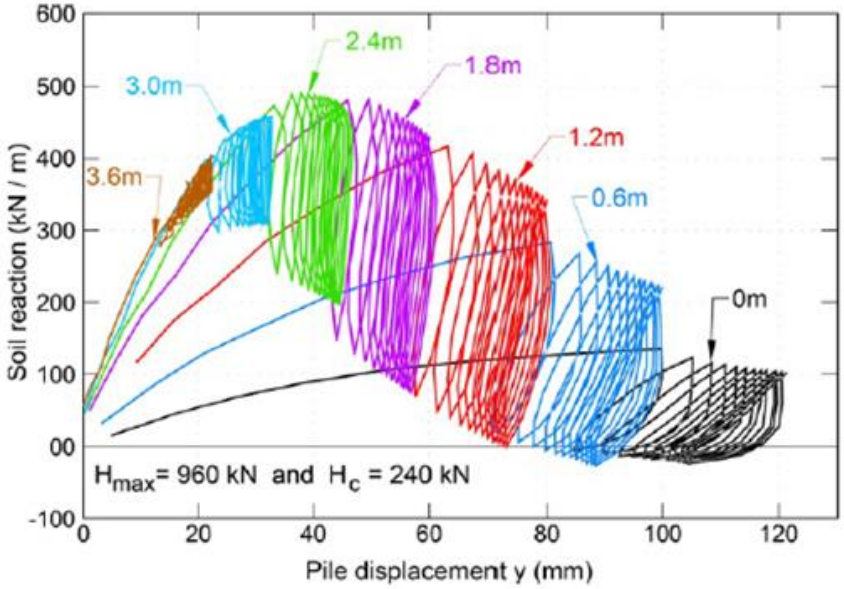

Figure 1-13. Effect of cyclic loading on p-y curves in sand (Rosquoët, 2004).

Zhang and Andersen (2017) proposed a new framework to compute site-specific p-y curves directly from direct simple shear (DSS) tests in clay (after the similarity concept proposed by Jeanjean et al., 2017). Zhang et al. (2018) further developed this framework by implementing consideration for cyclic loading. Based on the same approach, cyclic p-y curves can be scaled from soil DSS cyclic contour diagrams. Figure 1-14 presents the similarity between a laterally loaded pile element and a DSS soil element test. The ratio of mobilised soil lateral reaction upon cyclic loading over ultimate reaction (p/p_u) is considered analogous to the ratio of mobilised shear stress over shear strength (τ/s_u). Such procedure results require numerous cyclic laboratory experiments to build the cyclic contour diagram and hence is only practicable for later stages of design. The framework allows the computation of site-specific soil reaction curves.

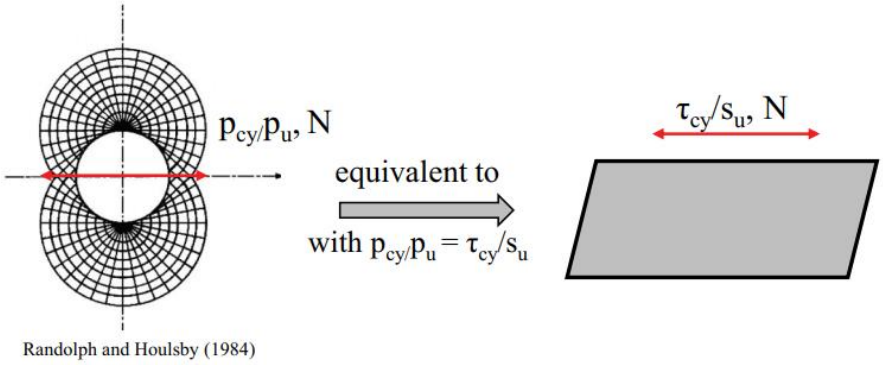

Figure 1-14. Analogy between pile lateral loading and Direct Simple Shear soil element test (Zhang et al. 2016).

Beucklears et al. (2022) have recently applied the Hyperplastic Accelerated Ratcheting Model (HARM) in a generalised Winkler model consistent with the PISA framework. HARM was originally developed for macro-element monopile modelling as discussed in the

next section. The simulated results showed a good match with PISA large scale field tests in both sand and clay (see Figure 1-15). However, this required the input parameters to be calibrated. The predictive capability of the approach was not fully demonstrated.

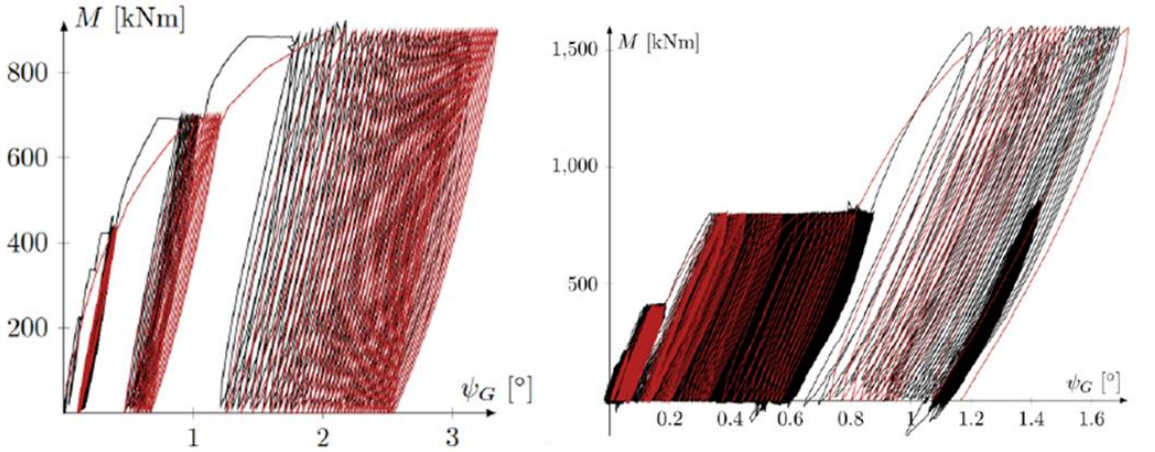

Figure 1-15. Comparison of PISA large scale field tests (black line) with results simulated by HARM implemented within a Winkler model (red line). Pile CM6 at the Cowden site (top) and pile DM2 at the Dunkirk site (bottom)

1.3.3.3 Macro-element models

Macro-element models are the most simplistic approach, incorporating the interactions between the pile and the soil into surface springs. Hence, such models provide no information on structural forces nor deflections along pile embedded length. They require limited input parameters and run very quickly. However, they are often calibrated for specific soil and load conditions, making it challenging to apply them directly to a real monopile design case. Macro-element models are best suited for early monopile design stage.

Most of the macro-element models existing in the literature predict the monopile mudline cyclic rotation, θ_{cyclic}, explicitly from the cycle number, N, and from the static rotation under the same load magnitude, θ_{static}. Most models are either power (e.g. Little & Briaud, 1988, Long & Vanneste, 1994, Leblanc, 2010, Klinkvort, 2012, Roesen et al., 2013, Albiker et al., 2016, Puech & Garnier, 2017) or log function (e.g. Hettler, 1981, Lin & Liao, 1999, Verdure et al., 2003, Li et al., 2010, Bienen et al., 2012, Puech & Garnier 2017) of the cycle number and can be simplified into equation (1.5) or (1.6), respectively. Cuéllar (2011) has also suggested a log-linear model based on cyclic tests done with very large number of cycles but this is not further discussed here. The parameters t and a represent the rate of accumulation are a function of pile geometry, characteristics of the cyclic loading and site conditions. In the literature, they are broadly found to range from 0.04 to 0.25 and from 0.072 to 0.31, respectively.

$$\theta_{cyclic} = \theta_{static}(1 + t \ln N) \tag{1.5}$$

$$\theta_{cyclic} = \theta_{static} N^{a} \tag{1.6}$$

The characteristics of the cyclic loading are commonly captured by two parameters as per Figure 1-16. The lateral load, H, applied at an eccentricity, e, above mudline corresponds to an overturning moment at mudline, M = H×e. Hence, ζ_b and ζ_c in equations (1.7) and (1.8) are expressed in terms of H or M where relevant. ζ_b characterises the magnitude of the cyclic loading (H_{max} or M_{max}) with respect to the pile lateral capacity (Hult or Mult). ζ_c characterises the direction of the cyclic loading: one-way ($\zeta_c = 0$), partial one-way ($0 < \zeta_c < 1$), two-way ($\zeta_c = -1$) or partial two-way ($-1 < \zeta_c < 0$).

$$\zeta_b = \frac{H_{max}}{H_{ult}} = \frac{M_{max}}{M_{ult}} \tag{1.7}$$

$$\zeta_c = \frac{H_{min}}{H_{max}} = \frac{M_{min}}{M_{max}} \tag{1.8}$$

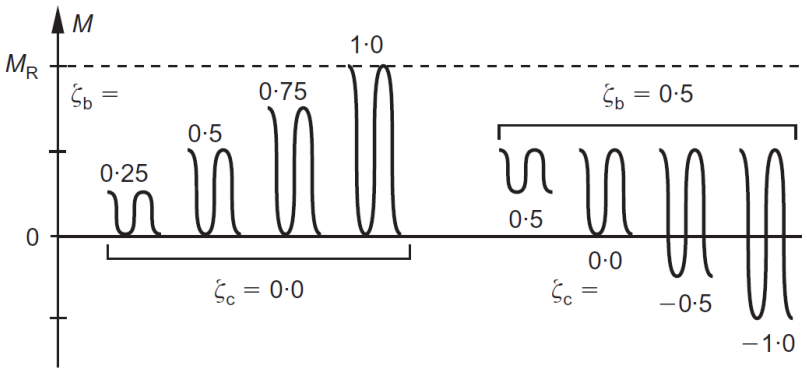

Figure 1-16. Characteristic of cyclic loading (Leblanc, 2010).

All researchers agreed that the two extreme cases ($\zeta_c = -1$ and $\zeta_c = 1$) lead to no accumulation of cyclic rotation (i.e. a = 0 or t = 0). However, there is no consensus for the intermediate cases. Most researchers found pure one-way loading to be the most detrimental. However, Leblanc (2010) and Klinkvort (2012) found the intermediate case $\zeta_c = -0.6$ to be the most detrimental. Similarly, although most researchers found the rate of accumulation to increase with ζ_b, there is no consensus on how to define monopile lateral capacity. For example, Leblanc (2010) defines capacity for a mudline rotation of 4 degrees, a limit of 2 degrees or 10% pile diameter were used during the PISA project, Albiker et al. (2016) used about 3 degrees, Verdure et al. (2003) considered a tangent-asymptote approach leading to about 1 pile diameter, Puech & Garnier (2017) considered a slightly different tangent approach for their global model (SOLCYP-G) leading to about 25% pile diameter, etc. Such disparities between models make the comparison of the different models and experimentations rather challenging.

Another difference concerns whether the approach predicts accumulated pile displacement or rotation. Most of the explicit models mentioned were developed for the accumulation of pile displacement. Rotation is more relevant for monopile design given the strict 0.25 degrees limit specified in DNV (2021). Hence, it is a common practice in the industry to use the same formulation for rotation. However, Li et al. (2015) show that accumulated rotation and displacement can both be depicted with log or power functions, but the parameters will not be the same. Only more recently, Leblanc et al. (2010), Klinkvort (2012) and Albiker et al. (2016) carried out 1-g or centrifuge laboratory experiments specifically for monopile, looking at accumulated rotation and taking care of using relevant pile geometry (small L/D) and load eccentricities (couple of diameters above soil surface).

Another difference between the models is whether the model aims to predict the maximum (peak) rotation or permanent (unloaded) rotation. Most explicit models predict the maximum rotation accumulated through the cyclic loading. However, Cuéllar (2011) found that a log-linear fit better the evolution of the permanent rotation with the number of cycles. If the model predicts maximum rotation, it is therefore necessary to estimate how much the rotation reduces upon unloading. Although some researchers reported increasing unloading-reloading stiffness upon cyclic loading, the monotonic (backbone) stiffness is usually conservatively considered. The unloading might be done following the initial monotonic linear stiffness or assuming Masing's rule as discussed by Prendergast & Igoe (2022).

Finally, all these models concern a single-load package. However, the monopiles experience multi-direction, multi-amplitude cyclic loading throughout their lifetime. Hence, based on Miner's superposition, researchers have developed approaches to define a number of cycles, Neq, equivalent to the entire cyclic load history. However, different researchers used different variables of interest to define Neq. For example, DGGT (2013) considers the total cyclic rotation to remain constant at the end of the load packet and at the beginning of the next one. This is disregarding the instantaneous change in pile rotation due to the increase of the lateral loading from one load packet to the next one. Hence, Leblanc et al. (2010) considered a constant increase due to cyclic loading (see Figure 1-17 where $\Delta\theta = \theta_{cyclic} - \theta_{static}$). Another approach suggested by Page et al. (2021) consists of considering constant accumulated permanent rotation.

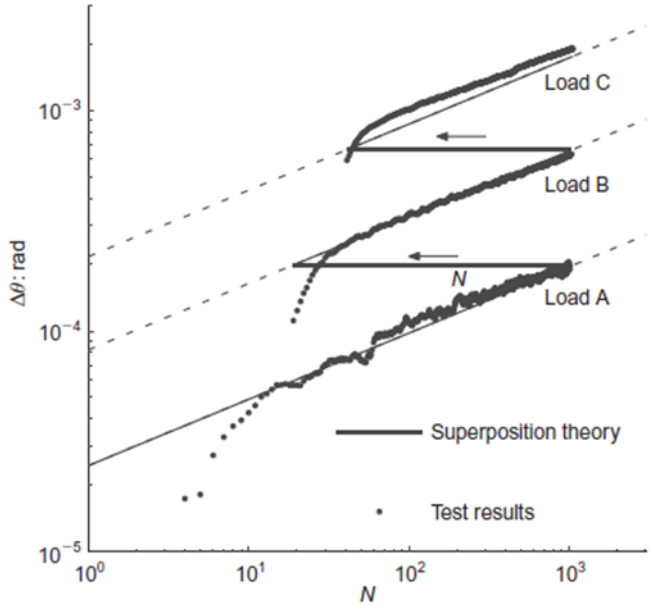

Figure 1-17. Superposition theory for accumulation of cyclic rotation from one load package to another (Leblanc et al. 2010b)

EA-Pfähle, the German recommendations for piling, recommends the model developed by Hettler (1981) to predict the deflection accumulation of piles subjected to cyclic lateral loading. The French committee for soil mechanics and geotechnics (CFMS, 2020) also recommends Hettler's model as well as models developed by Puech & Garnier (2017) and Leblanc et al. (2010). All three are macro-element models. They are the most likely to be used by the industry, especially at an early stage of design. Due to their simplicity, macro-element models allow for quick computation and require minimum design inputs.

Another macro-element model suggested by CFMS (2021) is the Hyperplastic Accelerated Ratcheting Model (HARM) developed by Houlsby and co-workers at Oxford (Houlsby et al., 2017; Abadie et al., 2019). HARM has been specially developed to study the monopiles response to cyclic loading. The model is derived from the hyper elasticity framework and provides a 0-D representation of the soil-pile macro response. It has been developed based on a series of specifically designed 1-g laboratory scale model tests in sand. Up to 100,000 cycles were applied to identify key mechanisms of piles response to cyclic loading. Among other observations, the experimental results showed an accumulation of pile deformation whose rate decreases with the number of cycles but always remains non-null. It was also shown that the cyclic hysteresis loops tend to tighten with an increased secant stiffness and decreased loop area. Finally, the extended Masing rule seems to apply as the pile static response after a cyclic loading history tends towards the initial static response. HARM is able to replicate the complete pile macro response to complex cyclic loading in terms of load-displacement curves as shown in Figure 1-18. The model showed good

predictions of not only the accumulation of pile displacement but also the secant stiffness increase, and hysteresis loop area decrease with increasing number of cycles. In order to reduce the computation time, the author implemented an accelerated procedure (Abadie et al., 2019). A high number of identical cycles can be simulated by a reduced number of equivalent cycles. Although this framework seems to mark a significant step forward in the modelling of monopiles response to cyclic loading, it has only been validated against small scale laboratory piles. Additional features such as gap formation between the pile and the soil may need to be implemented for the model to be applied to large scale monopiles. Gapping can have a significant impact on the pile response. It has been widely observed during the PISA field tests (Byrne et al., 2020; McAdam et al., 2020). Finally, even if the model has the advantage of being computationally efficient, it requires an extensive calibration exercise which is not yet practical or well understood for application in industry.

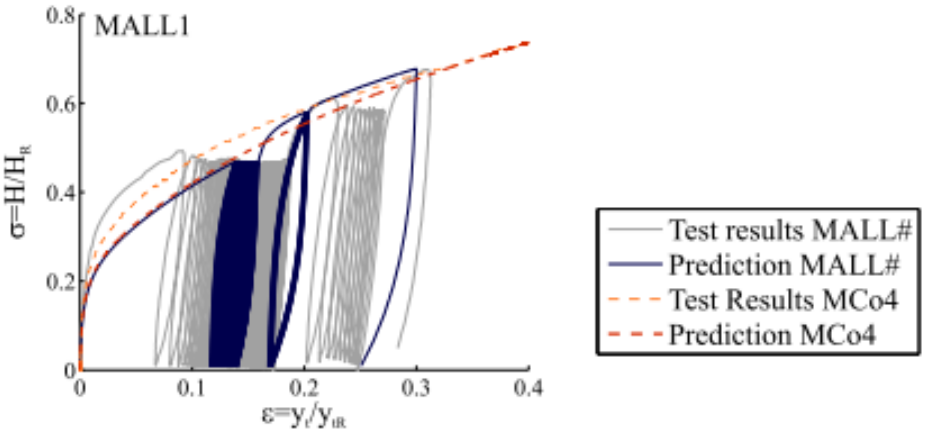

Figure 1-18. Comparison of experimental and HARM predicted load-displacement curves for complex cyclic loading. (Abadie, 2016).

1.4 RESEARCH OBJECTIVES

The main research objectives of this PhD are to:

a) Review the literature and identify shortcomings of current approaches to account for the effect of cyclic loading on monopile lateral response.
b) Develop high quality experimental data from lateral loading field tests on piles which are representative of offshore conditions.
c) Develop and validate methodologies to predict monopile lateral response under cyclic loading which are practical for use in monopile design practice.

1.5 THESIS OUTLINE

This thesis is divided into five main chapters for a clearer comprehension. It has been arranged as an introduction and a series of papers that have either been published or

submitted for publication. All the papers have been updated to avoid repetitions and to improve continuity.

This first chapter is an introduction to the offshore wind industry focusing on foundation design and the modelling of monopiles response to cyclic lateral loading.

The second chapter addresses the shortcomings of the approaches popular in the industry for predicting the response of monopiles to cyclic lateral loading. It is now widely acknowledged that there is no consensus and that the various cyclic models published in the literature lead to very different predictions. However, currently, the research focuses on pile response to constant amplitude cyclic loading although not realistic conditions. This chapter demonstrates that the choice of superposition theory to accumulate the effect of the different load magnitudes has as much influence as the choice of cyclic model. A new superposition theory matching with PISA field tests experimental results is proposed. This chapter has been published in Ocean Engineering in 2023.

The third chapter presents the details of a new campaign of pile lateral monotonic and cyclic field tests carried out in dense sands at the Blessington test site. The Chapter focused on the presentation of the experimental campaign and the results of the lateral monotonic tests. The monotonic response of three piles with a slenderness ratio ranging from 2.2 to 4.4 is reported. It is shown that the blind predictions based on three-dimensional finite-element analyses are in very good agreement with the experimental responses. The input parameters to the 3D FE soil constitutive model are based on the CPT profiles following an approach recently developed at Trinity College Dublin. This chapter is currently under preparation to be submitted to an international journal.

The fourth chapter is a follow-up from Chapter three, focusing on presenting the results of the lateral cyclic tests. Thousands of cycles were applied to four different piles with slenderness ratios ranging from 2.2 to 4.4 at various load levels up to about 65% of the pile ultimate capacity. The results are presented in terms of both accumulation of displacement at ground level and in terms of reduction of the secant stiffness upon cyclic loading. A macro-element model is fitted to the experimental data using two different approaches for comparison with the existing models in the literature. The superposition model proposed in Chapter 2 is found in much better agreement with the experimental data than any other superposition model from the literature. This chapter is currently under preparation to be submitted to an international journal.

The fifth chapter presents the step-by-step methodology and the validation of a new cyclic model for the design of monopiles in sand and clay. The model consists of the degradation of monotonic soil reaction curves based on soil cyclic contour diagrams. The

model is validated against PISA field tests and the Blessington field tests reported in chapters three and four. The model provides accurate and quick predictions of the monopiles cyclic response enabling the optimisation of monopiles geotechnical and structural design. This chapter has been submitted to Acta Geotechnica and is undergoing peer review.

The sixth chapter summarises the key findings and conclusions of the thesis and proposes future directions for the research.

(intentionally left blank)

Chapter 2: Assessment of cyclic superposition approaches for the cyclic design of monopiles supporting offshore wind turbines

Chapter 1 has shown that limiting the permanent rotation accumulated through the lifetime of the offshore wind turbines is a key design criterion for the monopile foundation, and macro-element semi-empirical models are often used to assess such accumulation. The procedure require 4 key components: (1) a static model, (2) a cyclic model for accumulating rotation for a given load package, (3) a superposition model for accumulating rotation between different load packages (4) an unloading model to assess the final permanent accumulated rotation once unloaded. However, to date, the literature has focused on the comparison of the cyclic accumulation models (component 2 solely) and the other components, yet essential, are often overlooked. To address this shortcoming, this chapter assesses the effect of using different cyclic superposition models. A new superposition approach is proposed which matches well with the results from a high-quality field test from the literature. The Chapter compares the permanent accumulated rotation from four widely used semi-empirical cyclic models (Hettler 1981; Puech & Garnier, 2017; Leblanc et al., 2010a; Klinkvort & Hededal, 2013) used in conjunction with four different superposition approaches. The results demonstrate that the choice of superposition approach can be as important as the choice of cyclic model, which is often overlooked in the literature but is critical for the estimation of accumulated permanent rotation.

2.1 PRESENTATION OF THE FRAMEWORK

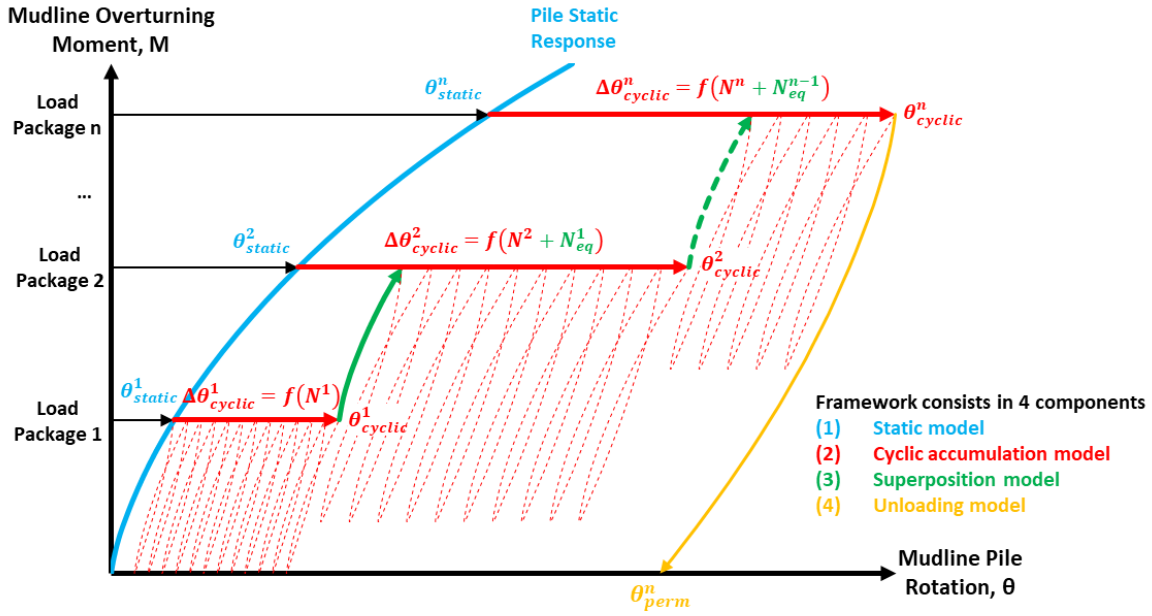

Figure 2-1. Framework for application of semi-empirical cyclic macro-model for estimation of accumulated permanent rotation.

Figure 2-1 proposes a framework for the application of macro-modelling approaches for predicting the accumulated permanent rotation for cyclic monopile design. In this type of approach, estimating the accumulated permanent rotation requires 4 key components: (1) a static model (in blue), (2) a cyclic model (in red), (3) a superposition model (in green) and (4) an unloading model (in orange).

2.1.1 Monotonic model

The static (monotonic) pile response is a key input to any semi-empirical cyclic macro-model. As shown in Figure 2-1, the accumulation of cyclic rotation θ^i_{cyclic} during a generic load package *i* (where *i* indicates the load package number increasing from *1* to *n* from the load package with the lowest to the highest peak load) is determined from the static rotation θ^i_{static} under the same loads ($\theta^i_{cyclic} = \theta^i_{static} + \Delta\theta^i_{cyclic}$). Therefore, the prediction of the cyclic response of a monopile can only be accurate if the static response is also accurately captured.

Historical shortcomings and recent developments in monotonic modelling have already been discussed in Chapter 1.

2.1.2 Cyclic accumulation model

The cyclic accumulation model predicts the monopile mudline cyclic rotation, θ_{cyclic}, explicitly from the cycle number, *N*, and from the static rotation under the same load magnitude, θ_{static}. Most models existing in the literature are either power (e.g. Little &

Briaud, 1988; Long & Vanneste, 1994; Leblanc, 2010a; Klinkvort & Hededal, 2013; Roesen et al., 2013; Albiker et al., 2016; Puech & Garnier, 2017) or log functions (e.g. Hettler, 1981; Lin & Liao, 1999; Verdure et al., 2003; Li et al., 2010; Bienen et al., 2012; Puech & Garnier, 2017) of the cycle number and can be simplified into equation (2.1) or (2.2), respectively. The parameters *t* and *a* in these equations govern the rate of rotation accumulation and they are a function of pile geometry, characteristics of the cyclic loading and site conditions. In the literature, they are broadly found to range from 0.04 to 0.25 and from 0.072 to 0.31, respectively.

$$\theta_{cyclic} = \theta_{static} + \Delta\theta_{cyclic} = \theta_{static}(1 + t \ln N) \quad (2.1)$$

$$\theta_{cyclic} = \theta_{static} + \Delta\theta_{cyclic} = \theta_{static} N^{a} \quad (2.2)$$

Numerous studies (e.g. Frick and Achmus, 2022; Jalbi et al., 2020; Puech & Garnier, 2017) pointed out the differences and inconsistencies between the various models, which lead to a broad range of predictions. However, to date, there is no consensus on the most generally accurate approach. The choice of the cyclic model is known to significantly impact the prediction of accumulated permanent rotation and in turn the monopile design. The interested reader is referred to the references cited above.

2.1.3 Superposition model

The cyclic load history considered for monopile design generally consists of a number of different load packages with various load magnitudes and number of cycles. Hence, a superposition model is required to make load packages equivalent to each other so that their respective contribution can be added. It is a common practice to pick the load package with the largest load as reference. Indeed, this usually leads to the largest accumulated pile deflection.

DGGT (2013) recommends two superposition approaches:

1. Each package can be made equivalent to the package with the largest loads; or
2. The package with the lowest loads is made equivalent to the package with the next lowest loads. This is repeated until the entire cyclic load history is made equivalent to the package with the largest loads.

In Approach 2, the N^1 cycles of package *1* are made equivalent to N_{eq}^1 cycles of package *2* before adding the N^2 cycle of the later package. This is repeated until the second last package *n-1* is made equivalent to N_{eq}^{n-1} cycle of the last package *n* (see Figure 2-1).

To compute N_{eq}^1, N_{eq}^2, ..., N_{eq}^{n-1}, one should define the reloading stiffness from one load package to the next (green arrow). Section 2.2 presents the existing approaches from DGGT (2013), Leblanc et al. (2010b) and Page et al. (2021). Given the shortcomings of

these existing approaches, a new approach is also suggested. The Chapter aims to assess the impact of the adopted superposition model on the prediction of monopile cyclic response and design.

2.1.4 Unloading model

The limit imposed by DNV (2021) for monopile geotechnical serviceability limit state applies to the accumulated permanent (unloaded) rotation. Hence, an unloading model is required at the end of the cyclic load history as shown in Figure 2-1 to compute $\theta_{perm}{}^{n}$. Three simple approaches could be adopted:

1. Using an unloading stiffness equal to the initial linear static (backbone) stiffness;
2. Using a Masing's rule unload based on monotonic response (i.e. scaling the static backbone curve by a factor of 2 and reversing the direction for unload);
3. Using an unloading-reloading stiffness which decreases/increases with cyclic loading.

Prendergast & Igoe (2002) and Thieken et al. (2018) suggest that the unloading stiffness compares relatively well with the monotonic (backbone) stiffness, thus implying that the use of unloading approaches 1 or 2 may be most suitable. Unloading models are much less studied than cyclic models and can also impact the prediction of accumulated permanent rotation and in turn the monopile design. In order to confine the scope of this Chapter to superposition models, only a simple linear unload model (approach 1) will be used in the subsequent analysis described in this Chapter.

2.2 PRESENTATION OF SUPERPOSITION MODELS

2.2.1 Superposition model recommended by EA-Pfahle

One of the most common models is presented in Figure 2-2 after DGGT (2013) and is termed the "EA-Pfahle" superposition model in this Chapter. As illustrated in Figure 2-2, the "EA-Pfahle" superposition model assumes that the mudline pile cyclic displacement (y_{cyclic} below) remains constant when going from one load package (i) to the next one (i+1). Hence, the N^{i} cycles of load package i are converted into $N_{eq}{}^{i+1}$ cycles of load package i+1 before adding the N^{i+1} cycles of load package i+1. The same assumption is generally equally applied to mudline pile rotation.

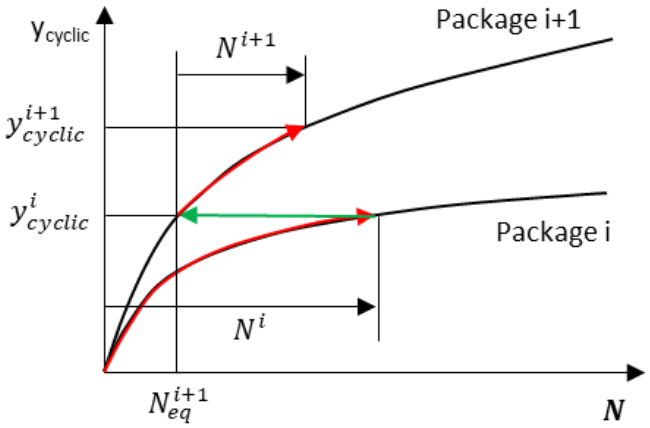

Figure 2-2. "EA-Pfahle" superposition model as suggested in DGGT (2013).

The "EA-Pfahle" superposition model is often considered the default design option due to its simplicity. However, one should note that the assumption of constant mudline pile displacement/rotation from one load package to another means that the reloading stiffness is infinite. The increasing loads from one load package to another lead to no extra deflection. In addition, the monopile can recover entirely from the previous load history if the loads of the next load package are sufficiently larger than the previous load package. In some instances, the cyclic response might even become stiffer than the monotonic response as illustrated in Figure 2-3.

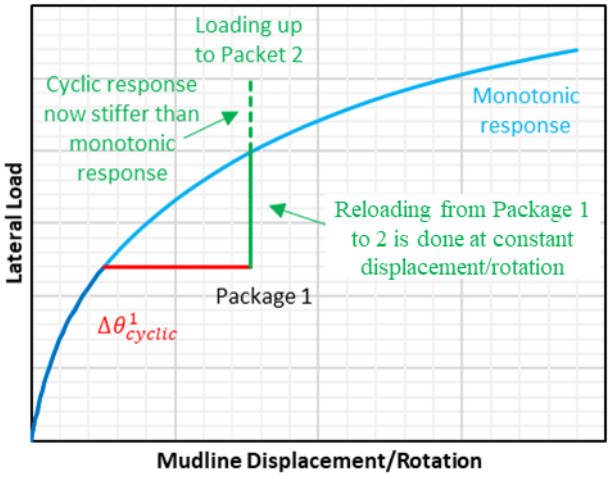

Figure 2-3. Illustration of the shortcoming of the "EA-Pfahle" superposition model.

2.2.2 Superposition model recommended by Leblanc et al. (2010b)

Leblanc et al (2010b) suggested another superposition model (termed "Leblanc" superposition model in this Chapter). Figure 2-4 presents the approach whereby N^i cycles of load package *i* are made equivalent to $N_{eq}{}^{i+1}$ cycle of load package *i+1* before adding N^{i+1} cycles. The equivalence is made considering constant $\Delta\theta^i$ which is the difference between

the cyclic rotation at the end of load package i and the static rotation under the same load level.

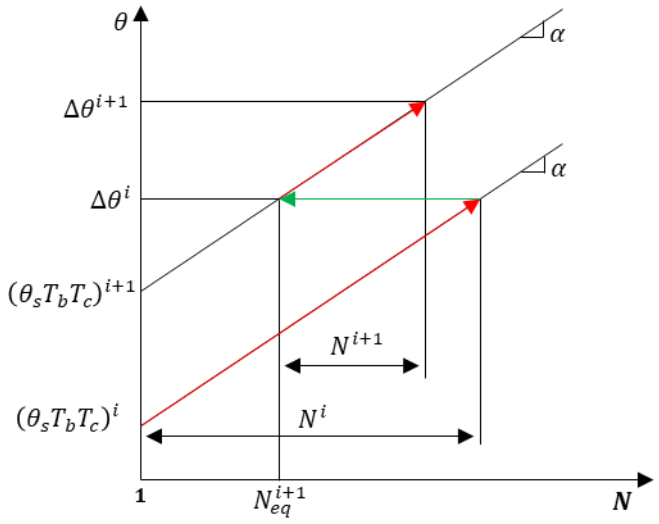

Figure 2-4. "Leblanc" superposition model as presented in Leblanc et al. (2010b)

In other words, "Leblanc" superposition model assumes that the loading stiffness after the first package 1 is the same as the virgin monotonic stiffness under the same load level as shown in Figure 2-5 where the difference between the cyclic response and the static response remains constant.

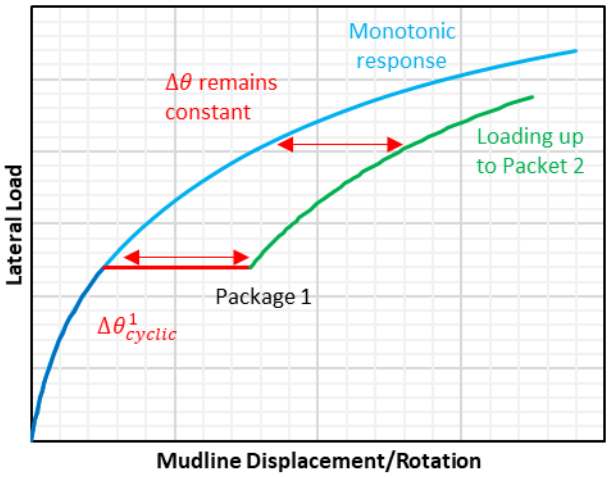

Figure 2-5. Illustration of the "Leblanc" superposition model.

2.2.3 Superposition model recommended by Page et al. (2021)

Page et al. (2021) presented an approach where permanent rotation at the start of one load packet is equal to the permanent rotation from the previous load packet plus an additional rotation due to the change in load characteristics as illustrated in Figure 2-6. Indeed, it is assumed that the change in average load acting on the monopile ΔM leads to an instantaneous change in permanent rotation $\Delta\theta_{perm}$. Page et al. (2021) suggest that change in permanent

rotation, $\Delta\theta_{perm}$, can be estimated from the equivalent change in load in the static (monotonic) moment-rotation curve $\Delta\theta_{static}$. This approach differs from the others in that it directly assumes the change in permanent rotation $\Delta\theta_{perm}$ (rather than $\Delta\theta_{cyclic}$) and therefore includes an unloading component. Page et al. 2021 assume a Masing's rule unloading response. This superposition model will be termed "Page" in this Chapter. No experimental evidence is provided by Page et al. (2021) to justify such superposition.

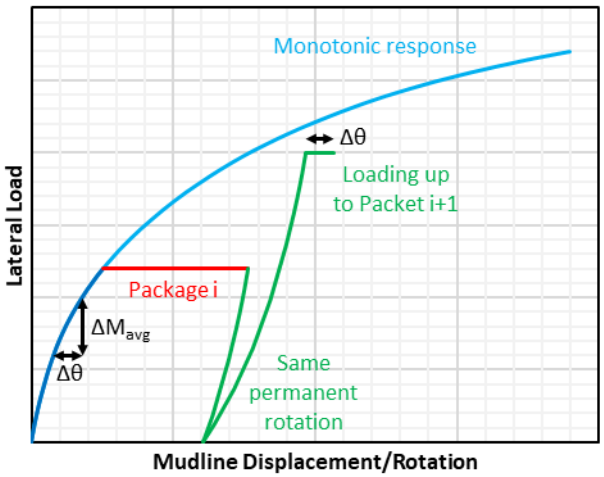

Figure 2-6. Illustration of the "Page" superposition model.

2.2.4 Superposition model recommended by this Chapter

Given the shortcomings of the existing approaches, a new superposition model is suggested in this Chapter. The approach is illustrated in Figure 2-7 where the pile cyclic rotation θ_i at the beginning of load packet i is the sum of the cyclic rotation θ_{i-1} at the end of load packet i-1 and the increase in rotation due to the increase in load $\Delta H=H_i-H_{i-1}$. The instant change in rotation due to the increased load is obtained from a scaled version of the monotonic (backbone) response as per equation (2.3).

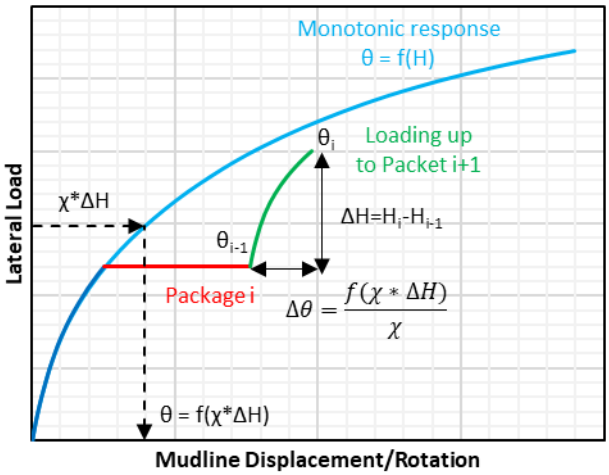

Figure 2-7. Illustration of the new superposition model suggested in this Chapter.

$$\theta_i = \theta_{i-1} + \frac{f\left(\chi * (H_i - H_{i-1})\right)}{\chi} \tag{2.3}$$

Where χ is a scaling factor which increases as the load magnitude of the previous load package H_{i-1} gets closer to pile ultimate capacity H_{ult}, as per Equation (2.4). The ultimate capacity is here defined for a mudline displacement of 10% pile diameter. Function $\theta = f(H)$ refers to the monotonic response.

$$\chi = \frac{H_{ult}}{H_{ult} - H_{i-1}} \tag{2.4}$$

This empirical approach is defined to match well with experimental data, as shown in the following section.

2.2.5 Comparison to PISA field tests

Three superposition models presented above are compared to the results of large-scale field tests carried out as part of the PISA project. Although the PISA project focused on monopile monotonic response, a few cyclic tests were also carried out. The results were disseminated through several publications (e.g. Beuckelaers, 2017; Byrme et al., 2020a; Byrme et al., 2020b; McAdam et al., 2020). It should be noted that gaping between the pile and the soil was observed upon cyclic loading, most likely affecting the unloading-reloading stiffness. Such gaping might not be observed offshore, depending on the soil conditions.

The load-displacement curves presented in Figure 2-8 relate to the response of the medium size piles DM4 and DM2 tested at the sand site in Dunkirk. The two piles had the same geometry with an outside diameter of 0.762 m, an embedded length of 4 m (L/D = 5.25), a wall thickness of 14 mm and the lateral load being applied 10 m above ground level.

DM4 was tested monotonically to define the backbone static curve for DM2 which was subject to cyclic loading.

The red arrow shows the superposition from load package 4 to load package 5 following the "EA-Pfahle" superposition model. As presented in section 2.2.1, EA-Pfahle assumes that the pile deflection remains constant (i.e. the pile has infinite stiffness when moving from a lower to a higher load packet). This is found to lead to a large underestimation of the cyclic rotation at the beginning of load package 5 in comparison to the experimental data as shown in Figure 2-8. On the contrary, the superposition according to the "Leblanc" model represented by the blue arrow leads to a large overestimation of the cyclic rotation at the beginning of load package 5. This result is in line with the expectations given the assumption of a constant difference between cyclic and static response in the "Leblanc" superposition model is preventing any recovery from previous cyclic history and a soft reloading behaviour.

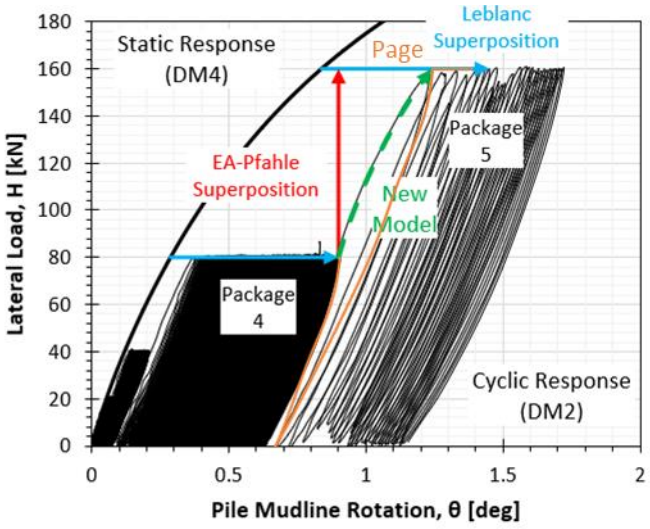

Figure 2-8. Comparison of the three different superposition models to the results of the PISA large scale field tests in sand at the Dunkirk site (adapted from Byrne et al. 2020b).

The shortcomings of the existing approaches led to the development of the new superposition model proposed in this Chapter. The new model presented in section 2.2.4 is represented by the green curve in Figure 2-8. It is shown that this new model lies between the two previous models and matches the experimental data very well.

The superposition model proposed by Page et al. (2021) is also plotted in orange in Figure 2-8. The results of the "Page" superposition model are found within the "New model" and "Leblanc" superposition models.

2.3 Case study: effect of superposition model on monopile cyclic response and design

The influence of the superposition model on the cyclic response of a monopile is demonstrated through a range of case studies, examining 4 relative densities from loose to very dense soil profiles and 4 separate load histories. Three of the load histories are based on the cyclic load history reported by Page et al. (2021) which is considered representative of typical offshore wind sites while a 4th load history is taken from a North Sea wind farm is also considered. For each of the case studies, the response of the monopile to the cyclic load history is calculated using the 4 cyclic accumulation models proposed by Hettler (1981), Puech & Garnier (2017), Leblanc et al. (2010a), Klinkvort & Hededal (2013) and the 4 superpositions models presented in section 3 and summarises in Table 2-1.

Table 2-1. Summary of the formulation and input parameters for each of the 4 cyclic accumulation models considered.

Reference	Formulation	Parameters
Hettler (1981)	$\frac{\theta_{cyclic}}{\theta_{static}} = 1 + t\ ln\ N$	$0.16 \leq t \leq 0.22$
Leblanc et al. (2010a)	$\frac{\theta_{cyclic}}{\theta_{static}} = 1 + T_b T_c N^a$	$T_b = f(\zeta_b, D_r)$ $T_c = f(\zeta_c)$ $a = 0.31$
Puech & Garnier (2017)	$\frac{\theta_{cyclic}}{\theta_{static}} = 1 + \alpha\ log_{10}\ N$	$\alpha = \frac{0.235\left(\frac{1-\zeta_c}{2}\right)^{0.35}}{CR}$
Klinkvort & Hededal (2013)	$\frac{\theta_{cyclic}}{\theta_{stat}} = N^{T_b T_c}$	$T_b = 0.61\zeta_b - 0.013$ $T_c = (\zeta_c + 0.63)(\zeta_c - 1)(\zeta_c - 1.64)$

2.3.1 Inputs to the case studies

2.3.1.1 Soil profiles

For the proposed case studies, the soil profiles are based on the representative offshore sites developed as part of the PISA project and reported by Burd et al. (2020). A homogeneous Flandrian sand profile is considered with a relative density estimated at 45%, 60%, 75% and 90% corresponding to an initial void ratio e_0 of 0.741, 0.685, 0.629, and 0.573 respectively. The water table is assumed at mudline and the soil profile fully saturated. The small strain shear modulus profile (G_0) is calculated as per equation (2.5) with a submerged unit weight (γ') of 10.09 kN/m^3, an earth pressure coefficient at rest (K_0) of 0.4 and the parameter B reported as 875 for p'_{ref} = 101.3 kPa (Burd et al., 2020).

$$G_0 = \frac{Bp'_{ref}}{0.3 + 0.7{e_0}^2}\sqrt{\frac{p'}{p'_{ref}}} \tag{2.5}$$

The monopile-soil lateral interactions are modelled using the PISA rule-based approach with depth variation parameters as reported by Burd et al. (2020). The 1-D finite element model is implemented in an in-house software.

2.3.1.2 Pile geometry

The monopile outside diameter (D) and wall thickness (t) are assumed as 9 m and 80 mm, respectively. The pile embedded length is initially set as 30 m. These monopile dimensions are representative of offshore wind turbine foundations. Geometrical and steel parameters are summarised in Table 2-2.

Table 2-2. Monopile geometry and steel parameters

D [m]	L [m]	t [mm]	E [GPa]	ν [-]
9	30	80	210	0.3

2.3.1.3 Cyclic load histories

In order to assess the impact of load history on the results, four separate cyclic load histories are considered, reported in Table 2-3. The first three load histories are modified from the 35h storm event and North Sea hindcast data reported by Bachynski et al. (2019) for a generic 10 MW turbine. The irregular load time histories were simplified into regular cyclic load packets, each of constant load amplitude, through rainflow counting. Assuming a wave dominated loading scenario, a constant load eccentricity (ratio of mudline overturning moment to lateral load, e = M/H) of 30 m equal to the water depth is used as reported in Page et al. (2021). The 4th cyclic load history is shown in Table 3. A constant load eccentricity e = 40 m was assumed.

Table 2-3. Cyclic load histories 1-3, modified after Page et al. (2021).

Cases 1 to 3				Case 1	Case 2	Case3
Load Packet	Number of Cycles	$e=M/H$ [m]	H_{max} [MN]	$\zeta_b=H_{min}/H_{max}$ [-]		
1	27,748	30	1.02	0	-0.7	0
2	9,413	30	3.06	0	-0.7	-0.51
3	6,340	30	4.76	0	-0.7	-0.71
4	2,560	30	6.80	0	-0.7	-0.81
5	1,055	30	9.52	0	-0.7	-0.88
6	94	30	13.60	0	-0.7	-0.89
7	4	30	16.32	0	-0.7	-0.88
8	1	30	19.38	0	-0.7	-0.85

Table 2-4. Cyclic load history case 4.

Load Packet	Number of Cycles	$e=M/H$ [m]	H_{max} [MN]	H_{min} [MN]
1	70,839	40	4.91	4.78
2	2,107	40	5.17	3.45
3	2,066	40	5.96	1.77
4	792	40	5.98	-2.19
5	3,286	40	5.98	2.99
6	1,629	40	6.06	-0.83
7	715	40	6.06	-3.09
8	2,553	40	6.29	0.87
9	666	40	6.31	-3.97
10	528	40	6.84	-5.07
11	233	40	7.41	-5.67
12	158	40	8.01	-6.11
13	184	40	8.55	-6.63
14	91	40	9.25	-7.43
15	29	40	10.20	-8.80
16	35	40	10.24	-7.79
17	11	40	11.76	-9.99
18	17	40	11.96	-8.22
19	5	40	12.97	-11.77
20	1	40	13.37	-9.40

2.3.2 Cyclic accumulation model considered

The cyclic accumulation models developed by Hettler (1981), Leblanc (2010a), Puech & Garnier (2017) and Klinkvort & Hededal (2013) are considered. A summary of their respective formulation and input parameters is provided in Table 4. Each model predicts the cyclic rotation (θ_{cyclic}) as a function of the static rotation (θ_{static}) and the number of cycles (N).

The rate of accumulation is constant (t = 0.22) for Hettler (1981) whereas Leblanc (2010a), Puech & Garnier (2017) and Klinkvort & Hededal (2013) account for the cyclic loading characteristics (ζ_b and ζ_c) as defined in equation (2.6). The evolution of parameters T_b and T_c for Leblanc (2010a) is reported in Figure 2-9. In addition, Puech & Garnier (2017) also accounts for the relative pile stiffness through the rigidity coefficient CR defined in equation (2.7) where $(EI)_{ref}$ is the actual bending stiffness of the monopile and $(EI)_{fl}$ is the limit stiffness for the pile flexible behaviour.

$$\zeta_c = \frac{M_{min}}{M_{max}} = \frac{H_{min}}{H_{max}} \quad \& \quad \zeta_b = \frac{M_{max}}{M_R} = \frac{H_{max}}{H_R} \tag{2.6}$$

$$CR = \sqrt[5]{\frac{(EI)_{ref}}{(EI)_{fl}}} \tag{2.7}$$

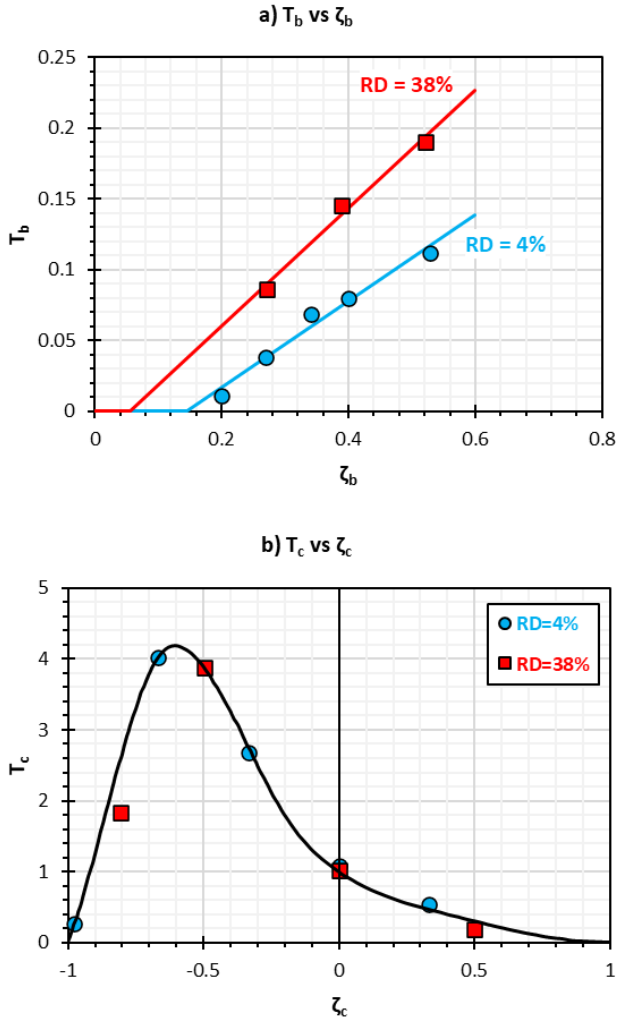

Figure 2-9. Functions relating (a) T_b and (b) T_c to relative density and cyclic loading characteristics ζ_b and ζ_c after Leblanc et al. (2010).

2.3.3 Example base case

In order to highlight the effect of the superposition method in detail, an example base case is first discussed before more general cases are introduced. For this base case, storm load history 1 is used (1-way loading, ζ_c=0) and a relative density of 75% is assumed.

2.3.3.1 Base case monopile monotonic response

The monopile monotonic response is a key input to each cyclic model and is reported in Figure 2-10 in terms of load-displacement and moment-rotation curves at mudline.

Particularly, the ultimate capacity of the monopile is used as a reference load to determine the rate of accumulation in the cyclic models by Leblanc et al. (2010a) and Klinkvort & Hededal (2013), and by Puech & Garnier (2017) to calculate the stiffness limit of flexible behaviour. For Klinkvort & Hededal (2013), H_R and M_R are defined at a mudline rotation of 4 degrees. The same limit is used by Leblanc et al. (2010a) but it applies to the

mudline rotation normalised by the vertical effective stress at pile toe (where the normalised rotation noted $\tilde{\theta}$ is calculated as $\theta\sqrt{\frac{p_a}{L\gamma'}}$). Both criteria are shown in Figure 2-10b.

As shown in Figure 2-10a, Puech & Garnier (2017) defines the ultimate capacity as $H_{lim} = 2H(y=D/2)-H(y=D)$. H_{lim} is required to calculate the stiffness limit for the pile flexible behaviour. This is done by plotting the mudline displacement under H_{lim} as a function of the pile bending stiffness (see Figure 2-11). As per Puech & Garnier (2017), (i) on the left-hand-side of Figure 2-11, the mudline displacement is proportional to the pile bending stiffness and hence the pile is considered flexible while (ii) on the right-hand-side of Figure 2-11, the pile is rigid and the response is driven by the soil stiffness which remains constant. For this case study, the limit stiffness of the flexible behaviour $(EI)_{fl}$ is found as $0.036(EI)_{ref}$, leading to *CR* equal to 1.94.

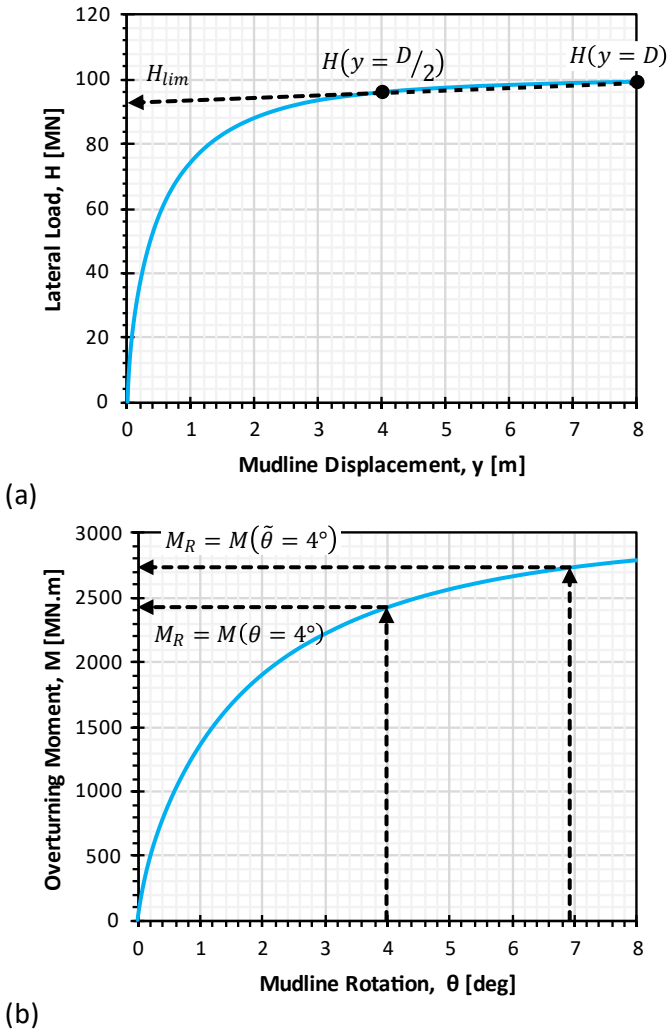

Figure 2-10. Monopile monotonic response in terms of (a) load-displacement and (b) moment-rotation curves at mudline presenting the definition of the reference load for each model.

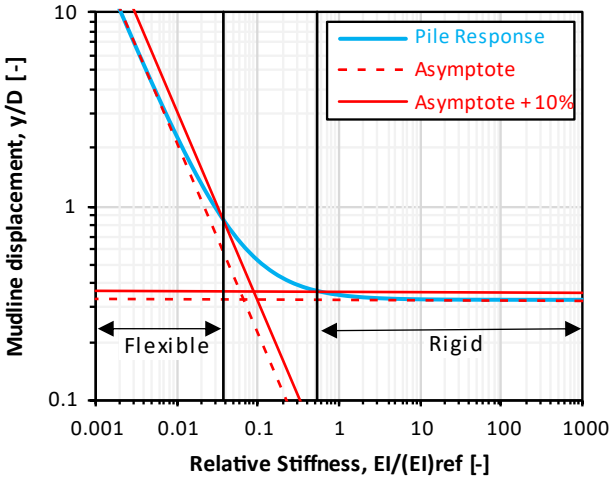

Figure 2-11. Calculation of the limit stiffness of the pile flexible behaviour for the definition of the rigidity coefficient for the Puech & Garnuer (2017) displacement accumulation model.

2.3.3.2 Base case comparison of monopile cyclic responses

The base case monopile cyclic response (for the initial geometry provided in Table 2-2) is calculated using the 4 different cyclic accumulation models presented in Table 4. For each model, the calculation is repeated based on 4 different superposition models as presented in section 2.2. The results are summarised in Figure 2-12 where the mudline cyclic rotation accumulated at the end of the storm event is plotted for each model. Taking the new superposition model suggested in this chapter as the reference, it is found that the "EA-Pfahle" superposition model was seen to predict up to 13% less cyclic rotation irrespective of the cyclic model considered. On the contrary, the "Leblanc" superposition model predicted up to 11% larger cyclic rotations. The "Page" superposition model resulted in slightly larger predicted cyclic rotations to the new model, with differences of up to 8%.

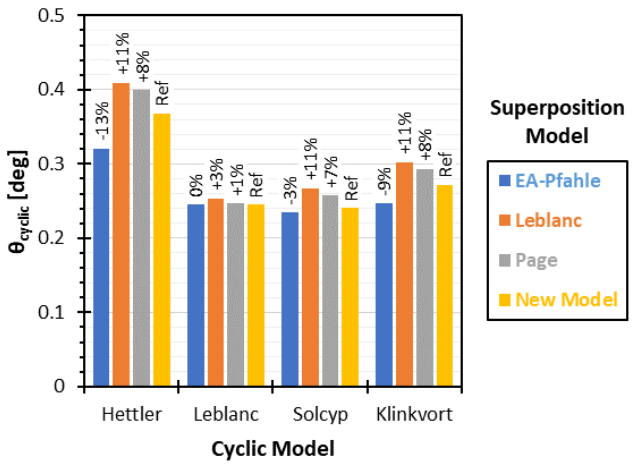

Figure 2-12. Summary of base case cyclic response for each cyclic and superposition model.

2.3.3.3 Base case comparison of required pile penetration

To assess the impact of the four different superposition models on the estimation of permanent rotation and monopile design, the base case study is extended by repeating the calculation for a range of pile embedded lengths. This is in line with the procedure typically taken by offshore geotechnical engineers for the optimisation of the monopile penetration. Since the limit imposed by DNV applies to the permanent rotation, unloading based on the monotonic initial stiffness is assumed at the end of the storm event. The obtained accumulated permanent rotation is plotted in Figure 2-13 as a function of the embedded length for each combination of cyclic and superposition models. The different combinations lead to a broad range of predictions. As expected, the accumulated permanent rotation reduces as the pile embedded length increases until reaching a plateau. The optimal pile penetration is obtained when the accumulated permanent rotation reaches the allowable limit. The limit on the accumulated permanent rotation at mudline is typically set at 0.5 degrees but may vary depending on project-specific requirements (DNV, 2021). For this base case study, the limit for in-place accumulation is arbitrarily set to 0.25 degrees (allowing for 0.25 degrees for installation tolerance).

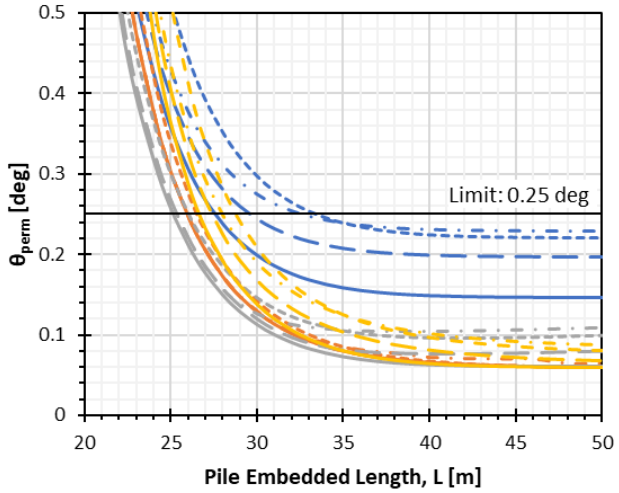

Superposition Model	Cyclic Model			
	Hettler	Leblanc	Solcyp	Klinkvort
EA-Pfahle				
Leblanc				
Page				
New Model				

Figure 2-13. Evolution of permanent rotation accumulated at the end of the storm event as a function of pile embedded length for each combination of cyclic and superposition models.

The required pile embedded lengths for the base case study using each combination of cyclic and superposition models are presented in Figure 2-14. Figure 2-14a highlights the effect of the superposition model for each cyclic model. Taking the new superposition model

suggested in this chapter as the reference, it is found that whatever cyclic model is considered, the "EA-Pfahle" superposition leads to shorter required pile lengths when compared to the new superposition model. The required pile penetration is up to 2 m shorter for the base case. As shown in Figure 2-13, the evolution of accumulated permanent rotation with pile embedded length is highly nonlinear and even a small change in pile embedded length may lead to large changes in accumulated permanent rotation. On the contrary, the "Leblanc" superposition model leads to longer required pile lengths, ranging from 0.6 m to 3.8 m depending on the cyclic model considered. The "Page" superposition model tends to predict either equal or longer pile lengths, depending on the cyclic model chosen.

Figure 2-14b presents the same results but highlights the effect of the cyclic model instead. Although discussing the difference between the different cyclic models is outside of the scope of this chapter, it is worth noticing that the variation in required pile embedded length from one cyclic model to another is similar to the variation due to the superposition model. Indeed, the 4 different cyclic models considered in this case study led to a variation of 2.4 m to 7.4 m depending on the superposition model considered. It is shown in Figure 2-14a that the superposition model leads to a variation of up to 5.8 m. It can therefore be concluded that in certain cases the choice of superposition model can be of equal importance to the cyclic model.

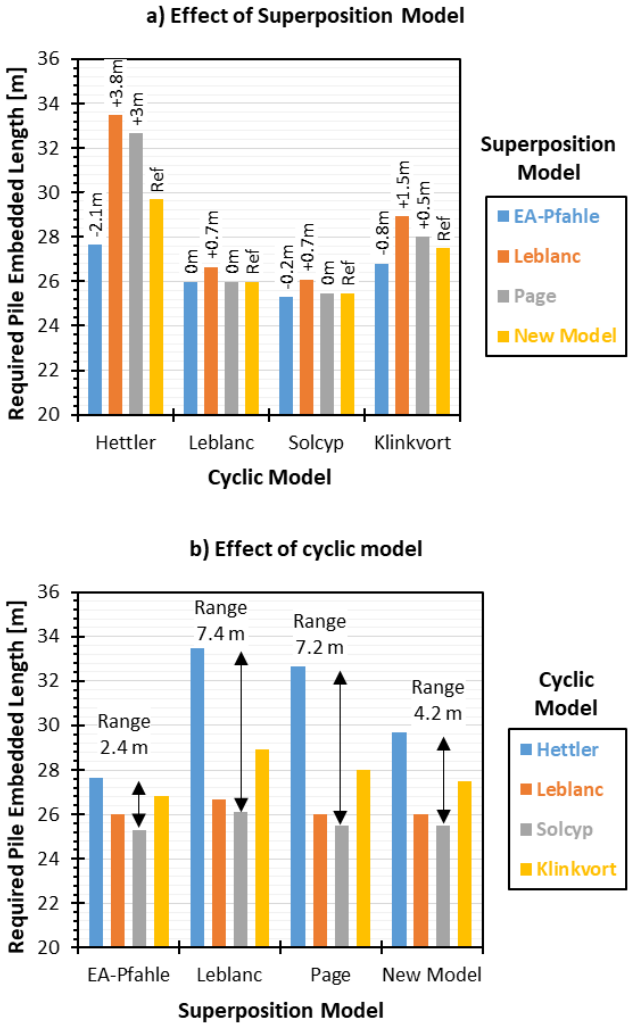

Figure 2-14. Summary of the pile penetration check for each combination of cyclic and superposition models highlighting (a) the effect of the superposition model and (b) the effect of the cyclic model.

2.3.4 Analyses of generalised cases

In order to assess the effect of the superposition model more generally, four separate cyclic load histories and four separate relative densities were analysed.

2.3.4.1 Analyses using different cyclic loading histories

Four separate cyclic load histories were analysed as detailed in Tables 2 and 3. The results considering a pile embedment length of 30 m in a homogenous soil profile with a relative density of 75% are presented in Figure 2-15. The permanent rotations, θ_{perm}, are compared for a range of cyclic models and superposition models. The permanent rotations for a static model are calculated by loading along the static (monotonic) curve and linearly unloading along the line of initial stiffness ($\Delta\theta_{cyclic} = 0$). The static model is included for comparison to show where the effect of load cycling (and therefore superposition model) is small. Overall, the trend for each load history is similar to what was observed for the base case. For

1-way loading (cyclic history 1), the "Page" superposition model tends to give slightly higher accumulated rotations compared with the new model, but both fall in the midway range between the "Hettler" and upper-bound "Leblanc" superposition models. For 2-way loading (cyclic histories 2-4), the "Page" superposition model and the new superposition model gave broadly similar results, falling between the lower-bound "Hettler" and upper-bound "Leblanc" superposition models.

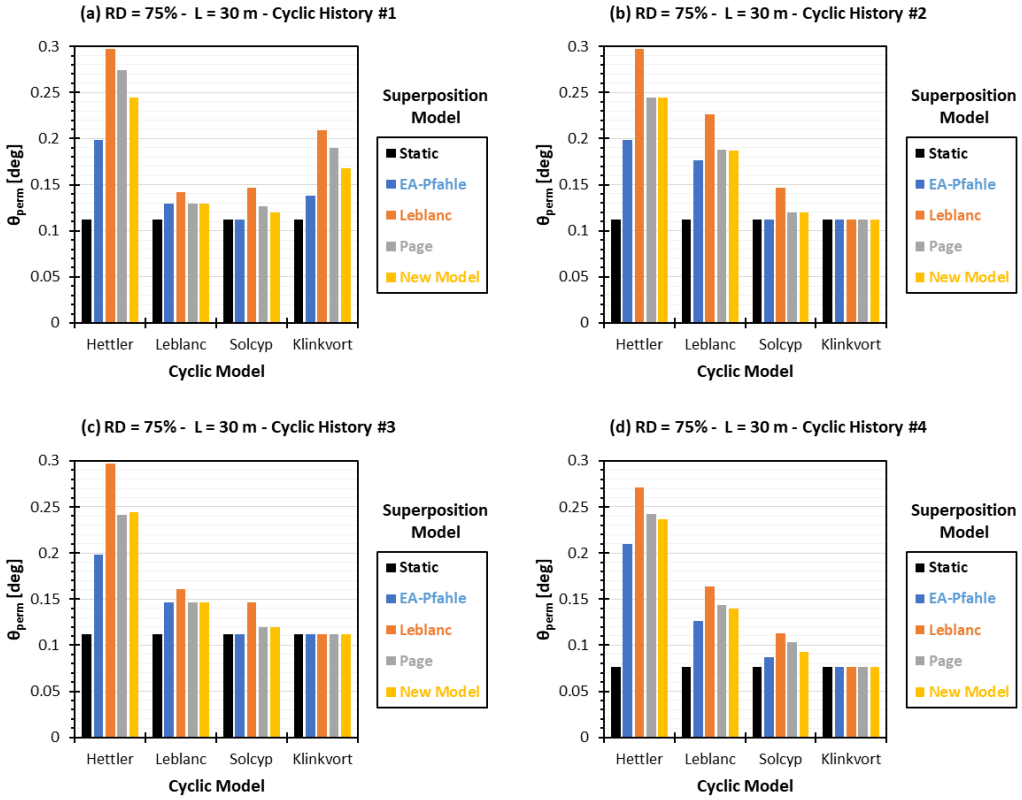

Figure 2-15. Sensitivity to cyclic load history.

2.3.4.2 Analyses using different relative densities

Four separate homogenous soil profiles were analysed with relative densities from 45 – 90% using cyclic load history 1 (1-way cyclic loading) and considering a pile embedment length of 30m. The results are presented in Figure 2-16. The same trends are noted where the effect of the superposition model is of equal importance to the cyclic accumulation model. The "Page" and new superposition models provide similar accumulated rotations with the page model predicting slightly higher accumulated rotations for the 1-way cyclic loading history.

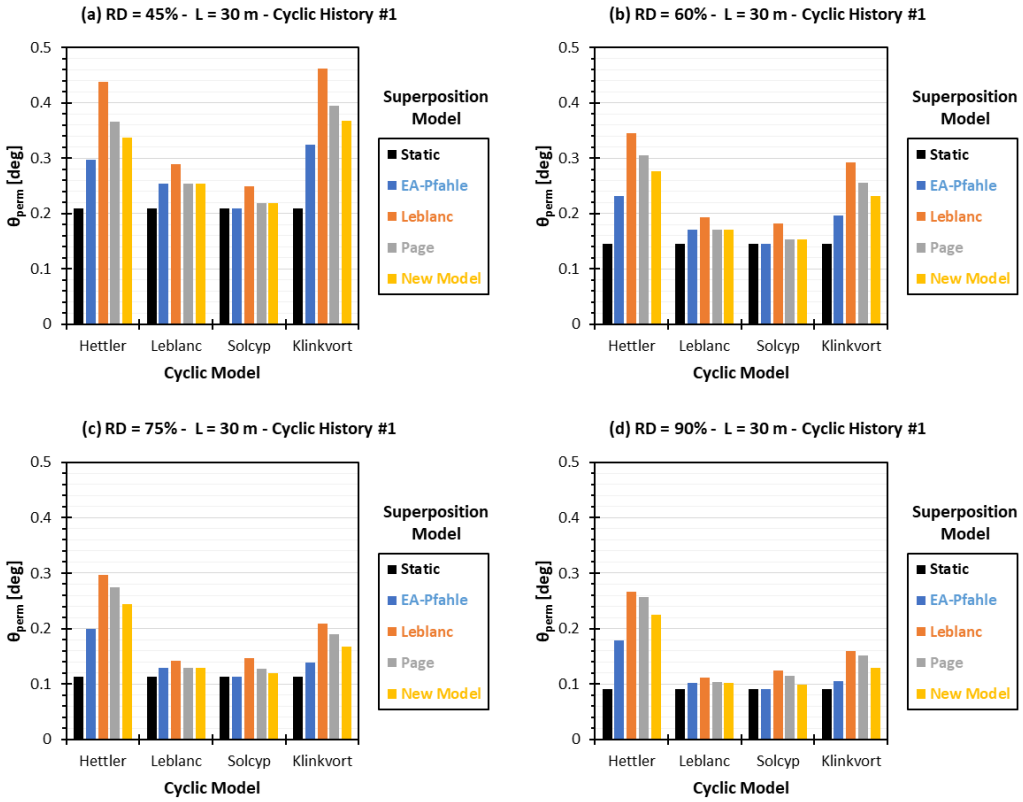

Figure 2-16. Sensitivity to relative density.

2.4 DISCUSSION

Through an example case study, the chapter demonstrated the importance of the superposition model on the prediction of monopile response under cyclic loading. It was shown that the choice of superposition model can significantly affect the predicted response. Some observations are as follows:

The "EA-Pfahle" superposition model suggested in DGGT (2013) systematically leads to lower accumulated rotation in comparison to the new superposition model recommended in this chapter. It was shown that the model assumes an unrealistically stiff reloading stiffness from one load package to another. The model considers constant monopile mudline displacement or rotation for each load increase. This assumption leads the "EA-Pfahle" superposition model to predict a relatively low accumulation of rotation upon cyclic loading since the monopile can recover entirely from the previous load history if the loads of the next load package are sufficiently larger than the previous load package.

The "Leblanc" superposition model suggested by Leblanc et al. (2010b) systematically leads to larger accumulated rotation in comparison to the new superposition model recommended in this chapter. The "Leblanc" superposition model (presented in section 2.2.2) was shown to assume a reloading stiffness equal to the virgin monotonic stiffness. This assumption leads the "Leblanc" superposition model to predict a relatively large

accumulation of rotation upon cyclic loading since the monopile cannot recover at all from the previous load history even if the loads are significantly larger.

Both the "Page" superposition model and the new superposition model suggested in this chapter as presented in section 2.2.3) lead to the prediction of accumulated rotation within the range of "EA-Pfahle" and "Leblanc" superposition models.

The analysis undertaken shows that the permanent accumulated rotation is sensitive to the choice of superposition model and in certain cases, the choice of superposition model can be of equal importance to the choice of cyclic accumulation model.

2.5 CONCLUSION

Predicting the permanent accumulated rotation under cyclic loading is a key requirement for offshore wind turbine foundation design. Semi-empirical cyclic macro-models, such as those proposed by Hettler (1981), Puech & Garnier, (2017), Leblanc et al. (2010a) and Klinkvort & Hededal (2013) can be conveniently used due to their simplicity, especially at early stages of design.

This chapter presented a framework for the application of such cyclic accumulation models, highlighting the importance of the superposition model. The superposition model allows computation of the monopile response to multi-amplitude cyclic loading. While many studies investigate the impact of the cyclic accumulation model, the impact of the superposition model is often overlooked. A new superposition model was proposed and compared with three existing superposition approaches described in the literature. This new model is found to be in good agreement with limited available experimental data (only the superposition from packages 4 to 5 for PISA test DM4 is presented). This new superposition model is empirical and was defined to offer a good match with the PISA field tests in sand. Additional experimental data are required to validate the proposed model.

The effect of the superposition model on monopile cyclic response and design was demonstrated through case studies covering a range of relative densities and loading conditions and the results show that the choice of superposition model can be of equal importance to the choice of cyclic accumulation model.

(intentionally left blank)

Chapter 3: Field lateral load tests on monopiles in dense sand at Blessington – Part 1 – Monotonic loading

This chapter is the first of two presenting the results from a recent pile lateral field-testing campaign carried out in dense sand at the Blessington test site, located approximately 25 km southwest of Dublin, Ireland. This experimental campaign aims to bridge the gap between the field test data available in the literature and current monopile design practices in the offshore wind industry. Previous lateral load monopile field tests reported in the literature have focused on piles with a slenderness ratio (L/D, where L is the embedded length of the pile and D is the external diameter) close to 6 which were representatives of monopile design practice at that time. However, large diameter monopiles are now typically designed with L/D closer to 3. Hence, this new experimental campaign considered pile slenderness ratios ranging from 2.2 to 4.4. The ground-level responses to both monotonic and cyclic lateral loading of 6 piles with an outer diameter of 457 mm are reported over the two chapters. This first chapter focuses on the monotonic response and comparisons to predictions which were required to plan the tests and size the loading system. Predictions made using a number of different approaches show the importance of the choice of design method for capturing the monotonic response. Blind predictions based on three-dimensional finite-element analyses, where all soil constitutive model parameters were derived from Cone Penetration Test (CPT) correlations, provided an excellent match with the experimental results.

3.1 SITE CONDITIONS

The Blessington test site is located in an active quarry, approximately 25 km southwest of Dublin, Ireland. The site has been used as a Geotechnical test site for piled foundation research for the past 20 years. The quarry had previously been divided into two research sites:

- Site 1 (previously referred to as the upper quarry) where axial pile research was performed by Igoe et al. (2010), Gavin et al. (2013), Gavin and Igoe (2020), Igoe and

Gavin (2021), and lateral pile research performed by Li et al. (2015), Prendergast and Igoe (2022)

- Site 2 (previously referred to as the lower quarry) where lateral pile research was performed by Doherty et al. (2015), Murphy et al. (2018), Igoe and Jalilvand (2020).

Igoe and Gavin (2020) provided a comprehensive overview of the geotechnical ground conditions at the site for Blessington Sites 1 & 2. Due to space restrictions at the previous sites, a new area of the quarry was used for the pile testing in this Chapter, referred to as Site 3. Site 3 is located approximately 100 m from site 1 and is several metres higher in elevation compared with site 1 (see Figure 3-1). Cone Penetration Testing (CPT) was undertaken at each desired pile location to ascertain site-specific conditions. Near the location of the lateral pile testing, a preliminary trial pit had identified the presence of 1 m of topsoil at the location, underlain by dense sand. For this reason, before CPT testing was undertaken, the top 1 m of soil was removed with an excavator to form the lateral pile test pit. The CPT locations with respect to the pit boundary are presented in Figure 3-2 for reference.

Figure 3-1. Site 3 location at Blessington

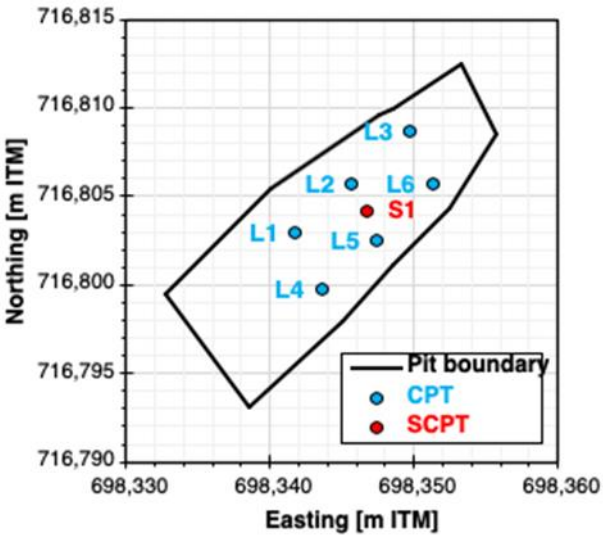

Figure 3-2. Cone Penetration Testing locations and lateral pile test pit boundary.

The results of the in-situ testing are presented in Figure 3-3. Seven CPTs were performed within the lateral pile test pit along with small strain shear modulus, G_0, determined from shear wave velocities measured from a seismic CPT test (SCPT01) and Multi-channel Analysis of Surface Waves (MASW). The CPT results confirm the homogeneity of the site with minimum lateral and vertical soil variation. Cone tip resistances (q_c) generally range from 10 MPa to 15 MPa, increasing with depth. Friction ratios (f_s/q_c) are found to be in the range of 1 % to 3 %. CPT correlations (provided in Table 3-3) indicated a sand relative density between 60 – 75% below 0.5 m depth. Significant differences were noted between the G_0 (determined from shear wave velocities) from the vertically propagating shear wave from CPT (S01) and the horizontally propagating shear wave from MASW. Long et al. (2023) suggested this difference may be a result of the anisotropy of the over-consolidated deposit. Estimation of G_0 from CPT tip resistance using correlations from Schnaid and Yu (2007) (see Table 3-3) matches better with the MASW when compared to the seismic CPT results and is used in subsequent analysis.

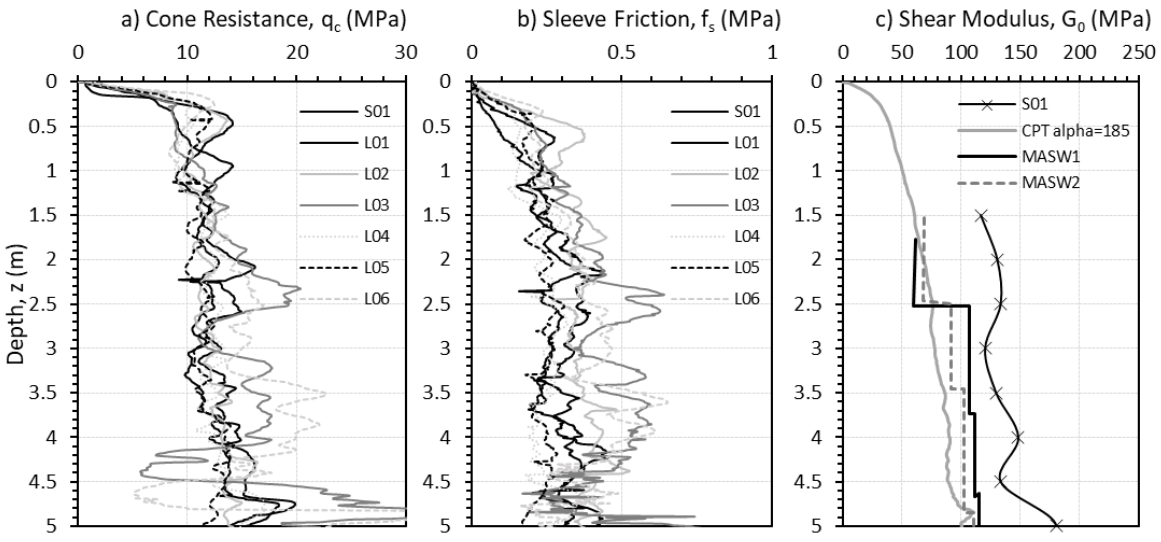

Figure 3-3. (a) CPT cone resistance, (b) CPT sleeve friction and (c) Seismic CPT and MASW from Blessington Site 3.

The water table is estimated to be >10m below ground level with the result that the sand in which the test pile was embedded is partially saturated. Similarly to the PISA field tests carried in Dunkirk marine dense sand, the suction caused by the partial saturation can act as an apparent cohesion (Taborda et al., 2020). However, this was not explicitly capture in the following analyses. The moisture content of the deposit is seen to range from approximately 8 - 15%. Laboratory testing was used to supplement the in-situ site investigation and establish basic soil properties. Particle size analyses classified the material as fine-grained, with a median particle size varying from 0.1 - 0.15 mm. The particle size distribution indicated a D_{60} of 0.18mm, a D_{10} of 0.07mm and a uniformity coefficient of 2.80

from an average of 8 samples. The fines content varied between 2 – 7% with a mean value of 5.05%. The specific gravity of the solid particles was measured at 2.675. Maximum density tests indicated a maximum bulk density of 2081.9 kg/m^3 at a moisture content of 18% and a maximum dry density of 1769.5 kg/m^3 averaged from 3 samples. The minimum dry density was measured at 1351.3 kg/m3 resulting in a minimum void ratio of 0.492 and a maximum void ratio of 0.980. Triaxial testing on reconstituted samples of Blessington Site 3 sand were carefully prepared at a relative density of 60%. The peak friction angle from 3 tests at confining pressures of 25, 50 and 100 kPa are shown in Figure 3-4. The measured peak friction angles are compared with those estimated from CPT correlations suggested by Bolton (1986) and as shown in Table 3-3.

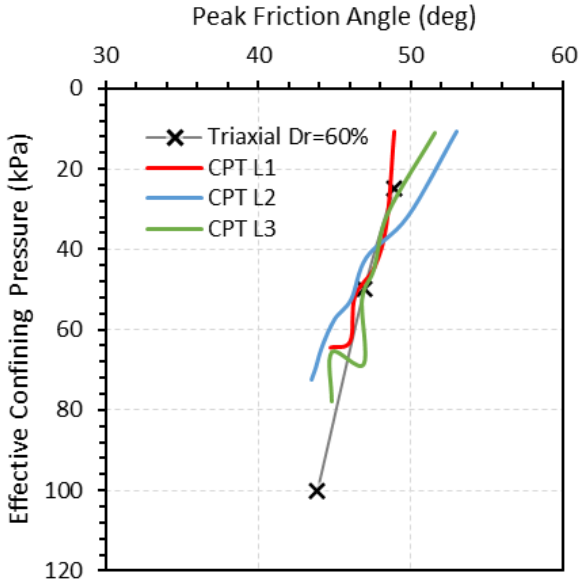

Figure 3-4. Peak friction angle for Blessington site 3.

3.2 TEST PROGRAM

3.2.1 Pile installation

A total of 6 piles were installed at CPT locations shown in Figure 3-5. All piles have an external diameter (D) of 457 mm and a wall thickness of 6.35 mm. The total lengths of the piles are in the range of 2.5 m to 3.5 m. Allowing for sufficient stick-up length, the piles are installed with embedded lengths (L) ranging from 1 m to 2 m (L/D ranging from 2.2 to 4.4). A summary of piles geometry is provided in Table 3-1.

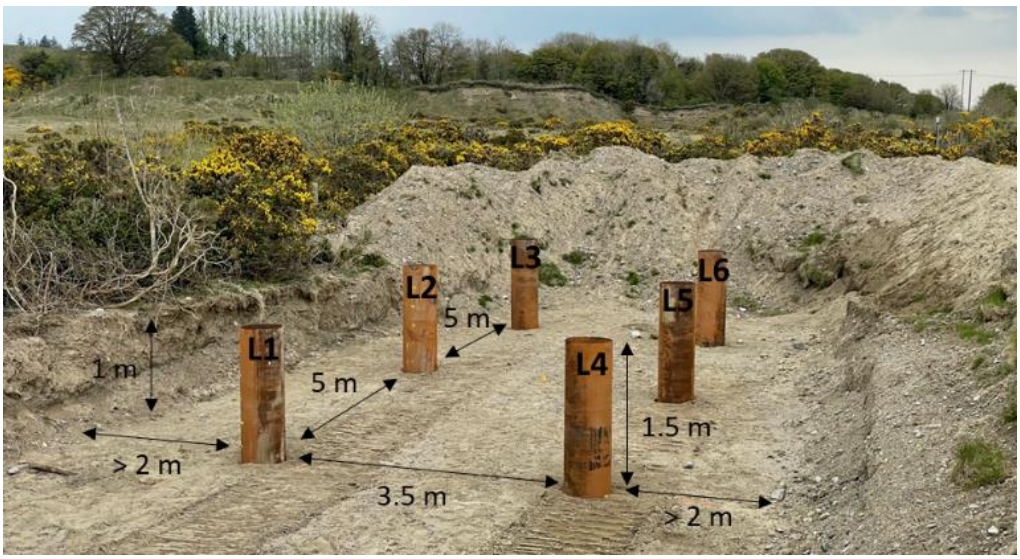

Figure 3-5. Overview of piles arrangement in lateral pile test pit.

Table 3-1. Summary of piles geometry.

Pile	L_{tot} [m]	D [m]	L [m]	L/D [-]	t [mm]
L1	2.5	0.457	1.0	2.2	6.35
L2	3.5	0.457	2.0	3.3	6.35
L3	3.0	0.457	1.5	4.4	6.35
L4	3.0	0.457	1.5	3.3	6.35
L5	3.5	0.457	2.0	4.4	6.35
L6	2.5	0.457	1.0	2.2	6.35

The piles were impact-driven into the ground using a Junttan 4-tonne piling hammer as shown in Figure 3-6. The blow count for each pile during installation is shown in Figure 3-7. The piles are installed in a 3x2 grid with the longer piles installed at the centre as shown in Figure 3-5 and Figure 3-8. Piles are installed 3.5 m to 5 m apart to avoid interaction effects. The piles are installed at least at a distance of 2 m from the pit boundary to avoid the effects of the additional overburden and the direction of loading between piles was chosen to minimize these effects. A stick-up length of 1.5 m is left out to ensure the lateral load can be applied with sufficient eccentricity to be representative of offshore conditions. The loads are applied at an eccentricity of 1.37 m (3 times the pile external diameter).

Figure 3-6. Pile installation.

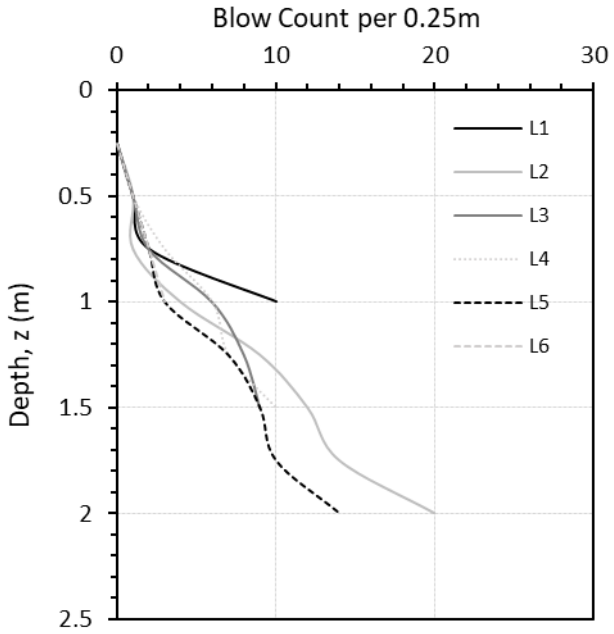

Figure 3-7. Blows count during pile installation.

3.2.2 Testing plan

Each test consists of two piles with tension lateral load applied between them. The longer piles with an L/D = 4.4 (L2 and L5) are used as reaction piles to test the shorter piles. The test campaign consisted of 5 tests (see Figure 3-8):

- Test 1: Monotonic test between L6 (L/D = 2.2) and L5 (L/D = 4.4)
- Test 2: Monotonic test between L4 (L/D = 3.3) and L5 (L/D = 4.4)
- Test 3: Cyclic test followed by monotonic pushover between L3 (L/D = 3.3) and L2 (L/D = 4.4)
- Test 4: Cyclic test followed by monotonic pushover between L1 (L/D = 2.2) and L2 (L/D = 4.4)
- Test 5: Cyclic test followed by monotonic pushover between L2 (L/D = 4.4) and L5 (L/D = 4.4)

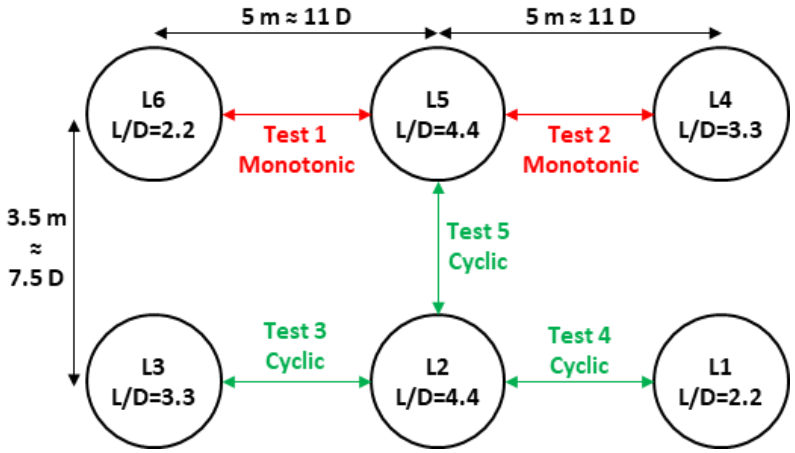

Figure 3-8. Summary of testing plan (not to scale).

The monotonic tests consist of a monotonic lateral pushover of the piles until failure (ground-level displacement of D/10) of the tested piles. A small number of unloading-reloading loops are applied at small displacements to capture the unloading-reloading stiffness and ensure all instrumentations are working correctly.

During the cyclic tests, it is targeted to apply 1,000 one-way cycles at 4 different load levels for a total of 4,000 cycles before application of a final monotonic lateral pushover. The load levels are targeted at 10%, 20%, 30% and 40% of the predicted ultimate capacity. Due to the partial factors included in the design, monopiles are typically only subjected to cyclic loads less than about 60% of their ultimate capacity with only a few cycles applied at the largest amplitude. A cyclic load period of 8 seconds was used in the tests as this was deemed representative of offshore conditions (wave loading typically close to 10 s). The

load period is slightly reduced compared to the expected offshore conditions to allow for up to 4,000 cycles to be completed in a working day.

3.2.3 Instrumentation

During each test, both the reaction and test piles were instrumented with inclinometers (SEIKA N2) and linear potentiometric position transducers (Novotechnik TR-0050) at ground level, as shown in Figure 3-9. The inclinometers were directly glued to each side of each pile. The LVDTs were mounted on reference frames.

The lateral load was applied with a hydraulic jack at 1.37 m above ground level (eccentricity equals 3 times the pile external diameter) and measured with a tension load cell (ETW-12t-015-000). The control unit and the pump apply the pressure to the hydraulic jack. The role of the custom-made control unit is essential for the application of thousands of cycles. Although the hydraulic jack was rated for 900 bar, the cyclic loading pump was only rated up to 200 bar which limits the cyclic lateral loads to about 30 kN. A hand pump is used for the monotonic test up to 135 kN. All instrumentations were connected to a Campbell scientific CR9000x datalogger recording 10 readings per second on all instruments. All measurements were observed in real-time to ensure all instruments were working correctly.

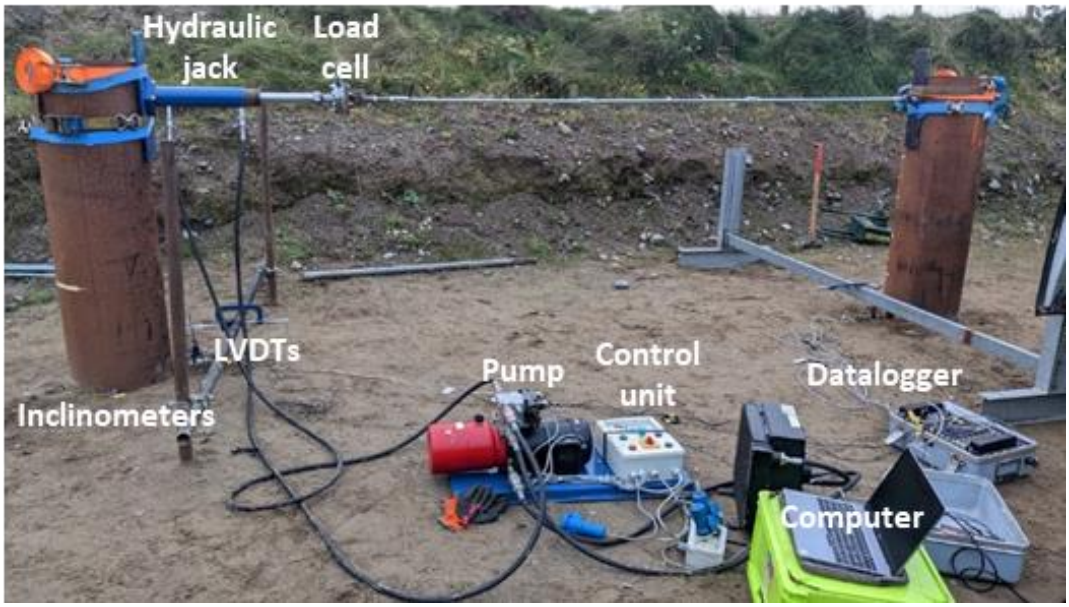

Figure 3-9. Overview of pile instrumentation.

3.2.4 Timeline

This experimental campaign took place over a relatively long period due to challenges with the COVID restrictions, the weather conditions, the availability of contractors and technicians, the accessibility of the test site, the occurrences of equipment breakdowns (especially with the hydraulic loading system), and the theft of equipment left overnight. Key dates are summarised below:

- Topsoil excavation: October 18th, 2021
- CPTs: October 19th to 20th 2021
- Pile installation: April 27, 2022
- Pile tests: See Table 3-2.

Table 3-2: Summary of test dates.

Test	Date	Test pile	L [m]	L/D [-]	Reaction pile	Test type
Test 1	10/11/2022	L6	1.0	2.2	L5	Monotonic
Test 2	21/01/2023	L4	2.0	3.3	L5	Monotonic
Test 3	13/06/2023	L3	1.5	4.4	L2	Cyclic + Pushover
Test 4	14/06/2023	L1	2.0	4.4	L2	Cyclic + Pushover
Test 5	15/06/2023	L2	1.0	2.2	L5	Cyclic + Pushover

3.3 BLIND MONOTONIC PREDICTIONS

Blind predictions of the pile response to monotonic lateral loading were required to plan the tests and size the loading system. The blind predictions were undertaken ahead of testing and were based on a number of different approaches including (1) API p-y approach, (2) PISA Rule 1D FE approach, (3) 3D FE using CPT correlations and (4) 3D FE analysis using Plaxis Monopile Designer. The results from the 4 methods are compared to the field lateral loading monotonic response in section 5.

3.3.1 API p-y approach

The traditional approach for modelling the lateral response of offshore piles from the oil and gas industry is referred to as the American Petroleum Institute (API) p-y approach where the pile is modelled as 1D elastic beam elements, and the soil is modelled using non-linear lateral soil reaction curves (referred to as p-y curves). Details are provided in section 1.3.2.1.

3.3.2 PISA rule approach

The PISA design model (Byrne et al. 2020, Burd et al., 2020) represents the current state-of-the-art design methodology for monopiles and is now widely used. Like API, the PISA approach relies on 1DFE analyses. One difference with API is the PISA design model considers other soil reaction components in addition to the distributed lateral load (p-y), namely: the distributed moment as a result of vertical tractions on the pile; the base shear; and the base moment. Details are provided in section 1.3.2.2.1,

3.3.3 3D FE with CPT correlations

The piles were modelled at full scale and half-space using the commercially available package PLAXIS 3D. An example model is presented in Figure 3-10.

The piles were modelled with linear elastic plate elements with Young's modulus of 210 GPa and Poisson's ratio of 0.3. The piles were considered weightless since the focus is on the lateral response. Interfaces were included at the outside and inside of the piles to allow for differential displacements and capture the pile-soil interactions. The piles are assumed wished in place with no effect of the installation taken into account. The lateral load is applied as a prescribed displacement in the y-direction at an eccentricity e = M/H until pile failure (considered to be reached at a ground-level displacement of 10% of the pile diameter).

Table 3-3. Summary of CPT-based correlations proposed by Igoe & Jalilvand (2020) for HS-small input parameters.

Correlations	References
$E_{50}^{ref} = E_{ur}^{ref}/3$	Brinkgreve et al. (2010)
$E_{oed}^{ref} = E_{50}^{ref}$	
$E_{ur}^{ref} = 0.00464 \cdot {E_0^{ref}}^{1.724} \quad (MPa)$ Where $E_0^{ref} = 2(1+\nu)G_0^{ref}$	Modified after Kirsh et al. (2014)
$m = 0.5$	Benz et al. (2009)
$\varphi' = {\varphi'}_{cv} + 3(D_R(10 - \ln {p'}_0) - 1)$	Bolton (1986)
$D_R = \sqrt{\frac{Q_{tn}}{305 \times OCR^{0.15}}}$	Kulhawy & Mayne (1990)
$Q_{tn} = \left(\frac{q_t - \sigma_{v0}}{p_{ref}}\right)\left(\frac{p_{ref}}{{\sigma'}_{v0}}\right)^n$ $n = 0.381 \cdot I_c + 0.05\frac{{\sigma'}_{v0}}{p_{ref}} - 0.15$ $I_c = \sqrt{(3.47 - \log_{10} Q_{tn})^2 + (1.22 + \log_{10} F_r)^2}$ $F_r = \frac{f_s}{q_t - \sigma_{v0}}$	Roberston & Cabal (2014)
$\sin\psi' = \frac{\sin\varphi' - \sin{\varphi'}_{cv}}{1 - \sin\varphi'\sin{\varphi'}_{cv}}$	Brinkgreve et al. (2018)
$G_0 = \alpha\left(q_t \cdot {\sigma'}_{v0} \cdot p_{ref}\right)^{1/3}$	Schnaid and Yu (2007)
$\gamma_{0.7} = 1.5 \cdot 10^{-4}$	Benz et al. (2009)
$G_0^{ref} = G_0\left(\frac{p_{ref}}{K_0^{nc}{\sigma'}_v}\right)^m$	Brinkgreve et al. (2018)
$K_0 = K_{0,NC} \times OCR^{\sin\varphi'}$ $K_{0,NC} = 1 - sin\,\varphi'$	Mayne & Kulhawy (1982)
$OCR = \left(\frac{1.33{q_t}^{0.22}}{K_{0,NC}{{\sigma'}_{v0}}^{0.31}}\right)^{\frac{1}{\sin\varphi' - 0.27}}$	Mayne (2001)

The soil (sand for this study) is modelled using the hardening soil small-strain stiffness constitutive model. Igoe and Jalilvand (2020) developed an approach to derive all of the required HS-small input parameters from CPT data. All parameter (including small strain shear modulus) were derived from the CPT correlations summarised in Table 3-3. Some of the correlations are interdependent and require iterative computations until convergence. The approach has been calibrated and validated against a database of large-scale field tests

including PISA tests in the Dunkirk marine sand and was shown to offer better predictive accuracy metrics for piles tested in the database than correlations suggested by the Plaxis Monopile Designer manual (Panagoulias et al., 2021). Although the piles are wished in place in the 3D FE analyses, the CPT-based correlations were calibrated for impact-driven piles and account for installation effects intrinsically. Additional discussion on the soil parameters and choice of correlation are provided in Igoe and Jalilvand (2020).

Interfaces were added between the pile and the soil (inside and outside) to allow for differential displacements between the pile and soil elements. Following the recommendations of the Plaxis Monopile Designer manual, additional soil models were created for the interfaces. The stiffness properties of the interfaces were kept similar to the soil, while strength properties were reduced by specifying an interface friction angle of 29 degrees and reducing the dilatancy angle to 0.

A relatively coarse mesh was considered with fine local refinement around the pile as shown in Figure 3-10. This is to ensure accurate predictions and reduced computation time following a mesh sensitivity study. The example shown in Figure 3-10 is for pile L2 and consists of 10,359 10-node tetrahedral elements.

The whole process was automated in PYTHON using the PLAXIS API scripting interface. The automation allows for quick model set-up and results extraction. In addition, it ensures consistency across all the analyses by avoiding human error.

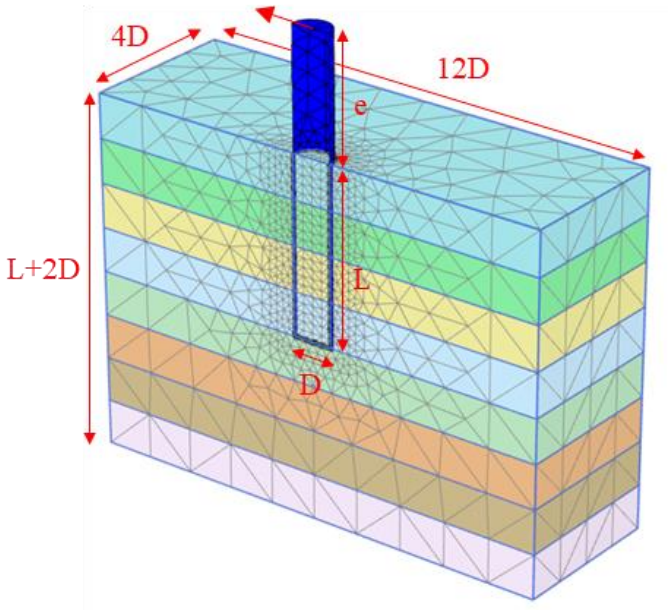

Figure 3-10. Example 3D FEA model in Plaxis 3D.

For reference, the correlated HS-small input parameters for piles L1 to L6 are summarised in Table 3-4 to Table 3-9, respectively. The tables of parameters show high

relatively K_0 values due to large over-consolidation. This was expected as 1-1.5 m of topsoil were excavated and the history of the site as documented in (Igoe and Gavin (2020).

The blind monotonic predictions for all 6 piles are reported in Figure 3-11 in terms of load-displacement response at ground level. The ultimate capacity is defined at a ground-level displacement of 10% of the pile diameter. The predictions suggest ultimate capacities of about 25 kN for the short piles (L1 and L6, L/D = 2.2), 65 kN for the medium piles (L3 and L4, L/D = 3.3), and 140 kN for the long piles (L2 and L5, L/D = 4.4). The blind predictions capture the soil lateral variability. Indeed, piles with the same geometry show different responses: L1, L4 and L5 are softer than L6, L3 and L2, respectively.

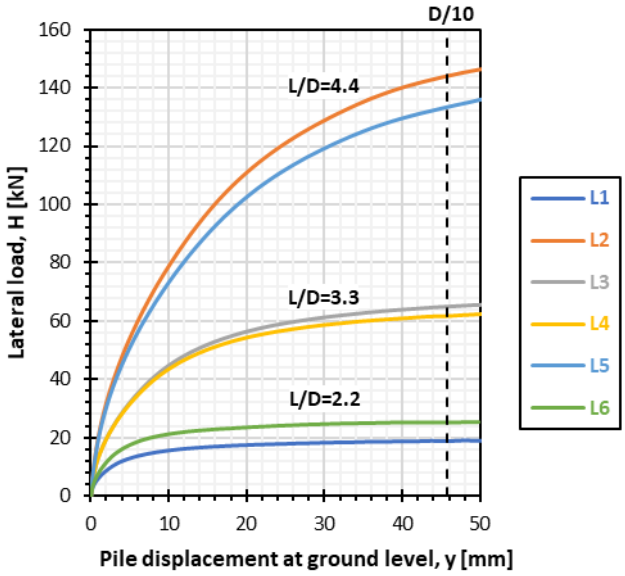

Figure 3-11. Blind predictions for all 6 piles reported in terms of load-displacement response at ground level.

Table 3-4. HS-small soil model parameters for L1.

Z_{top} [mBGL]	Z_{bot} [mBGL]	γ [kN/m^3]	E_{50}^{ref} [MPa]	E_{oed}^{ref} [MPa]	E_{ur}^{ref} [MPa]	m [-]	φ' [deg]	ψ' [deg]	$y_{0.7}$ [-]	G_0^{ref} [MPa]	K_0 [-]
0	0.5	17.8	100.8	100.8	302.5	0.5	48.9	17.3	1.5E-04	247.8	2.4
0.5	1	20.2	102.6	102.6	307.7	0.5	48.4	16.6	1.5E-04	250.3	2.2
1	1.5	20.9	88.8	88.8	266.3	0.5	47.6	15.4	1.5E-04	230.1	1.7
1.5	2	21.1	76.3	76.3	229.0	0.5	46.3	13.6	1.5E-04	210.8	1.4
2	2.5	21.5	76.3	76.3	228.8	0.5	46.0	13.2	1.5E-04	210.7	1.3
2.5	3	21.3	64.0	64.0	192.0	0.5	44.7	11.4	1.5E-04	190.3	1.1

Table 3-5. HS-small soil model parameters for L2.

Z_{top} [mBGL]	Z_{bot} [mBGL]	γ [kN/m^3]	E_{50}^{ref} [MPa]	E_{oed}^{ref} [MPa]	E_{ur}^{ref} [MPa]	m [-]	φ' [deg]	ψ' [deg]	$y_{0.7}$ [-]	G_0^{ref} [MPa]	K_0 [-]
0	0.5	19.3	144.3	144.3	433.0	0.5	53.0	23.4	1.5E-04	305.1	2.2
0.5	1	21.2	103.6	103.6	310.7	0.5	49.8	18.6	1.5E-04	251.7	2.0
1	1.5	21.0	80.0	80.0	240.0	0.5	47.1	14.7	1.5E-04	216.6	1.6
1.5	2	21.4	72.2	72.2	216.7	0.5	46.1	13.4	1.5E-04	204.2	1.4
2	2.5	21.3	64.3	64.3	192.9	0.5	45.0	11.8	1.5E-04	190.8	1.2
2.5	3	21.2	58.8	58.8	176.3	0.5	44.2	10.7	1.5E-04	181.2	1.1
3	3.5	21.3	57.1	57.1	171.3	0.5	43.8	10.1	1.5E-04	178.2	1.0
3.5	4	21.5	56.0	56.0	168.0	0.5	43.5	9.7	1.5E-04	176.2	0.9

Table 3-6. HS-small soil model parameters for L3.

Z_{top} [mBGL]	Z_{bot} [mBGL]	γ [kN/m^3]	E_{50}^{ref} [MPa]	E_{oed}^{ref} [MPa]	E_{ur}^{ref} [MPa]	m [-]	φ' [deg]	ψ' [deg]	$y_{0.7}$ [-]	G_0^{ref} [MPa]	K_0 [-]
0	0.5	19.3	114.2	114.2	342.6	0.5	51.6	21.3	1.5E-04	266.3	2.3
0.5	1	20.7	92	92	276.1	0.5	48.5	16.8	1.5E-04	235.0	2.0
1	1.5	21.1	87.7	87.7	263.2	0.5	47.6	15.4	1.5E-04	228.6	1.7
1.5	2	21.4	81.3	81.3	244.0	0.5	46.8	14.2	1.5E-04	218.7	1.4
2	2.5	21.8	87.5	87.5	262.6	0.5	46.9	14.4	1.5E-04	228.3	1.4
2.5	3	21.7	63.9	63.9	191.8	0.5	44.8	11.5	1.5E-04	190.2	1.1
3	3.5	21.8	67.9	67.9	203.8	0.5	44.8	11.5	1.5E-04	197.1	1.1

Table 3-7. HS-small soil model parameters for L4.

Z_{top} [mBGL]	Z_{bot} [mBGL]	γ [kN/m^3]	E_{50}^{ref} [MPa]	E_{oed}^{ref} [MPa]	E_{ur}^{ref} [MPa]	m [-]	φ' [deg]	ψ' [deg]	$y_{0.7}$ [-]	G_0^{ref} [MPa]	K_0 [-]
0	0.5	19.2	128.3	128.3	385.0	0.5	52.1	22.1	1.5E-04	285.0	2.2
0.5	1	20.2	88.8	88.8	266.3	0.5	47.9	15.8	1.5E-04	230.1	2.0
1	1.5	20.4	78.8	78.8	236.5	0.5	46.5	13.9	1.5E-04	214.8	1.6
1.5	2	20.9	73.7	73.7	221.2	0.5	46.0	13.2	1.5E-04	206.6	1.4
2	2.5	20.9	66.8	66.8	200.4	0.5	45.1	11.9	1.5E-04	195.1	1.2
2.5	3	21.1	63.1	63.1	189.3	0.5	44.6	11.2	1.5E-04	188.8	1.1
3	3.5	21.0	57.3	57.3	171.9	0.5	43.8	10.1	1.5E-04	178.6	1.0

Table 3-8. HS-small soil model parameters for L5.

Z_{top} [mBGL]	Z_{bot} [mBGL]	γ [kN/m^3]	E_{50}^{ref} [MPa]	E_{oed}^{ref} [MPa]	E_{ur}^{ref} [MPa]	m [-]	φ' [deg]	ψ' [deg]	$y_{0.7}$ [-]	G_0^{ref} [MPa]	K_0 [-]
0	0.5	19.2	135.8	135.8	407.3	0.5	52.4	22.5	1.5E-04	294.4	2.2
0.5	1	20.5	97.6	97.6	292.8	0.5	48.7	17	1.5E-04	243.1	2.1
1	1.5	20.8	80.6	80.6	241.8	0.5	46.9	14.5	1.5E-04	217.6	1.6
1.5	2	20.7	67.5	67.5	202.6	0.5	45.5	12.4	1.5E-04	196.4	1.3
2	2.5	20.9	61.9	61.9	185.8	0.5	44.7	11.4	1.5E-04	186.8	1.2
2.5	3	21.0	59.6	59.6	178.9	0.5	44.2	10.7	1.5E-04	182.7	1.1
3	3.5	20.8	53.4	53.4	160.1	0.5	43.4	9.6	1.5E-04	171.3	0.9
3.5	4	20.8	54.2	54.2	162.6	0.5	43.3	9.4	1.5E-04	172.9	0.9

Table 3-9. HS-small soil model parameters for L6.

Z_{top} [mBGL]	Z_{bot} [mBGL]	γ [kN/m^3]	E_{50}^{ref} [MPa]	E_{oed}^{ref} [MPa]	E_{ur}^{ref} [MPa]	m [-]	φ' [deg]	ψ' [deg]	$y_{0.7}$ [-]	G_0^{ref} [MPa]	K_0 [-]
0	0.5	19.8	149.4	149.4	448.2	0.5	54.0	25.0	1.5E-04	311.2	2.1
0.5	1	20.5	86.5	86.5	259.5	0.5	48.1	16.1	1.5E-04	226.7	2.0
1	1.5	20.8	78.5	78.5	235.4	0.5	46.8	14.3	1.5E-04	214.2	1.6
1.5	2	21.3	77.4	77.4	232.1	0.5	46.4	13.8	1.5E-04	212.5	1.4
2	2.5	21.5	78.8	78.8	236.4	0.5	46.2	13.4	1.5E-04	214.8	1.3
2.5	3	21.7	72.4	72.4	217.2	0.5	45.4	12.4	1.5E-04	204.5	1.2

3.3.4 Plaxis monopile designer

In addition to the PISA rule-based approach described previously, the PISA design model included provision for using bespoke 3D FE analysis which could be applied within the PISA framework, referred to as the PISA numerical approach. To facilitate easy implementation in the industry, the Plaxis Monopile Designer software was developed. For piles in sand, the hardening soil with a small-strain stiffness constitutive model is used. The user is required

to input values for the soil unit weight, γ, peak friction angle, ϕ', dilation angle, ψ, small strain shear modulus, G_0, in-situ lateral stress coefficient, K_0 and relative density, D_r. All other parameters are derived through correlations described in the Plaxis Monopile Designer manual (see Panagoulias et al. 2018 for full details). In this Chapter, the main differences between the CPT based 3D FE approach and the Plaxis Monopile Designer approach relate to the reference secant triaxial stiffness, which is calculated as follows:

$$E_{50}{}^{ref} = 60 \times D_r \quad \text{(MPa)} \tag{3.1}$$

In addition, Plaxis Monopile Designer uses $\gamma_{0.7} = 0.0001$ by default (rather than 0.00015 used by the authors), although a sensitivity analysis undertaken by the authors indicates this change will have minimal effect on the load-displacement response. For the predictions using Plaxis Monopile Designer, all the user-defined inputs described above were the same as for the CPT based 3DFE approach with the exception of $\gamma_{0.7}$ and $E_{50}{}^{ref}$ (and consequently $E_{oed}{}^{ref}$ and $E_{ur}{}^{ref}$ as they are dependent).

3.4 RESULTS

Figure 3-12 presents the results of the monotonic tests 1 and 2 for piles L6 (L/D = 2.2), pile L4 (L/D = 3.3) and pile L5 (L/D = 4.4) in terms of load-displacement and load-rotation response at ground level. All the tests were load-controlled. Although the tests were carried to assess the monotonic response of the piles, an unloading-reloading loop was carried at very small displacement to ensure all the equipment was working correctly and capture the small-strain unloading-reloading response. This is not deemed to affect the monotonic response of the piles.

The experimental results are compared to the blind predictions following the approaches presented in section 4. For all piles API p-y approach, PISA Rule and Plaxis monopile designer significantly underpredict both the stiffness and ultimate capacity. The 3DFE approach based on CPT correlations suggested by Igoe et al. (2020) is seen to provide an excellent match with the both ultimate capacity and initial stiffness of the load-displacement and load-rotation responses. None of the approaches predicted the post-peak behaviour showing softening, especially for the shortest pile (Pile L6, L/D = 2.2). Although not explicitly discussed, similar softening is observed in the PISA field test logs in sand for DM5 which was the shorted pile tests with L/D close to 3 (McAdam et al, 2020). This post peak softening seems to be characteristic of short piles which exhibit large toe displacements and require special attention to ensure safe monopile design as slenderness ratio decreases.

Table 3-10 provides a quantitative comparison of measured ultimate capacity for each pile and that predicted using the CPT based 3DFE approach. Relative errors of -1.9 % and

3.7% are observed. Table 3-11 provides a similar comparison for initial stiffness. Relative errors of 4.5% to 8.7% are observed. Ultimate capacity and initial stiffness are defined at a ground level displacement of 10% and 0.1% of the pile external diameter, respectively. This comparison demonstrates the accuracy of the approach recently developed by Igoe and Jalilvand (2020). Although the approach has been calibrated based on a database of field tests with larger slenderness ratios, it captures both the strength and stiffness of these shorter piles.

Table 3-10. Comparison of predicted and experimental monotonic ultimate capacities (at D/10).

Pile	L/D [-]	Ultimate capacity [kN]		Relative error [%]
		Predicted	Experimental	
L6	2.2	25.0	25.5	- 1.9
L4	3.3	61.8	59.5	+ 3.7
L5	4.4	133.4	-	-

Table 3-11. Comparison of predicted and experimental monotonic initial stiffness (at D/1000).

Pile	L/D [-]	Initial stiffness [kN/mm]		Relative error [%]
		Predicted	Experimental	
L6	2.2	11.3	10.7	L6
L4	3.3	18.6	17.1	L4
L5	4.4	25.5	24.4	L5

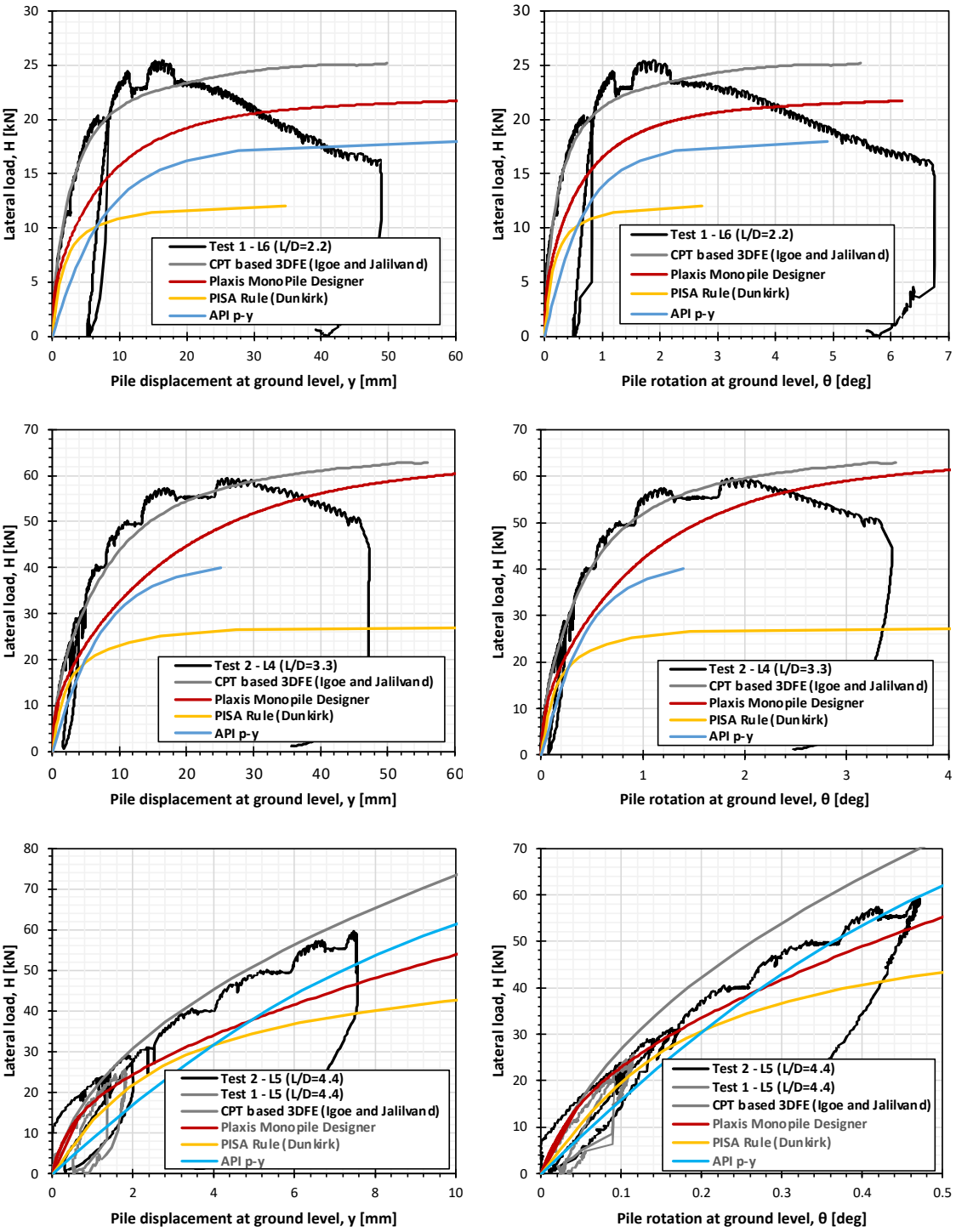

Figure 3-12. Results of monotonic tests 1 and 2 in terms of load-displacement response (a, c and e) and load-rotation response (b, d and f) at ground level for piles L6 (L/D = 2.2) (a and b), pile L4 (L/D = 3.3) (c and d) and pile L5 (L/D = 4.4) (e and f). Experimental responses are compared to predicted responses.

Upon completion of the monotonic tests, significant gap formation was noticed between the pile and the soil at the back of the pile (with respect to the loading direction) as shown on Figure 3-13. The depth of gapping was measured at about 2/3 of the pile penetration, in line with the expected rotation point depth. The soil cracks observed at the back of the pile on Figure 3-13 suggest a wedge failure mechanism, as expected, with the

soil heaving as the pile is rotating. The longer pile (L4) shows less cracks than the shorter one (L6).

Figure 3-13. Example of gaping and soil cracks after completion of the monotonic tests for L6 (L/D=2.2) and L4 (L/D = 3.3).

3.5 CONCLUSION

This chapter presents the results of a recent pile lateral field-testing campaign carried out in dense sand at the Blessington test site, located approximately 25 km southwest of Dublin in Ireland. This experimental campaign aims to bridge the gap between the existing database of field tests and current monopile design practices in the offshore wind industry. Most data available in the literature pertains to piles with a large slenderness ratio (L/D, where L is the pile embedded length and D is the pile external diameter) while monopiles (which are the most popular foundation type for offshore wind turbines) are characterised by small L/D, typically close to 3.

Hence, this new experimental campaign considered pile slenderness ratios ranging from 2.2 to 4.4. Ground-level responses for monotonic loading of 3 piles with an outer diameter of 457 mm are reported. Blind monotonic predictions were required to plan the tests and size the loading system. The predictions are based on four different approaches reported in the literature. A recently developed approach developed by Igoe and Jalilvand (2020), based on 3DFE analysis where all the soil constitutive model parameters were correlated from the CPT (Cone Penetration Test) data, was seen to provide an excellent match with the experimental results. All other approaches examined significantly underestimated the initial stiffness and ultimate capacity of the piles.

Chapter 4: Field lateral load tests on monopiles in dense sand at Blessington – Part 2 – Cyclic loading

This chapter is the second part presenting the results from a recent pile lateral field-testing campaign carried out in dense sand at the Blessington test site in Ireland. This chapter focuses on cyclic loading field tests. Building upon the findings of Chapters 1 and 2, a macro-element model is fitted to this new experimental data and the superposition models are assessed.

4.1 CYCLIC TESTS RESULTS

4.1.1 Cyclic loading applied

Figure 4-1 presents the cyclic load histories applied during the three cyclic tests (tests 3, 4 and 5, as presented in Figure 3-8).

During test 3, the lateral load was applied between piles L3 (L/D = 3.3) and pile L2 (L/D = 4.4). The test consisted of 5 sets (see Figure 4-1a), following the initial plan:

1. Set 1: 1,000 one-way cycles at 6.4 kN (about 10% of the predicted capacity of the smaller pile).
2. Set 2: 1,000 one-way cycles at 12.5 kN (about 20% of the predicted capacity of the smaller pile).
3. Set 3: 1,000 one-way cycles at 18.8 kN (about 30% of the predicted capacity of the smaller pile).
4. Set 4: 1,000 one-way cycles at 26.1 kN (about 40% of the predicted capacity of the smaller pile).
5. Final pushover until pile failure

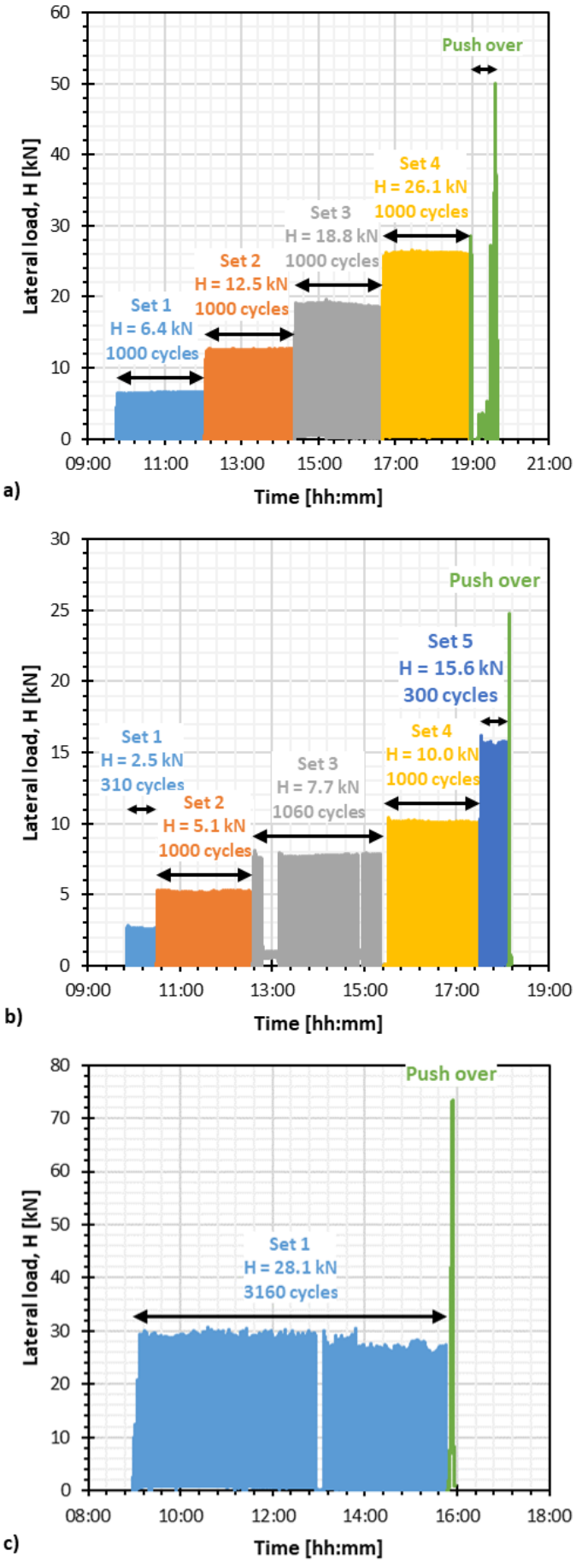

Figure 4-1. Cyclic load history applied during test 3 (a), test 4 (b) and test 5 (c).

During test 4, the lateral load is applied in tension between pile L1 (L/D = 2.2) and pile L2 (L/D = 4.4). The test consists of 6 phases (see Figure 4-1b):

1. Set 1: 300 one-way cycles at 2.5 kN (about 10% of the pile predicted capacity). This set was interrupted early (compared to the 1,000 cycles initially planned) because a very limited accumulation of displacement was observed.
2. Set 2: 1,000 one-way cycles at 5.1 kN (about 20% of the predicted capacity of the smaller pile).
3. Set 3: 1,060 one-way cycles at 7.7 kN (about 30% of the predicted capacity of the smaller pile). 60 extra cycles were applied after an unexpected failure of the control system around 13:00 due to excessive heat.
4. Set 4: 1,000 one-way cycles at 10.0 kN (about 40% of the predicted capacity of the smaller pile).
5. Set 5: 300 one-way cycles at 15.6 kN (about 65% of the predicted capacity of the smaller pile). This additional set was allowed by the time saved during set 1.
6. Final pushover until pile failure

During test 5, the lateral load is applied in tension between pile L5 (L/D = 4.4) and pile L2 (L/D = 4.4). Both piles were previously tested in the perpendicular direction up to 60 kN and 50 kN, respectively. This represents about 35% to 45% of the predicted pile capacity which may have some notable effect on the results. The test consists of 2 phases (see Figure 4-1c):

1. Set 1: 3,160 cycles at 28.1 kN (about 20 % of the predicted capacity of both piles). Only one load level is considered because: a) Pile L2 has already been loaded at various lower load levels and b) the hydraulic control unit cannot accommodate larger loads. Hence, it was decided to run only 1 load level but with a larger number of cycles.
2. Final pushover until pile failure. The test stopped at 74 kN due to an unexpected failure of the loading system likely due to the fatigue damage caused by the load cycles. None of the piles reached failure.

It should be noted that the loads reported in the paragraphs above and in Figure 4-1 are averages of the peak loads applied. As shown in Figure 4-2, small variations of peak load are noticed due to the limited accuracy of the hydraulic control unit. In addition, the hydraulic control unit only allow the application of quasi square wave form. This is not deemed to significantly affect the results compare to the sinusoidal wave form expected

offshore. As detailed in the paragraphs above, all load parcels were applied in ascending order (as typically assumed during monopile design).

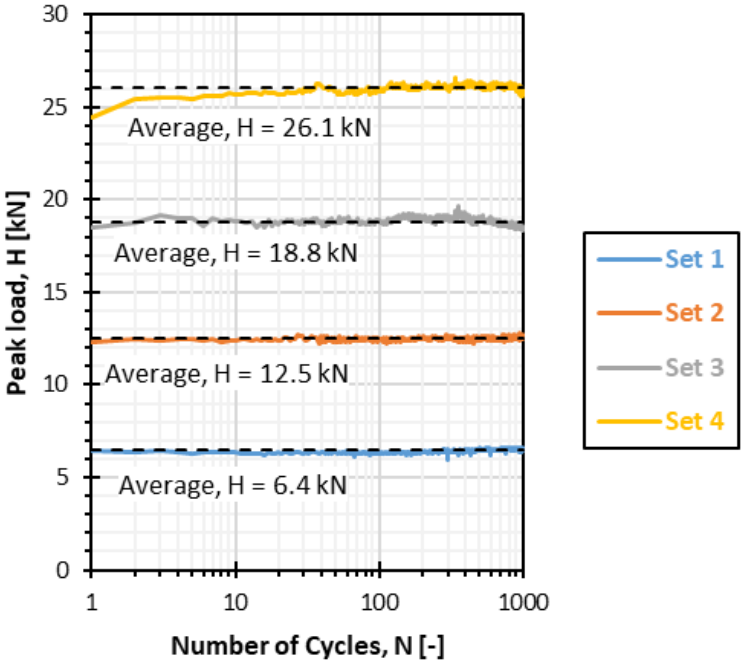

Figure 4-2. Example evolution of peak load through each load set for test 3.

4.1.2 Data processing

Two features are extracted from the pile load-displacement response at ground level: a) the accumulation of displacement, and b) the change in secant stiffness (as shown in Figure 4-3).

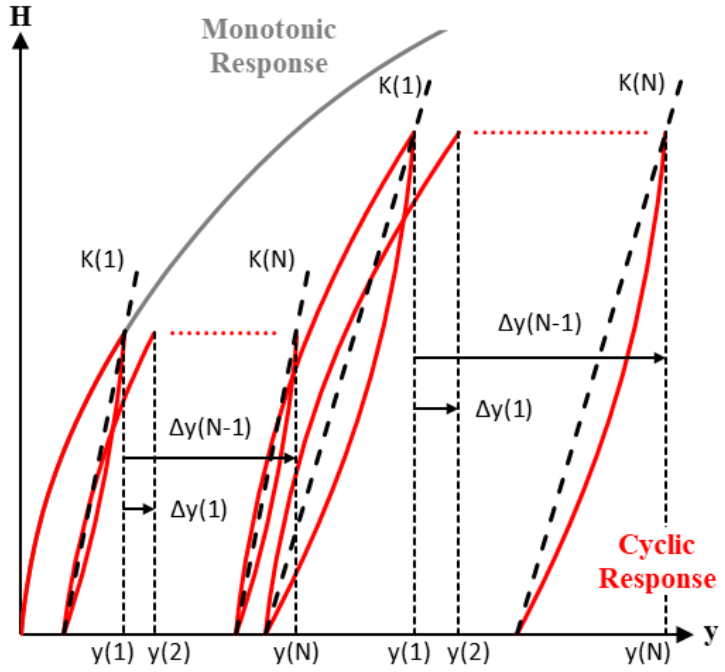

Figure 4-3. Example pile load-displacement response and definition of accumulated displacement and secant stiffness.

The secant stiffnesses (K) reported in Figure 4-4c, Figure 4-4d, Figure 4-5c, Figure 4-5d, Figure 4-6c, Figure 4-6d, Table 4-1, Table 4-2 and Table 4-3 are defined in Figure 4-3. K(i) denotes the unloading secant stiffness during load cycle i. The secant stiffness might be affected by the formation of gapping (as identified during the monotonic tests). However,

The displacements (y) reported in Figure 4-4c, Figure 4-4d, Figure 4-5c, Figure 4-5d, Figure 4-6c, Figure 4-6d, Table 4-1, Table 4-2 and Table 4-3 are defined in Figure 4-3. During the first load set, y(1) coincides with the monotonic (static) response. However, this is not the case during any subsequent load sets as some displacement will have accumulated due to the cyclic loading history. Therefore, y(1) denotes the pile displacement when applying the peak load for the first time in a given load set. The displacement is reported for N = 1 although only one-half cycle is applied as no unloading has occurred. Alternatively, the accumulated displacement can be defined in terms of increased displacement (Δy) compared to the displacement during the first cycle y(1). Hence, Δy(1) captures the effect of 1 full cycle, between y(1) and y(2).

The displacements reported are corrected for small peak load variations as per equation (1) below where y(i) and y*(i) are the corrected and uncorrected peak displacements during cycle i, H(i) is the peak load during cycle i and H_{avg} the average peak load during the load set.

$$y(i) = y^*(i) + \frac{H_{avg} - H(i)}{K(i)} \tag{4.1}$$

4.1.3 Results

The results of test 3, test 4 and test 5 are presented in Figure 4-4, Figure 4-5 and Figure 4-6 respectively. The left-hand side of the figures presents the results of the ‘test’ piles L3 (L/D = 3.3), L1 (L/D = 2.2) and L5 (L/D = 4.4) for test 3, test 4 and test 5, respectively. While the right-hand side of the figures presents the results for the ‘reaction’ pile L2 (L/D = 4.4). The results are presented in terms of load-displacement response at ground level (top), ground level displacement vs number of cycles (middle) and secant stiffness vs number of cycles (bottom).

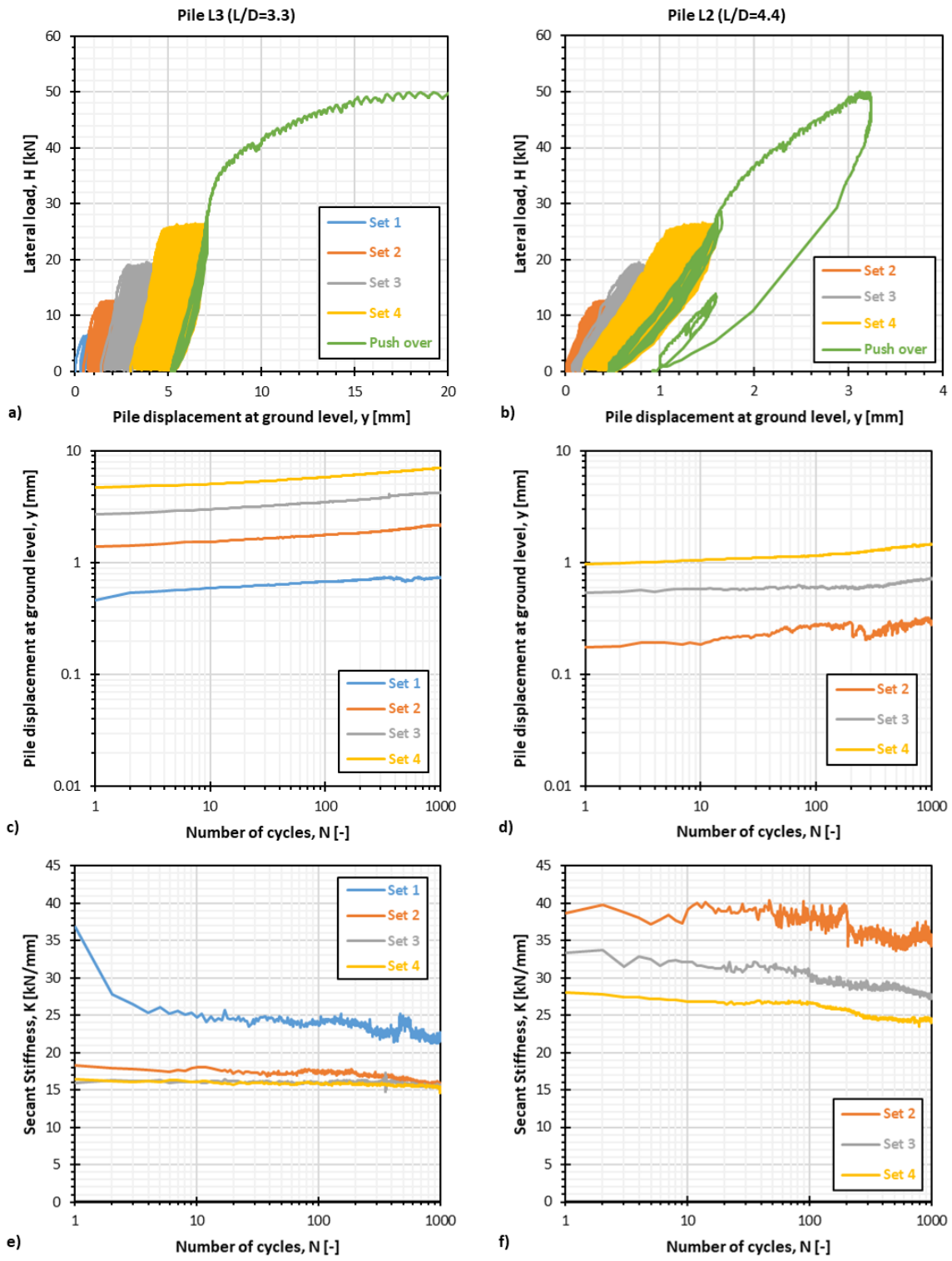

Figure 4-4. Results of cyclic test 3 in terms of load vs displacement (a and b), displacement vs number of cycles (c and d) and secant stiffness vs number of cycles (e and f) for pile L3 (L/D=3.3) (a, c and e) and pile L2 (L/D=4.4) (b, d and f).

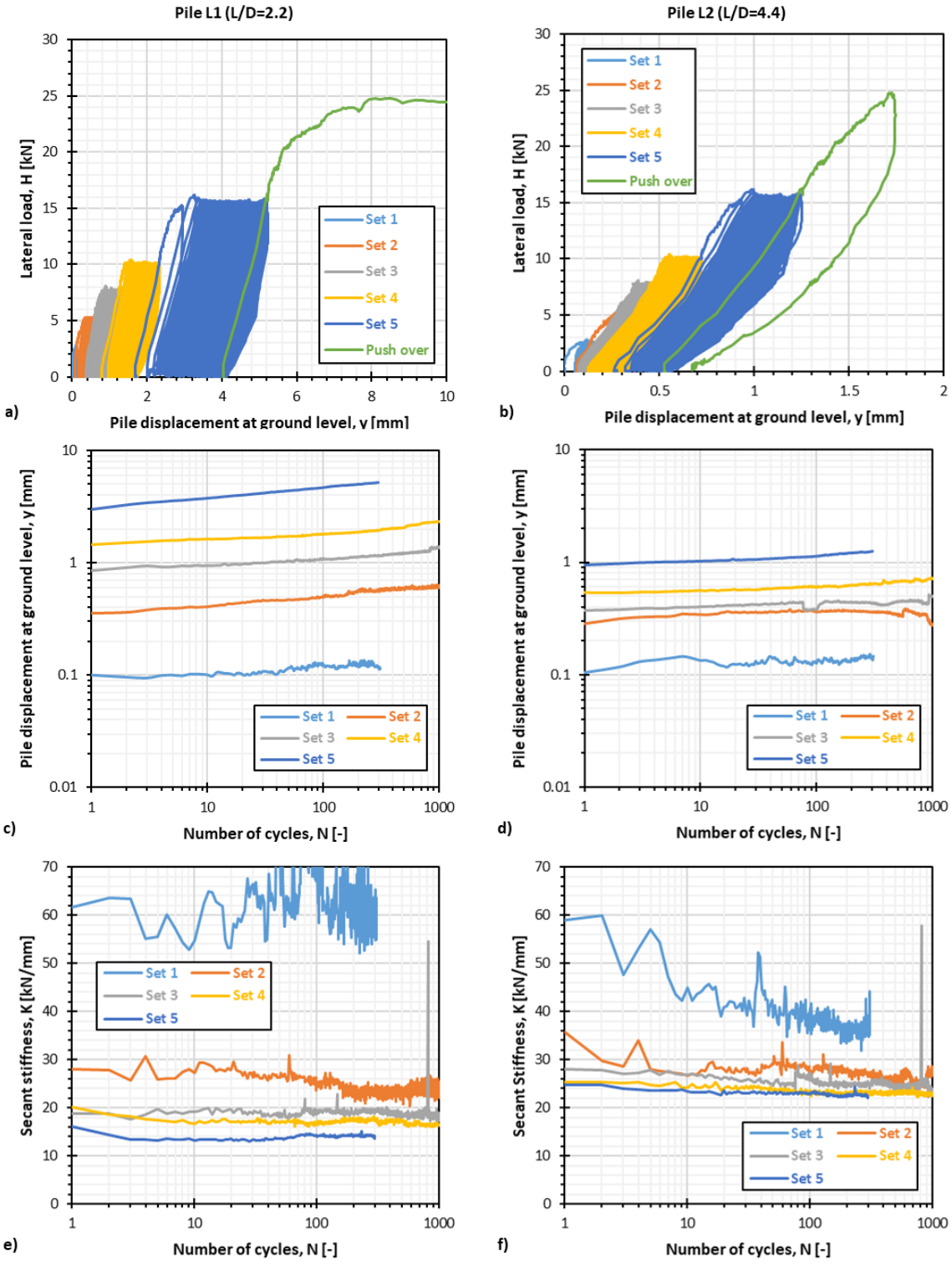

Figure 4-5. Results of cyclic test 4 in terms of load vs displacement (a and b), displacement vs number of cycles (c and d) and secant stiffness vs number of cycles (e and f) for pile L2 (L/D=2.2) (a, c and e) and pile L2 (L/D=4.4) (b, d and f).

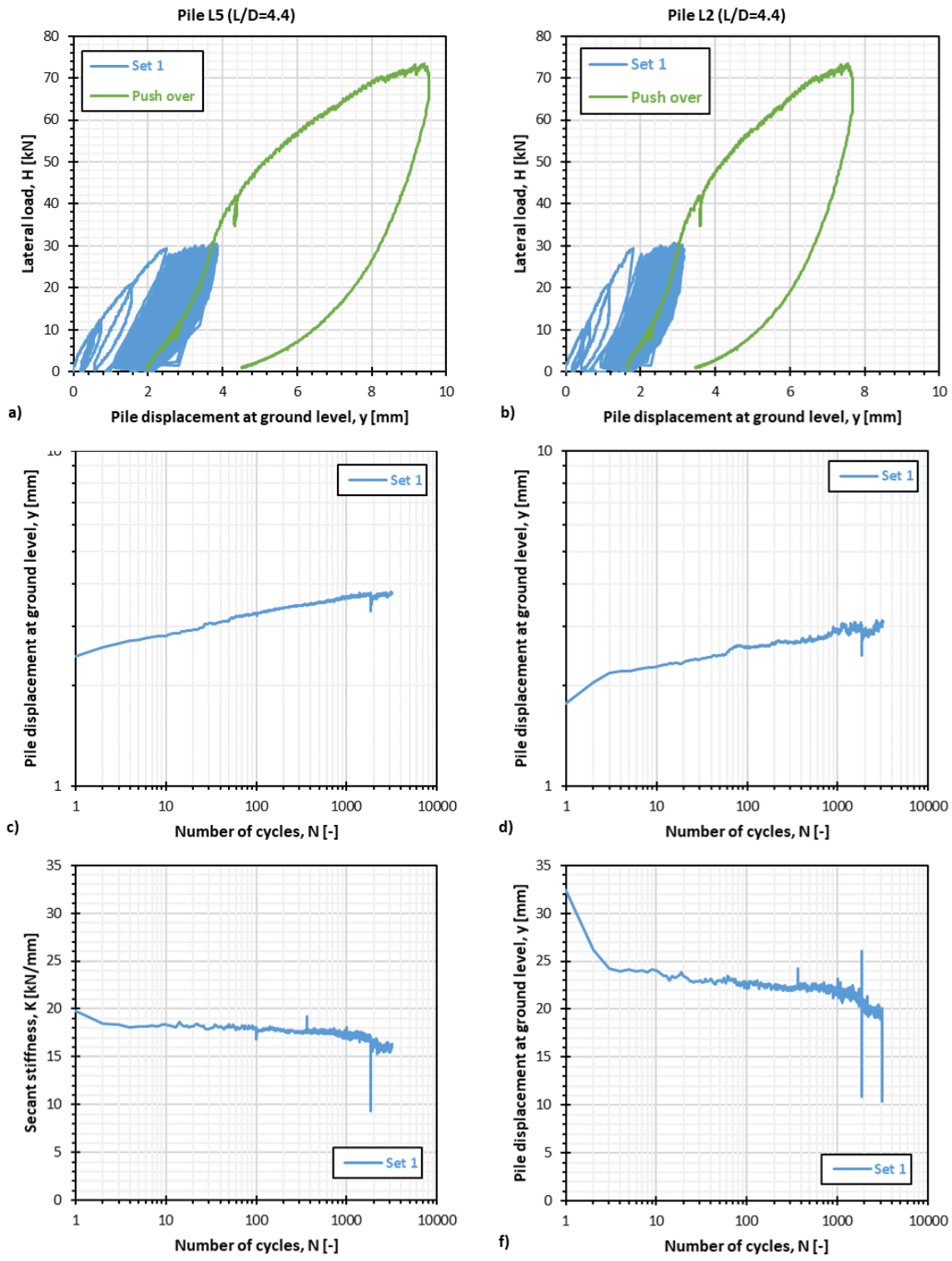

Figure 4-6. Results of cyclic test 5 in terms of load vs displacement (a and b), displacement vs number of cycles (c and d) and secant stiffness vs number of cycles (e and f) for pile L5 (L/D=4.4) (a, c and e) and pile L2 (L/D=4.4) (b, d and f).

Due to some inaccuracy at small displacement, pile L2 (L/D = 4.4) response during set 1 of test 2 is not shown. The inclinometers were found very sensitive to the unloading / reloading dynamic effects during each load cycle. In addition, significant drift due to

temperature change during up to 10 hours of continuous testing was also noticed. Hence, pile rotations are not shown.

Figure 4-4a shows that the ultimate reaction mobilised by pile L3 (L/D = 3.3) after 4,000 cycles at various load levels reaches 50.0 kN only. This is less than the predicted monotonic capacity of 64.7 kN (-22.7%). This could be attributable to a loss of capacity due to cyclic loading. However, Figure 4-5a shows that the ultimate reaction mobilised by pile L1 (L/D = 2.2) after 3,670 cycles at various load levels reaches 24.8 kN. This is notably more than the predicted monotonic capacity of 18.9 (+31.4%). Ultimate capacity is not defined for piles L2 and L5 (L/D = 4.4). Such discrepancies between the predicted and experimental capacities are typical of lateral loading field tests (see McAdam et al. 2020) where soil spatial variability (particularly over the top 1 m) may play a crucial role.

Figure 4-4c, Figure 4-4d, Figure 4-5c, Figure 4-5d, Figure 4-6c and Figure 4-6d presents the accumulation of pile displacement at ground level with the number of cycles. All the results are consistent and show that pile displacement at ground level increases with the number of cycles and with the load magnitude. The experimental results plot linearly on a log-log scale suggesting a power relationship as recommended by some macro-element models in the literature (e.g. Leblanc et al.,2010; Klinkvort and Hededal, 2013). Extending the number of cycles applied beyond 1,000 during test 5 confirms that the linear relationship in the log-log scale still holds beyond 3000 cycles. The longer piles (right-hand side of the figure) systematically present smaller pile ground level displacement than the smaller piles (left-hand side) for the same number of cycles and load level. This is expected since the additional pile penetration increases the pile stiffness. The only exception is when comparing Figure 4-5c and Figure 4-5d for set 1 where both piles have similar responses although one (L2 L/D = 4.4, right-hand side) is twice longer than the other (L1 L/D = 2.2, left-hand side). This is because the entire pile embedded length is not fully mobilised at a very small displacement (0.1 mm is about D/5000). When comparing Figure 4-6c and Figure 4-6d, both piles have the same geometry (L/D = 4.4) but pile L5 (left-hand side) is found significantly softer than pile L2 (right-hand side). Again, this could be attributable to the difference in the load histories applied to the piles in the perpendicular direction. However, this is more likely due to the soil spatial variability as captured by the monotonic predictions in Chapter 3 identifying L5 as softer than L2. Plotting the accumulation of displacement in terms of Δy instead of total displacement y shows that the two piles have similar behaviour (see Figure 4-7).

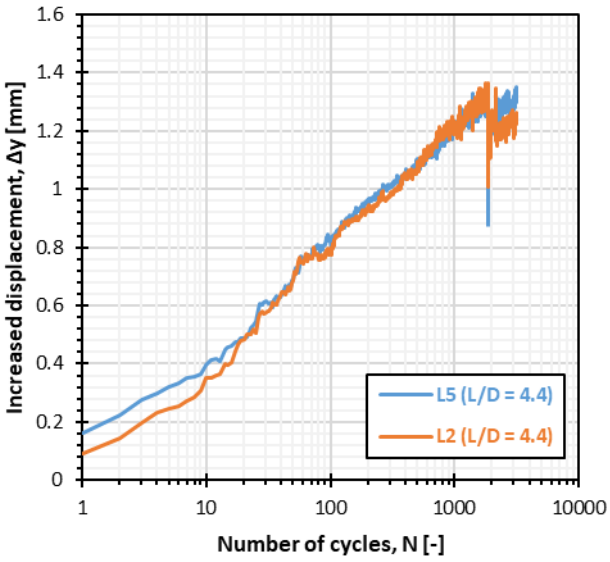

Figure 4-7. Increase in pile displacement at ground level for piles during test 5.

This data can be used to calibrate and/or validate models capturing the accumulation of pile deflection upon cyclic loading which is critical for monopile geotechnical design in serviceability limit states (e.g. DNV-ST0126). In addition to capturing the accumulation of pile deflection with the number of cycles, Chapter 2 showed that the assumptions regarding superposition between load sets greatly affect the overall pile response to cyclic loading. The results from the cyclic field tests 3, 4 and 5 are summarised in Table 4-1,

Table 4-2 and

Table 4-3, respectively for further analysis.. The results are tabulated for both piles in terms of predicted and measured ultimate capacity, pile displacement at ground level at the start and end of each load set and pile secant stiffness at ground level at the start and end of each load set.

Table 4-1. Summary of the results for test 3 between pile L3 (L/D = 3.3) and pile L2 (L/D = 4.4).

Set	H [kN]	N [-]	L3 (L/D = 3.3)						L2 (L/D = 4.4)					
			H_{ult} [kN]		y [mm]		K [kN/mm]		H_{ult} [kN]		y [mm]		K [kN/mm]	
			Pred.	Exp.	Start	End	Start	End	Pred.	Exp.	Start	End	Start	End
1	6.4	1,000	64.7	50.0	0.46	0.74	36.9	22.7	144.2	-	-	-	-	-
2	12.5	1,000			1.39	2.19	18.3	15.4			0.17	0.28	38.6	35.8
3	18.8	1,000			2.74	4.23	16.0	15.1			0.54	0.72	33.3	27.8
4	26.1	1,000			4.73	7.05	16.4	14.5			0.98	1.46	28.0	23.9

Table 4-2. Summary of the results for test 4 between pile L1 (L/D = 2.2) and pile L2 (L/D = 4.4).

Set	H [kN]	N [-]	L1 (L/D = 2.2)						L2 (L/D = 4.4)					
			H_{ult} [kN]		y [mm]		K [kN/mm]		H_{ult} [kN]		y [mm]		K [kN/mm]	
			Pred.	Exp.	Start	End	Start	End	Pred.	Exp.	Start	End	Start	End
1	2.5	310	18.9	24.8	0.10	0.11	61.7	61.7	144.2	-	0.10	0.15	59.0	44.2
2	5.1	1000			0.36	0.60	28.0	23.5			0.29	0.28	35.7	26.9
3	7.7	1060			0.85	1.37	18.7	18.1			0.37	0.49	27.9	22.2
4	10.0	1000			1.46	2.34	20.2	16.6			0.54	0.72	25.4	23.3

5	15.6	300			2.98	5.21	16.1	13.5			0.95	1.25	24.8	22.1

Table 4-3. Summary of the results for test 5 between pile L5 (L/D = 4.4) and pile L2 (L/D = 4.4).

Set	H [kN]	N [-]	L5 (L/D = 4.4)						L2 (L/D = 4.4)					
			H_{ult} [kN]		y [mm]		K [kN/mm]		H_{ult} [kN]		y [mm]		K [kN/mm]	
			Pred.	Exp.	Start	End	Start	End	Pred.	Exp.	Start	End	Start	End
1	28.1	3,160	133.4	-	2.51	3.77	19.8	15.9	144.2	-	1.81	3.10	32.4	20.0

Similarly to the monotonic tests, significant gapping and cracks were observed at the end of the tests as shown on Figure 4-8. However, the gaps and cracks formation were mostly observed during the final push-over after the cyclic testing. Limited gapping was observed during the cyclic tests and this is supported by the load-displacement responses which do not exhibit a pronounced "banana shape" (see Figure 4-4a, Figure 4-4b, Figure 4-5a, Figure 4-5b, Figure 4-6a, and Figure 4-6b). The cyclic tests were carried in June 2023 after a particular dry and warm period and some vegetation has grown since excavation of the topsoil. This explains why the cracks are significantly more pronounced than after the monotonic tests (see Figure 3-13). This difference in hydraulic conditions of the site might have affected the pile response.

Figure 4-8. Example of gaping and soil cracks after completion of the cyclic tests for pile L1 (L/D = 2.2)

4.2 MACRO-ELEMENT MODEL

In order to fit a macro model to capture the effect of displacement accumulation due to cyclic loading at groundline it is common to examine either the accumulation of total displacement,

y, (similar to the approach adopted by Klinkfort and Hededal, 2013; equation (4.2)) or the accumulated change in displacement due to cyclic loading, Δy (similar to LeBlanc et al., 2010; equation (4.3)).

$$y(N) = aN^b \tag{4.2}$$

$$\Delta y(N) = y(N) - y(1) = cN^d \tag{4.3}$$

Two separate approaches for the fitting of the macro model to the experimental data have been examined:

1. Fitting parameters for each load set for each test individually using least squares regression and examining trends in the fitting parameters
2. Using an optimization algorithm to fit parameters for the combined dataset of all pile geometries and all load sets simultaneously.

4.2.1 Fitting to each individual load package

Fitting parameters for each load set for each test individually is useful to better understand how these fitting parameters change with respect to pile geometry, cyclic load level etc. It should be noted that this approach of fitting each load set individually ignores the effect of previous cycling history (i.e. from previous load sets). In order to achieve this fitting, least squares regression was applied to the data using a log distribution of sample points to avoid the fitting being biased towards larger values of N. The results of the fitting for both total displacement, y, and change in displacement due to cyclic loading, Δy, are provided in Figure 4-9 and Table 4-4. The exponent parameters, b and d, control the slope of the response on a log-log scale. With respect to the total displacement, y, the exponent parameter b was seen to vary between 0.02 – 0.09 with a mean value of ~0.06. With respect to the change in displacement, Δy, the exponent parameter d was seen to vary between 0.2 – 0.5 with a mean value of ~0.33. This is in reasonable agreement with the mean value of 0.31 reported by LeBlanc et al. (2010a). Figure 4-9 shows the exponent fitting parameters b and d for each test as a function of relative load level (H_{max} / H_{ult}). When plotted this way, the data shows a large scatter with no clear trend with load level evident.

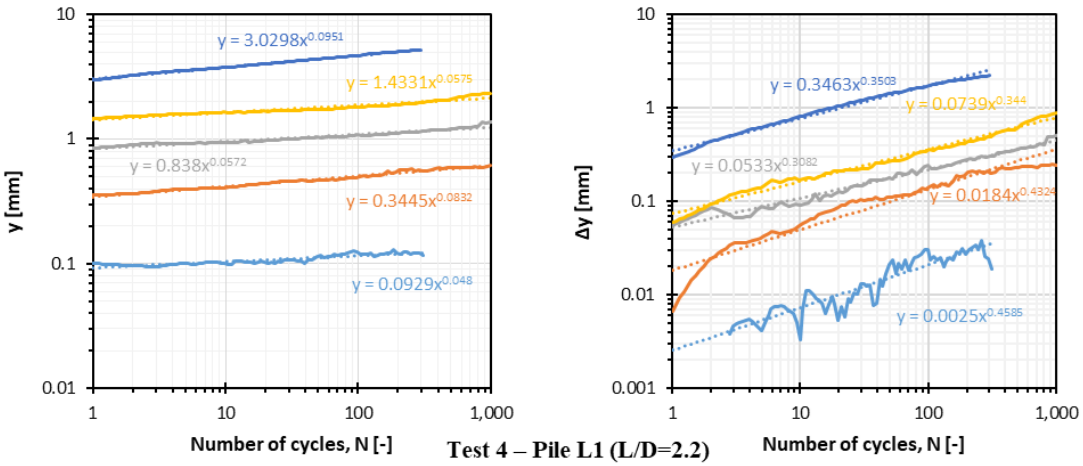

Test 4 – Pile L1 (L/D=2.2)

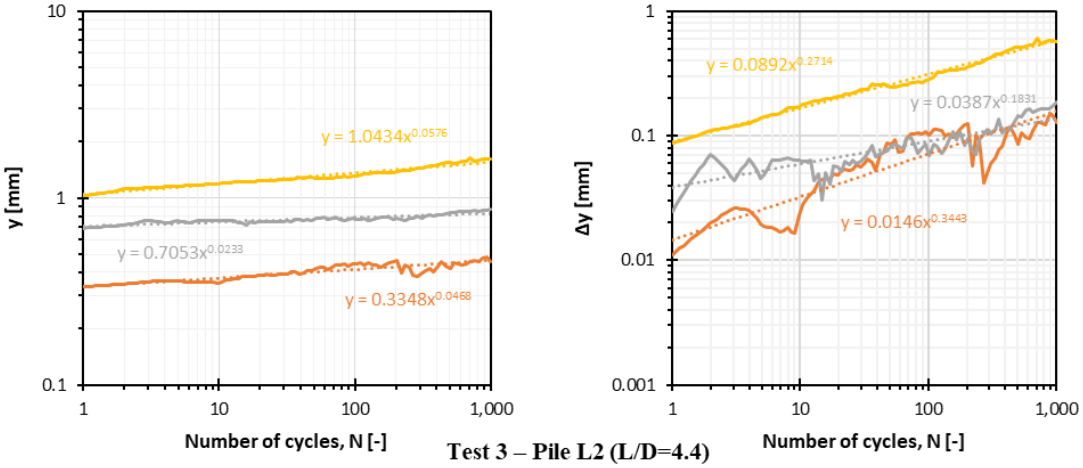

Test 3 – Pile L2 (L/D=4.4)

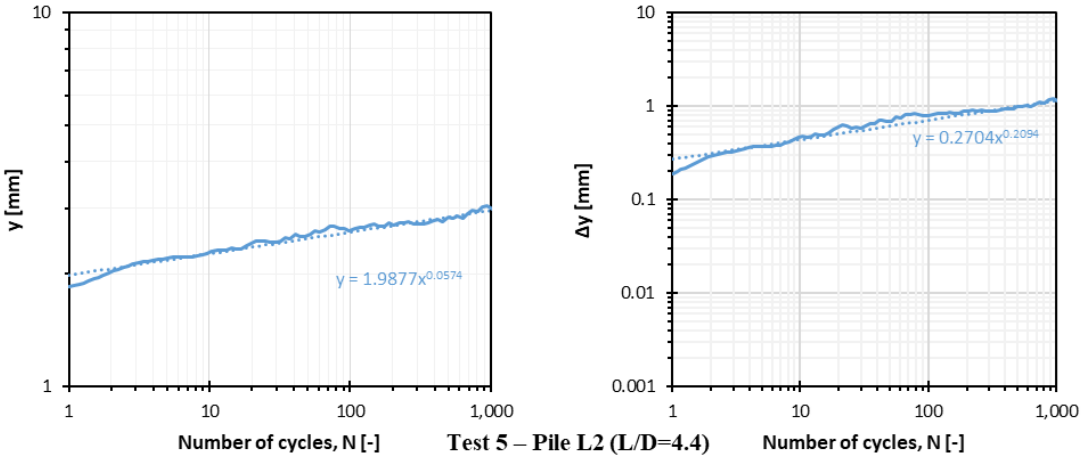

Test 5 – Pile L2 (L/D=4.4)

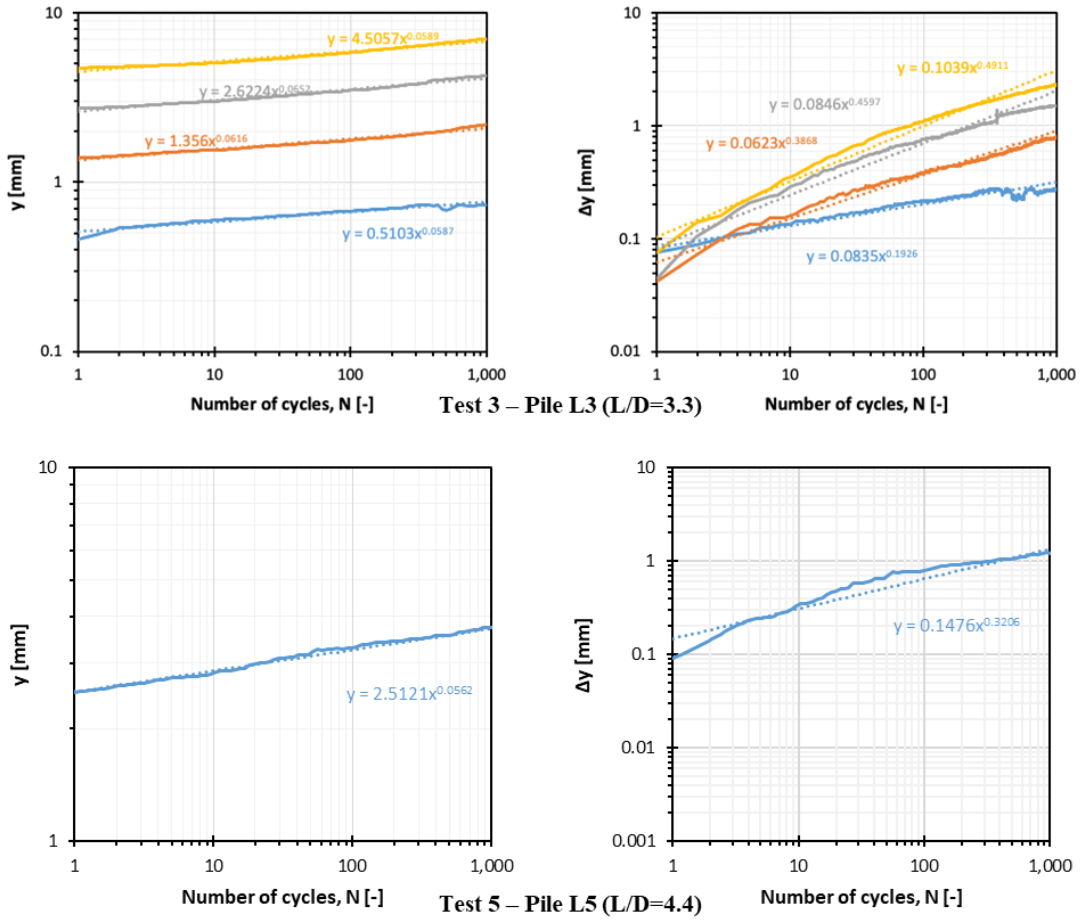

Figure 4-9. Individual fitting of cyclic test results in terms of total displacement (left) and change in displacement (right) for (a) Pile L1 test 4, (b) Pile L2 test 3, (c) Pile L2 test 5, (d) Pile L3 test 3 and (e) Pile L5 test 5.

Table 4-4. Table of individual fitting parameters for macro model (see equations 2 and 3)

Test	Pile	Set	H [kN]	H_{ult} [kN]	H/H_{ult} [%]	a	b	c	d
4	L1	1	2.5	24.8	10	0.0929	0.048	0.0025	0.4585
4	L1	2	5.1	24.8	21	0.3445	0.0832	0.0184	0.4324
4	L1	3	7.7	24.8	31	0.838	0.0572	0.0533	0.3082
4	L1	4	10	24.8	40	1.4331	0.0575	0.0739	0.344
4	L1	5	15.6	24.8	63	3.0298	0.0951	0.3463	0.3503
3	L2	1	6.4	144.2	4	-	-	-	-
3	L2	2	12.5	144.2	9	0.3348	0.0468	0.0146	0.3443
3	L2	3	18.8	144.2	13	0.7053	0.0233	0.0387	0.1831
3	L2	4	26.1	144.2	18	1.0434	0.0576	0.0892	0.2714
5	L2	1	28.1	144.2	19	1.9877	0.0574	0.2704	0.2094
3	L3	1	6.4	50	13	0.5103	0.0587	0.0835	0.1926
3	L3	2	12.5	50	25	1.356	0.0616	0.0623	0.3868
3	L3	3	18.8	50	38	2.6224	0.0652	0.0846	0.4597
3	L3	4	26.1	50	52	4.5057	0.0589	0.1039	0.4911
5	L5	1	28.1	133.4	21	2.5121	0.0562	0.1476	0.3206

4.2.2 Fitting one single model to combined dataset

An alternative to fitting each load set individually, is to use optimisation to fit parameters for the combined dataset of all pile geometries and all load sets simultaneously. One advantage of this approach is the ability to account for the effects of previous loading

history and to develop a single set of fitting parameters for all tests. In order to achieve this, a modified version of equation 2 was used as shown in equation 4.

$$y(H,N) = y_{static}(H) \times (1 + T_b T_c N^{S_b S_c}) \quad (4)$$

Where:

$$T_c = S_c = 1 \text{ for one-way loading} \quad (5)$$

$$T_b = max\left(0, \alpha \frac{H}{H_{ult}} + \beta\right) \quad (6)$$

$$S_b = max\left(0, \gamma \frac{H}{H_{ult}} + \delta\right) \quad (7)$$

Where α, β, γ and δ are optimised to offer the best match between the model and experimental data. This equation is a modified and combined form of that proposed by LeBlanc et al. (2010a) and Klinkfort and Hededal (2013). In order to perform the optimization for multiple piles and different load sets, there is a need to first estimate the static (monotonic) load-displacement response, y_{static}, often referred to as the backbone curve. There is also a need to use a cyclic superposition model when moving from one load to another to account for the loading history. The approach used in this Chapter for both these are described below.

4.2.2.1 Fitting monotonic model

The monotonic model was defined by adopting a PISA rule-based method for sand and scaling the soil reaction curves with so-called p- and y-factors to best match the backbone response from the cyclic field tests. The p- and y-factors were applied directly to all soil reaction components with the exception of the distributed moment which already scales with the lateral soil reaction, p. A similar approach was adopted in Beuckelaers (2017). The fitting of the p- and y- factors was achieved by sampling points along the back-bone curve of the field tests and using optimisation in MATLAB with a least square error cost function to minimize the error in monotonic prediction at these sample points. Separate p- and y- factors were optimised for each test pile. Figure 4-10 shows the fitted backbone monotonic response against the field test data and Table 4-5 provides the list of p- and y-factors.

Table 4-5. Best fit p- and y-factors from optimisation

Pile	p-factor	y-factor
L1	4.32	1.30
L2	1.28	0.13
L3	4.82	5.28

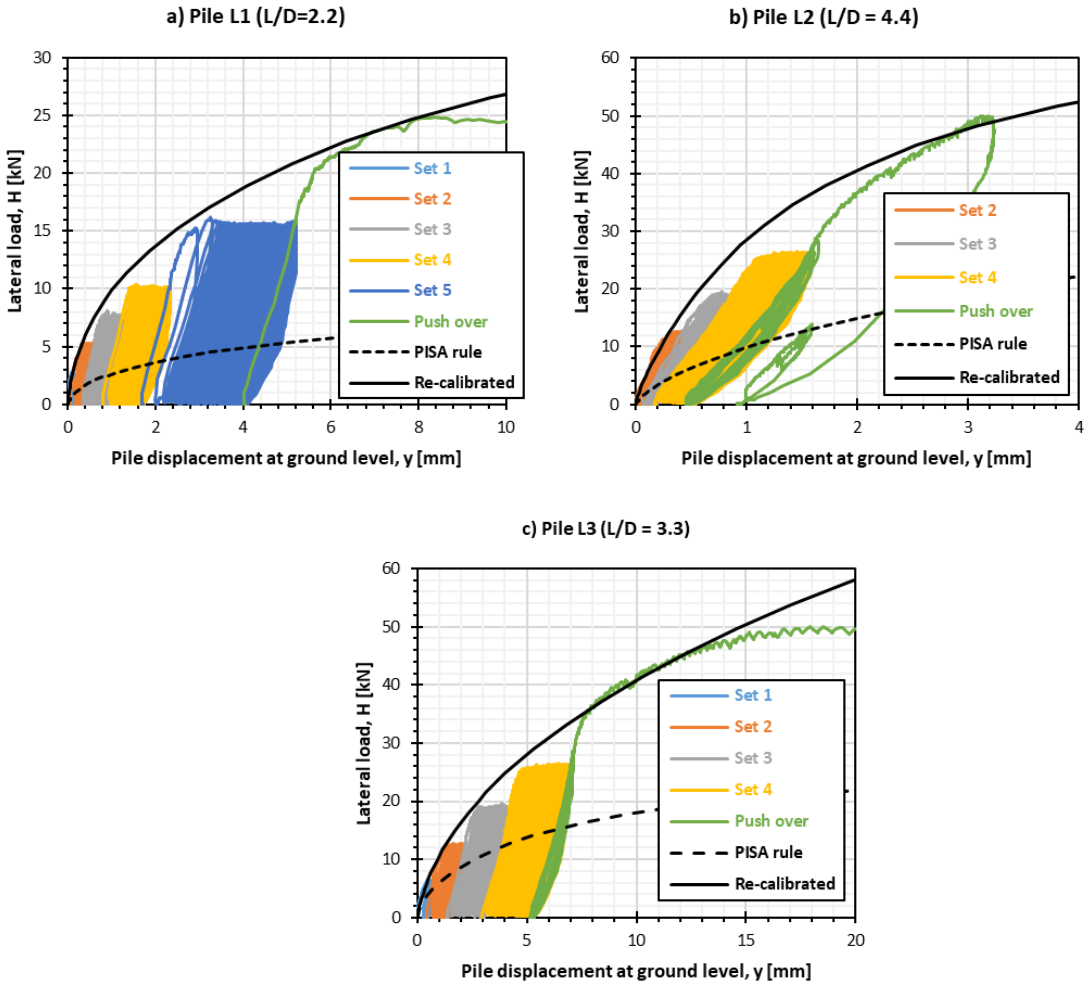

Figure 4-10. Fitting of PISA p- and y-factors to cyclic response backbone curve for (a) Pile L1, (b) Pile L2 and (c) Pile L3

4.2.2.2 Superposition model

A comparison between the measured instantaneous change in displacement between different load packets and that predicted from the various different superposition approaches described in the literature (as discussed in Chapter 2) is provided in Figure 4-11. From the figure, it is evident that the approach in Chapter 2 provides the best match with the experimental results and therefore this approach was adopted in order to reduce the uncertainty in the fitting of the cyclic accumulation model.

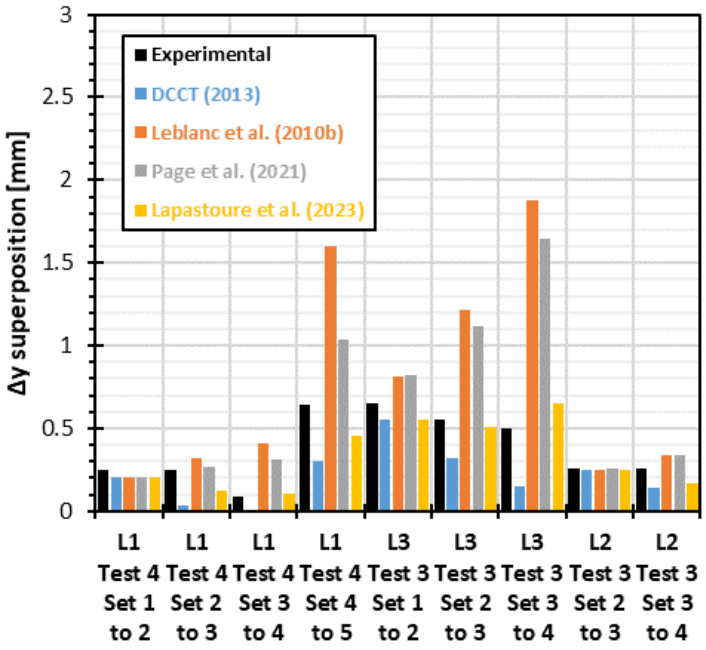

Figure 4-11. Comparison between instantaneous change in displacement during transition between load packets compared with that predicted from different cyclic superposition approaches.

4.2.2.3 Fitted cyclic accumulation model

The fitting parameters for the cyclic accumulation model provided in equation 4 were found through constrained optimisation using the "fmincon" function in MATLAB. All test loads from all piles were used in the optimisation. Lower- and upper-bound limits to the values of α, β, γ and δ used in the optimisation along with the final optimised values of the parameters are given in Table 4-6. The predictions from equation 4 and using the fit parameters below are provided in Figure 4-12. It is evident that this single set of fitting values gives an excellent fit with the experimental data for a range of load levels and pile geometries.

Table 4-6. Lower- and Upper-bound limits and optimised parameters for cyclic macro-element model presented in equations 4 to 7.

Parameter	Lower bound	Upper bound	Optimised values
α	0	10	0.08
β	-10	10	0.09
γ	0	10	0.00
δ	-10	10	0.26

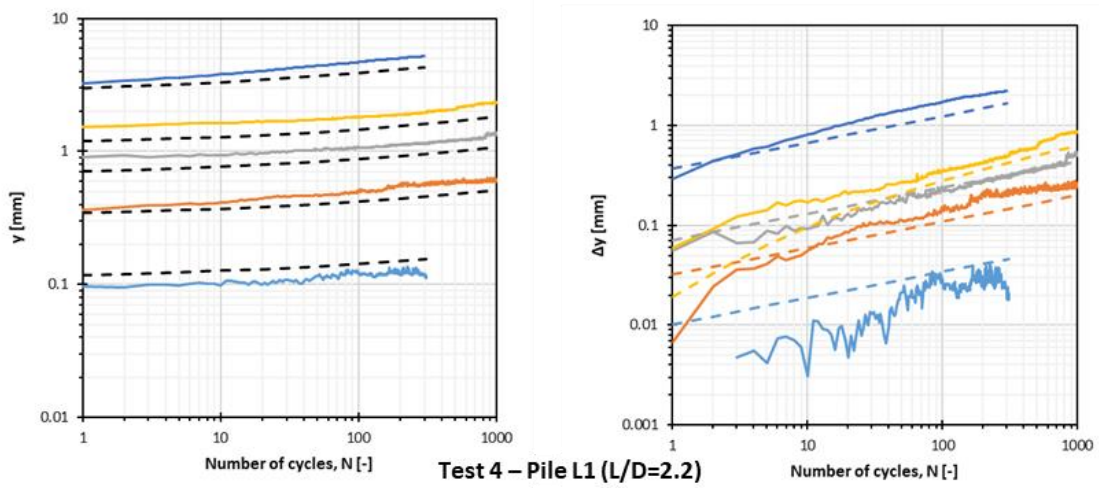
y [mm]
Number of cycles, N [-]
Δy [mm]
Number of cycles, N [-]
Test 4 – Pile L1 (L/D=2.2)

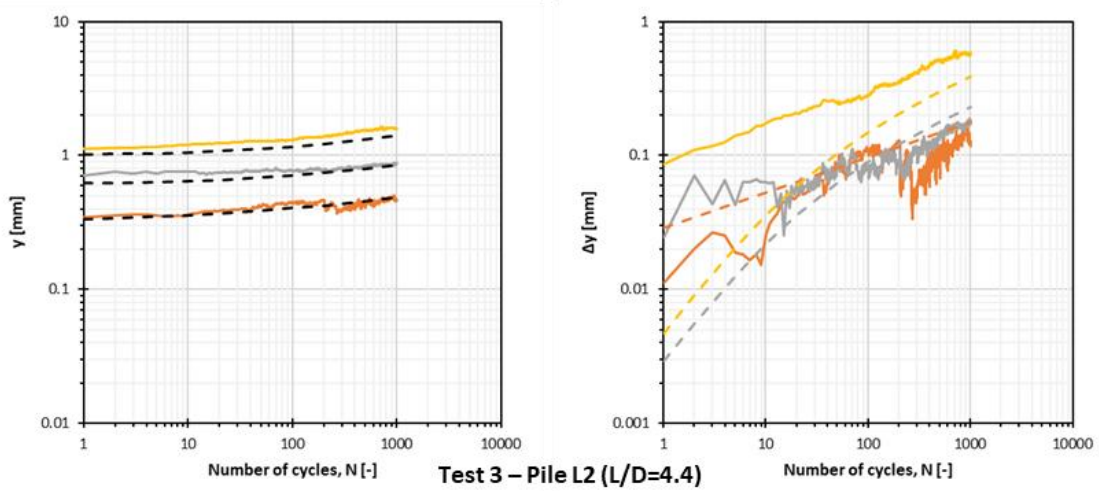
y [mm]
Number of cycles, N [-]
Δy [mm]
Number of cycles, N [-]
Test 3 – Pile L2 (L/D=4.4)

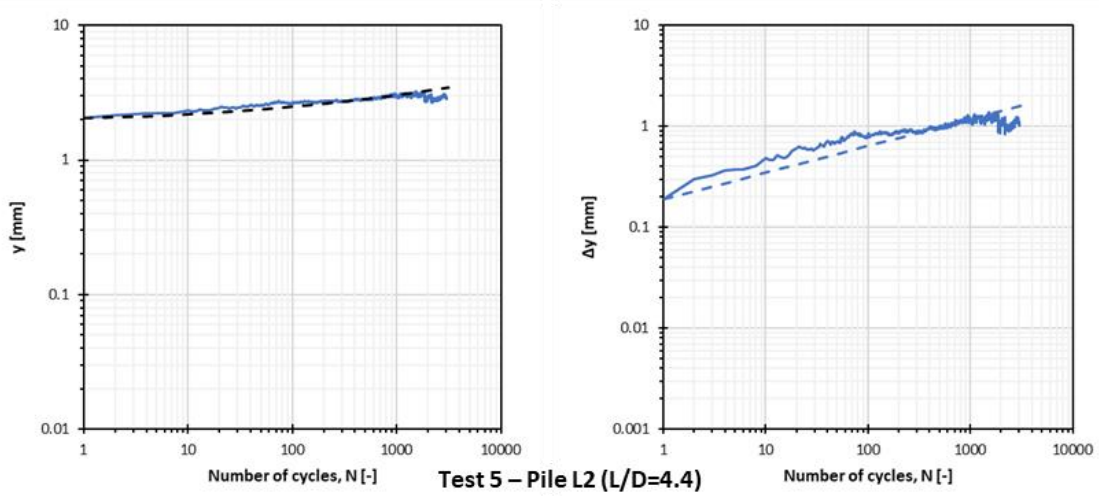
y [mm]
Number of cycles, N [-]
Δy [mm]
Number of cycles, N [-]
Test 5 – Pile L2 (L/D=4.4)

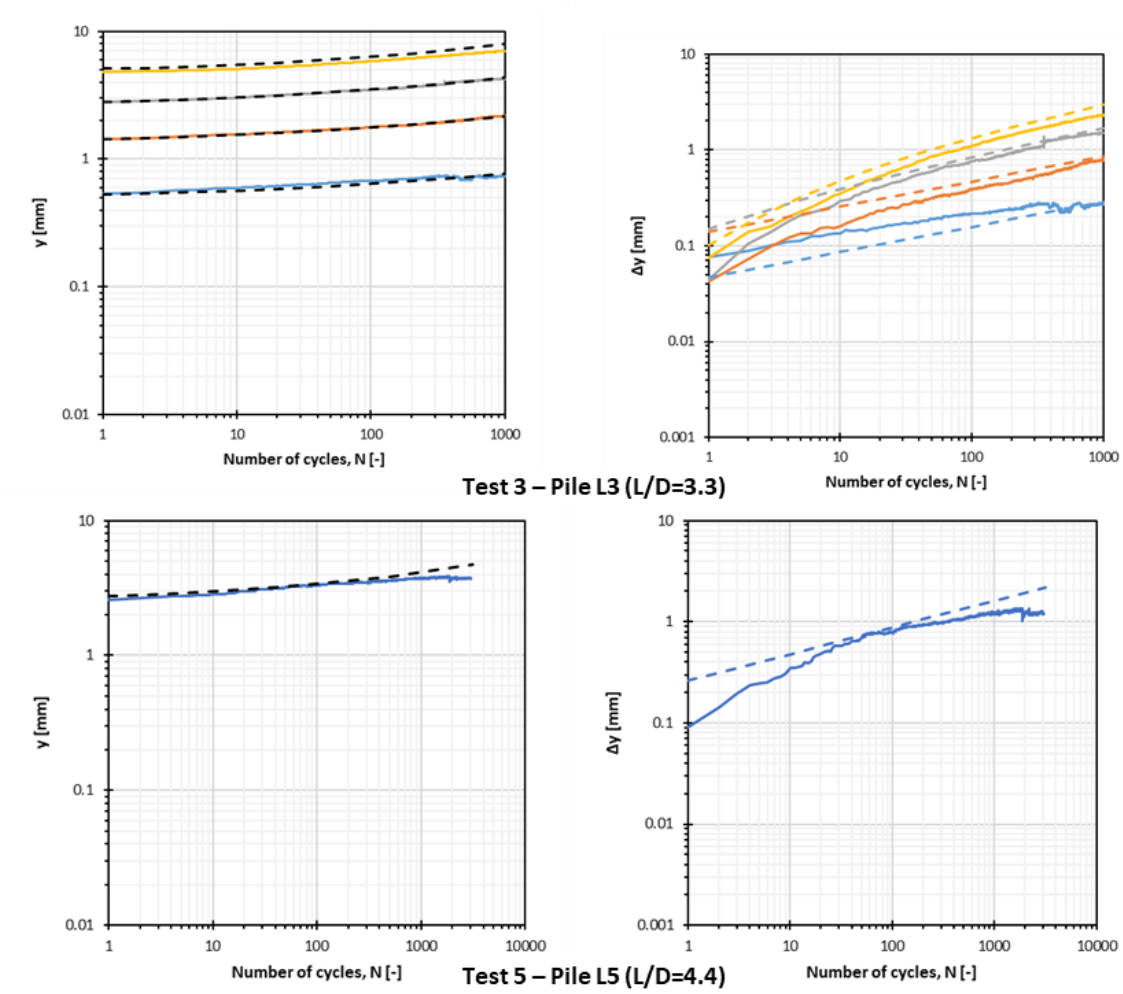

Figure 4-12. Comparison of experimental test data (full lines) and optimised macro-element model (dashed lines) in terms of pile displacement (left) and change in displacement (right).

4.3 CONCLUSION

This Chapter presents the results of a recent pile lateral cyclic loading field testing campaign carried out in dense sand at the Blessington test site, southwest of Dublin in Ireland. This experimental campaign adds valuable field test data with piles with slenderness ratios which cover the range currently seen in in the offshore wind industry.

Three piles with an outer diameter of 457 mm, a wall thickness of 6.35mm and slenderness ratios (L/D) of 2.2, 3.3 and 4.4 were load tested under lateral cyclic loading with up to 4,000 load cycles applied per pile. The results of the cyclic tests are presented in terms of accumulated ground level displacement with the number of cycles and unloading secant stiffness with the number of cycles. This data was used to calibrate simple macro element cyclic accumulation models using 2 different approaches. The first approach was to fit simple power-law accumulation model to each load set individually and examining the trends in the fitting parameters. The 2nd approach involved fitting a backbone curve to the test data and applying a cyclic superposition model to account for the loading history. Once this was implemented an optimisation algorithm was used to find best fit parameters to all

the data simultaneously. An excellent match was achieved to the data using both methods. An examination of a recently developed cyclic superposition approach developed in Chapter 2 was shown to provide the best match with the experimental results when compared with a range of methods described in the literature.

Chapter 5: Validation of a contour diagram based model for monopile cyclic design in sand and clay

As discussed in Chapter 1, Monopiles are the most popular type of foundation for offshore wind turbines. Although capturing the effects of cyclic loading is critical to the design of monopiles, there is no recommended approach in the main design standards and no consensus in the literature as to how this can be achieved. In addition, Chapter 2 has shown the shortcomings of cyclic models typically used in the industry.

Hence, this chapter presents the step-by-step methodology and validation of a new cyclic model in sand and clay. The model consists of the degradation of monotonic soil reaction curves based on soil cyclic contour diagrams. The model is found to provide a very satisfactory match with the PISA field tests in Dunkirk dense marine sand and Cowden stiff glacial till. In addition, a preliminary comparison to cyclic field tests carried out in Blessington dense sand (Chapters 3 and 4) with low pile slenderness ratios further confirms that the proposed approach is suitable for monopile design at different sites.

5.1 CYCLIC METHODOLOGY

This section presents a new cyclic model for the design of monopiles supporting offshore wind turbines. This methodology aims at capturing the accumulation of pile deformation, the potential reduction in pile capacity and the redistribution of stresses along the pile which are critical for monopile geotechnical and structural design.

The methodology consists of the degradation of previously calibrated monotonic soil reaction curves to account for cyclic loading. The degraded cyclic soil reaction curves are then incorporated into a beam element solver to get the monopile cyclic response. This approach ensures fast computation and easy integration into the structural design process which is critical for design optimisation and ease of application in industry. The same formulation is adopted for cohesive and cohesion-less soils which makes it convenient for layered soils as typically encountered offshore.

The magnitude of the cyclic degradation is based on the soil mobilization under design lateral loads, the number of cycles and the soil cyclic contour diagrams. The calculation of cyclic degradation is inspired by the interaction diagram approach recommended by DGGT (2013) for pile axial cyclic loading. The cyclic degradation is applied to the monotonic soil reaction curves in terms of p-multipliers which affect both strength and stiffness (see section 5.4 and Figure 5-10). The cyclic degradation is applied to both the distributed lateral reaction (p-y curve), the distributed moment, the base shear and the base moment.

The approach is summarised in the following 5 steps:

1. Initialisation, which consists of the compiling of all the necessary inputs;
2. Calculation of soil mobilisation after application of the design lateral loads into a 1D beam element solver with monotonic soil reaction curves;
3. Calculation of cyclic degradation based on the soil mobilisation, number of load cycles and soil cyclic contour diagrams;
4. Calculation of cyclic response after application of the design lateral loads into a beam element solver with cyclic soil reaction curves;
5. Superposition of the effect of the different load parcels making up the cyclic load history.

5.1.1 Initialisation

The key inputs to the cyclic model are:

- The pile dimensions and stiffness properties: pile embedment length (L), pile diameter (D), wall thickness (t), Young's modulus (E) and Poisson's ratio (ν).
- The monotonic soil reaction curves. These can either be directly extracted from three-dimensional finite-element analysis or generated following approaches such as PISA rule or PISA numerical.
- The soil cyclic contour diagrams. The approach only requires the failure contours only which capture the number of cycles to failure as a function of average and cyclic stress ratios. These can be generated from site-specific cyclic laboratory tests or scaled from the database reported in Andersen (2015) following the approach recommended in Andersen et al. (2023).
- The cyclic lateral load history. The load time series resulting from a design storm event must be simplified into load parcels following approaches such as rainflow counting or mean crossing counting. The loads are expressed at mudline and each load parcel consists of a minimum load (H_{min}), a maximum load (H_{max}), a number of load cycles (N) and a load eccentricity (e).

5.1.2 Soil mobilisation

The soil mobilisation is a key input to the cyclic model. The soil mobilisation is calculated after the application of the lateral loads in the beam element solver with monotonic soil reaction curves. The lateral load, H, is applied at an eccentricity e above ground level to produce the corresponding overturning moment, M = H*e. The soil mobilisation is calculated in terms of the ratio p/p_u, where p is the soil reaction mobilised and p_u is the ultimate soil reaction at a given depth. As shown in Figure 5-1, the soil mobilisation is usually maximum at shallow depth, decreases with depth to be minimum close to the point of rotation (about 70% of pile embedment length) and increases slightly again getting closer to pile toe. The soil mobilisation is usually close to 1 at shallow depth due to the large pile displacement mobilising relatively large soil reaction curves and the limited vertical effective stress leading to a relatively small ultimate reaction.

The profile of minimum soil reaction p_{min} is obtained after the application of the minimum lateral load H_{min}. The profile of maximum soil reaction p_{max} is obtained after the application of the maximum lateral load H_{max}. Then, the profile of average soil reaction is computed as $p_{avg} = (p_{max} + p_{min}) / 2$ and the profile of cyclic soil reaction is computed as $p_{cyc} = (p_{max} - p_{min}) / 2$.

The soil mobilisation is independent of the number of load cycles.

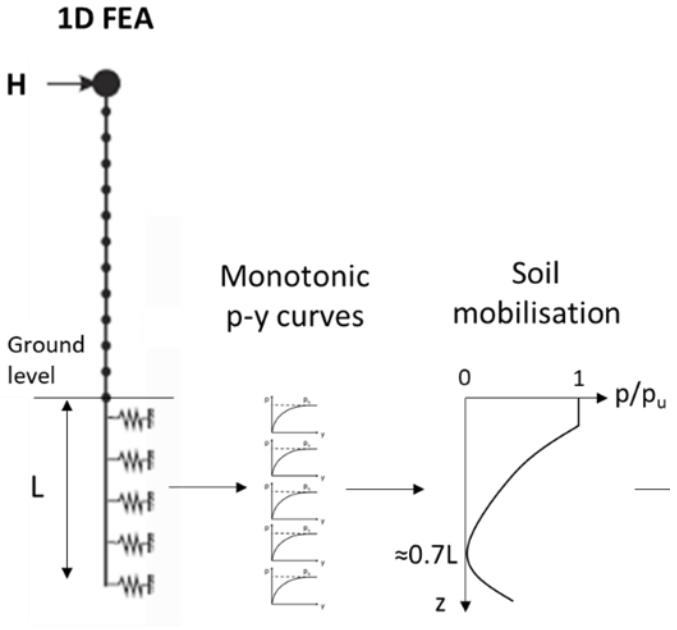

Figure 5-1. Summary of step 2 - calculation of soil mobilisation.

5.1.3 Cyclic degradation

Due to the similarities between the interaction diagram on the left of Figure 5-2 and the soil cyclic failure contour diagram on the right of Figure 5-2, the cyclic degradation is

inspired by the interaction diagrams concept recommended in Appendix D2.2.1 of EA-Pfahle (DGGT, 2013) for pile axial cyclic loading.

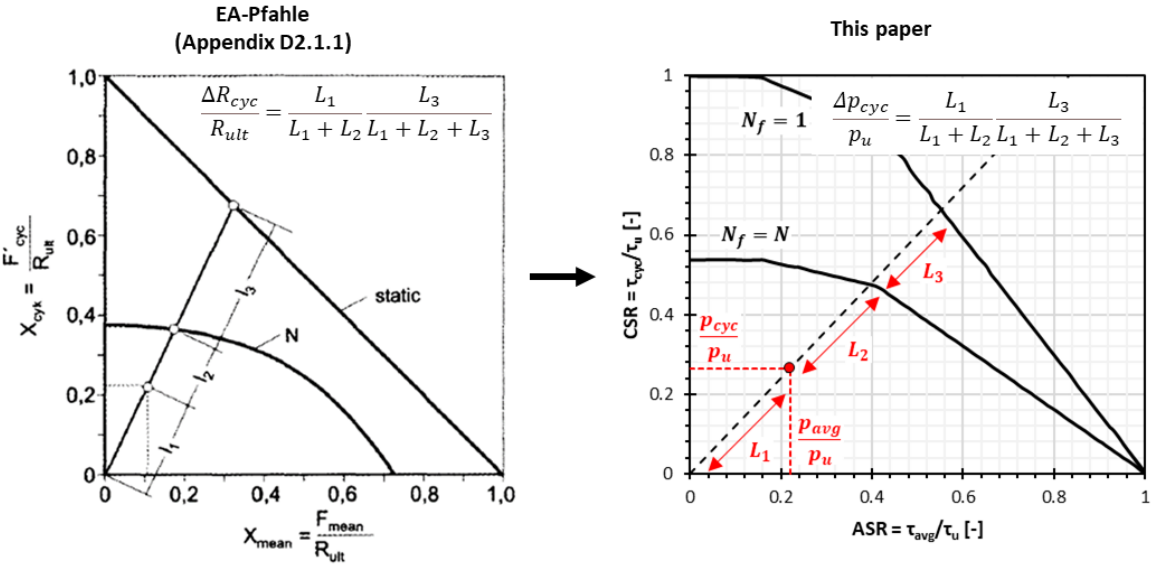

Figure 5-2. Summary of the calculation of step 3 – computation of cyclic degradation (right) and comparison to EA-Pfahle interaction diagram approach for pile axial cyclic loading (left).

In Appendix D2.2.1 of EA-Pfahle (DGGT, 2013), the axial cyclic degradation, ΔR_{cyc}, is calculated based on the ultimate capacity, R_{ult}, and the distances L_1, L_2 and L_3 measured directly on the interaction diagram as per equation (5.1) and as shown on the left of Figure 5-2. The ratio $L_3/(L_1+L_2+L_3)$ captures how much the pile cyclic capacity is reduced compared to the pile static capacity. The larger the ratio, the larger the cyclic degradation. The ratio $L_1/(L_1+L_2)$ captures how close the current load level is to cyclic failure. The cyclic degradation also increases with this ratio. This approach is very convenient and has a long track record for pile axial cyclic loading. Detailed explanations are provided in Appendix D2.2.1 of EA-Pfahle (DGGT, 2013).

$$\frac{\Delta R_{cyc}}{R_{ult}} = \frac{L_1}{L_1 + L_2} \frac{L_2}{L_1 + L_2 + L_3} \tag{5.1}$$

Hence for lateral loading, it is proposed to calculate cyclic degradation based on the average and the cyclic soil mobilisations (p_{avg}/p_u and p_{cyc}/p_u, respectively), the number of load cycles (N) and the cyclic failure contour diagram following the approach summarised on the right of Figure 5-2. The cyclic failure contour diagram plots the number of cycles to failure N_f as a function of the average stress ratio (ASR = τ_{avg}/τ_u) and the cyclic stress ratio (CSR = τ_{cyc}/τ_u). Following the analogy between the soil mobilisation (p/p_u) and the stress ratio (τ/τ_u) proposed in Jeanjean et al. (2017), the average and cyclic soil mobilisations can be plotted on the same diagram. In line with EA-Pfahle (DGGT, 2013), the reduction in distributed lateral reaction due to cyclic loading, Δp_{cyc} is computed based on, p_u, and the distances L_1, L_2 and L_3 measured directly on the cyclic failure contour diagram as per

equation (5.2). The cyclic degradation increases with the soil mobilisation and the number of cycles. The distance L_3 is measured relative to $N_f = 1$ rather than the static line. Hence, this approach adopts the convention that 1 single load cycle leads to no degradation.

$$\frac{\Delta p_{cyc}}{p_u} = \frac{L_1}{L_1 + L_2} \frac{L_2}{L_1 + L_2 + L_3} \tag{5.2}$$

The cyclic degradation is applied to the monotonic soil reaction curves as a p-multiplier computed as $1-\Delta p_{cyc}/p_u$. The p-multiplier affects both strength and stiffness (see section 5.5 and Figure 5-10). The cyclic degradation is applied to both the distributed lateral reaction (p-y curve), the distributed moment, the base shear and the base moment. If the PISA framework is used to generate the soil reaction curves, the normalised distributed moment curves in sand are not factored to avoid double counting.

The cyclic degradation is done independently at each discretisation depth which is convenient for layered soil. The same formulation applies to cohesive soil (clay) and to cohesion-less soil (sand).

With this formulation, there is no so-called "stable" zone (e.g. Jardine and Standing, 2012). Any instance of cyclic loading leads to some degree of degradation. However, at very small load level the soil mobilisation is minimal leading to very marginal cyclic degradation which will barely affect the monopile response.

5.1.4 Cyclic response

The pile response to lateral cyclic loading is computed by applying the lateral loads into a beam element solver with the cyclic soil reaction curves rather than monotonic soil reaction curves as shown in Figure 5-3. Looking at the load-displacement or the moment-rotation response at ground level, one can assess the accumulation of pile deflection and the reduction in pile lateral due to cyclic loading. The redistribution of stresses along the pile can also be assessed by looking at the change in shear force and bending moment profiles.

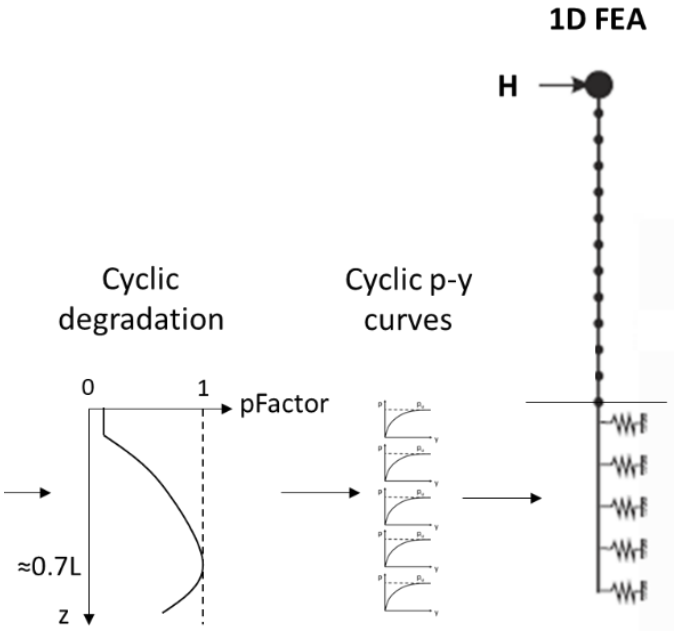

Figure 5-3. Summary of step 4 – computation of cyclic response

5.1.5 Superposition

One can use the approach presented in section 2.3 to track the effect of an increasing number of load cycles, but the approach is only valid for a single load level. However, the design cyclic load history for the design of monopile typically involves numerous load parcels with increasing load level. Hence, to account for the cumulative effect of the different load parcels, each load parcel is made equivalent to the next one until the entire load history is made equivalent to the last load parcel with the largest load.

A superposition model is required to define the "equivalence". Chapter 2 showed that the choice of the superposition model can greatly affect the cyclic response. The superposition model suggested in Chapter 2 is preferred over Leblanc et al. (2010b), Page et al. (2021) or EA-Pfahle (DGGT, 2013) since Chapter 4 showed it better matches experimental pile responses.

Figure 5-4 presents an example superposition procedure for a typical monopile design case. For convenience, the Leblanc (2010b) superposition model is used since its visualisation is simpler. The superposition model by Leblanc (2010b) assumes that the increase in rotation at ground level due to cyclic loading $\Delta\theta_{cyclic}(H,N) = \theta_{cyclic}(H,N) - \theta_{static}(H)$ remains constant at the end of a load parcel and at the beginning of the next one. In Figure 5-4, each colour line represents a different applied load amplitude and shows the increase in rotation due to cyclic loading for an increasing number of load cycles for that constant load amplitude. The black line shows the cumulative effect of over 20 loads parcels with over 60,000 cycles in total. For this example, this superposition procedure suggests that the entire load history is equivalent to about 30 cycles at the largest load level.

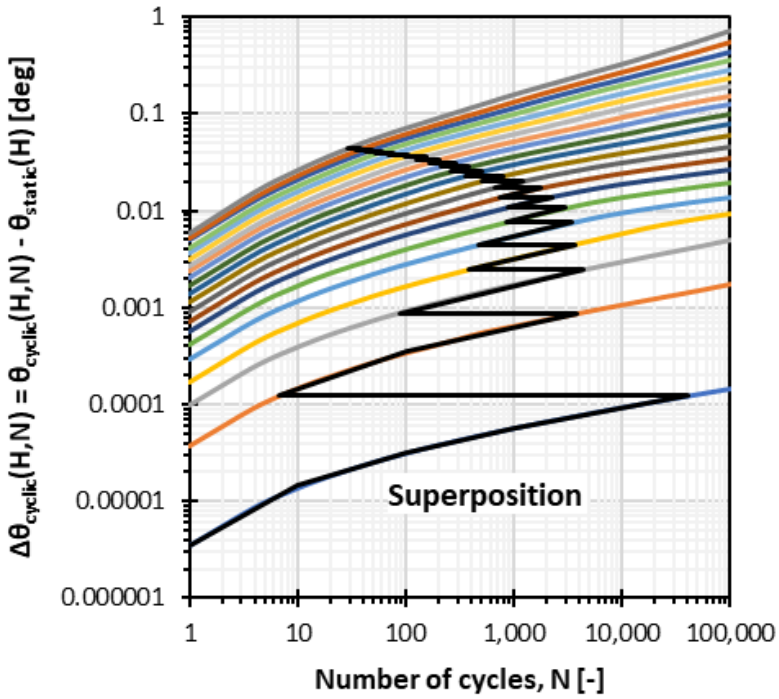

Figure 5-4. Example superposition procedure.

5.2 EXPERIMENTAL DATA FOR VALIDATION

This section provides a summary of the pile lateral field test data used to validate the proposed approach in sand and clay. The PISA medium-scale piles (D = 0.762 m) tested monotonically and cyclically at the Dunkirk and Cowden test sites are considered in this study.

5.2.1 Soil conditions

The conditions at both sites are presented comprehensively in Zdravkovic et al. (2020). The following briefly summarises the soil profiles and the main input parameters of this study.

The Dunkirk site consists of normally consolidated dense sand. The small strain shear modulus profile is reported in Figure 5-5a. A relative density of 100% is assumed for the top 3 m and 75% below. The soil unit weight equals 19.9 kN/m^3 above the water table and 17.1 kN/m^3 below. The water table is at 5.4 mBGL.

The Cowden site consists of over-consolidation low-plasticity glacial clay till. The profiles of small strain shear modulus, undrained shear strength and over-consolidation ratios are reported in Figure 5-5a, Figure 5-5b and Figure 5-5c, respectively. The soil unit weight equals 21.19 kN/m^3. The plasticity index averages 18%, except for the top 1 m reported with a plasticity index of 37%. The water table is at 1 mBGL.

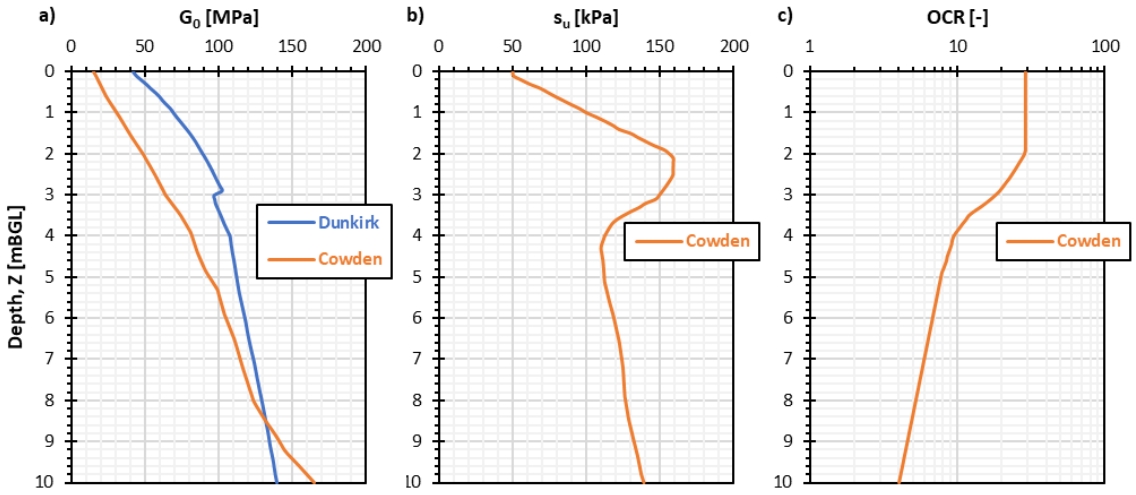

Figure 5-5. Profiles of small strain shear modulus (a), undrained shear strength (b) and over-consolidation ratio (c) at both sites (modified after Zdravkovic et al., 2020).

5.2.2 Pile geometries

Table 5-1 summarises the PISA field test used in this study.

Although the PISA field test campaign focused on pile response to monotonic lateral loading, few cyclic tests have been carried out as well. Piles DM2 and CM5 with a diameter of 0.762 m and a slenderness ratio (L/D, ratio of pile embedded length L over pile diameter D) of about 5.3 were the two main cyclic tests at the Dunkirk site and the Cowden site, respectively.

Hence, DM2 and CM5 are considered in this study to validate the cyclic prediction of the proposed model. Pile DM4 and CM9 which have a similar geometry as pile DM2 and CM5, respectively, are considered for the calibration of the monotonic response which is a key input to the cyclic model. In addition to DM4 and CM9, piles DM4, DM3, CM2 and CM3 are also considered for the monotonic calibration as they have the same diameter but smaller/larger pile penetration. This is to ensure the robustness of the monotonic calibration.

Table 5-1. Summary of PISA field tests used in this study.

Pile	D [m]	L [m]	t [mm]	e [m]	Note
DM7	0.762	2.2	10	10.0	Monotonic
DM4	0.762	4.0	14	10.0	Monotonic
DM2	0.762	4.0	14	10.0	Cyclic
DM3	0.762	6.0	25	10.0	Monotonic
CM2	0.762	2.2	10	10.0	Monotonic
CM9	0.762	4.0	11	10.0	Monotonic
CM5	0.762	4.0	11	10.0	Cyclic
CM3	0.762	7.6	25	10.0	Monotonic

5.2.3 Monotonic test results

The response of the piles to monotonic lateral loading is reported in terms of a load-displacement curve at ground level in Figure 5-6 after Byrne et al. (2020) for the Dunkirk (sand) tests and in Figure 5-7 after McAdam et al. (2020) for the Cowden (clay) tests. This is to carry the monotonic calibration and ensure accurate monotonic soil reaction curves are inputted to the cyclic model.

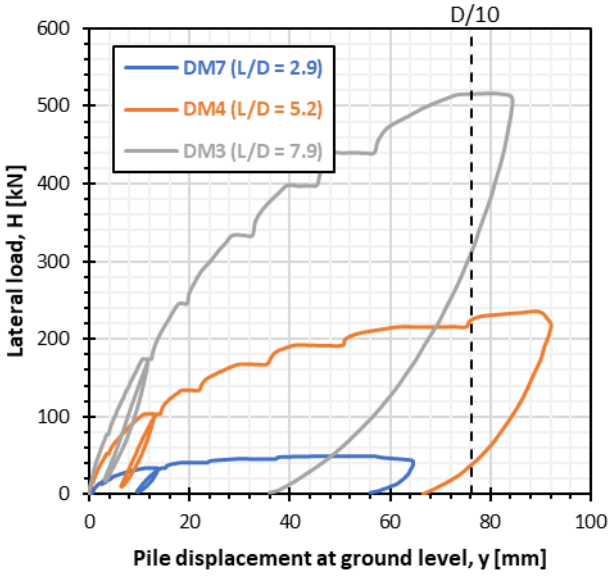

Figure 5-6. Monotonic lateral response at ground level of piles DM7, DM4 and DM3 (modified after Byrne et al., 2020).

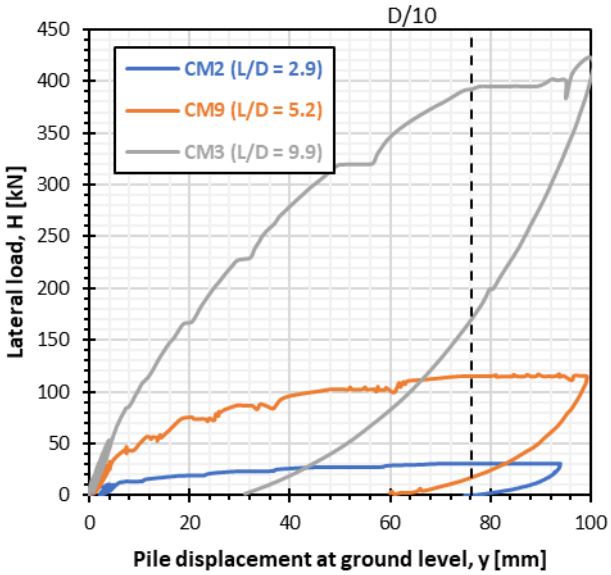

Figure 5-7. Monotonic lateral response at ground level of piles DM7, DM4 and DM3 (modified after McAdam et al., 2020).

5.2.4 Cyclic test results

The response of the piles to cyclic lateral loading is reported in terms of the relative rotation versus the number of cycles after Beuckelaers (2017) for piles DM2 and CM5 in Figure 5-8

and Figure 5-9, respectively. For a given load set, the relative rotation is defined as the difference between the pile ground level rotation after the first cycle and after N cycles. The relative rotation increases with the number of cycles and the load magnitude. In Figure 5-8 and Figure 5-9, each colour line represents a different load set. The pile cyclic response is used to validate the cyclic model.

The cyclic loading sequence applied to DM2 is summarised in Table 5-2. Over 27,000 cycles were applied across 5 load sets with loads ranging from 10 kN to 160 kN. The lateral loads are applied at an eccentricity of 10 m above ground level. Hence, overturning moments up to 1,600 kN.m were applied during the test. Assuming DM2 exhibits the same ultimate reaction as DM4 (same soil profile, same pile geometry), the loads applied represent 4% to 68% of the ultimate capacity. All cyclic loads were applied one-way ($\zeta_c=H_{min}/H_{max}=0$**).**

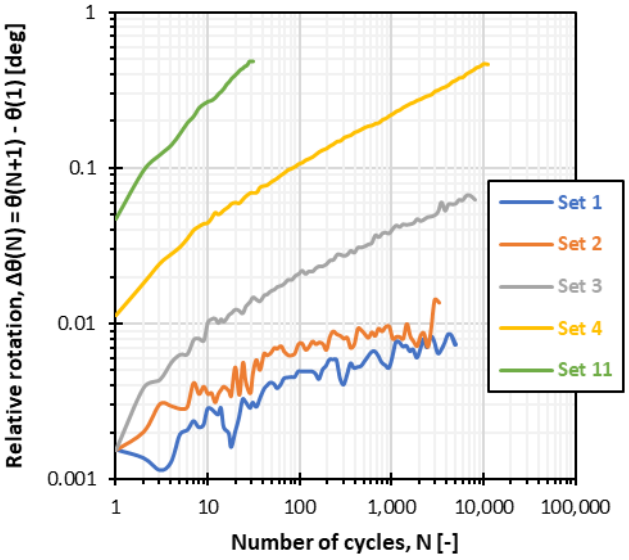

Figure 5-8. Cyclic response of pile DM2 (modified after Beuckelaers, 2017).

Table 5-2. Cyclic loading sequence applied to DM2.

Set	N [-]	H [kN]	ζ_b [%]	ζ_c [%]
1	5,100	10	4	0
2	3,300	20	8	0
3	8,100	40	17	0
4	11,110	80	34	0
11	31	160	68	0

The cyclic loading sequence applied to CM5 is summarised in Table 5-3. Over 16,000 cycles were applied across 4 load sets with loads ranging from 10 kN to 90 kN. The lateral loads are applied at an eccentricity of 10 m above ground level. Hence, overturning moments up to 900 kN.m. Assuming CM5 exhibits the same ultimate reaction as CM9 (same soil

profile, same pile geometry), the loads applied represent 9% to 78% of the ultimate capacity ($\zeta_b = H_{max}/H_{ult}$). All cyclic loads were applied one-way ($\zeta_c = H_{min}/H_{max} = 0$).

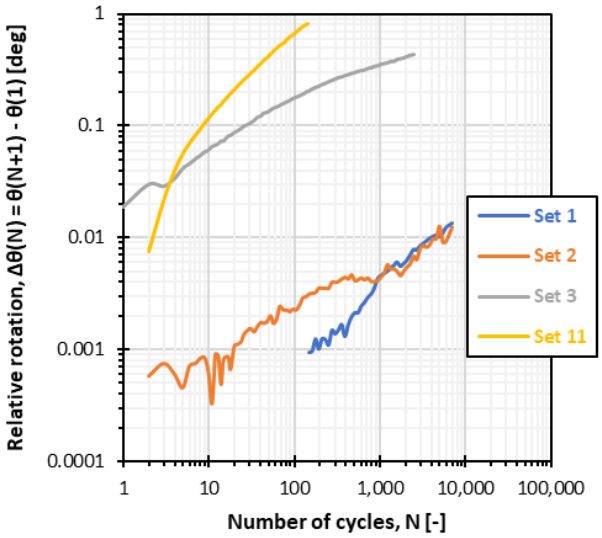

Figure 5-9. Cyclic response of pile CM5 (modified after Beuckelaers, 2017).

Table 5-3. Cyclic loading sequence applied to CM5.

Set	N [-]	H [kN]	ζ_b [%]	ζ_c [%]
1	7,000	10	9	0
2	7,000	20	17	0
3	2,500	60	52	0
11	145	90	78	0

5.3 CALIBRATION OF THE MONOTONIC RESPONSE

The PISA rule-based approach (after Burd et al., 2020 in sand and after Byrne et al., 2020 in clay) fails to capture the response of the piles to monotonic loading although the depth variation functions were calibrated based on these exact same tests. This is due to the diameter difference between the field tests ($D \leq 2$ m) and the 3-dimensional finite-element models used for calibration ($D \geq 5$ m). Hence, p- and y- multipliers are introduced to scale the PISA rule soil reaction curves and improve the match with the experimental monotonic response. A similar procedure was previously adopted by Beuckelaers (2017) and Balaam (2020).

Figure 5-10 presents the effects of the p- and y- multipliers on the shape of the soil reaction curves. The p-multiplier scales the y-axis, affecting both strength and stiffness, while the y-multiplier scales the x-axis, only affecting the stiffness. A p-multiplier larger than 1 makes the soil reaction curve stiffer and increases the plateau of ultimate reaction. A p-multiplier smaller than 1 causes the opposite effects. On the contrary, a y-multiplier larger than 1 makes the soil reaction curves softer while a y-multiplier smaller than 1 makes it stiffer.

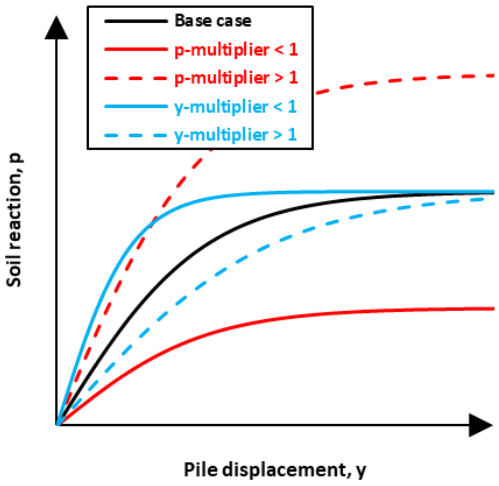

Figure 5-10. Effects of p- and y- multipliers on the shape of the soil reaction curves.

The p- and y- multipliers are applied to all soil reaction curves: p-y curves, distributed moment, base shear, and base moment. In sand, the p- and y- multipliers are not applied to the distributed moment to avoid double accounting given the distributed moment is de-normalised by the lateral reaction which is already factored.

The Trinity College Dublin one-dimensional finite-element solver is used to optimize the set of p- and y- multipliers to minimize the root mean squared error between the experimental and simulated pile response. At each site, the 3 piles are optimised simultaneously to get a robust calibration suitable for a range of pile penetrations.

5.3.1 Results of the calibration at the Dunkirk site

Figure 5-11 provides a comparison of the experimental and the simulated pile monotonic responses based on the PISA rule-based approach (Burd et al., 2020). The comparison is provided for piles DM7 (L/D = 2.9), DM4 (L/D = 5.2) and DM3 (L/D = 7.9), in Figure 5-11a, Figure 5-11b and Figure 5-11c, respectively. PISA rule largely underestimates both initial stiffness and ultimate reaction across all pile penetrations.

After optimisation, the set of p- and y- multipliers reported in Table 5-4 is found to lead to a very satisfactory match with the initial stiffness and the ultimate reaction across all pile penetrations. Different multipliers are applied above and below 3 m due to the change in relative density and small strain shear modulus observed in the soil profile at the Dunkirk site.

Table 5-4. Calibrated set of p- and y- multipliers for the Dunkirk tests.

Depth, Z	p-multiplier [-]	y-multiplier [-]
< 3 mBGL	1.39	0.82
> 3 mBGL	2.42	0.67

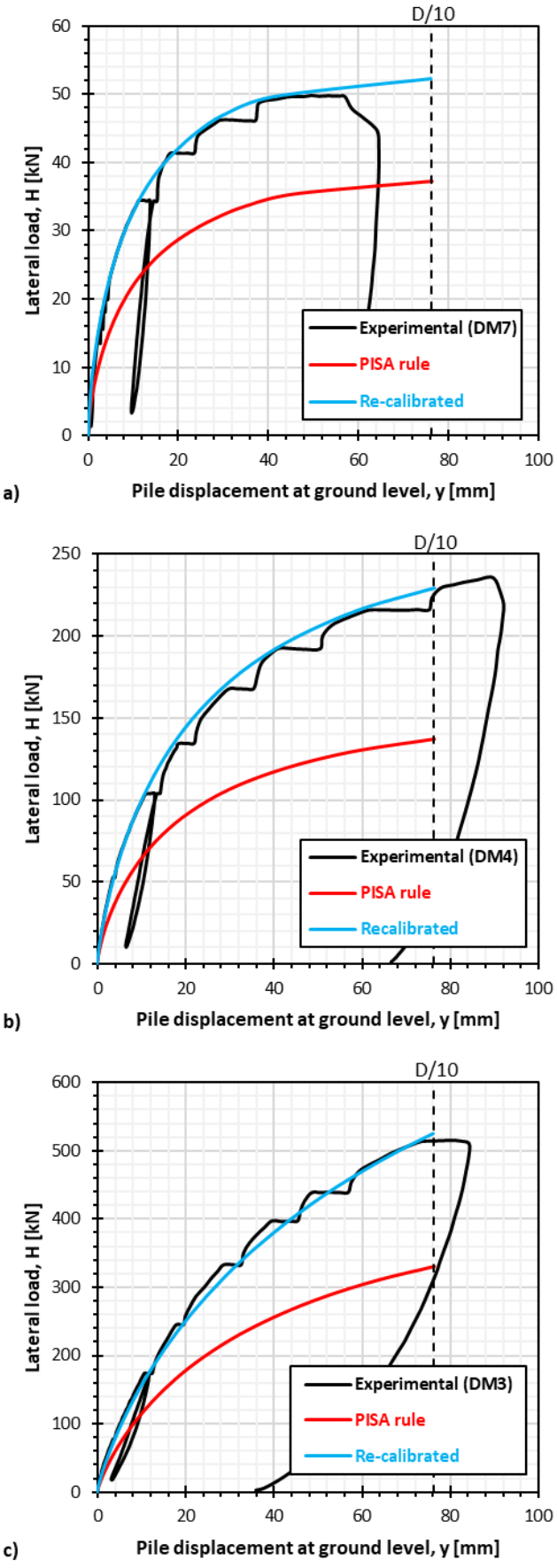

Figure 5-11. Results of the monotonic calibration compared to the experimental response of piles DM7 (a), DM4 (b) and DM3 (c).

5.3.2 Results of the calibration at the Cowden site

Figure 5-12 provides a comparison of the experimental and the simulated pile monotonic responses based on the PISA rule-based approach (Byrne et al., 2020). The comparison is provided for piles CM2 (L/D = 2.9), CM9 (L/D = 5.2) and CM3 (L/D = 9.9), in Figure 5-12a, Figure 5-12b, and Figure 5-12c, respectively. PISA rule generally overestimates the ultimate reaction.

This finding is in line with the trend reported by Byrne et al. (2020): the cases with D = 5 m overestimate stiffness and capacity while cases with D = 10 m underestimate both. The behaviour of CM3 is different due to the large L/D (about 10), outside of the calibration space (2 < L/D < 6). This is causing some of the depth variation functions (k_p, n_{Mb}, M_{bu}) to turn negative. Hence, CM3 is not considered in the monotonic calibration process.

After optimisation, the set of p- and y- multipliers reported in Table 5-5 is found to lead to a very good match with initial stiffness and ultimate reaction across all pile penetrations. The change of calibration parameters at 1 mBGL coincides with the change in plasticity index and the depth of the water table as reported by Zdravkovic et al. (2020).

Table 5-5. Calibrated set of p- and y- multipliers for the Cowden tests.

Depth, Z	p-multiplier [-]	y-multiplier [-]
< 1 mBGL	0.50	0.93
> 1 mBGL	0.94	0.90

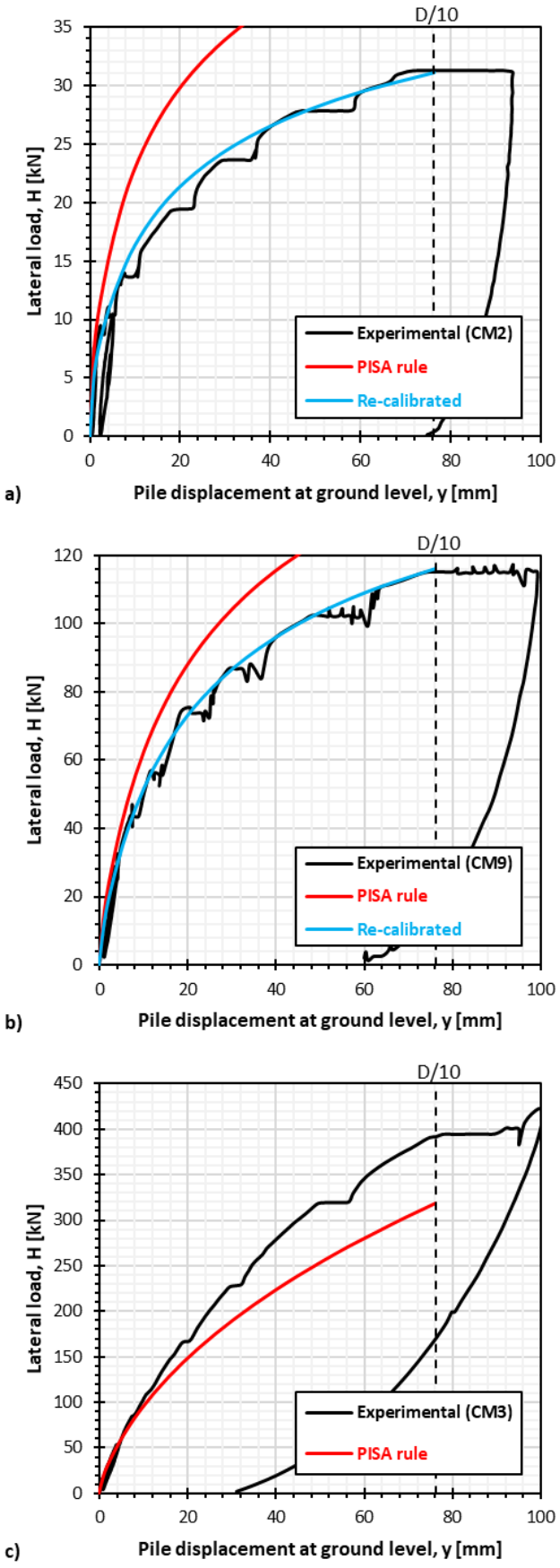

Figure 5-12. Results of the monotonic calibration compared to the experimental response of piles CM2 (a), CM9 (b) and CM3 (c).

5.4 DERIVATION OF CYCLIC CONTOUR DIAGRAMS

Soil cyclic failure contour diagrams are a key input to the cyclic model proposed in this Chapter. Due to the lack of site-specific contour reported in the original PISA ground characterisation (Zdravkovic et al., 2020), the contours for the validation exercise are scaled from the database reported in Andersen (2015) following the approach recommended in Andersen et al. (2023). This section summarises the procedure and presents the resulting diagrams for both sites (Dunkirk and Cowden).

5.4.1 Cyclic contour diagrams for the Dunkirk site

The failure contour diagrams considered for the Dunkirk site are coming from a database of DSS tests on normally consolidated sand and silt with different average shear stresses (τ_{avg}) applied drained (Figure 12.16 in Andersen, 2015). The cyclic shear stresses (τ_{cyc}) were applied at a much faster rate and considered undrained. Five diagrams are reported in Andersen (2015) and labelled A, B, C, D, and E. They are representative of cyclic shear strengths $(\tau_{cyc,f}/\sigma'_{ref})_{N=10}$ for τ_{avg} = 0 of 0.19, 0.25, 0.60, 1.00 and 1.80, respectively.

The cyclic shear strength can be estimated from the relative density as per Figure 5-13 and after Andersen (2015). At the Dunkirk site, the top 3 m are reported with a relative density of 100% which leads to a cyclic shear strength of 1.20, making diagram D (Figure 5-14a) the most representative. Below, with a relative density reported at 75%, the cyclic shearing strength is estimated at 0.24 and diagram B (Figure 5-14d) is selected.

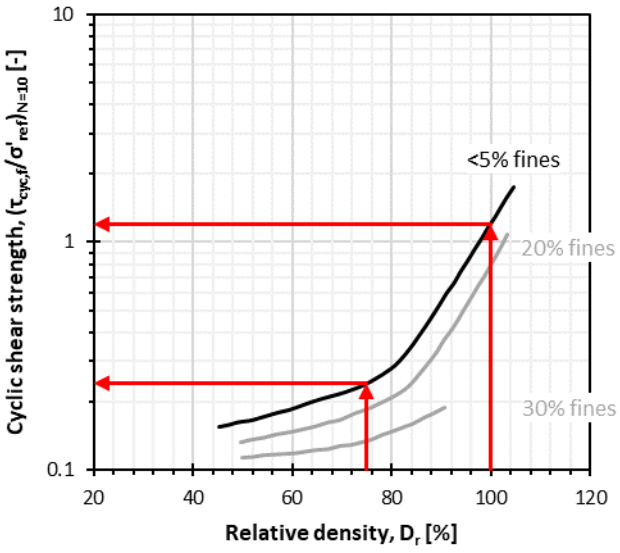

Figure 5-13. Cyclic shear strength as a function of relative density (modified after Andersen, 2015).

After being selected, the diagrams are scaled to the site-specific conditions (see Figure 5-14b and Figure 5-14e). Firstly, the X-axis is scaled to adjust the diagram to the correct drained static shear strength calculated as per equation (5.3) after Andersen et al (2023). For

relative densities of 100% and 75%, tan α' equals 0.97 and 0.8, respectively. Where tan α' = τ_u/σ'_{ref} is the drained static shear strength. Then, the Y-axis is scaled to adjust the cyclic shear strength at 10 cycles with the cyclic shear strength calculated in Figure 5-13. Following the approach suggested by Andersen et al. (2023), the Y-axis should also be scaled to account for the over-consolidation ratio. However, this is not required here since the site is reported as normally consolidated (OCR = 1).

$$\tan\alpha' = \tan(0.21RD + 23) \tag{5.3}$$

In order to make the diagrams compatible with the approach detailed in section 5.2, the axes are normalised so that the stresses are expressed in terms of τ/τ_u rather than τ/σ'_{ref} (see Figure 5-14c and Figure 5-14f). At the Dunkirk site, the water table is located below the tip of DM2, hence the tests are fully drained. Therefore, the ultimate shear stress (τ_u) is defined as τ_u/σ'_{ref} = tan α' (which correspond to the drained static shear strength) for the X-axis. For the Y-axis, the shear strength reported in the contour diagrams are for undrained conditions and are much different than the shear strength reported for drained conditions on the X-axis. Given the cyclic loading is fully drained, τ_u/σ'_{ref} is set a $(\tau_{cyc,f}/\sigma'_{ref})_{N=1}$ for the Y-axis to ensure both X-axis and Y-axis are consistently representative of drained conditions. This normalisation might not be applicable to an offshore site where undrained conditions might be expected due to the rate of cyclic loading.

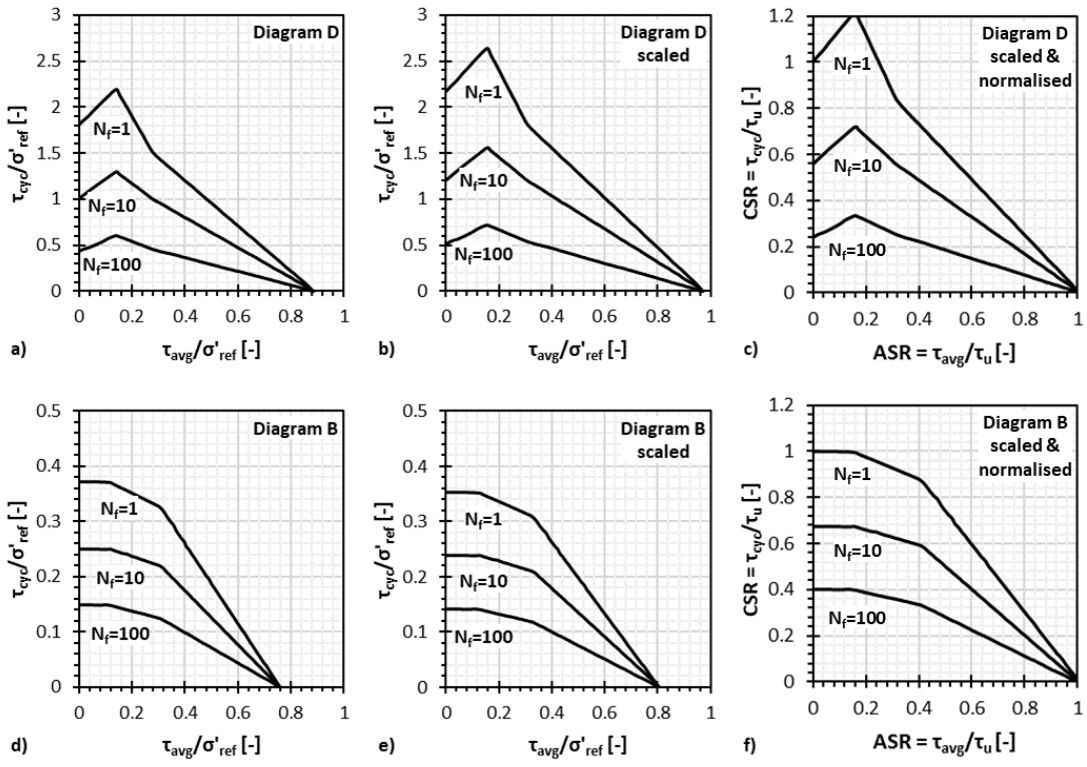

Figure 5-14. Cyclic failure contour diagrams for the Dunkirk site: (a), (b) and (c) for the top 3 m (relative density of 100%) and (d), (e) and (f) below (relative density 75%). Figures (a) and (d) are the generic diagrams, figures (b) and (e) are scaled to the site-specific conditions and figures (c) and (f) are normalised.

5.4.2 Cyclic contour diagrams for the Cowden site

For the Cowden site, the DSS cyclic contour diagrams reported by Andersen et al. (1988) for Drammen clay with OCR of 1, 4 and 40 are considered. These contour diagrams are less relevant for Cowden Glacial Till than the cyclic triaxial results reported in Ushev and Jardine (2020). However, the results obtained with Drammen clay were deemed satisfactory and have the benefit of presenting the contour diagram scaling approach in clay.

The OCR at the Cowden site reduces from above 29 at ground level down to about 4 at 10 mBGL. The diagram for OCR = 40 is used from 0 to 3.5 mBGL, and the diagram for OCR = 4 is used below. The diagrams in Andersen et al. (1988) are presented for a default plasticity index of 27%.

After being selected, the diagrams are scaled to the site-specific conditions following the approach presented by Andersen et al. (2023). No scaling is applied to the X-axis. The Y-axis is scaled to account for the actual OCR and account for the plasticity index. Figure 5-16 presents example diagrams for the first top 1 m at the Cowden site. The generic diagram in Figure 5-16a is scaled to Figure 5-16b to account for the actual OCR of 29 and PI of 37% representative of the first 1 m at Cowden. Below, PI of 18% is considered with the OCR profile presented in Figure 5-15c.

No further normalisation is required given all the diagrams are already plotted in terms of τ/τ_u where $\tau_u = s_u$.

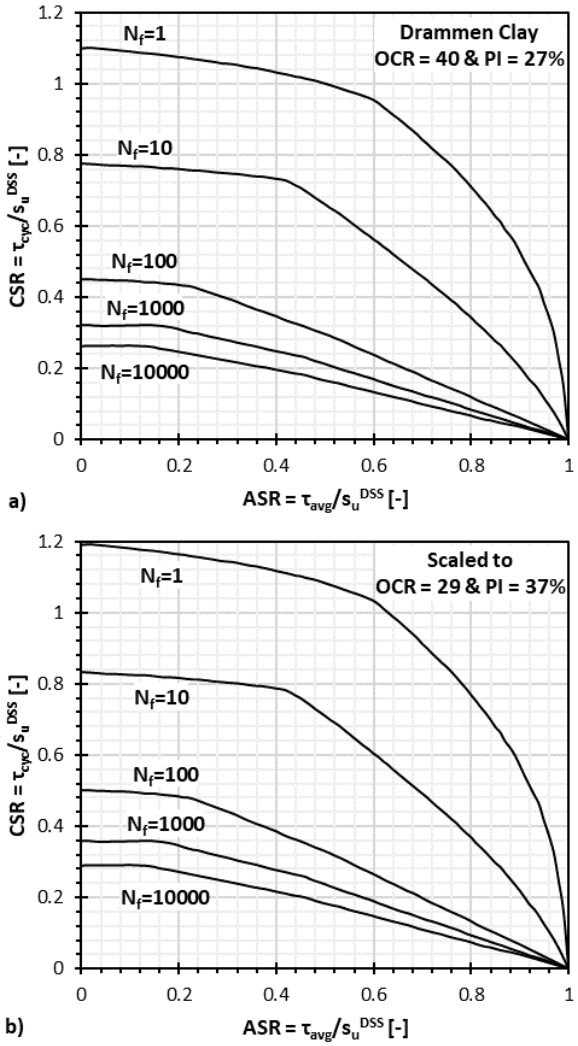

Figure 5-16. Example of cyclic contour diagrams for the Cowden site for the first top 1 m. (a) Generic diagram for OCR = 40 and PI = 27%. (b) Scaled diagram for OCR = 27 and PI = 37%.

5.5 RESULTS

This section presents the comparison of the experimental cyclic response of piles DM2 (at the Dunkirk site, in sand) and CM5 (at the Cowden site, in clay) to the predictions made by the model proposed in this Chapter. This is to showcase the capability of the model in both sand and clay.

5.5.1 Comparison to experimental response in sand

Figure 5-17 shows the comparison of DM2 experimental cyclic response to the cyclic model proposed in this Chapter. The cyclic response is plotted in terms of the relative rotation at ground level versus the number of cycles. Each coloured line represents the effect of one cyclic load set. For a given load set, the relative rotation is defined as the difference between the pile ground level rotation after the first cycle and after N cycles. Five cyclic load sets were modelled with lateral load increasing from 10 kN for set 1 to 160 kN for set 11. The

full lines represent the experimental response, and the dashed lines represent the response predicted by the model proposed in this Chapter.

Figure 5-17 shows that the model provides a very satisfactory match with the experimental. The effects of the number of cycles and load magnitude are properly captured for all load sets. Only Set 1 is slightly off. However, it is assumed that this is due to inaccuracies of the experimental data because the loads applied during set 2 were twice larger than set 1 so set 1 should show less accumulation of rotation.

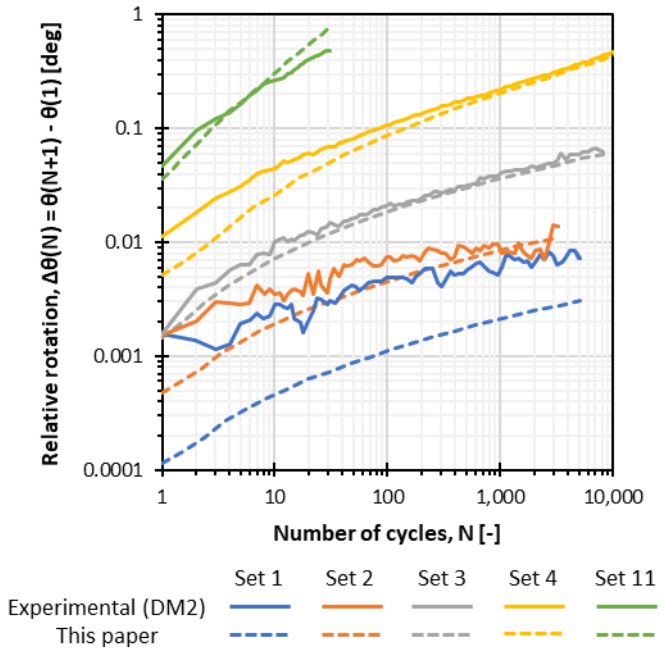

Figure 5-17. Comparison of DM2 experimental cyclic response to the cyclic model proposed in this Chapter.

To put the previous comparison in perspective, the same DM2 experimental response is also compared to Leblanc et al (2010a; 2010b) cyclic macro-element model in Figure 5-18. The macro-element model by Leblanc et al (2010a; 2010b) is based on laboratory pile cyclic lateral tests for sand conditions similar to the Dunkirk site. Macro-element models are typically used by engineers at early stage of monopile design to estimate the accumulation of rotation upon cyclic loading as recommended in CFMS (2020).

Figure 5-18 shows that Leblanc et al (2010a; 2010b) model, although popular in the industry, does not capture the experimental pile cyclic response well. The macro-element model underestimates the relative rotation, especially at low number of cycles and for the largest load set. The predicted response for set 1 cannot be plotted on a log scale because this macro-element model predicts no accumulation of rotation ($\Delta\theta = 0$) for loads less than 5.5% of the ultimate capacity.

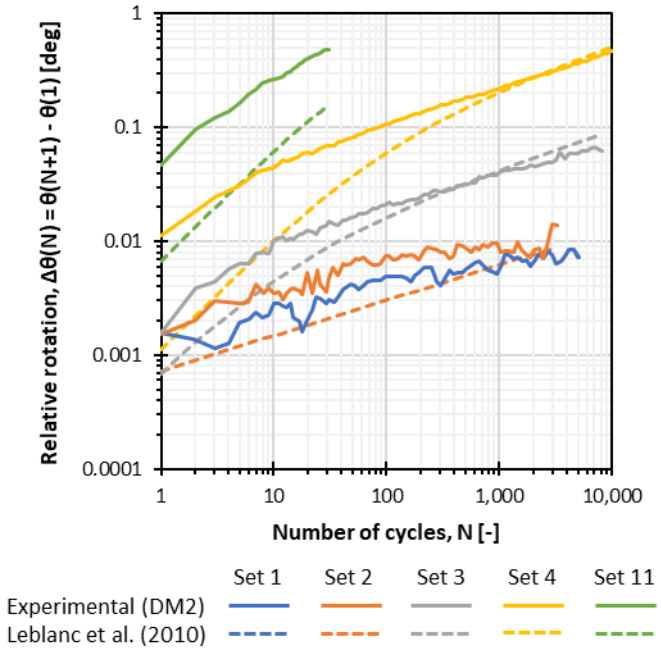

Figure 5-18. Comparison of DM2 experimental cyclic response to the cyclic model proposed by Leblanc et al. (2010).

Further results are presented in Figure 5-19 where soil mobilisation (a), cyclic degradation (b) and bending moment (c) profiles along the pile embedded length are plotted. The example results are provided for pile DM2 under set 4 (H = 80 kN) with the number of cycles applied ranging from 1 to 10,000. These example results are presented to demonstrate that:

- Unlike the cyclic degradation recommended by API (2014) for sands which does not account for the number of cyclic or the load magnitude, the model presented in this Chapter accounts for both. The cyclic degradation reported in Figure 5-19b is proportional to the soil mobilisation reported in Figure 5-19a and increases (decreasing p-multiplier means higher degradation) with the number of cycles. The soil mobilisation and cyclic degradation are maximum at shallow depth, then decrease to a minimum close when close to the point of rotation (found at 2.5 m ≈ 0.63L) before increasing again until pile toe.
- Unlike macro-element models which can only track the ground-level response of the pile upon cyclic loading, the model proposed in this Chapter can be used to capture the effect along the entire pile embedded length. Figure 5-19c shows how the bending moment profile is affected by cyclic loading. As the number of cycles increases, the depth and magnitude of the maximum bending moment increases. This is in line with observations reported by Puech and Garnier (2017) and can be critical for monopile structural design.

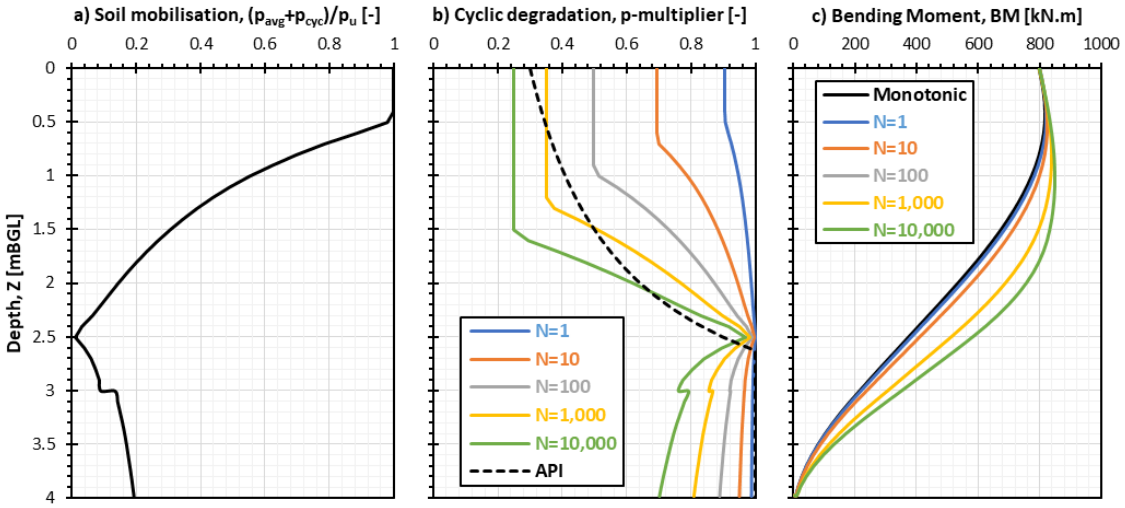

Figure 5-19. Example results for DM2 set 4 (H = 80 kN) with N ranging from 1 to 10,000 presented in terms of a) soil mobilisation, b) cyclic degradation and c) bending moment profiles along pile embedded length.

It should be noted that the cyclic degradation is applied as a p-multiplier, which not only affects the stiffness of the soil reaction curves but also their ultimate reaction. This is consistent with the API cyclic p-y curves formulation (API, 2014) and EA-Pfahle (DGGT, 2013). However, the application of a large reduction in ultimate reaction (p-multiplier as low as 0.25 show in the example on Figure 5-19b) might lead to a large reduction in pile lateral capacity after cyclic loading. This is not supported by experimental results in the literature, which instead suggests that the pile lateral capacity is not significantly affected by cyclic loading. To overcome this shortcoming, the superposition approach presented in section 5.1.5 should be adopted to compute the post-cyclic lateral capacity when the lateral loads are ramped up.

5.5.2 Comparison to experimental response in clay

Figure 5-20 shows the comparison of CM5 experimental cyclic response to the cyclic model proposed in this Chapter. The cyclic response is plotted in terms of relative rotation at ground level versus number of cycles. Each coloured line represents the effect of one cyclic load set. For a given load set, the relative rotation is defined as the difference between the pile ground level rotation after the first cycle and after N cycles. Four cyclic load sets were modelled with lateral load increasing from 10 kN for set 1 to 90 kN for set 11. The full lines represent the experimental response, and the dashed lines represent the response predicted by the model proposed in this Chapter.

Figure 5-20 shows that the model provides a very satisfactory match with the experimental results. The effect of the number of cycles and load magnitude is properly captured for all load sets. Again, only set 1 seems off but it is assumed that this is suggested to be due to inaccuracies of the experimental data at extremely low rotations. The loads

applied during set 2 were twice larger than set 1 so set 1 was expected to show less accumulation of rotation.

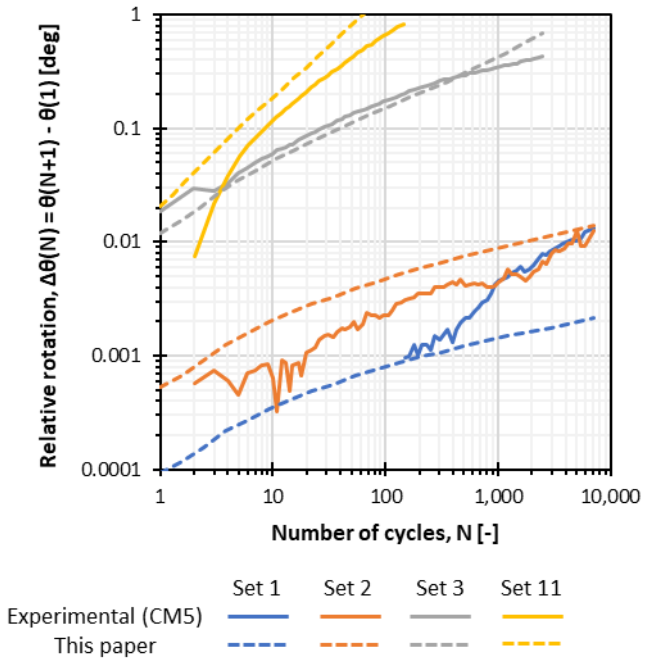

Figure 5-20. Comparison of CM5 experimental cyclic response to the cyclic model proposed in this Chapter.

5.6 DISCUSSION

Section 6 showed that the cyclic model presented in this Chapter offers an excellent match with PISA cyclic experimental data in both sand and clay. However, the piles DM2 and CM5 have a slenderness ratio of 5.5 (L/D, ratio of embedded length, L, to diameter, D). This was representative of monopile design at the time of the project but monopiles have grown in diameter since then and are typically designed with slenderness ratios closer to 3 now. This limitation motivated the experimental pile field tests presented in Chapters 3 and 4.

Figure 5-21 presents the experimental cyclic response of pile L1 (L/D = 2.2) as reported in Chapter 4 compared to the predictions made by the model proposed in this Chapter. Five load sets were applied for a total of 3,669 cycles and with loads ranging from about 10% to 65% of the pile ultimate capacity. The results are presented in terms of relative displacement at ground level (instead of relative rotation previously). Again, the model from this Chapter is found to capture relatively well the accumulation of displacement with number of cycles for a range of load magnitude. The small mismatches are attributed to the relatively poor preliminary monotonic calibration which will be improved in the future before further publications. This comparison still suggests that the model is adequate to predict the accumulation of pile displacement of short piles upon cyclic loading.

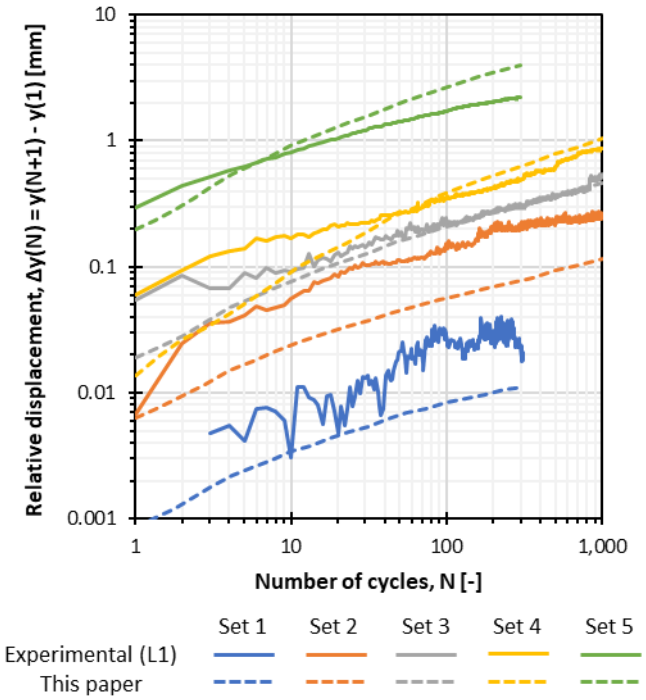

Figure 5-21. Comparison of L1 experimental cyclic response to the cyclic model proposed in this Chapter.

5.7 CONCLUSION

A new cyclic model for the design of monopiles supporting offshore wind turbines is presented in this Chapter. The methodology consists of the degradation of monotonic soil reaction curves to account for cyclic loading. The cyclically degraded soil reaction curves can then be fed into a beam element solver to predict the pile lateral response to cyclic loading. The magnitude of the cyclic degradation is based on the soil mobilisation, the number of cycles and the soil cyclic contour diagrams. This model is inspired by an approach for pile axial cyclic loading recommended by EA-Pfahle. This is due to the similarities between the pile axial interaction diagrams and the soil cyclic failure contour diagrams.

The approach is validated against PISA field tests in sand and clay as well as recent field tests carried out by TCD at the Blessington test site. The details of the calibration of the monotonic soil reaction curves and the derivation of the cyclic contour diagram for the PISA sites are provided. It is shown that the approach predicts well the accumulation of both pile ground level displacement and rotation in both sand and clay for pile slenderness ratio (L/D) ranging from 2.2 to 5.25.

This approach can be a good option for monopile design because:

- The validation range covers the current monopile design practices (L/D ranging from 2.2 to 5.25)

- It accounts for site specific data. At an advanced stage of design, the results of in-situ and laboratory tests can be used to derive the monotonic soil reaction curves and cyclic contour diagrams
- It can still be used at an early stage of design based on generic monotonic soil reaction curves (such as PISA rule) and cyclic contour diagrams (following Andersen et al., 2023 approach)
- The same formulation is adopted for cohesive and cohesion-less soils which makes it convenient for layered soils as typically encountered offshore. Complex layering can be analysed as the degradation is computed at each discretisation depth along the pile embedded length.
- Unlike API recommended cyclic degradation, it can capture the effect of the load magnitude and the number of cycles.
- Unlike macro-element models, it is not limited to the prediction of ground-level response and so it can be used for structural design as well
- It runs much faster than 3D FEA based approaches making it possible to optimise the design across an entire wind farm

Future work will look at further validating the approach in sand and clay based on recently carried field tests as well as experimental results reported in the literature. The cyclic degradation is currently applied as a strength degradation, consistently with API (2014) and EA-Pfahle (DGGT, 2013). However, experimental results suggests that the pile lateral capacity is not significantly affect by cyclic loading. Hence, the approach might be updated in the future to apply the cyclic degradation as a stiffness degradation rather than strength degradation. The current approach is relatively simpler and hence limited. It does not explicitly account for drainage conditions, rate effects or gapping. Rate effects and drainage conditions are accounted for indirectly by the provided cyclic contour diagrams.

(intentionally left blank)

Chapter 6: Conclusion

This thesis is a summary of research undertaken in partnership with Trinity College Dublin and Gavin and Doherty Geosolutions to enable better optimisation of offshore wind turbine foundation design for a safe and more sustainable future. Although significant work has also been carried out on the monotonic lateral response of monopiles, the thesis focuses on the development of advanced numerical models capturing the effect of cyclic loading. The work is based on experimental data from the literature as well as a new field test campaign carried at the Blessington test site, presented in the thesis.

The four main contributions presented in the thesis are:

1. A new set of monotonic and cyclic lateral field tests on low slenderness piles.
2. A new superposition model to account for the multi-amplitude cyclic loading conditions experienced offshore.
3. The validation for short piles of the CPT based correlations of HS-small parameters recently developed by Trinity College Dublin.
4. A new contour diagram-based model to account for the effect of cyclic loading on monopile lateral response

In addition, this work has led to many publications which are not all discussed in the main body of the thesis. These are attached as appendices for references.

Finally, as an industry-based research project, the work presented in this thesis has already been applied to approximately 30 offshore foundation design projects all over the world. From conceptual to detailed design, all the development mentioned above have allowed significant cost savings to be achieved for offshore wind foundation design.

6.1 FIRST CONTRIBUTION

The first contribution relates to a new set of monotonic and cyclic lateral field tests on low slenderness piles. The aim of this experimental campaign was to extend the database available in the literature to lower pile slenderness ratios, which are more representative of current monopile design practices. Six piles with an outer diameter of 457 mm and penetration ranging from 1 m to 2 m have been tested in dense sand at the Blessington test site, located 25 km south to Dublin. The piles were subjected to both monotonic and lateral

loading, applied at an eccentricity of about 3 times the diameter above ground level to be representative of offshore conditions. The piles were instrumented with linear variable differential transducers and inclinometers at ground level. The results of both monotonic and cyclic tests are reported.

This experimental campaign has proven to be particularly challenging due to the COVID restrictions, the weather conditions, the availability of contractors, the limited accessibility of the test site, the occurrences of equipment breakdowns (especially with the hydraulic loading system), and the theft of equipment left overnight. The campaign lasted over 2.5 years and represents most of the work done during the project.

The processing of such large amount of data was challenging as well. The inclinometers were found particularly sensitive to the dynamic pile response when unloading and reloading (cyclic loading) and to the temperature changes, despite efforts made to protect the sensor from direct sunlight. Unfortunately to date, the inclinometers data could not be corrected for the cyclic tests.

In this thesis, most of the work is focused on the accumulation of pile displacement upon cyclic loading. This relates to one of the main geotechnical design checks required by DNV (2021) and it is critical for monopile design. Additionally, valuable data relating to the change in unloading-reloading stiffness due to cyclic loading is also provided. This may prove to affect the natural frequency of the structure significantly and can be critical for monopile design as well. However, this has not been the focus in this thesis.

The aim of this new experimental campaign was to extend the existing database to lower slenderness ratio (L/D). Piles with slenderness ratio as low as 2.2 were tested. It was shown that such short piles exhibit a brittle behaviour. However, none of the current approaches could capture such significant post peak softening. The short pile failed well before the D/10 displacement limit typically employed for monopile design, at a rotation of 2 degrees. All these findings should be carefully taken into account when designing monopiles will low slenderness ratio.

Additional information will be made available in the future by the research group at Trinity College Dublin as soil samples were collected at the Blessington site to carry advanced laboratory tests to supplement the CPTs.

6.2 SECOND CONTRIBUTION

A new superposition model to account for the multi-amplitude cyclic loading conditions experienced offshore. Although not widely studied in the literature, the superposition model was found to greatly influence the predictions of monopiles response

to realistic cyclic loading. A new superposition model was proposed based on observations from the PISA field tests. The new superposition model was found to match with the recent field tests at Blessington much better than any other superposition model suggested in the literature.

Although this superposition model offers a convenient way to account for multi-amplitude loading and was found to match pretty well with experimental data, it is highly empirical and might not be appropriate for other site and/or loading conditions.

The creation of a robust and holistic superposition model is particularly challenging as it would require the knowledge of both the monotonic and the cyclic pile response for the exact same conditions. This is very challenging experimentally due to inherent soil variability and experimental uncertainty. However, this might be possible numerically with an advanced soil constitutive models, able to accurately capture the cyclic and post cyclic response, and properly calibrated. SANISAND-MS recently made available in Plaxis 3D might be a good candidate, but this was not investigated in this thesis.

The focus was put on the superposition model, but the framework presented in this thesis also shows the importance of the unloading model. Capturing accurately the unloading stiffness after cyclic loading is also critical for monopile design since current design criteria applies to the unloaded accumulated rotation. Again SANISAND-MS might be a good candidate to study this aspect numerically

6.3 THIRD CONTRIBUTION

The validation for short piles of the CPT based correlations of HS-small parameters recently developed by Trinity College Dublin. This approach offers a simple, consistent and accurate approach to derive all the required soil constitutive model input parameters for three-dimensional finite-element analysis of monopiles. This approach was found to offer excellent predictions of the new lateral monotonic field tests on short piles in dense sand carried at Blessington.

This set of CPT correlations has allowed for accurate blind predictions which were critical for the success of the experimental campaign. Accurate blind predictions are required to correctly size the loading system as well as define the different load level for the cyclic tests.

To date, this set of CPT based correlations has only been tested and validated against medium scale field tests. Additional validation against centrifuge tests might be required to bring confidence in the approach prior to offshore applications.

As vibro-driving is starting to be a popular alternative to impact-driving to reduce the driving fatigue or comply with stricter environmental regulations, the effect of pile installation on the CPT correlations and pile response should be investigated. All piles considered for the validation of this approach so far were impact driven.

Finally, the derivation of soil reaction curves from 3D FE analyses is not straightforward. Although the PISA numerical based framework is available in the commercially available Plaxis Monopile Designer software, this implementation seems to lack the 2nd stage optimisation potentially leading to inaccurate calibrated soil reaction curves. Appendix B shows how the PISA numerical based framework has been re-implemented thanks to the Python API of Plaxis 3D. The soil reaction curves are automatically extracted from Plaxis output and the DVFs are adjusted to get an optimal match between 1D FEA and 3D FEA. It is noted that optimising a function of 24 (in sand) to 28 (in clay) parameters is cumbersome. The cost function to be minimised by the optimisation algorithm was simplified instead of the accuracy metric initially proposed in the original PISA publications. In addition, it can be seen as a convenient alternative to optimise only a set of p- and y- multipliers (as presented in Chapter 5) rather than the full DVFs when trying to match 3D FEA and 1D FEA analyses.

6.4 FOURTH CONTRIBUTION

A new contour diagram-based model to account for the effect of cyclic loading on monopile lateral response. The model consists of the degradation of monotonic soil reaction curves based on soil mobilisation and soil cyclic contour diagrams. The model was shown to offer satisfactory match with the PISA field tests in both sand and clay and the new Blessington field tests. Over the typical API cyclic formulation, this model has the advantage of accounting for the effect of number of cycles and load magnitude. Over typical cyclic macro-element model, this model has the advantage of capture the effect of cyclic degradation on the soil reaction, rather than only the mudline response. Notably, this allows the inspection of the effect of cyclic loading on the bending moment distribution which might be critical for the monopile structural design.

The cyclic degradation is currently applied as a strength degradation, consistently with API and EA-Pfahle. However, experimental results suggests that the pile lateral capacity is not significantly affect by cyclic loading. Hence, the approach might be updated in the future to apply the cyclic degradation as a stiffness degradation rather than strength degradation.

Once properly validated, this cyclic model has the advantage of being applicable at any stage of design. At early stage, when limited site-specific data is available, the input

cyclic contour diagrams can be scaled from a database as demonstrated. At later stage of design, site specific contour diagrams can directly be inputted. It is convenient for actual monopile design to have the same formulation for sand and clay, allowing streamlined application to layered soils, as typically encountered offshore.

The current approach is relatively simpler and hence limited. It does not explicitly account for drainage conditions, rate effects or gapping. Rate effects and drainage conditions are accounted for indirectly by the provided cyclic contour diagrams. If proven too simplistic, the approach can be further developed. An overview of the advanced procedure has already been published and is attached in Appendix D.

(intentionally left blank)

References

Abadie, C. (2015). Cyclic lateral loading of monopile foundations in cohesionless soils. PhD Thesis. University of Oxford.

Abadie, C. N., Houlsby, G. T., & Byrne, B. W. (2019). A method for calibration of the Hyperplastic Accelerated Ratcheting Model (HARM). Computers and Geotechnics, 112, 370–385. https://doi.org/10.1016/J.COMPGEO.2019.04.017

AFNOR. (2012). NF P 94-262, Justification des ouvrages géotechniques, Norme d'application nationale de l'Eurocode 7, Fondations profondes.

Albiker, J., Achmus, M., Frick, D., & Flindt, F. (2017). 1 g model tests on the displacement accumulation of large-diameter piles under cyclic lateral loading. Geotechnical Testing Journal, 40(2), 173–184. https://doi.org/10.1520/GTJ20160102

Andersen, K. H. (2015). Cyclic soil parameters for offshore foundation design. The 3rd McClelland Lecture. In Meyer (Ed.), Frontiers in Offshore Geotechnics III, ISFOG'2015 (pp. 5–82). Taylor & Francis Group.

Andersen, K. H. (1976). Behavior of clay subjected to cyclic loading. International Conference on Offshore Structures, Trondheim.

Andersen, K. H., Engin, H. K., D'Ignazio, M., & Yang, S. (2023). Determination of cyclic soil parameters for offshore foundation design from an existing data base. Ocean Engineering, 267, 113180. https://doi.org/10.1016/J.OCEANENG.2022.113180

Andersen, K. H., & Lauritzsen, R. (1988). Bearing capacity for foundations with cyclic loads. Journal of Geotechnical Engineering, 114(5), 540–555.

API. (2014). API Recommended Practice 2GEO. First edition, April 2011 + addendum 2014.

Arany, L., Bhattacharya, S., Macdonald, J., & Hogan, S. J. (2017). Design of monopiles for offshore wind turbines in 10 steps. Soil Dynamics and Earthquake Engineering, 92, 126–152. https://doi.org/10.1016/J.SOILDYN.2016.09.024

Bachynski-Polić, E., Page, A., & Katsikogiannis, G. (2019). Dynamic Response of a Large-Diameter Monopile Considering 35-Hour Storm Conditions. ASME 2019 38th

International Conference on Ocean, Offshore and Arctic Engineering. https://doi.org/10.1115/OMAE2019-95170

Balaam, T. (2020). Development and calibration of cyclic loading models for monopile foundations in clays. PhD Thesis. University of Oxford.

Benz, T., Schwab, R., & Vermeer, P. (2009). Small-strain stiffness in geotechnical analyses. Bautechnik, 86(S1), 16–27. https://doi.org/https://doi.org/10.1002/bate.200910038

Beuckelaers, W. (2017). Numerical modelling of laterally loaded piles for offshore wind turbines. PhD Thesis. University of Oxford.

Beuckelaers, W. J. A. P., Burd, H. J., Houlsby, G. T., Mcadam, R. A., & Byrne, B. W. (2020). A GENERALISED WINKLER MODEL FOR THE HYSTERETIC AND RATCHETING BEHAVIOUR OF MONOPILES IN CLAY AND SAND. 4th International Symposium on Frontiers in Offshore Geotechnics (ISFOG 2020 in 2022).

Bienen, B., Dührkop, J., Grabe, J., Randolph, M. F., & White, D. J. (2012). Response of Piles with Wings to Monotonic and Cyclic Lateral Loading in Sand. Journal of Geotechnical and Geoenvironmental Engineering, 138(3), 364–375. https://doi.org/10.1061/(ASCE)GT.1943-5606.0000592

Bolton, M. D. (1986). The strength and dilatancy of sands. Géotechnique, 36(1), 65–78. https://doi.org/10.1680/geot.1986.36.1.65

Brinkgreve, R. B. J., Engin, E., & Engin, H. K. (2010). Validation of empirical formulas to derive model parameters for sands. In T. Benz & S. Nordal (Eds.), Numerical methods in geotechnical engineering Numge 2010 (pp. 137–142). CRC Press.

Brinkgreve, R., Engin, E., & Swolfs, W. (2018). Plaxis 3D Materials Manual.

Burd, H. J., Taborda, D. M. G., Zdravković, L., Abadie, C. N., Byrne, B. W., Houlsby, G. T., Gavin, K. G., Igoe, D. J. P., Jardine, R. J., Martin, C. M., McAdam, R. A., Pedro, A. M. G., & Potts, D. M. (2020). PISA design model for monopiles for offshore wind turbines: application to a marine sand. Géotechnique, 70(11), 1048–1066. https://doi.org/10.1680/jgeot.18.P.277

Byrne, B. W., Houlsby, G. T., Burd, H. J., Gavin, K. G., Igoe, D. J. P., Jardine, R. J., Martin, C. M., McAdam, R. A., Potts, D. M., Taborda, D. M. G., & Zdravković, L. (2020). PISA design model for monopiles for offshore wind turbines: application to a stiff glacial clay till. Géotechnique, 70(11), 1030–1047. https://doi.org/10.1680/jgeot.18.P.255

Byrne, B. W., McAdam, R. A., Beuckelaers, W. J. A. P., Burd, H. J., Gavin, K., Houlsby, G. T., Igoe, D. J. P., Jardine, R., & Martin, C. M. (2020). Cyclic laterally loaded

medium scale field pile testing for the PISA project. 4th International Symposium on Frontiers in Offshore Geotechnics (Postponed), 1323–1332.

Byrne, B. W., McAdam, R. A., Burd, H. J., Beuckelaers, W. J. A. P., Gavin, K. G., Houlsby, G. T., Igoe, D. J. P., Jardine, R. J., Martin, C. M., Muir Wood, A., Potts, D. M., Skov Gretlund, J., Taborda, D. M. G., & Zdravković, L. (2020a). Monotonic laterally loaded pile testing in a stiff glacial clay till at Cowden. Géotechnique, 70(11), 970–985. https://doi.org/10.1680/jgeot.18.PISA.003

Byrne, B. W., McAdam, R. A., Burd, H. J., Beuckelaers, W. J. A. P., Gavin, K. G., Houlsby, G. T., Igoe, D. J. P., Jardine, R. J., Martin, C. M., Muir Wood, A., Potts, D. M., Skov Gretlund, J., Taborda, D. M. G., & Zdravković, L. (2020b). Monotonic laterally loaded pile testing in a stiff glacial clay till at Cowden. Géotechnique, 70(11), 970–985. https://doi.org/10.1680/jgeot.18.PISA.003

Byrne, B. W., McAdam, R., Burd, H. J., Houlsby, G. T., Martin, C. M., Zdravkovic, L., Taborda, D. M. G., Potts, D. M., Jardine, R. J., & Sideri, M. (2015). New design methods for large diameter piles under lateral loading for offshore wind applications. Frontiers in Offshore Geotechnics III, 705–710.

Cuéllar, P. (n.d.). Pile Foundations for Offshore Wind Turbines: Numerical and Experimental Investigations on the Behaviour under Short-Term and Long-Term Cyclic Loading. https://doi.org/https://doi.org/10.14279/depositonce-2760

Dafalias, Y. F., & Manzari, M. T. (2004). Simple Plasticity Sand Model Accounting for Fabric Change Effects. Journal of Engineering Mechanics, 130(6), 622–634. https://doi.org/10.1061/(ASCE)0733-9399(2004)130:6(622)

DECC. (2021). Climate Action Plan 2021.

DGGT. (2013). Analysis Methods and Examples for Cyclically Loaded Piles (Informative). In Recommendations on Piling (EA-Pfähle) (pp. 417–458). John Wiley & Sons, Ltd. https://doi.org/https://doi.org/10.1002/9783433604113.app4

DNV. (2021). DNV-ST-0126: Support structure for wind turbines. DNV AS: Oslo, Norway.

DNV-GL. (2014). DNV-OS-J101: Design of offshore wind turbine structures. DNV GL: Oslo, Norway.

Dyvik, R., Andersen, K. H., Hansen, S. B., & Christophersen, H. P. (1993a). Field Tests of Anchors in Clay. I: Description. Journal of Geotechnical Engineering, 119(10), 1515–1531. https://doi.org/10.1061/(ASCE)0733-9410(1993)119:10(1515)

Dyvik, R., Andersen, K. H., Hansen, S. B., & Christophersen, H. P. (1993b). Field Tests of Anchors in Clay. I: Description. Journal of Geotechnical Engineering, 119(10), 1515–1531. https://doi.org/10.1061/(ASCE)0733-9410(1993)119:10(1515)

European Commission. (2020). An EU Strategy to harness the potential of offshore renewable energy for a climate neutral future.

Frick, D., & Achmus, M. (2022). A model test study on the parameters affecting the cyclic lateral response of monopile foundations for offshore wind turbines embedded in non-cohesive soils. Wind Energy Science, 7(4), 1399–1419. https://doi.org/10.5194/wes-7-1399-2022

Gavin, K. G., Igoe, D. J. P., & Kirwan, L. (2013). The effect of ageing on the axial capacity of piles in sand. Proceedings of the Institution of Civil Engineers - Geotechnical Engineering, 166(2), 122–130. https://doi.org/10.1680/geng.12.00064

Gavin, K., & Igoe, D. (2021). A field investigation into the mechanisms of pile ageing in sand. Géotechnique, 71(2), 120–131. https://doi.org/10.1680/jgeot.18.P.235

Hettler, A. (1981). Verschiebungen starrer und elastischer Gründungskörper in Sand bei monotoner und zyklischer Belastung. https://api.semanticscholar.org/CorpusID:36508197

Houlsby, G. T., Abadie, C. N., Beuckelaers, W. J. A. P., & Byrne, B. W. (2017). A model for nonlinear hysteretic and ratcheting behaviour. International Journal of Solids and Structures, 120, 67–80. https://doi.org/10.1016/J.IJSOLSTR.2017.04.031

Igoe, D., & Gavin, K. (2019). Characterization of the Blessington sand geotechnical test site. AIMS Geosciences, 5(2), 145–162. https://doi.org/10.3934/geosci.2019.2.145

Igoe, D., & Gavin, K. (2021). Investigation of Cyclic Loading of Aged Piles in Sand. Journal of Geotechnical and Geoenvironmental Engineering, 147(4), 4021011. https://doi.org/10.1061/(ASCE)GT.1943-5606.0002451

Igoe, D. J. P., Gavin, K. G., & O'Kelly, B. C. (2011). Shaft Capacity of Open-Ended Piles in Sand. Journal of Geotechnical and Geoenvironmental Engineering, 137(10), 903–913. https://doi.org/10.1061/(ASCE)GT.1943-5606.0000511

Igoe, D., & Jalilvand, S. (2020). 3D finite element modelling of monopiles in sand validated against large scale field tests. Proc. Int. Symp. Frontiers in Offshore Geotechnics, ISFOG, 1231–1242.

Igoe, D., Lapastoure, L., & Jalilvand, S. (2022). Comparison of geotechnical design criteria for offshore monopiles. Geotechnical Society of Ireland Conference, 37–42.

Igoe, D., & Lapastoure, L.-M. (2024a). Field lateral load tests on monopiles in dense sand at Blessington - Part 1 - Monotonic Loading. Submitted to Géotechnique.

Igoe, D., & Lapastoure, L.-M. (2024b). Field lateral load tests on monopiles in dense sand at Blessington - Part 2 - Cyclic Loading. Submitted to Géotechnique.

Jalbi, S., Hilton, J., & Jacques, L. (2020). Assessment of Practical Methods to Predict Accumulated Rotations of Monopile-Supported Offshore Wind Turbines in Cohesionless Ground Profiles. Energies, 13(15). https://doi.org/10.3390/en13153915

Jardine, R.J. and Standing, J.R. (2012) "Field axial cyclic loading experiments on piles driven in sand," Soils and Foundations, 52(4), pp. 723–736. Available at: https://doi.org/https://doi.org/10.1016/j.sandf.2012.07.012.

Jostad, H. P., Grimstad, G., Andersen, K. H., Saue, M., Shin, Y., & You, D. (2014). A fe procedure for foundation design of offshore structures–applied to study a potential owt monopile foundation in the korean western sea. Geotechnical Engineering Journal of the SEAGS & AGSSEA, 45(4), 63–72.

Kirsch, F., Richter, T., & Coronel, M. (2014). Geotechnische Aspekte bei der Gründungsbemessung von Offshore-Windenergieanlagen auf Monopfählen mit sehr großen Durchmessern. Stahlbau, 83(S2), 61–67.

Klinkvort, R. T. (2013). Centrifuge modelling of drained lateral pile - soil response: Application for offshore wind turbine support structures. Technical University of Denmark.

Klinkvort, R. T., & Hededal, O. (2013). Lateral response of monopile supporting an offshore wind turbine. Proceedings of the Institution of Civil Engineers-Geotechnical Engineering, 166(2), 147–158.

Kulhawy, F. H., & Mayne, P. W. (1990). Manual on estimating soil properties for foundation design. Electric Power Research Inst., Palo Alto, CA (USA); Cornell Univ., Ithaca.

Lapastoure, L.-M., Diambra, A., Jalilvand, S., & Igoe, D. (2023). Assessment of cyclic superposition approaches for the cyclic design of monopiles supporting offshore wind turbines. Ocean Engineering, 287, 115759.

Leblanc, C., Byrne, B. W., & Houlsby, G. T. (2010). Response of stiff piles to random two-way lateral loading. Géotechnique, 60(9), 715–721.

LeBlanc, C., Houlsby, G. T., & Byrne, B. W. (2010). Response of stiff piles in sand to long-term cyclic lateral loading. Géotechnique, 60(2), 79–90.

Li, W., Igoe, D., & Gavin, K. (2015). Field tests to investigate the cyclic response of monopiles in sand. Proceedings of the Institution of Civil Engineers-Geotechnical Engineering, 168(5), 407–421.

Li, Z., Haigh, S. K., & Bolton, M. D. (2010). Centrifuge modelling of mono-pile under cyclic lateral loads. Physical Modelling in Geotechnics, 2, 965–970.

Lin, S.-S., & Liao, J.-C. (1999). Permanent strains of piles in sand due to cyclic lateral loads. Journal of Geotechnical and Geoenvironmental Engineering, 125(9), 798–802.

Little, R. L., & Briaud, J.-L. (1988). Full Scale Cyclic Lateral Load Tests on Six Single Piles in Sand. https://api.semanticscholar.org/CorpusID:127745497

Liu, H. (2020). Constitutive modelling of cyclic sand behaviour for offshore foundations. PhD Thesis. TU Delft.

Liu, H., Diambra, A., Abell, J. A., & Pisanò, F. (2020). Memory-Enhanced Plasticity Modeling of Sand Behavior under Undrained Cyclic Loading. Journal of Geotechnical and Geoenvironmental Engineering, 146(11), 4020122. https://doi.org/10.1061/(ASCE)GT.1943-5606.0002362

Liu, H., Kementzetzidis, E., Abell, J. A., & Pisanò, F. (2022). From cyclic sand ratcheting to tilt accumulation of offshore monopiles: 3D FE modelling using SANISAND-MS. Géotechnique, 72(9), 753–768.

Liu, H. Y., Abell, J. A., Diambra, A., & Pisanò, F. (2019). Modelling the cyclic ratcheting of sands through memory-enhanced bounding surface plasticity. Géotechnique, 69(9), 783–800. https://doi.org/10.1680/jgeot.17.P.307

Long, J. H., & Vanneste, G. (1994). Effects of cyclic lateral loads on piles in sand. Journal of Geotechnical Engineering, 120(1), 225–244.

Matlock, H. (1970). Correlation for design of laterally loaded piles in soft clay. Offshore Technology Conference, OTC-1204.

Mayne, P. W., & Kulhawy, F. H. (1982). Ko-OCR relationships in soil. Journal of the Geotechnical Engineering Division, 108(6), 851–872.

McAdam, R. A., Byrne, B. W., Houlsby, G. T., Beuckelaers, W. J. A. P., Burd, H. J., Gavin, K. G., Igoe, D. J. P., Jardine, R. J., Martin, C. M., & Muir Wood, A. (2020). Monotonic laterally loaded pile testing in a dense marine sand at Dunkirk. Géotechnique, 70(11), 986–998.

Niemunis, A., & Herle, I. (1997). Hypoplastic model for cohesionless soils with elastic strain range. Mechanics of Cohesive-frictional Materials: An International Journal on Experiments, Modelling and Computation of Materials and Structures, 2(4), 279–299.

Niemunis, A., Wichtmann, T., & Triantafyllidis, T. (2005). A high-cycle accumulation model for sand. Computers and Geotechnics, 32(4), 245–263.

Page, A. M., Jostad, H. P., & Saue, M. (2013). Application of an undrained and a partially drained cyclic accumulation model for monopile design. Proceedings of the 5th International Young Geotechnical Engineers' Conference, 205–208.

Page, A. M., Klinkvort, R. T., Bayton, S., Zhang, Y., & Jostad, H. P. (2021). A procedure for predicting the permanent rotation of monopiles in sand supporting offshore wind turbines. Marine Structures, 75, 102813.

Panagoulias, S., Brinkgreve, R., & Zampich, L. (2021). Plaxis Monopile Designer CE V21 Manual.

Patrick Berthelot, Alain Puech, & Françoise Ropers. (2020). Recommendations for planning and designing foundations of offshore wind turbines. Version 2.1.

Plaxis. (2021). PLAXIS 3D CE V21 - Material Models Manual.

Prendergast, L. J., & Igoe, D. (2022). Examination of the reduction in natural frequency of laterally loaded piles due to strain-dependence of soil shear modulus. Ocean Engineering, 258, 111614.

Puech, A., & Garnier, J. (2017). Design of piles under cyclic loading: SOLCYP recommendations. John Wiley & Sons.

Richards, I. A., Byrne, B. W., & Houlsby, G. T. (2020). Monopile rotation under complex cyclic lateral loading in sand. Géotechnique, 70(10), 916–930.

Robertson, P. K., & Cabal, K. L. (2015). Guide to cone penetration testing for geotechnical engineering. Signal Hill, CA: Gregg Drilling & Testing.

Roesen, H. R., Ibsen, L. B., Hansen, M., Wolf, T. K., & Rasmussen, K. L. (2013). Laboratory testing of cyclic laterally loaded pile in cohesionless soil. ISOPE International Ocean and Polar Engineering Conference, ISOPE-I.

Rosquoët, F. (2004). Pieux sous charge latérale cyclique. PhD Thesis. École Centrale de Nantes et Université de Nantes.

Schnaid, F., & Yu, H. S. (2007). Interpretation of the seismic cone test in granular soils. Geotechnique, 57(3), 265–272.

Smith, C. (2018). Renewable energy: Powering up for the future. Ground Engineering.

Ushev, E., & Jardine, R. (2020). The behaviour of Bolders Bank glacial till under undrained cyclic loading. Géotechnique, 1–46. doi:10.1680/jgeot.18.p.236

Verdure, L., Garnier, J., & Levacher, D. (2003). Lateral cyclic loading of single piles in sand. International Journal of Physical Modelling in Geotechnics, 3(3), 17–28.

Wichtmann, T. (2016). Soil behaviour under cyclic loading: experimental observations, constitutive description and applications.

Wind Europe. (2022). Offshore wind in Europe: key trends and statistics 2021.

Zachert, H., Wichtmann, T., Triantafyllidis, T., & Hartwig, U. (2015). Simulation of a full-scale test on a gravity base foundation for offshore wind turbines using a high cycle

accumulation model. Frontiers in Offshore Geotechnics III: Proceedings of the 3rd International Symposium on Frontiers in Offshore Geotechnics (ISFOG 2015), 1, 819–824.

Zdravković, L., Jardine, R. J., Taborda, D. M. G., Abadias, D., Burd, H. J., Byrne, B. W., Gavin, K. G., Houlsby, G. T., Igoe, D. J. P., & Liu, T. (2020). Ground characterisation for PISA pile testing and analysis. Géotechnique, 70(11), 945–960.

Zhang, Y., & Andersen, K. H. (2017). Scaling of lateral pile p-y response in clay from laboratory stress-strain curves. Marine Structures, 53, 124–135. https://doi.org/10.1016/J.MARSTRUC.2017.02.002

Zhang, Y., Andersen, K. H., & Jeanjean, P. (2020). Verification of a framework for cyclic py curves in clay by hindcast of Sabine River, SOLCYP and centrifuge laterally loaded pile tests. Applied Ocean Research, 97, 102085.

Zhang, Y., Andersen, K. H., Klinkvort, R. T., Jostad, H. P., Sivasithamparam, N., Boylan, N. P., & Langford, T. (2016). Monotonic and cyclic py curves for clay based on soil performance observed in laboratory element tests. Offshore Technology Conference, D031S035R005.

Zhang, Y., Andersen, K., Jeanjean, P., Mirdamadi, A., Gundersen, A., & Jostad, H. (2017). A framework for cyclic p-y curves in clay and application to pile design in GoM. 8th Int. Conf.: Offshore Site Investigation Geotechnics, 108–141.

Appendix A

Lapastoure, L.-M. and David, Igoe (2022). A comparison of soil lateral reaction models for monopile design in clay. 20th International Conference on Soil Mechanics and Geotechnical Engineering (ICSMGE), Sydney, Australia.

A comparison of soil lateral reaction models for monopile design in clay

Comparaison de modèles de réaction latérale pour le dimensionnement de monopieux dans l'argile

Louis-Marin Lapastoure & David Igoe
Department of Civil Structural and Environmental Engineering, Trinity College Dublin, Dublin, Ireland. lapastol@tcd.ie

ABSTRACT: In recent years there has been an increase in the size of offshore wind turbines along with the water depth in which they are being installed. As a result, the loads are increasing and geotechnical engineers need accurate models to deliver safe and cost-effective foundations. Monopile foundations are the most popular foundation type, covering about 80% of the installed offshore wind turbines in Europe to date. Monopiles mobilise lateral soil reactions to withstand the large environmental loads carried by the wind turbine. This paper presents a comparison of the main approaches used in the industry (API, PISA, 3D FE). Their performances are compared for an example of monopile design in a range of homogenous clay profiles. Finally, a refinement of the current industry design approach is proposed to improve accuracy of the modelling.

RÉSUMÉ : Ces dernières années, la taille des éoliennes offshore et la profondeur des eaux dans lesquelles elles sont installées ont augmenté. En conséquence, les charges augmentent et les ingénieurs ont plus que jamais besoin de modèles précis pour dimensionner des fondations sûres et optimisées. Les fondations monopieux sont le type de fondation le plus populaire, couvrant environ 80 % des éoliennes offshore installées en Europe à ce jour. Les monopieux mobilisent les réactions latérales du sol pour résister aux importantes charges environnementales exercées sur l'éolienne. Cet article présente une comparaison des principales approches utilisées dans l'industrie (API, PISA, 3D FE). Leurs performances sont comparées pour le dimensionnement d'un monopieu dans différents sols argileux. Enfin, des pistes d'améliorations sont proposées.

KEYWORDS: offshore, wind turbine, monopile, geotechnical, lateral design.

1 INTRODUCTION.

Monopiles are large diameter open ended steel pipe driven into the seabed. During the first years of the offshore wind energy industry, monopiles were design with a diameter of about 4 m. As the industry is maturing, diameters up to 10 m are being designed, and up to 12 m are expected in the future. Monopiles are relatively short with slenderness ratios (*L/D*, where *L* is the embedded length and *D* the diameter) historically lower than 6, and now typically around 3. One of the main design drivers is to avoid resonance of the whole structure with the forcing frequencies. Monopiles are typically designed in the soft-stiff domain where the first mode of vibration must fit between the rotor frequency (*1P*) and the blade passing frequency (*3P* for a three bladed turbine) as shown on Figure 1. Excessive conservatism in the design approaches may not only lead to uneconomical design but may also make the foundation stiffer than expected. There is a risk that the natural frequency of the structure will coincide with the blade passing frequency leading to excessive deflections and fatigue. Hence, geotechnical engineers need accurate design approach to correctly size monopiles supporting offshore wind turbine.

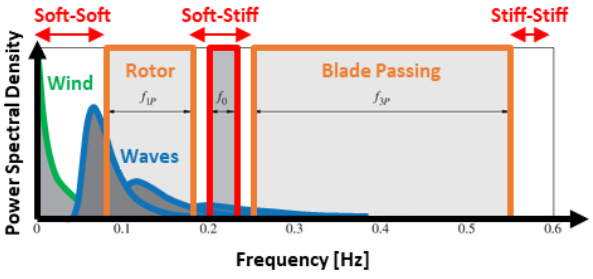

Figure 1. Natural frequency criterion for monopile design (modified after Kallehave et al. 2015).

2 MODELLING SOIL LATERAL REACTIONS

This section briefly presents the main approaches to model soil lateral reactions used in the offshore wind industry for monopile design.

2.1 *Traditional API 'p-y' approach*

The traditional industry approach consists in modelling the embedded part of the monopile using discrete Euler-Bernoulli beam element as shown on Figure 2. Soil lateral reactions are modelled as a series of independent non-linear springs. Theses curves, called 'p-y' curves, give the lateral reaction force *p* pushing against the pile as a result of the pile lateral displacement *y*. This approach is directly taken from the oil and gas industry (API 2014) and is recommended in the main offshore wind standards (DNV 2014).

The shape of the 'p-y' curves is provided in the standards. For example, in soft clay the API (API 2014) recommends curves based on the work of Matlock (1970) as below:

$$\frac{p}{p_u} = \frac{1}{2}\left(\frac{y}{y_c}\right)^{\frac{1}{3}} \leq 1 \quad (1)$$

Where p_u is the ultimate lateral reaction calculated from the undrained shear strength (s_u), the depth (z), the effective unit weight (γ'), the pile diameter (D) and an empirical dimensionless constant (J) in the range of 0.25 to 0.5 as per:

$$p_u = \left(3s_u + z\gamma'\right)D + Js_u z \leq 9s_u D \quad (2)$$

And y_c is the reference displacement at which 50% of the ultimate capacity is mobilized. It is directly scaled from the strain at one-half of the maximum stress in undrained tri-axial compression test (ε_{50}) as per:

$$y_c = 2.5\varepsilon_{50}D \quad (3)$$

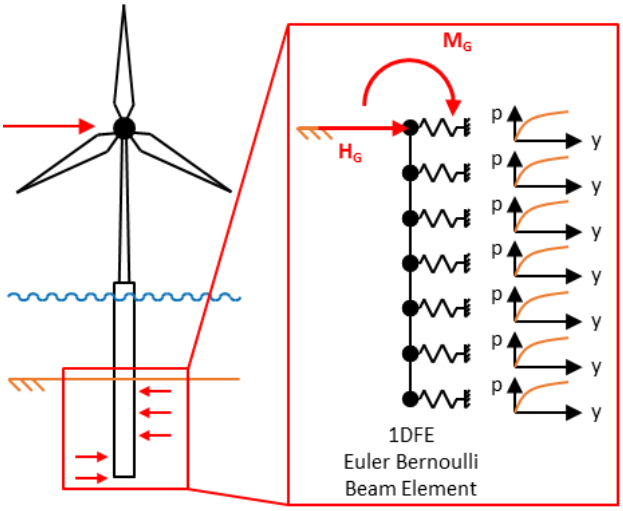

Figure 2. Representation of the API 'p-y' approach.

The API 'p-y' approach has been successfully used in the oil and gas industry for decades and was used at the early stage of the offshore wind industry. However, it is now widely acknowledged that this approach is unsuitable for monopile design due to fundamental differences between the two industries. It has only been validated against a small database of field tests on long and slender piles with diameter up to about 1 m. In contrast, monopiles are short with diameter larger than 6 m, up to 10 m. DNV-ST-0126 clause 7.6.2.6 now recommends validating the use of p-y curves for monopiles by means of finite element analysis (DNV 2018).

2.2 *State of the art PISA approach*

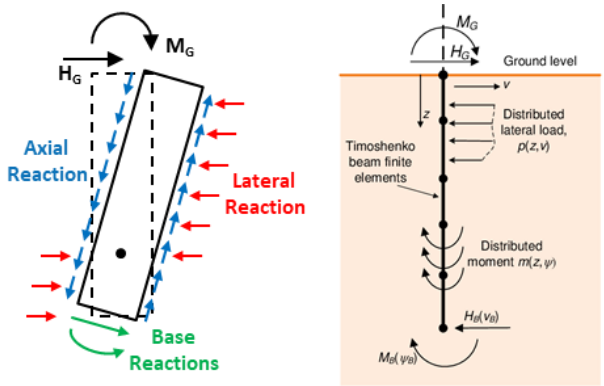

Figure 3. Representation of the PISA approach (modified after Byrne et al. 2019).

Due to the shortcomings of the API 'p-y' approach, the recently completed PISA project aimed at developing state-of-the-art design methodology for monopiles. One of the key differences is the addition of other soil reaction components such as distributed moment, base shear and base moment (see Figure 3). Upon lateral loading, monopiles not only mobilise soil lateral reactions but also axial reactions as a result of their rotation due to their large diameter. Also, monopiles typically behave rigidly (due to their low slenderness ratio) and show significant toe displacement mobilising base shear force and base resisting moment. Similarly to API 'p-y' approach, these four soil reaction components are integrated into 1D finite element. However, PISA investigators preferred Timoshenko beam element type over Euler-Bernoulli in order to take into account shear deformations. Byrne et al. (2015) compared monopile load-displacement curves at mudline obtained from 3D and 1D finite element modelling. The response considering 'p-y' curves only was found to be significantly softer. The principal investigators of the PISA project showed that adding these additional soil reactions makes the response stiffer and in better agreement with 3D FE. It was also shown that their contributions become more significant as pile diameter increases.

In the PISA framework, the soil reaction curves are normalised. Figure 4 shows a 'p-y' curve as an example. The lateral reaction p is normalised over the pile diameter (D) and the undrained shear strength (s_u) while the displacement y is normalised by the ratio of shear modulus at small strain (G_0) over pile diameter and undrained shear strength. Then, the curves are parameterised according to a conic function (see Eq. 4) with 4 parameters (x_u, k, n, y_u) to be fitted. Each of them relates to a particular aspect of the curve as shown on Figure 4.

$$-n\left(\frac{\bar{y}}{\bar{y_u}}-\frac{\bar{x}}{\bar{x_u}}\right)^2+(1-n)\left(\frac{\bar{y}}{\bar{y_u}}-\frac{\bar{x}k}{\bar{y_u}}\right)\left(\frac{\bar{y}}{\bar{y_u}}-1\right)=0 \qquad (4)$$

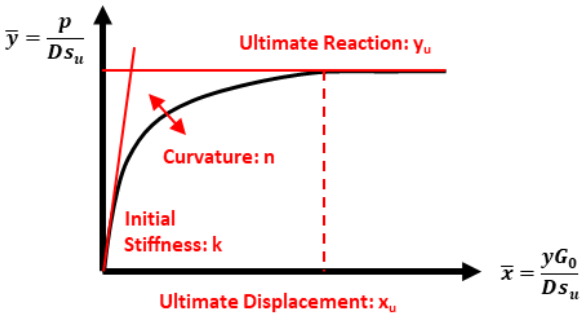

Figure 4. Example of PISA normalisation and parameterisation.

The PISA project developed two approaches: the 'rule-based' approach and the 'numerical-based' approach. These are discussed in the following sections.

2.2.1 *PISA rule-based approach*

In the PISA rule-based approach, generic depth variation functions give profiles of these 4 parameters with depth for each soil reaction component, giving a total of 16 depth variation functions. Table 1 reports the depth variation functions that were calibrated for the Cowden till for a wide range of pile geometry examined during the PISA project. At monopile concept design stage, these could be used in any similar clay profile. Only a limited number of soil input parameters are required (s_u and G_0) to de-normalise the soil reaction curves. Monopile mudline response under any loads can then be quickly estimated in a 1D finite element solver for a range of pile geometries.

Table 1. Depth variation functions calibrated in Cowden till (Byrne et al. 2019).

Soil Reaction Component	Parameter	Depth Variation Function
Distributed lateral load, p	x_u	241.4
	k	10.60 - 1.650 * Z/D
	n	0.9390 - 0.03345 * Z/D
	y_u	10.70 - 7.101 * exp(-0.3085 * Z/D)
Distributed moment, m	x_u	Given by y_u/k
	k	1.420 - 0.09643 * Z/D
	n	0
	y_u	0.2899 - 0.04775 * Z/D
Base shear, H_b	x_u	235.7
	k	2.717 - 0.3575 * L/D
	n	0.8793 - 0.03150 * L/D
	y_u	0.4038 + 0.04812 * L/D
Base Moment, M_b	x_u	173.1
	k	0.2146 - 0.002132 * L/D
	n	1.079 - 0.1087 * L/D
	y_u	0.8192 - 0.08588 * L/D

2.2.1 *PISA numerical-based approach*

The PISA framework also offers the possibility to develop site specific soil reaction curves. This approach involves running numerous advanced 3D finite element models for a range of pile geometries. For each geometry, the soil rection curves are extracted, normalised and parameterised, giving site-specific fitting parameters (x_u, k, n, y_u). The 16 depth variation functions are then fitted to the site-specific fitting parameters. Figure 5 shows an example of such fitting for the normalized ultimate lateral distributed load in Cowden till (Byrne et al. 2019). Dots show fitting parameters from different pile geometries while the lines show successive fitting attempts.

This is not a straight-forward process as most 3D FE software will not provide soil reaction curves directly. This approach is implemented in the commercially available Plaxis Monopile Designer software (Panagoulias et al. 2021), which can automatically extract the soil reaction curves and fit the depth variation functions.

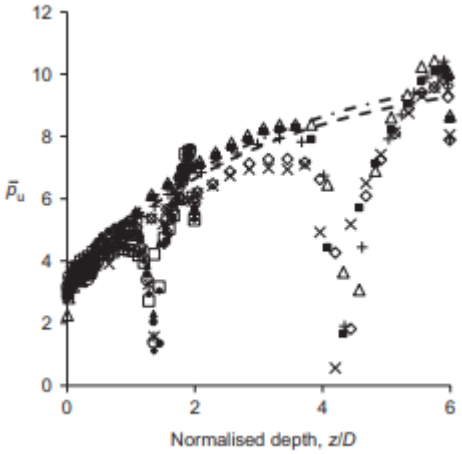

Figure 5. Example of depth variation function fitted to normalised ultimate lateral distributed load in Cowden till (Byrne et al. 2019).

2.2 *Reference 3D finite element modelling*

A full 3D finite element modelling comes at expensive computation cost but is a more rigorous approach to model the pile-soil interaction. The accuracy of the 3D FE analysis is dependent on choice of constitutive soil model and the availability of high-quality ground investigation data to define the required input parameters (as it is with the PISA numerical approach). The constitutive model should be able to capture the nonlinear stress-strain behaviour of the soil.

Figure 6 shows a typical monopile model using the commercial finite element package Plaxis 3D. The monopile is modelled using shell elements with elastic properties of structural steel (i.e. E = 210 GPa, ν = 0.3). Interface elements are introduced between pile and soil to allow for differential displacements. To obtain the required overturning moment M at mudline, the lateral force H is applied at an eccentricity e=M/H above mudline. Taking advantage of the plan of symmetry, the model is set up in half-space in order to reduce computation time.

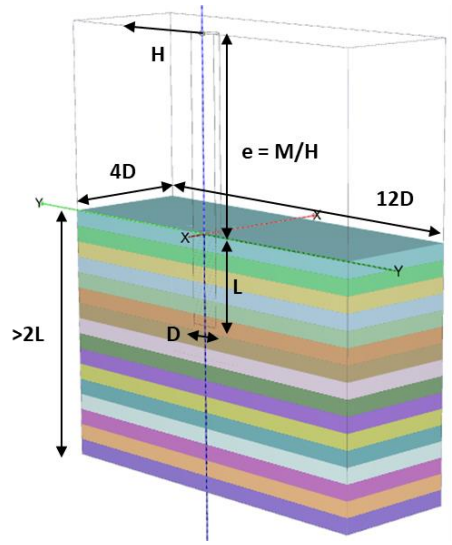

Figure 6. Model set up in Plaxis 3D.

3 APPLICATION TO MONOPILE DESIGN

In this section, the different soil lateral reaction models are compared for an example monopile design.

3.1 *Inputs for monopile design*

For simplicity, a number of input parameters for this monopile design exercise are assumed based on experience and engineering judgement (see Figure 7). A Serviceability Limit State (SLS) lateral load of 10 MN applied 60 m above the seafloor is deemed representative of a large capacity offshore wind turbine installed in typical water depth. The pile diameter, D, is assumed at 9 m with a constant wall thickness, t, of 90 mm (D/t = 100). This optimised geometry should be based on natural frequency assessment and to avoid fatigue or resonance issues but these assessments are omitted here for the sake of conciseness. Only the pile embedded length is considered for optimisation. A range of synthetic homogeneous clay profiles are considered. Soil effective unit weight and coefficient of earth pressure are kept constant with depth at value of 10 kN/m^3 and 1, respectively. A total of three profiles are considered here with constant undrained shear strength, s_u, with depth as shown in Figure 8. Although a constant s_u profile with depth is unrealistic, this is chosen for simplicity, as the aim of this study is to compare different methods. The stiffness to strength ratios (G_0/s_u) are taken as 800 for all three profiles.

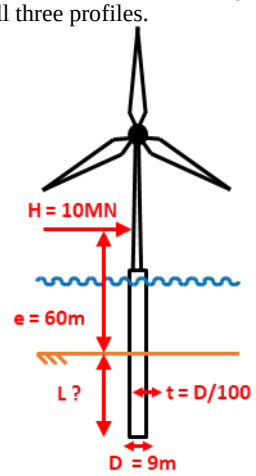

Figure 7. Inputs for example monopile design.

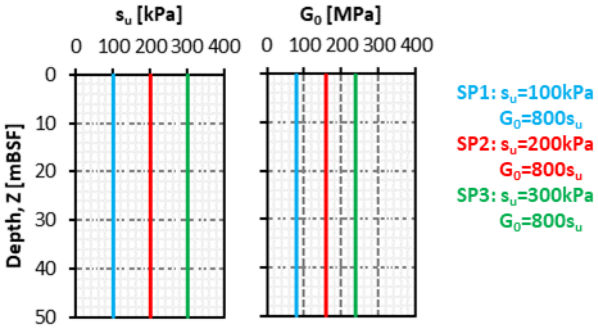

Figure 8. Range of undrained shear strength and small strain shear modulus profiles considered.

3.2 *Implementation of the different approaches*

The API 'p-y' approach and the PISA rule-based approach are implemented in a MATLAB 1D finite element solver. For the API approach, 'p-y' curves are computed as per API (2014) and the work of Matlock (1970) for soft clay (s_u < 96 kPa) and as per Reese et al. (1975) for stiffer clay. For the PISA rule-based approach, the depth variation functions calibrated in Cowden till (Byrne et al. 2019) are considered.

The implementation of the PISA numerical-based approach was undertaken in PLAXIS Monopile Designer V21. For each soil profile, the depth variation functions are fitted based on 8 calibrating 3D FE models where the pile length range from 20 m to 55 m. Pile diameter, wall thickness and load eccentricity are kept constant as assumed in the previous section.

For the 3D finite element modelling, the soil is modelled using the NGI-ADP model for clay in Plaxis 3D CE V21. The missing parameters are correlated with s_u and G_0 according to the recommendations made by Panagoulias et al. (2021). These correlations and the use of NGI-ADP to model monopiles in clay was validated against PISA field tests in Cowden till (Minga & Burd 2019).

3.3 *Design pile embedded length*

Based on each approach considered, the monopile rotation at sea floor under the assumed SLS load was calculated for a range pile embedded length (see Figure 9 for an example in SP1). The SLS-GEO lateral check typically requires limiting the permanent accumulated rotation at mudline due to cyclic loading to 0.25 degree (DNV 2018). For the sake of simplicity, the 0.25 degree criterion is directly applied to the static rotation here. This is deemed acceptable here because the aim is not to actually design the monopile but to compare the different approaches. The 3D FE analysis case is considered to be the reference case, as all other cases require simplifications (i.e. Winkler approach) or empiricism (e.g. API method) to be introduced. 3D FE leads to required pile embedded length of about 37 m in this case. The API 'p-y' approach results in a significantly larger pile penetration with about 52 m. The PISA approaches are closer to 3D FE with 35 m for the rule-based approach and 33 m for the numerical-based approach. Surprisingly, the numerical based approach which use the same 3D FE analyses to extract site-specific set of depth variation functions are seen to perform worse than the generic rule-based functions.

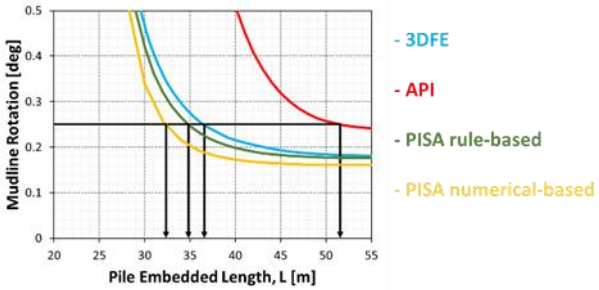

Figure 9. Example of pile embedded length design in SP1.

3.4 *Comparison of the different approaches*

Extending the analysis to all the 3 clay profiles, we observe the same trend. The API 'p-y' approach, shown in red in Figure 10 largely overestimates the pile length from 3D FE in blue. For the three clay profiles considered here, the required pile lengths were 26% to 41% larger. The PISA approaches in green for rule-based and yellow for numerical based are a significant improvement with much closer prediction (from -4% to -12%). However, the PISA numerical-based approach was expected to better match with the 3D FE result than PISA rule-based but it is not the case here.

Foundation design at the scale of an entire offshore wind farm cannot solely rely on 3D finite element modelling. Indeed, 3D FE can be very accurate once properly calibrated but are computationally expensive. Fast design approaches are required for early design stage but need to remain accurate to enable optimisation at later stage of design which may require many thousands of different analysis cases. Even a few metres of pile penetration change can significantly impact fabrication, transportation and installation costs at the scale of the entire offshore wind farm.

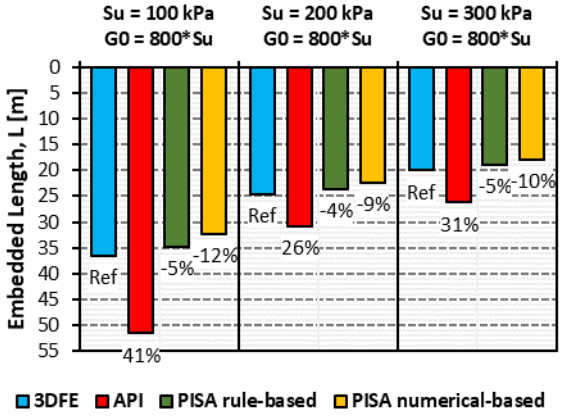

Figure 10. Comparison of design pile embedded lengths.

4 REFINEMENT OF PISA NUMERICAL-BASED APPROACH

4.1 *Current shortcomings*

For all three homogeneous clay profiles considered here, the PISA numerical-based approach (implemented in Plaxis Monopile Designer V21) estimated embedded lengths which were marginally unconservative (up to 12%) in comparison with the reference 3D FE models. Design pile lengths estimated with the PISA rule-based approach (generic depth variation functions calibrated in Cowden till as reported in Table 1) were closer to the 3D FE than the numerical-based approach using depth

variation functions calibrated with PLAXIS Monopile Designer V21. Potential causes are listed below:

- The addition of distributed moment, base shear and base moment is a significant improvement of the API 'p-y' only framework. However, the implementation in 1D FE remains an approximation and simplification of the 3D pile-soil interactions.
- Each parameter of each soil reaction component is fitted independently of the other. There is no guarantee that the fittings of the 16 depth variation functions are fully compatible.
- Parameters fitted from soil reaction curves form a scattered point cloud which is hard to fit with depth variation functions. This is due to different soil responses for different pile geometries, a lack of soil reaction close to point of rotation and interactions between distributed and base soil reactions close to the pile toe among other errors. Plaxis Monopile Designer CE V21 does not show the points cloud and hence the user cannot assess the quality of the fit for the depth variation functions. **Error! Reference source not found.** shows an example of a point cloud extracted from 3D FE using the Python interface of Plaxis for SP1.
- The goodness of the match between 1D FE and 3D FE is assessed based on two accuracy metrics comparing the integral of difference over integral of 3D FE load displacement curves. One metric is computed for very small displacements (lower than D/10000) and the other one for large displacements (up to D/10). These metrics are not meaningful a geotechnical engineer as they do not report if 1D FE is overestimating or underestimating the 3D FE response. Also, it is hard to define what is a good accuracy metric as they are all typically high.

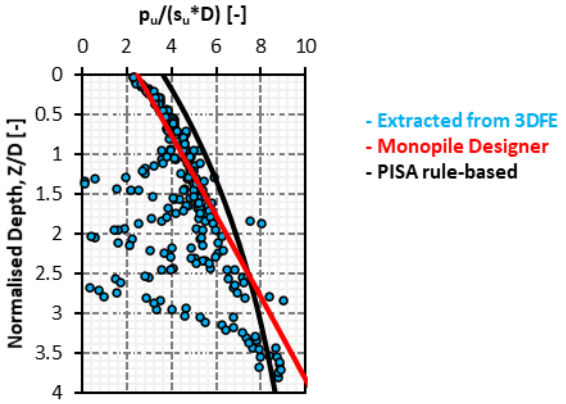

Figure 11. Comparison of 3D FE extract lateral ultimate reaction and depth variation functions fitted by Plaxis Monopile Designer V21 and calibrated in Cowden tillB

4.2 *Proposed solutions*

The PISA numerical-based approach as implemented in Plaxis Monopile Designer V21 corresponds to the first stage calibration reported in Byrne et al. (2019). Site-specific depth variation functions are fitted based on a range of 3D FE models with different pile geometries but keeping the same soil profile. Each depth variation function is fitted independently to offer the best match with the scattered point cloud. During the calibration exercise in Cowden till, Byrne et al. (2019) reported accuracy metrics in the range of 77% to 92% for small displacement and 90% to 98% for large displacement. Depth variation functions were then adjusted during a second stage calibration. The aim was no longer to fit each scattered point cloud individually, but instead to offer the highest accuracy metrics. Metrics in the range of 95% to 99% for small displacement and 90% to 96% for large displacement have been reported in this way.

The first point of improvement to be suggested is to implement the second stage calibration into the PISA numerical-based approach. This second stage calibration seems to be a key aspect of the PISA project and is lacking in Plaxis Monopile Designer CE V21. Recently, a calibration of PISA depth variation functions using in-situ measurements from an instrumented offshore wind turbine founded on monopile was reported (Jurado 2021). The authors reported the use of a Bayesian optimization approach to improve the match between the predicted and measured bending moment profile by applying scaling factor to the initial stiffness (k) and ultimate reaction (y_u) parameters in the PISA approach. This is deemed very interesting as it offers a clear optimization framework with limited number of parameters to account for.

The second point of improvement concern the metrics used to compare 1D FE and 3D FE responses. Accuracy metrics defined within the PISA framework, while useful to gauge model performance, are arguably not ideally suited for monopile geotechnical design. Arguably the three most important criteria for the design of a monopile are:

1. Pile ultimate capacity to ensure minimum factor of safety against failure under extreme loads. There is often no clear plateau in the load-displacement curve and ultimate capacity can be hard to define. It is proposed here to define the ultimate capacity as the lateral load at which pile displacement at sea floor reach 10% of the pile diameter.
2. Pile sea floor rotation under maximum operational loads to verify serviceability limit state. From experience, typical large diameter monopile design are found to have a high margin of safety against failure. Considering a load partial factor of 1.35, material partial factor of 1.25 and a typical ULS utilisation (ratio of design load to design resistance) of 50 – 70%, it is proposed here to estimate operational loads as 1/3 of 3D FE ultimate capacity.
3. Pile stiffness to assess the natural frequency of the structure. It is proposed here to define the small-strain stiffness as the secant stiffness in the load-displacement curve at seafloor under loads equivalent of 2% of the 3D FE ultimate capacity.

Hence, 3 new metrics based are proposed for calculating relative error for pile ultimate capacity (Eq. 5), pile sea floor rotation under operational loads (Eq. 6) and pile small-strain strain stiffness (Eq. 7). A metric value of zero is equivalent to a perfect match, a negative value implies the 1D FE is underestimating compared to the 3D FE and a positive value implies the 1D FE is overestimating compared to the 3D FE. Overestimation of ultimate capacity or underestimation of rotation under operational loads leads to unconservative design. For the stiffness, both may lead to unconservative design as discussion in the introduction.

$$\delta_{ULS} = \frac{H_{ult}^{1DFE} - H_{ult}^{3DFE}}{H_{ult}^{3DFE}} \quad (5)$$

$$\delta_{SLS} = \frac{\theta_{ult/3}^{1DFE} - \theta_{ult/3}^{3DFE}}{\theta_{ult/3}^{3DFE}} \quad (6)$$

$$\delta_{FLS} = \frac{K_{ult/50}^{1DFE} - K_{ult/50}^{3DFE}}{K_{ult/50}^{3DFE}} \quad (7)$$

4.3 *Future works*

Plaxis Monopile Designer is a commercial software and users do not have access to all functions and variables required to implement new functionalities. Hence, current works consist in developing a new tool to implement the proposed solution as presented in Figure 12. Python was selected as the programming

language as it enables interface with Plaxis 3D to automate the setup of 3D FE models and the extraction of soil reaction curves. Future works will consist in transferring the current Matlab 1D finite element solver used in this paper to Python in order to streamline the workflow. An optimisation procedure will be introduced in order to update the depth variation functions in a second stage calibration phase. The aim is to ensure the best match with 3D FE mudline response. Although the three new metrics need to be reported to understand the performance of 1D FE with respect to 3D FE, the optimisation procedure needs the three metrics to be assembled in a cost function. The optimisation procedure will aim at minimizing the cost function *C* below where *n* is the number of 3D FE models used for the calibration of the depth variation functions:

$$C = \sqrt{\frac{1}{n}\sum_{i=1}^{n} \delta_{ULS,i}{}^2} + \sqrt{\frac{1}{n}\sum_{i=1}^{n} \delta_{SLS,i}{}^2} + \sqrt{\frac{1}{n}\sum_{i=1}^{n} \delta_{FLS,i}{}^2} \quad (8)$$

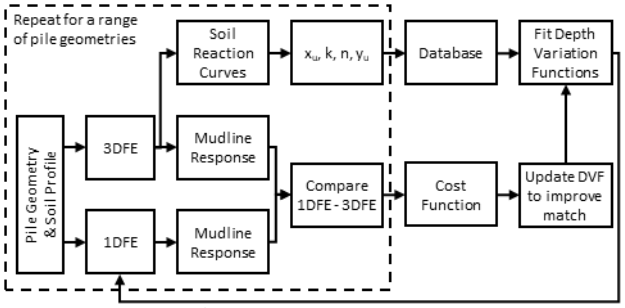

Figure 12. Flowchart of proposed solutions.

Once fully implemented, this tool will be used to populate a database of depth variation functions in a range of representative clay profiles, which may then use without the need for new 3D FE analysis (i.e. as per PISA rule-based approach).

5 CONCLUSIONS

This paper presented the main industry approaches used for the geotechnical design of monopile supporting offshore wind turbines. The traditional API 'p-y' approach, the state-of-the-art PISA rule-based and numerical-based approaches and 3D finite element modelling were considered for a typical monopile design in clays. It was shown that:

- API largely overestimated the required pile penetration in comparison to 3D FE and would lead to an uneconomical design. While this might be conservative for ultimate capacity check or serviceability limit check, it might be unconservative for the natural frequency check.
- The PISA approaches are a significant improvement although they were found slightly unconservative in this case.
- The PISA numerical-based approach as implemented in Plaxis Monopile Designer CE V21 is not performing as expected. The fitted depth variations functions led to a worse match with 3D FE than the generic functions calibrated in Cowden till. A number of limitations of Plaxis Monopile Designer CE V21 were discussed. The main limitation appears to be the lack of a second stage calibration of the depth variation functions to ensure maximum match with 3D FE mudline response.

Hence, current and future works consist in the implementation of a Python code able to automate the setting up of Plaxis 3D models, the extraction, normalisation and fitting of soil reaction curves and the two-stage calibration of depth variation functions. Also, new accuracy metrics are considered in order to better assess the performance of the PISA numerical-based approach. These new metrics are based on meaningful criterion for the geotechnical design of monopile. Once fully implemented, this tool will be used to populate a database of depth variations functions in a range of representative clay profiles.

6 ACKNOWLEDGEMENTS

The first author would like to acknowledge funding under the Irish Research Council (IRC) employment-based postgraduate program.

7 REFERENCES

API (2014). API-RP-2GEO Geotechnical and Foundation Design Considerations. First Edition. American Petroleum Institute, April 2011 + Addendum 1: 2014-10.

DNV (2014). DNV-OS-J101 Design of Offshore Wind Turbine Structures.

DNV (2016). DNVGL-ST-0126 Support structures for wind turbines.

Byrne, B.W., Houlsby, G.T., Burd, H.J., Gavin, K.G., Igoe, D.J.P., Jardine, R.J., Martin, C.M., McAdam, R.A., Potts, D.M., Taborda, D.M.G. and Zdravković, L. (2019). PISA design model for monopiles for offshore wind turbines: application to a stiff glacial clay till. Géotechnique, https://doi.org/10.1680/jgeot.18.P.255.

Byrne et al. (2015). New design methods for large diameter piles under lateral loading for offshore wind applications. Proceedings of the Third International Symposium on Frontiers in Offshore Geotechnics, Oslo, Norway.

Jurado, C. S. (2021). Calibration of soil-monopile interaction model using in-situ measurements from an instrumented offshore wind turbine. Proceedings of the 2021 Wind Energy Science Conference, Hannover, Germany.

Kallehave, D., Byrne B.W., Leblanc C., Mikkelsen K. (2015). Optimization of monopiles for offshore wind turbine. Phil. Trans. R. Soc. A. 373: 20140100. 20140100. https://doi.org/10.1098/rsta.2014.0100

Matlock, H. (1970). Correlations for design of laterally loaded piles in soft clay. Proceedings of the II Annual Offshore Technology Conference, Houston, Texas, (OTC 1204): 577-594.

Panagoulias, S., Brinkgreve, R.B.J., Zampich, L., (2021), "PLAXIS Monopile Designer CE V21 - Manual".

Reese, L.C., W.R. Cox & F.D. Koop (1975). Field testing and analysis of laterally loaded piles in stiff clay. Proceedings of the VII Annual Offshore Technology Conference, Houston, Texas, 2(OTC 2312): 672-690.

(intentionally left blank)

Appendix B

Lapastoure, L.-M. and Igoe, D. (2022). Implementation of PISA numerical framework for offshore wind foundation design. Civil Engineering Research in Ireland (CERI) conference, Dublin, Ireland

Recipient of the best geotechnical stream presentation award and the best paper award.

Implementation of PISA numerical framework for offshore wind foundation design

Louis-Marin LAPASTOURE[1,2], David IGOE[1]
[1]Department of Civil, Structural and Environmental Engineering, Trinity College Dublin, College Green, Dublin 2, Ireland
[2]Gavin and Doherty Geosolutions, Unit A2, Nutgrove Office Park, Dublin 14, Ireland
email: lapastol@tcd.ie, igoed@tcd.ie

ABSTRACT: Monopiles are the most common foundation type for offshore wind turbines representing about 80% of the offshore wind turbine installations to date. The recently completed PISA project developed state of the art design practices to model the pile soil interactions for monopiles. The PISA rule-based approach provides equations, referred to as 'depth variation functions', to generate monopile soil reaction curves which can be used in a non-linear beam-spring analysis. These depth variation functions were calibrated to match the results of Finite Element models which were validated against large scale pile tests in Cowden TILL and Dunkirk SAND. The PISA numerical based approach sets out a framework to calibrate site specific depth variation functions based on the results of bespoke 3D finite element modelling. The approach is quite complex requiring extraction of soil reaction curves, curve fitting and multi-variate optimisation. PLAXIS Monopile Designer (previously MoDeTo) is the first commercial implementation of the PISA framework. The software is very user friendly but is lacking a component, referred to as 2nd stage calibration. The 2nd stage calibration is essential to fine tune the depth variation functions in order to obtain best match with pile response. This paper presents key considerations and challenges for the implementation of the PISA numerical framework. Significant improvements are proposed, including the definition of new more time efficient cost function. It is shown that the proposed implementation provides more accurate results than PLAXIS Monopile Designer for a given design example.

KEY WORDS: Offshore Wind; Monopile; Geotechnical Engineering; PISA.

1 INTRODUCTION

In Ireland, no offshore wind farms have been built since the 24 MW Arklow Bank Wind Park Phase 1 in 2004. The offshore wind industry is now gaining momentum with the Climate Action Plan 2021 targeting 5 GW of offshore wind to be commissioned by 2030 [1], the launch of the new Marine Area Consent regime [2] and the release of draft terms and conditions of the first offshore subsidy [3].

Monopiles are the most common foundation type supporting offshore wind turbines, representing about 80% of the installation to date [4]. Monopiles are large diameter (6 – 10 m) open ended piles driven into the seabed. The popularity of monopiles is due to their simple design which allows for quick fabrication and installation. Traditional industry practices for monopile design were based on the American Petroleum Institute (API) standards [5] developed from a limited number of long and flexible pile field tests. It is now widely recognized as being unsuitable for short and rigid monopile design [6].

Due to the shortcomings of the API 'p-y' approach, the PISA project was formed in 2013 with the aim of developing new design methods specifically for the offshore wind industry. The new PISA design method represents the state-of-the-art design methodology for monopiles [7] and is now used globally for monopile design. Parts of the PISA design method have been implemented into the commercial software PLAXIS Monopile Designer [8]. Although the approach is quite complex, the software interface is very simple to use, making state-of-the-art research available for day-to-day engineering. However, the software is lacking an essential component to ensure the best results: the so-called '2nd stage calibration' [9]. Hence, this paper presents key considerations and challenges for the implementation of the PISA numerical framework. The proposed implementation, with a new more time efficient cost function, is also compared to PLAXIS Monopile Designer.

2 PISA FRAMEWORK

2.1 General principle

In the traditional API method for analysing laterally loaded piles, a 1D Finite Element (FE) analysis is used where the pile is modelled as a linear elastic beam and the soil lateral reaction is modelled using decoupled non-linear 'p-y' springs. One of the key differences between the PISA framework and the traditional API 'p-y' approach is the addition of three other soil reaction components to the distributed lateral load: the distributed moment, the base shear and the base moment (see Figure 1). The soil reaction curves can be constructed from a set of equations referred to as 'depth variation functions' following the PISA rule-based approach or using site specific advanced three-dimensional finite-element analysis following the PISA numerical-based approach.

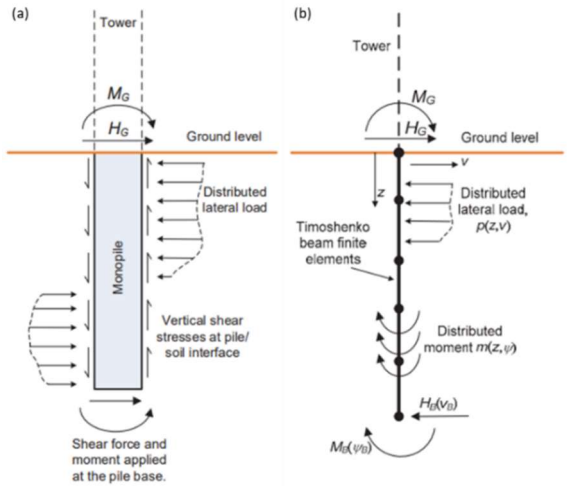

Figure 1. PISA design model: (a) soil reaction components acting on the pile; (b) implementation in 1D FE [10].

2.2 PISA rule-based approach

In the PISA framework the soil reaction curves are normalised by the pile outside diameter (D) and by local stiffness and strength soil parameters: small-strain shear modulus (G_0), initial vertical effective stress (σ'_v) in sand and undrained shear strength (s_u) in clay. The formulae are presented in Table 1 for both sand [11] and clay [12].

One may notice the coupling between distributed moment and distributed lateral load in sand. This coupling requires special attention when implementing the approach. Indeed, the distributed moment is a function of both the lateral displacement and the cross-section rotation.

Table 1. Soil reaction curves normalisation [11,12].

Normalised Variable	Dimensionless form	
	in SAND	in CLAY
Lateral displacement, $\bar{v}$	$\frac{vG_0}{D\sigma'_v}$	$\frac{vG_0}{Ds_u}$
Pile cross-section rotation, $\bar{\psi}$	$\frac{\psi G_0}{\sigma'_v}$	$\frac{\psi G_0}{s_u}$
Distributed lateral load, $\bar{p}$	$\frac{p}{D\sigma'_v}$	$\frac{p}{Ds_u}$
Distributed moment, $\bar{m}$	$\frac{m}{D\lvert p\rvert}$	$\frac{m}{D^2 s_u}$
Base horizontal load, $\bar{H}_B$	$\frac{H_B}{D^2\sigma'_V}$	$\frac{H_B}{D^2 s_u}$
Base moment, $\bar{M}_B$	$\frac{M_B}{D^3\sigma'_v}$	$\frac{M_B}{D^3 s_u}$

In the PISA framework, each soil reaction curve is described using a four-parameter conic function. In both sand and clay, any normalised soil reaction ($\bar{y}$) can be determined explicitly from the corresponding normalised displacement or rotation ($\bar{x}$) as per equation (1).

$$\bar{y} = \begin{cases} \bar{y}_u \dfrac{2c}{-b+\sqrt{b^2-4ac}} & \text{for } \bar{x} < \bar{x}_u \\ \bar{y}_u & \text{for } \bar{x} \geq \bar{x}_u \end{cases} \quad (1)$$

Where a, b and c are computed as per below:

$$a = 1 - 2n \quad (2)$$

$$b = 2n\frac{\bar{x}}{\bar{x}_u} - (1-n)\left(1+\frac{\bar{x}k}{\bar{y}_u}\right) \quad (3)$$

$$c = \frac{\bar{x}k}{\bar{y}_u}(1-n) - n\left(\frac{\bar{x}}{\bar{x}_u}\right)^2 \quad (4)$$

Each of the four parameters employed in the conic function have a clear physical meaning (see Figure 2):

- $\bar{y}_u$ is the ultimate normalised reaction. The reaction is any of the 4 soil reaction components ($\bar{p}$, $\bar{m}$, $\bar{H}_B$ or $\bar{M}_B$).
- $\bar{x}_u$ is the corresponding ultimate displacement or rotation at which the ultimate reaction is reached.
- k is the initial stiffness of the normalised reaction curve.
- n is a curvature parameter ranging from 0 to 1. The curved conic function is simplified to a bi-linear form when $n = 0$ or $n = 1$.

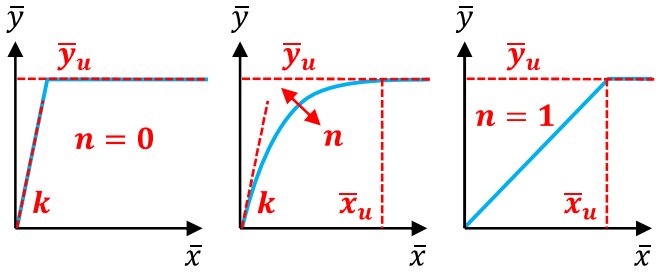

Figure 2. Signification of the four shape parameters.

The variations with depth of the 4 parameters ($\bar{x}_u$, k, n and $\bar{y}_u$) describing the shape of the 4 soil reaction components (distributed lateral load, distributed moment, base moment and base shear) are captured by the depth variation functions (DVF). The 16 DVFs are defined by 24 parameters in sand and 28 in clay (see Table 2). While some parameters remain constant with depth (z), most of them vary linearly with the normalised depth (z/D) at which the soil reaction curve is considered. In sand, the ultimate distributed lateral load and ultimate distributed moment are a function of z/L instead where L is the pile embedded length. In clay, the ultimate distributed lateral is an exponential function of z/D.

These DVF parameters, s_1 to s_{24} in sand and c_1 to c_{28} in clay, were calibrated using a set of three-dimensional finite-element analyses (11 analyses for each soil profile with D ranging from 5 m to 10 m and L/D ranging from 2 to 6) and are provided in [11] and [12], respectively. The 3D FE models were themselves validated against onshore large scale field tests (pile diameter up to 2 m) in Dunkirk dense marine sand [13] and Cowden stiff glacial clay till [14]. Since the vertical effective stress used in the normalisation process in sand does not adequately capture the soil strength, the DVF parameters are defined as a linear function of the relative density in [11] (validated for D_r ranging from 45% to 90%).

Table 2: Depth variation functions [11,12].

Soil Reaction Curve	Shape Parameter	Depth Variation Function	
		in SAND	in CLAY
Distributed lateral load, $\bar{p}$-$\bar{v}$	$\bar{x}_u$	s_1	c_1
	k	$s_2 + s_3 z/D$	$c_2 + c_3 z/D$
	n	s_4	$c_4 + c_5 z/D$
	$\bar{y}_u$	$s_5 + s_6 z/L$	$c_6 + c_7 e^{c_8 z/D}$
Distributed moment, $\bar{m}$-$\bar{\psi}$	$\bar{x}_u$	s_7	c_9
	k	s_8	$c_{10} + c_{11} z/D$
	n	s_9	c_{12}
	$\bar{y}_u$	$s_{10} + s_{11} z/L$	$c_{13} + c_{14} z/D$
Base horizontal force, $\bar{H}_B$-$\bar{v}$	$\bar{x}_u$	$s_{12} + s_{13} L/D$	c_{15}
	k	$s_{14} + s_{15} L/D$	$c_{16} + c_{17} L/D$
	n	$s_{16} + s_{17} L/D$	$c_{18} + c_{19} L/D$
	$\bar{y}_u$	$s_{18} + s_{19} L/D$	$c_{20} + c_{21} L/D$
Base moment, $\bar{M}_B$-$\bar{\psi}$	$\bar{x}_u$	s_{20}	c_{22}
	k	s_{21}	$c_{23} + c_{24} L/D$
	n	s_{22}	$c_{25} + c_{26} L/D$
	$\bar{y}_u$	$s_{23} + s_{24} L/D$	$c_{27} + c_{28} L/D$

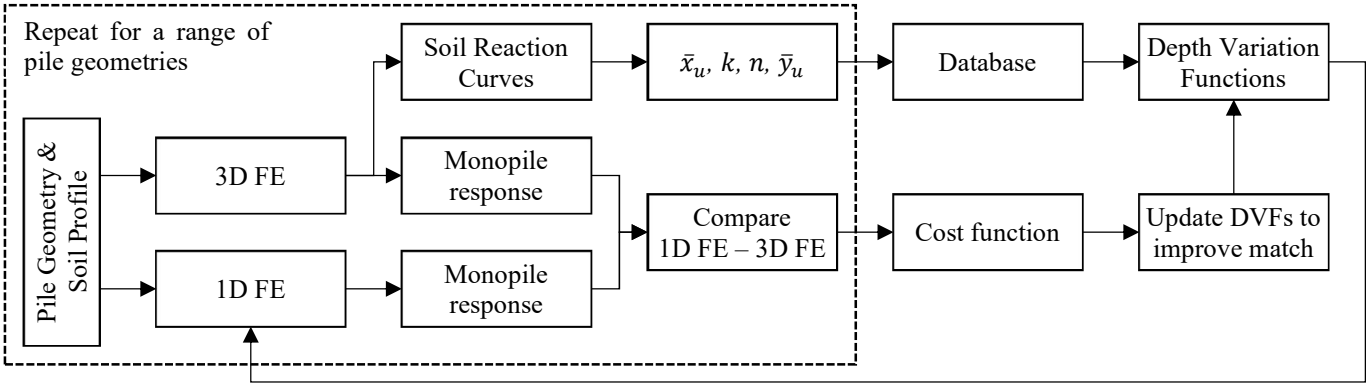

Figure 3. Flowchart of the PISA numerical based approach.

2.3 PISA numerical- based approach

At early stage of design, the PISA rule-based approach offers a simple and quick method to predict monopile responses. However, the predictions may be inaccurate as the soil profiles and pile geometries may be different from those used for calibration original PISA calibration. At later stage of design, when appropriate site investigations have been carried out, the PISA numerical based approach may be more accurate.

Carefully calibrated three-dimensional finite-element analyses are often regarded as the most accurate approach to predict monopile response to lateral loading. However, relying solely on 3D FE would be too time consuming to optimise the foundation design across the entire wind farm. Instead, the PISA numerical based approach offers a good trade-off between 3D FE accuracy and 1D FE computational efficiency. It employs a suite of 3D FE analyses to calibrate site-specific depth variation functions. Those depth variation functions can then be used in 1D FE (similarly to the PISA rule-based approach) to predict monopile response. Pile geometry and load combination can easily be varied in 1D FE at no extra computation cost compared to 3D FE. In addition, the PISA framework was initially only calibrated for a homogeneous soil profile but was later extended to layered soils [15]. Once the DVFs are calibrated for each soil unit, the thickness and arrangement of the different soil layers can be varied to match with the soil profile at different location across the wind farm.

Figure 3 presents the key aspects of the PISA numerical based approach which are detailed below:

- 3D FE analyses for a range of pile geometries are required to calibrate the depth variation functions. The accuracy of the overall approach relies on the accuracy of the 3D FE analyses. Any constitutive model may be considered but it needs to be carefully calibrated to replicate the soil response over the required strain range. The accuracy of the approach is naturally directly affected by the extent and quality of the site investigations.
- Soil reaction curves (distributed lateral load, distributed moment, base shear and base moment) are extracted from each 3D FE model.
- After normalisation, each soil reaction curve is fitted according to the PISA framework presented in section 2.2. A procedure to fit each of the 4 shape parameters for each of the 4 soil reaction components is presented in [11] for sand and [12] for clay.
- The 16 depth variation functions can then be fitted from the database of 3D FE extracted and fitted parameters. This concludes what is described as 'the first stage calibration' [11,12]. However, 1D FE pile response based on those DVFs may not compare exactly with the 3D FE response. Accuracy metrics (defined in Figure 4) as low as 77% were reported in [12] after the first stage calibration.
- A 'second stage calibration' is then required. It consists in fine tuning the DVFs until a good match between 3D FE and 1D FE responses is obtained. It requires the definition of a cost function to define what a good match is. Equation (5) is proposed in [11] and [12]. Then the DVFs can be fine-tuned using standard multi-variate optimisation algorithms available in computing environments such as MATLAB or PYTHON. Accuracy metrics as high as 99% were reported in [12] after the second stage calibration.

$$C = \sqrt{\sum_{i=1}^{N}\left(1-\eta_{ult_i}\right)^2} + \sqrt{\sum_{i=1}^{N}\left(1-\eta_{sd_i}\right)^2} \qquad (5)$$

Where:

- C is the cost function to be minimised
- N is the number of 3D FE calibration models
- η_{ult_i} is the large displacement accuracy metric for model i as defined in Figure 4a.
- η_{sd_i} is the small displacement accuracy metric for model i as defined in Figure 4b.

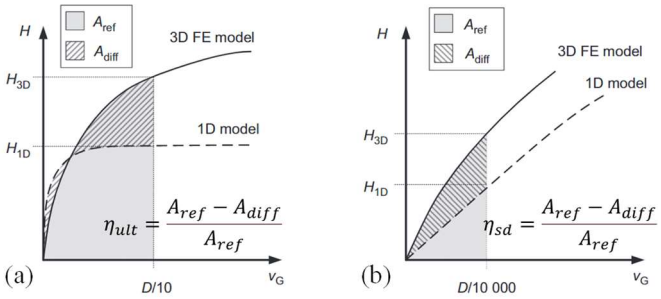

Figure 4. PISA accuracy metrics based on the pile mudline load (H) – displacement (v_g) response for (a) large displacements; (b) small displacements. Modified after [11,12].

3 IMPLEMENTATION OF PISA NUMERICAL-BASED MODELLING APPROACH

Although the PISA numerical based approach is quite complex, its commercial implementation into PLAXIS Monopile Designer offers a very simple user interface, making state-of-the-art research available for day-to-day engineering. However, the software is lacking an essential component to ensure best results: the 2nd stage calibration [8,9].

Hence, the PISA numerical framework has been re-implemented into PYTHON. The following sections presents the key considerations and challenges.

3.1 3-D finite-element modelling

The FE package PLAXIS 3D is commercially available and was selected to model the laterally loaded monopiles due to its popularity in the industry. The monopiles are modelled at full scale and half space (see Figure 5). Being consistent with PLAXIS Monopile Designer [8], the soil is modelled using the NGI-ADP model for clay and Hardening Soil small-strain (HSsmall) model for sand. A fully undrained behaviour is assumed for clay while a fully drained behaviour is considered for sand. The pile structure is modelled using linear-elastic isotropic plate elements with standard steel properties (Young's modulus of 210 GPa and Poisson's ratio of 0.3). The pile is weightless since the focus is on lateral loading. Interfaces at the outside and inside of the pile capture the soil-structure interactions. The undrained NGI-ADP model is replaced by a drained Mohr-Coulomb model at interfaces in clay to allow for tension cut-off. The stiffness parameters are kept the same, but the strength is reduced to 65% of the original value. In sand, the dilation angle is set to 0° and friction angle is reduced to 29° at the interfaces. After the pile is wished-in-place (i.e. no effect of installation), a prescribed displacement is applied in the y-direction at the top of pile until the mudline displacement reaches failure (considered to be 10% of the pile diameter). An additional interface with no strength reduction is added at pile toe to extract soil base reactions. Dummy horizontal surfaces are generated at 1 m intervals along the pile length to facilitate extraction of the soil reaction curves.

The whole process was automated in PYTHON using the PLAXIS API scripting interface. This is to ensure not only minimum computation time but also consistent modelling through all the calibration analyses by avoiding human error.

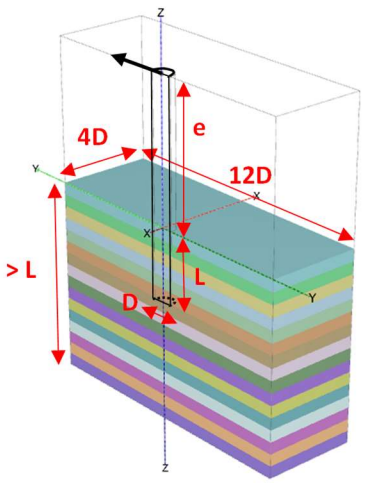

Figure 5. Example monopile model in PLAXIS 3D.

3.2 Extraction of soil reaction curves

It is typical and straight forward to extract mudline load-displacement and moment-rotation curves from laterally loaded pile 3D FE models. However, extraction of soil reaction curves along the pile length is less common and can be more cumbersome. The whole process was also automated in PYTHON using the PLAXIS API scripting interface.

The distributed lateral reaction and moments are extracted from the external vertical interfaces at 1 m intervals ($\Delta Z = 1$ m). Base shear and base moment are only extracted at pile base from the additional horizontal interfaces.

The distributed lateral reaction (p) at any depth (Z) is computed from integration of the interface forces in the y direction, while the distributed moment (m) is computed from integration of forces in the z direction multiplied by the lever arm y. This is presented in equations (6)-(7) and Figure 6a-b.

$$p(Z) = \frac{\int_{Z-\Delta Z/2}^{Z+\Delta Z/2} F_y(z)\,dz}{\Delta Z} \tag{6}$$

$$m(Z) = \frac{\int_{Z-\Delta Z/2}^{Z+\Delta Z/2} y \times F_z(z)\,dz}{\Delta Z} \tag{7}$$

However, in PLAXIS 3D Output, vertical and horizontal forces acting at the interfaces are not accessible. Only stress in local coordinates at either stress points or nodes are accessible. At each stress-point, knowing its coordinates (X, Y), the area of the element (A) and its integration weight (w), the stresses are translated into forces as per equations (8)-(9) and Figure 6c. The same process is applied to base shear and base moment curves.

$$F_y = w\mathrm{A}(\sin\theta\,\sigma_n - \cos\theta\,\tau_2) \tag{8}$$

$$F_z = w\mathrm{A}\tau_1 \tag{9}$$

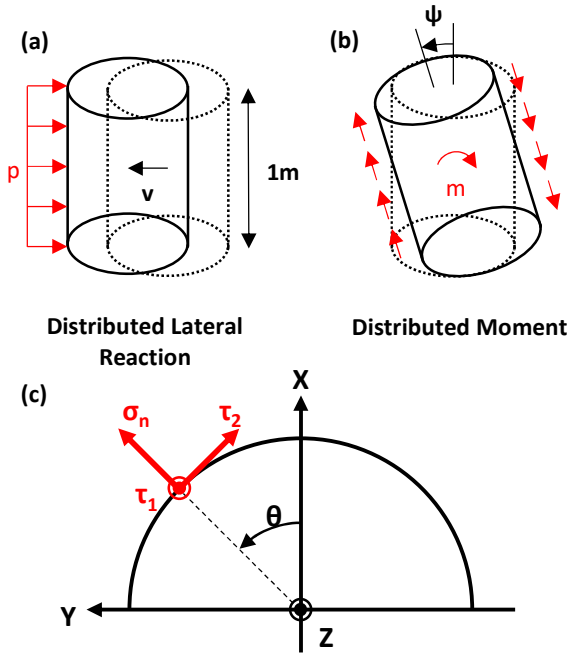

Figure 6. Extraction of soil reaction curves: (a) distributed lateral load; (b) distributed moment; (c) local coordinates system.

3.3 *Normalisation and curve fitting*

Once extracted, the soil reaction curves are normalized as per Table 1. The normalisation process is straightforward.

However, the curve fitting is more challenging. The ultimate reaction ($\bar{y}_u$) and the ultimate displacement ($\bar{x}_u$) can only be properly fit if sufficient pile displacements are achieved. The left-hand side of Figure 7 shows that, upon lateral loading, very little soil reactions are mobilized along the pile embedded length, even when large displacements are achieved at the mudline. Even the initial stiffness (k) might be problematic close to the point of rotation where no reactions are mobilized at all.

This issue is acknowledged in [11] and [12] where different processes are proposed depending on the soil reaction component (distributed lateral load, distributed moment, base shear or base moment) to be fitted and the soil type (sand or clay). These 8 processes are quite cumbersome to implement and require some user inputs. Hence, a simplified and unique approach is considered as part of this study:

- The initial stiffness, k, is determined by minimizing the root mean square error between the curve extracted from 3D FE and the linear expression $\bar{y} = k\bar{x}$ for the range of data at which the mudline displacement is less than $D/10000$.
- The ultimate reaction, $\bar{y}_u$, is defined as the reaction reached at the end of the analysis (largest displacement or rotation).
- The ultimate displacement or rotation, $\bar{x}_u$, is defined as the displacement or rotation as which $\bar{y}_u$ is reached for the first time.
- The curvature, n, is determined by minimizing root mean square error between the curve extracted from 3D FE and the conic function being fitted.

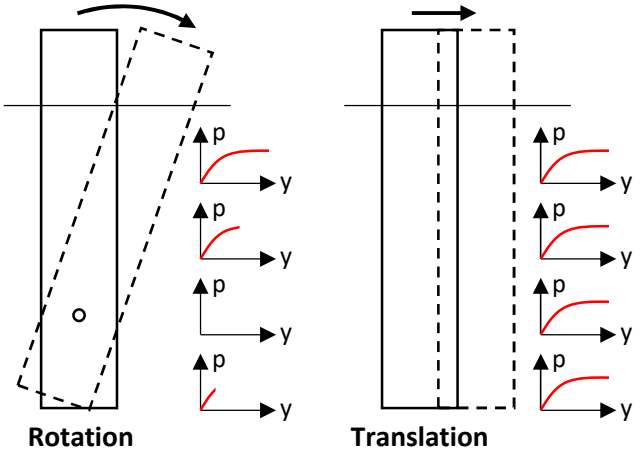

Figure 7. Limitation of the current rotation approach and proposed alternative approach.

3.4 *Optimisation of depth variation functions*

The so called 'second stage calibration' is a key component of the PISA numerical based approach. As presented previously and in [11] and [12], it consists in optimizing the depth variation functions in order to improve the match between the 3D FE and 1D FE responses. The soil reaction curves extracted from 3D FE, normalized and fitted are only used as a starting point for the optimization procedure. The *minimize* function from the *Scipy.optimise* library in PYTHON is used as part of this study. It allows the definition of bounds and linear constraints to ensure all parameters to be optimized remain in their range of validity. The optimization of 24 to 28 parameters (sand or clay) requires a significant number of iterations and function evaluations (typically more than 1000).

The cost function proposed by [11] and [12] (see equation (5)) was found to be too computationally expensive. The small and large displacement accuracy metrics are based on integration of the differences which may only be accurate if many small increments are summed. Instead, another cost function is implemented as part of this study and presented in equation (10). It only requires 4 loads increment per calibration models, dramatically reducing the computation time. The cost function accounts for both mudline displacement (y) and rotation (θ), minimising the difference between the 1D FE and 3D FE models.

$$C = \sqrt{\sum_{i=1}^{N} C_i(H_{ult}) + C_i\left(\frac{H_{ult}}{3}\right) + C_i\left(\frac{H_{ult}}{10}\right) + C_i\left(\frac{H_{ult}}{100}\right)} \quad (10)$$

Where:

- C is the cost function to be minimised
- N is the number of 3D FE calibration models
- H_{ult} is the ultimate capacity defined for a mudline displacement of D/10.
- $C_i(H)$ is the cost function evaluated for model i under lateral load H computed as per equation (11).

$$C_i(H) = \left(\frac{y_i^{1D}(H) - y_i^{3D}(H)}{y_i^{3D}(H)}\right)^2 + \left(\frac{\theta_i^{1D}(H) - \theta_i^{3D}(H)}{\theta_i^{3D}(H)}\right)^2 \quad (11)$$

4 COMPARISON TO PLAXIS MONOPILE DESIGNER

The implementation of the PISA numerical based approach presented in this paper is compared to PLAXIS Monopile Designer in this section. For the purpose of the comparison, the following inputs are considered:

- Soil profile: homogenous normally consolidated dense sand profile. A CPT based correlation for HSS parameters for monopile modelling was proposed by [16]. The equations were re-arranged to define the parameters assuming $D_r = 80\%$, $\phi'_{cv} = 32°$, $\gamma = 19.5\ \mathrm{kN/m^3}$, $f_s = 0.1q_c$ and $\beta^{CPT} = 185$.
- Loads: Lateral load of 12 MN acting 50 m above mudline.
- Pile geometry: D/t assumed as 110. A total of 9 calibration models were considered (Figure 8), pile diameters ranging from 6 m to 10 m and slenderness ratios (L/D) ranging from 2 to 6 are considered.

The SLS-Geo check [6] requires to limit the permanent (after unloading) mudline rotation accumulated through the cyclic load history to 0.250 degrees. For the sake of simplicity, the cyclic effects are not taken into account here and Figure 9 compares permanent static rotation for pile embedded length ranging from 20 to 50 m, assuming a diameter of 7 m. These piles' geometries fall in the range of validity for which the PLAXIS Monopile Designer and this paper's implementation were calibated.

Additional 3D FE models were run to find out that the design pile embedded length should be 29.5 m. This paper's

implementation compares very well with a design penetration of 29.2 m. However, the PLAXIS Monopile design compares poorly with a required penetration of 26.3 m. This is due to the lack of second stage calibration. See comparison on Figure 9.

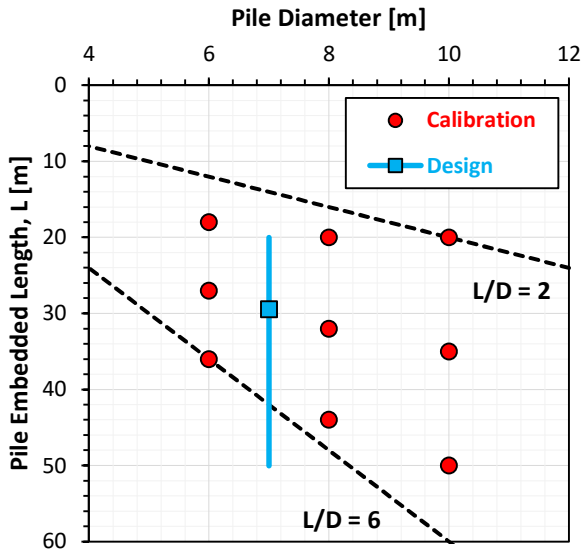

Figure 8. Calibration space and final design.

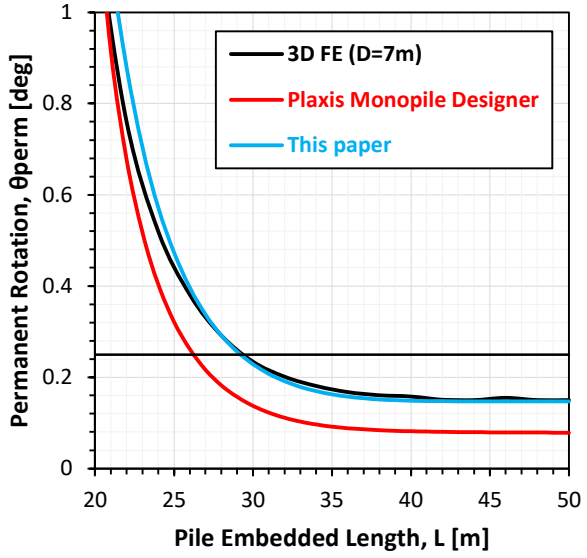

Figure 9. Comparison of PLAXIS Monopile designer results to the PISA numerical-based approach implemented in this paper.

5 DISCUSSION AND CONCLUSION

The PISA framework is the latest state of the art development for monopile design. This paper presented key considerations and challenges for the implementation of the PISA numerical-based approach. For a design example, the poor accuracy of PLAXIS Monopile Designer due to the lack of the 'second stage calibration' is demonstrated. The implementation proposed in this paper, with a new more efficient cost function and simplified curve fitting approach, provides a very satisfactory match with the base case 3D FE models. The implementation could be further improved by considering the following points:

- Fitting the soil reaction curve is challenging because there is little to no soil reaction close to point of rotation. An alternative approach where the pile model in 3D FE would be translated rather than rotated is envisaged (Figure 7 right). This would ensure large mobilization at all depths hence easier and more accurate curve fitting.
- Significant computation efforts are required to extract, normalize and fit the soil reaction curves. However, these curves are only used as a starting point for the second stage calibration. It is also possible to use PISA rule DVFs as a starting point instead, to reduce computation time.
- The cost function only considers mudline displacement and rotation. This ensures best match between the mudline responses in 1D FE and 3D FE. However, it is uncertain how the deflection profiles along the pile embedded length compare. Given that the piles are rigid, it is envisaged to add the toe displacement and rotation into the cost function evaluation to ensure better match of the overall pile response at no extra computation cost.

ACKNOWLEDGEMENT

This research is funded under the IRC employment based postgraduate program (EBPPG/2019/4).

REFERENCES

[1] https://www.gov.ie/en/publication/6223e-climate-action-plan-2021/
[2] https://www.gov.ie/en/press-release/f4c68-ireland-moves-a-step-closer-to-energy-independence/
[3] https://www.gov.ie/en/press-release/f6070-consultation-opens-on-first-auction-to-supply-electricity-from-offshore-wind-under-the-renewable-electricity-support-scheme-oress-1/
[4] Wind Europe (2020). Offshore wind in Europe - key trends and statistics 2020
[5] API (2014). APIRP2GEO Geotechnical and Foundation Design Consideration
[6] DNV (2021). DNV-ST-0126 Support structures for wind turbines.
[7] Byron W. Byrne, Harvey J. Burd, Lidija Zdravković, Ross A. McAdam, David M.G. Taborda, Guy T. Houlsby, Richard J. Jardine, Christopher M. Martin, David M. Potts, Kenneth G. Gavin (2019). PISA: new design methods for offshore wind turbine monopiles. Rev. Fr. Geotech. (158) 3. DOI: 10.1051/geotech/2019009
[8] Plaxis (2022). PLAXIS Monopile Designer CONNECT Edition Version 22 Manual.
[9] Brinkgreve, Ronald, Diego Lisi, Miquel Lahoz, and Stavros Panagoulias. 2020. "Validation and Application of a New Software Tool Implementing the PISA Design Methodology" Journal of Marine Science and Engineering 8, no. 6: 457. https://doi.org/10.3390/jmse8060457
[10] Byrne BW, McAdam RA, Burd HJ, Houlsby GT, Martin CM, Beuckelaers W, Zdravkovic L, Taborda DMG, Potts DM, Jardine RJ, Ushev E, Liu T, Abadias, D, Gavin K, Igoe D, Doherty P, Skov Gretlund J, Pacheco Andrade M, Muir Wood A, Schroeder FC (2017). PISA: New Design Methods for Offshore Wind Turbine Monopiles (Keynote). In: 8th International Conference on Offshore Site Investigations and Geotechnics. DOI: 10.3723/OSIG17.142
[11] Harvey J. Burd, David M. G. Taborda, Lidija Zdravković, Christelle N. Abadie, Byron W. Byrne, Guy T. Houlsby, Kenneth G. Gavin, David J. P. Igoe, Richard J. Jardine, Christopher M. Martin, Ross A. McAdam, Antonio M. G. Pedro, and David M. Potts (2020). PISA design model for monopiles for offshore wind turbines: application to a marine sand. Géotechnique 2020 70:11, 1048-1066. DOI: 10.1680/jgeot.18.P.277
[12] Byron W. Byrne, Guy T. Houlsby, Harvey J. Burd, Kenneth G. Gavin, David J. P. Igoe, Richard J. Jardine, Christopher M. Martin, Ross A. McAdam, David M. Potts, David M. G. Taborda, and Lidija Zdravković (2020). PISA design model for monopiles for offshore wind turbines: application to a stiff glacial clay till. Géotechnique 2020 70:11, 1030-1047. DOI: 10.1680/jgeot.18.P.255
[13] David M. G. Taborda, Lidija Zdravković, David M. Potts, Harvey J. Burd, Byron W. Byrne, Kenneth G. Gavin, Guy T. Houlsby, Richard J. Jardine, Tingfa Liu, Christopher M. Martin, and Ross A. McAdam (2020). Finite-element modelling of laterally loaded piles in a dense marine sand at Dunkirk. Géotechnique 2020 70:11, 1014-1029. DOI: jgeot.18.PISA.006
[14] Lidija Zdravković, David M. G. Taborda, David M. Potts, David Abadias, Harvey J. Burd, Byron W. Byrne, Kenneth G. Gavin, Guy T. Houlsby, Richard J. Jardine, Christopher M. Martin, Ross A. McAdam, and Emil Ushev (2020). Finite-element modelling of laterally loaded piles in a stiff glacial clay till at Cowden. Géotechnique 2020 70:11, 999-1013. DOI: 10.1680/jgeot.18.PISA.005
[15] Harvey J. Burd, Christelle N. Abadie, Byron W. Byrne, Guy T. Houlsby, Christopher M. Martin, Ross A. McAdam, Richard J. Jardine, Antonio M. G. Pedro, David M. Potts, David M. G. Taborda, Lidija Zdravković, and Miguel Pacheco Andrade (2020). Application of the PISA design model to monopiles embedded in layered soils. Géotechnique 2020 70:11, 1067-1082. DOI: jgeot.20.PISA.009
[16] Igoe. D. and Jalilvand, S. (2020). "3D finite element modelling of monopiles in sand validated against large scale field tests." Proceedings to the Fourth International Symposium on Frontiers in Offshore Geotechnics in Houston, USA.

(intentionally left blank)

Appendix C

Lapastoure, L.-M. and Igoe, D. (2022). 3D FE derivation of CPT based soil reaction curves for monopile lateral static design in sand. 5th International Symposium on Cone Penetration Testing (CPT'22), Bologna, Italy.

3D FE derivation of CPT based soil reaction curves for monopile lateral static design in sand

Louis-Marin Lapastoure
Department of Civil, Structural & Environmental Engineering, Trinity College Dublin, Dublin, Ireland
Gavin and Doherty Geosolutions Ltd, Dublin 14, Ireland

David IGOE
Department of Civil, Structural & Environmental Engineering, Trinity College Dublin, Dublin, Ireland

ABSTRACT: This paper aims to offer novel correlation between all 4 components of PISA soil reaction curves for monopile modelling and Cone Penetration Testing (CPT) data. This approach requires minimum user inputs and offers a consistent approach to develop site-specific soil reaction curves when CPT data are made available. The procedure developed by Igoe and Jalilvand was used to derive small-strain hardening (HS-small) soil model parameters from a range of CPT profile. HS-small parameters are then used to model the monopile response to static lateral loading in sand using Plaxis 3D. This procedure has been validated by the authors against a database of large-scale field tests including PISA tests in the Dunkirk marine sand. Soil reaction curves were directly extracted from the Plaxis models then applied into Timoshenko beam elements to match the 3D FE response and validated the extraction process. It is demonstrated that current CPT based correlations do not match the shape nor the ultimate reaction of 3D FE extracted soil reaction curves. It is also shown that all four components of soil reactions are required to accurately model monopiles which are short and rigid.

1 INTRODUCTION

1.1 *Context*

Monopiles are the main foundation type supporting about 80% of the installed offshore wind turbines to date in Europe (Wind Europe, 2020). The traditional industry design approach for monopile was adopted from the oil and gas industry. The 'p-y' approach recommended in the main design standards (API 2011, DNV 2013) was validated against a rather small database of long slender piles with diameter smaller than 1 m. On the contrary, monopiles are now designed with a low slenderness ratio (L/D ≈ 3) and a large diameter up to 10 m. Since 2014, it is warned that the API approach has "not been calibrated for monopiles with larger diameters and are in general not valid for such monopiles" (DNV 2014).

The recently completed PISA project was developed with the aim of improving on the traditional API design approach for monopile. In the PISA design model, pile-soil interactions are not limited to the distributed lateral reaction (p-y curves) but also include distributed moment, base shear and base moment (Burd et al. 2020). The PISA framework has now been implemented into the commercial software PLAXIS Monopile Designer (formerly MoDeTo) and is being commonly used in the industry (Minga and Burd 2019). It offers the option to extract site-specific soil reaction curves from 3D finite element models. However, this can be seen as computationally costly and requires careful calibration of the 3DFE soil input parameters.

Soil strength and stiffness parameters are often determined using correlations with Cone Resistance Testing (CPT) results, and therefore researchers have been looking at correlating soil reaction curves with CPT directly. Broms (1964) originally proposed relationship between ultimate lateral reaction, p_u, as a function of the cone resistance, q_c, in silica sands as per equation (1) where D is the pile diameter, p' is the mean effective stress and p_a is a reference stress taken as 100 kPa.

$$\frac{p_u}{D} = 0.1959 \cdot \left(\frac{q_c}{p_a}\right)^{0.4719} \cdot \left(\frac{p'}{p_a}\right)^{-0.6281} \quad (1)$$

Suryasentana and Lehane (2014) developed new p-y formulations for piles in sand based entirely on 3D finite element modelling, as opposed to back analysis of small scale instrumented laterally loaded pile tests as was the traditional approach. Equation (2) below has been calibrated against FE models using the hardening soil model (HS) in Plaxis 3D foundation and validated against lateral pile field tests with diameters of about 0.6 m and pile penetrations of 17 m (L/D > 28). γ denotes the soil unit weight and Z the depth at which the soil reaction is calculated.

$$\frac{p_u}{D} = 2.4 \cdot \gamma \cdot Z \cdot \left(\frac{q_c}{\gamma \cdot Z}\right)^{0.67} \left(\frac{Z}{D}\right)^{0.75} \quad (2)$$

However, these CPT based correlations are not compatible with the PISA framework and, as only the p-y response is considered, they might not be suitable for modelling monopiles (similarly to API).

1.2 *Proposed approach*

It is proposed here (see Figure 1) to use 3D finite element modelling to derive CPT based correlations of soil reaction curves including distributed lateral reaction, distributed moment, base shear and base moment (as per PISA framework).

Soil parameters required as inputs for the 3D FE are directly derived from CPT profiles as per the approach proposed by Igoe and Jalilvand (2020). This approach requires minimum user inputs and has been validated against a database of lateral pile field tests including PISA tests in the Dunkirk marine sand.

All components of soil reaction are extracted from the 3D FE models for a range of pile geometries and CPT profiles. CPT based correlations are calibrated from this database of soil reaction curves and by matching the 3D FE and 1D FE mudline responses.

The approach is then validated against large scale pile field tests (the same database used by Igoe and Jalilvand 2020).

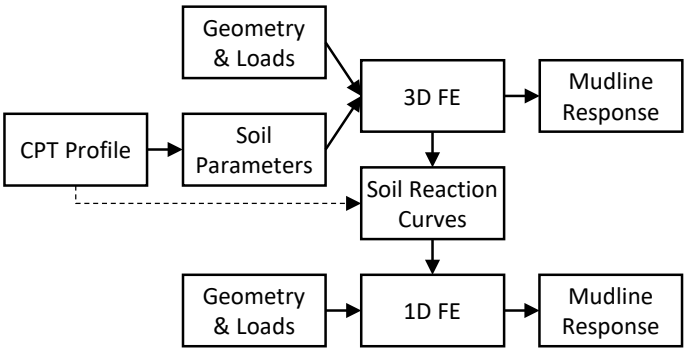

2 PLAXIS 3D FINITE ELEMENT MODELLING

This section presents how the 3D finite element models are set up in PLAXIS 3D and how results are being post-processed.

2.1 *Model set up*

Monopiles are modelled at full scale and half space using the commercially available finite element package PLAXIS 3D (see Figure 2). They are modelled with linear elastic plate elements with Young's modulus of 210 GPa and Poisson's ratio of 0.3. Since the lateral response is the main concern, the self-weight of the monopile is omitted. The piles are assumed wished in-place with no effect of the installation taken into account.

This study is limited to monopile modelling in sand. The hardening soil model with small-strain stiffness (HS-small) is an improvement of the HS model used by Suryasentana and Lehane (2014). It has been successfully used to accurately model monopile lateral response in sand (Igoe and Jalilvand 2020), and thus is considered here. Vertical interfaces are added between the pile shaft and the soil to allow for differential displacements, to introduce an interface strength reduction factor (set to 0.7 here) and to allow extraction of soil distributed reactions (distributed lateral load and distributed moment). At pile toe, an additional horizontal interface is added to allow for extraction of base reactions (base shear and base moment) but with no strength reduction considered.

The lateral loading as a result of wind and wave action is applied as a prescribed displacement at a height, e, above mudline. Burd et al. (2020) showed that there is negligible effect of the loading eccentricity on soil reaction curves. Hence the value of e is taken as 60 m (a mean value to represent both wave and wind dominated scenarios). The lateral loading is applied in the y direction. The size of the domain is taken as 12D in the direction of loading and 4D in the perpendicular direction as recommended in the PLAXIS Monopile Designer manual (Panagoulias et al. 2021), where D is the monopile diameter. The depth of the model is here set to 80 m with 16 soil layers of 5 m thickness each. This is to ensure the soil domain is large enough to avoid boundary effects.

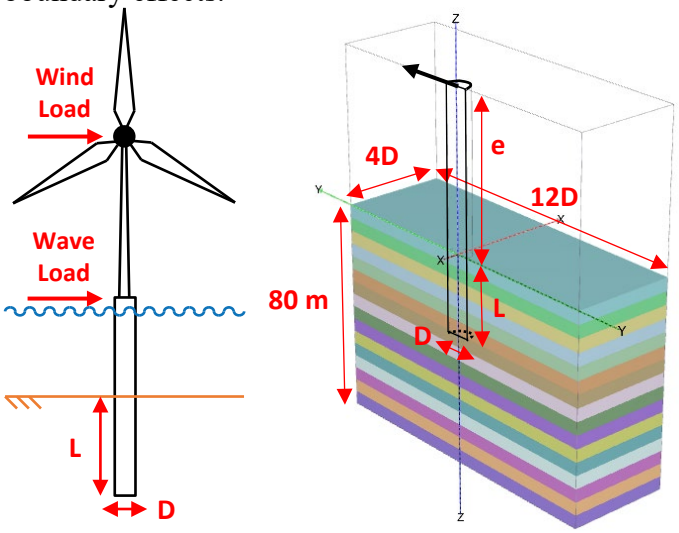

2.2 *Soil parameters*

Igoe and Jalilvand (2020) developed an approach to derive all of the required HS-small input parameters using widely used CPT correlations. All correlations used are summarised in Table 1. The approach has been validated against a database of large scale field tests including PISA tests in the Dunkirk marine sand and offers better predictive accuracy metrics than correlations suggested for the Plaxis Monopile Designer (Panagoulias et al. 2021).

By re-arranging the correlations presented in Table 1, synthetic CPT profiles for constant sand relative density are generated. Relative densities of 30% (loose), 50% (medium dense), 70% (dense) and 90% (very dense) are considered. At this stage, only normally consolidated state is considered with OCR set to 1. A constant ratio sleeve friction to cone resistance, f_s/q_c, of 1% is assumed. The constant volume friction angle is taken as 32 degrees for all profiles. The soil unit weight is taken ranging from 17 kN/m^3 to 20 kN/m^3 depending (linearly) on relative density. Finally, the small strain shear modulus profiles are estimated from the cone resistance with α set to 185 as recommended by Igoe & Jalilvand (2021).

Table 1. Correlations used by Igoe & Jalilvand (2021).

Correlations	References
$E_{50}^{ref} = E_{ur}^{ref}/3$	Brinkgreve et al. (2010)
$E_{oed}^{ref} = E_{50}^{ref}$	Brinkgreve et al. (2010)
$E_{ur}^{ref} = 0.00464 \cdot {E_0^{ref}}^{1.724}$ Where $E_0^{ref} = 2(1+\nu)G_0^{ref}$	Modified after Kirsh et al. (2014)
$m = 0.5$	Benz et al. (2009)
$\varphi' = \varphi'_{cv} + 3(D_R(10 - \ln p'_0) - 1)$	Bolton (1986)
$D_R = \sqrt{\frac{Q_{tn}}{305 \times OCR^{0.15}}}$	Kulhawy & Mayne (1990)
$Q_{tn} = \left(\frac{q_t - \sigma_{v0}}{p_{ref}}\right)\left(\frac{p_{ref}}{\sigma'_{v0}}\right)^n$ $n = 0.381 \cdot I_c + 0.05\frac{\sigma'_{v0}}{p_{ref}} - 0.15$ $I_c = \sqrt{(3.47 - \log_{10} Q_{tn})^2 + (1.22 + \log_{10} F_r)^2}$ $F_r = \frac{f_s}{q_t - \sigma_{v0}}$	Roberston & Cabal (2014)
$\sin\psi' = \frac{\sin\varphi' - \sin\varphi'_{cv}}{1 - \sin\varphi'\sin\varphi'_{cv}}$	Brinkgreve et al. (2018)
$G_0 = \alpha(q_t \cdot \sigma'_{v0} \cdot p_{ref})^{1/3}$	Schnaid and Yu (2007)
$\gamma_{0.7} = 1.5 \cdot 10^{-4}$	Benz et al. (2009)
$G_0^{ref} = G_0\left(\frac{p_{ref}}{p'_0}\right)^m$	Brinkgreve et al. (2018)
$K_0 = (1 - sin\,\varphi') \times OCR^{\sin\varphi'}$	Mayne & Kulhawy (1982)

2.3 *Monopile geometry*

To allow for the calibration of the CPT based correlations, a range of monopile geometries is considered. Literature showed that there is negligible effect of the pile wall thickness and load eccentricity on the soil reaction curves so these are kept constant as t = D/110 and e = 60 m, respectively (representative values based on experience). Outside diameters (D) of 6 m, 8 m, 10 m and 12 m are considered. Slenderness ratios (L/D) of 2, 3, 4, 5 and 6 are considered. This results in pile embedded length (L) ranging from 12 m to 72 m. Hence a total of 20 geometries are considered for each soil profile covering recent, current and future design.

2.4 *Soil reaction curves extraction*

Unlike Suryasentana and Lehane (2014), soil reaction curves are not calculated from the derivative of shear and bending moment diagrams. The approach briefly presented in the PLAXIS Monopile Designer manual (Panagoulias et al. 2021) has been preferred as it allow for extraction of all components of the soil reaction.

Distributed lateral load and distributed moment are calculated from integration of the normal and tangential stresses acting on monopile shaft (vertical interface). Soil reactions are integrated along 1 m (ΔZ) intervals as shown on Figure 3 and as per equations (3) and (4). Resulting lateral forces, Fy, and vertical forces, Fz, are calculated at each of the 6 Gaussian stress points of each interface elements as per equations (5) and (6), respectively. Where σ_n, τ_1 and τ_2 are the stresses directly extracted from Plaxis, X and Y are the coordinates of the stress point, D is the pile diameter, A is the area of the interface element and w is the weight of the stress point (0.11 for stress points 1 to 3 and 0.22 for stress points 4 to 6).

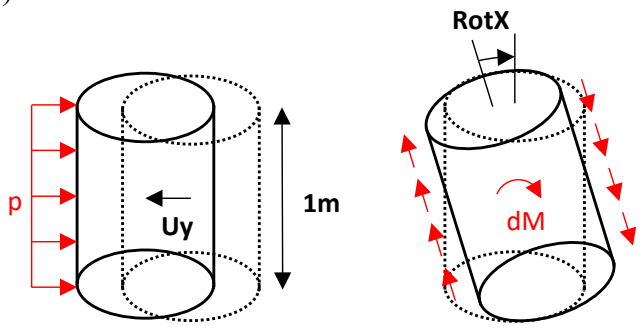

Figure 3. Integration of distributed lateral reaction and distributed moment.

$$p(Z) = \frac{\int_{Z-\Delta Z/2}^{Z+\Delta Z/2} F_y(z)dz}{\Delta Z} \quad (3)$$

$$dM(Z) = \frac{\int_{Z-\Delta Z/2}^{Z+\Delta Z/2} y \times F_z(z)dz}{\Delta Z} \quad (4)$$

$$F_y = wA\left(\frac{2Y}{D}\sigma_n - \frac{2X}{D}\tau_2\right) \quad (5)$$

$$F_z = wA\tau_1 \quad (6)$$

The base shear and base moments are calculated from the horizontal interface. This is not detailed here as the approach is very similar. All calculations are

repeated for each load increment in order to build the full reaction curves. These are then saved in a formatted .csv file for later use.

3 PRELIMINARY RESULTS

With 4 relative densities considered and 20 monopile geometries for each soil profile, the database consists in 80 3D FE models. On average, it took 1 hour to set up, run and process each model on a relatively high capacity computer (Intel(R) Xeon(R) W-1270P CPU @ 3.80GHz, 32 GB DDR4). The computation times were greatly reduced thanks to the automation of most aspects of the PLAXIS modelling through the PYTHON scripting interface. The database has been recently completed and this section presents and discuss preliminary results obtained.

3.1 *Comparison 1D FE – 3D FE responses*

In order to make sure soil reaction curves are being correctly extracted from PLAXIS, 3D FE and 1D FE monopile response are compared.

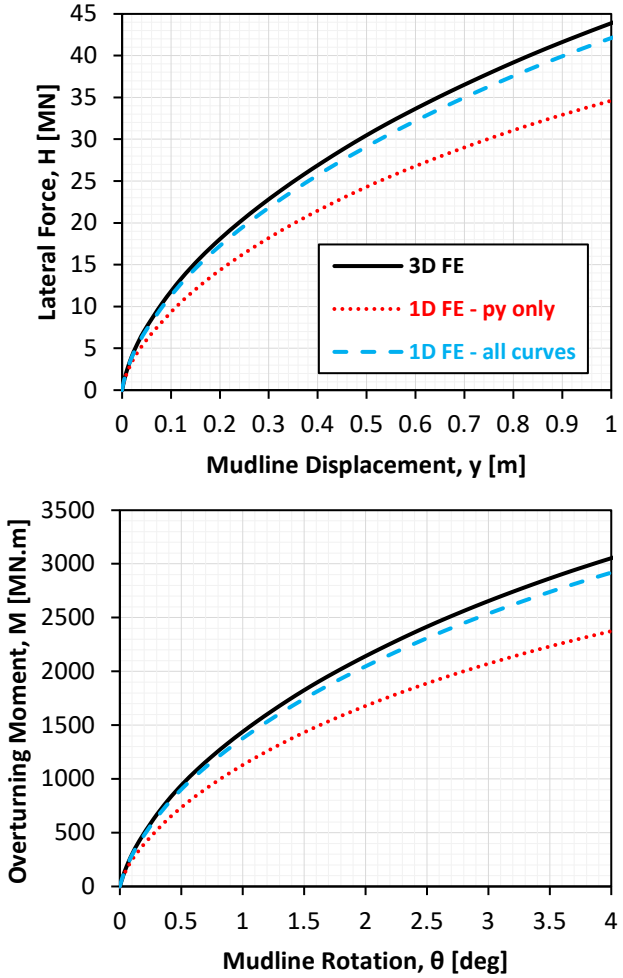

Figure 4. Comparison of 1D FE and 3D FE monopile lateral responses for case RD70%_D10L30.

For the sake of conciseness, only one model with pile diameter of 10 m, embedment length of 30 m in 70% relative density sand (case RD70%_D10L30) is presented in Figure 4 but all other models show similar results. Both load-displacement (top of the figure) and moment-rotation (bottom of the figure) curves compare relatively well when all reaction components are considered in the 1D FE model. However, when only p-y curves are being considered, the 1D FE response is found to be considerably softer than the 3D FE response. This is in agreement with findings from the PISA project (Byrne et al. 2015) and confirms the need of CPT based correlations including all components of pile-structure interactions and not limited to p-y curves only.

To add to this qualitative assessment, Table 2 compare initial stiffnesses, SLS rotations and ultimate capacities from 1D FE and 3D FE for the same model. The initial stiffness and ultimate capacity are defined at a mudline displacement of D/10000 and D/10, respectively. From experience, monopiles are subjected to strict serviceability requirements leading to low utilization in ULS GEO checks (≈ 1/2). When the load partial factor of ≈1.35 and material partial factor of 1.15 is considered, the SLS load is approximately defined as 1/3 of the ultimate capacity. One may consider that the 1D FE with p-y only may be considered overly conservative with underestimation of the initial stiffness and the ultimate capacity by 16.4% and 21.1%, respectively. The "SLS" rotation is overestimated by 47.7%. When adding other component of soil reactions to the 1D FE model, the match is much better with only a 4% underestimation of initial stiffness and ultimate capacity. The "SLS" rotation is only overestimated by 6.9%.

Table 2. Comparison of 1D FE and 3D FE initial stiffnesses, SLS rotations, and ultimate capacities for case RD70%_D10L30.

Model	Initial Stiffness [MN/m]	SLS Rotation [deg]	Ultimate Capacity [MN]
3D FE	244.4	0.450	43.9
1D FE py only	204.2 (- 16.4 %)	0.664 (+ 47.7 %)	34.6 (- 21.1 %)
1D FE all curves	234.5 (- 4.0 %)	0.481 (+ 6.9 %)	42.1 (- 4.0 %)

This quantitative assessment has been repeated for all 80 models. Only results pertaining to the estimation of ultimate capacity are presented in Figure 5 but the other two metrics show the same trend. For a typical slenderness ratio (L/D) of 3, the pile ultimate capacity is underestimated by more than 20% if only 'p-y' curves are used in 1D FE while the error is reduced to about 5% when all components are considered. For any L/D, the error is always larger when considering p-y curves only which suggests the need for the other component of soil reaction (distributed moment, base shear and base moment). For the p-y only scenario there is a clear trend for the errors to reduce when L/D increases. This is in agreement with the results of Byrne et al. (2015) and

it explains why approaches validated for slender piles (API 2011, Broms 1964, Suryasentana and Lehane 2014) had satisfactory results for slender piles. However, for current monopile design with L/D of as low as 3, these approaches are no longer applicable.

It is not yet clear why the errors with all curves included tend to slightly increase with L/D. However, the errors are deemed small enough (typically less than 5%) and the extracted soil reaction curves are deemed satisfactory.

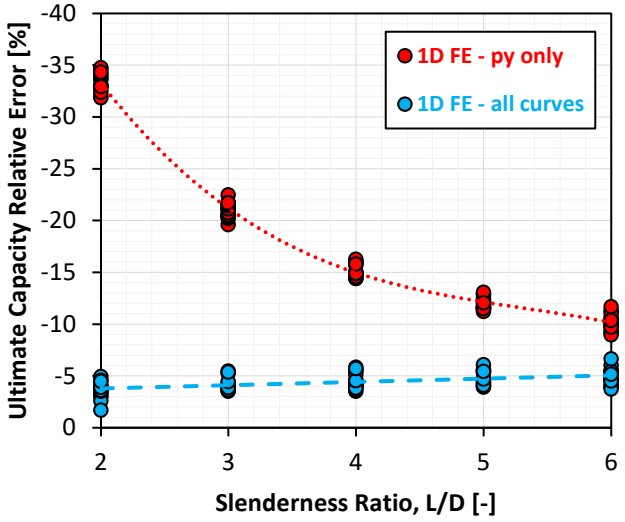

Figure 5. Comparison of ultimate capacity relative errors.

3.2 *Comparison soil reaction curves*

For the same case (RD70%_D10L30), Figure 6 shows the distributed lateral reaction curves (p-y curve) at a depth of 4.5 m as extracted from the 3D FE model and calculated as per API (2011), PISA rule (Burd et al. 2020) and Broms (1964). Input parameters required for API (friction angle) and PISA rule (relative density) are calculated as per approach set out in Table 1. Broms (1964) approach is directly based on the synthetic CPT profiles presented in section 2.2.

Figure 6 highlights the need to not only correctly match the ultimate reaction but also accurately describe the shape of the reaction curves. Broms (1964) overly simplify the problem by considering that the full reaction is mobilised at any displacement. In the API (2011), a hyperbolic tangent function is considered with the initial stiffness being a function of sand peak effective friction angle and depth. Although both approaches underestimate the ultimate capacity they will results in stiffer response in most practical cases (until a displacement of about 3% of pile diameter). On the contrary, the initial part of the PISA rule curve match relatively well with 3D FE. Although the ultimate capacity is underestimate again, they will results in similar response in most practical case.

In the PISA framework each of the reaction curves (distributed lateral reaction, distributed moment, base shear and base moment) are fitted with 4 parameters: the initial stiffness, the curvature, the ultimate reaction and the displacement at which the ultimate reaction is reached. This results in a total of 16 functions to correlate with CPT.

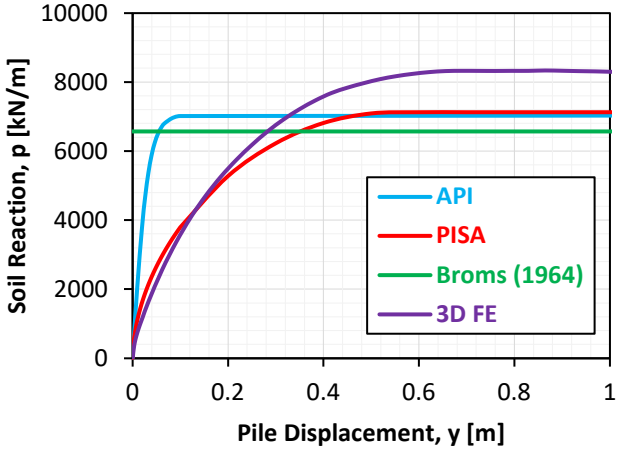

Figure 6. Comparison of distributed lateral reactions (p-y curves) at 4.5 m depth for case RD70%_D10L30.

4 ALTERNATIVE APPROACH

To date, no satisfactory CPT based correlations could be achieved due to a number of limitations with the current approaches. The main one (see sketch on Figure 7) is the lack of reaction close to pile point of rotation due to insufficient displacement. Although the pile is pushed until failure (mudline displacement larger than 10% of the pile diameter), the ultimate reactions are only reached for the top first 30%-40% of the pile length. No reaction at all is recorded close to point of rotation (at about 70% of pile length).

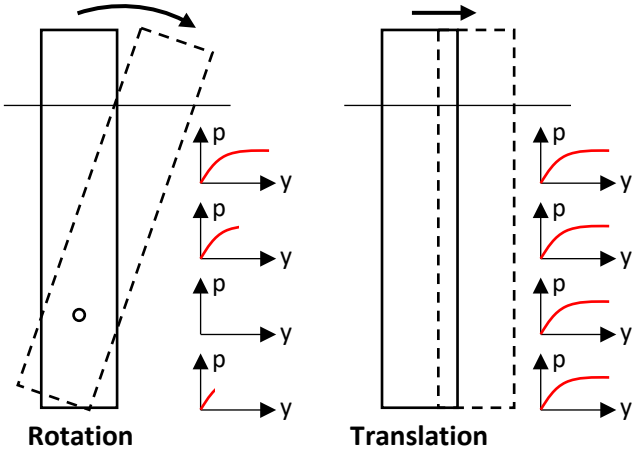

Figure 7. Limitation of the current rotation approach and proposed alternative approach.

An alternative approach is being considered where the pile would be laterally translated rather than rotated. This would allow for full mobilisation of reaction at any depth. Some components of the soil reaction may not be capture (distributed moment, base moment) and will still need to be extracted from the original models or correlated with the other component (distributed lateral reaction, base shear).

On-going works are focusing on comparing p-y curves extracted from both approaches to make sure they are comparable.

5 CONCLUSION

This paper presents a novel approach to derive CPT based correlation of soil reaction curves including distributed lateral reaction (p-y curves) but also distributed moment, base shear and base moment. This approach relies on finite element modelling in Plaxis 3D and the CPT based correlation of hardening soil model with small strain stiffness (HS-small) parameters developed by Igoe and Jalilvand (2020).

A total of 80 FE model are considered based on a range of pile geometry and synthetic CPT profiles for relative densities ranging from 30% (loose sand) to 90% (very dense sand).

All soil reaction curves are directly extracted from Plaxis 3D. Soil reactions are calculated from integration of stress at the pile-soil interface rather than derivation of pile shear force and bending moment profiles with depth. These are incorporated in a 1D FE solver and the obtained responses is compared with 3D FE to ensure the reaction curves are correctly extracted. Both initial stiffness, ultimate capacity and rotation under representative SLS loads are found to match well. By comparing the 1D FE responses when only p-y curves are considered, it is showed that existing approaches relying on p-y curves solely are not satisfactory for monopile modelling with slenderness ratio (L/D) of about 3.

Comparison of 3D FE extracted curves with existing approach shows that the ultimate distributed lateral soil reaction seems to be currently under-estimated, but this may not necessarily translate into an under-estimation of the pile response depending on the curve stiffness (and the account of other soil reaction components).

Current work is focusing on the derivation of CPT based correlations for all soil reaction curves including distributed lateral load, distributed moment, base shear and base moment. However, no satisfactory results could be obtained so far.

It is being investigated if the current 3D modelling approach should be revised. The current approach involves rotation of the monopile around of point of rotation. There is no pile displacement close to the point of rotation and hence no soil reactions making most of the data extracted from the 3D FE models un-usable. An alternative approach is being considered where the pile is being laterally translated in order to record soil reaction along the whole length of the monopile rather than only the top 30%-40%.

6 ACKNOWLEDGEMENT

The research conducted in this publication was funded by the Irish Research Council Postgraduate Employment-based Programme under grant number EBPPG/2019/4.

7 REFERENCES

API (2011). “API RP2GEO: Geotechnical and Foundation Design Considerations.”

Benz, T., Schwab, R., and Vermeer, P. (2009). “Small-strain stiffness in geotechnical analyses.” Bautechnik, 86(SUPPL. 1), 16–27.

Bolton, M. D. (1986). “The strength and dilatancy of sands.” Géotechnique, 36(1), 65–78.

Brinkgreve, R. B. J., Engin, E., and Swolfs, W. M. (2018). “Plaxis 3D Materials Manual.”

Brinkgreve, R., Engin, E., and Engin, H. (2010). “Validation of empirical formulas to derive model parameters for sands.” Numerical Methods in Geotechnical Engineering, (June), 137–142.

Burd, H., Taborda, D., Zdravković, L., Abadie, C., Byrne, B., Houlsby, G., Gavin, K., Igoe, D., Jardine, R., Martin, C., McAdam, R., Pedro, A. and Potts, D. (2020). “PISA design model for monopiles for offshore wind turbines: application to a marine sand.” Géotechnique, 70:11, 1048-1066.

Byrne, B. MacAdam, R., Burd, H. and Houlsby, G. (2015). “New design methods for large diameter piles under lateral loading for offshore wind applications.” Proceedings to the Third International Symposium on Frontiers in Offshore Geotechnics in Oslo, Norway.

DNV (2013). DNV OS-J101: Design of offshore Wind Turbine Structures.

DNV (2014). DNV OS-J101: Design of offshore Wind Turbine Structures.

Igoe. D. and Jalilvand, S. (2020). “3D finite element modelling of monopiles in sand validated against large scale field tests.” Proceedings to the Fourth International Symposium on Frontiers in Offshore Geotechnics in Houston, USA.

Kirsch, F., Richter, T., and Coronel, M. (2014). “Geotechnische Aspekte bei der Gründungsbemessung von Offshore-Windenergieanlagen auf Monopfählen mit sehr großen Durchmessern.” Stahlbau Spezial 2014 – Erneuerbare Energien, 83(SUPPL. 2), 61–67.

Kulhawy, F. H., and Mayne, P. W. (1990). „Manual on Estimating Soil Properties for Foundation Design.” EPRI-EL-6800.

Mayne, P. W., and Kulhawy, F. (1982). “K0 - OCR relationships in soils.” Journal of Geotechnical Engineering Division, 108(6), 851–872.

Minga, E. and Burd, H. (2019). “Validation of the PLAXIS MoDeTo 1D model for dense sand”.

Panagoulias, S., Brinkgreve, R. and Zampich, L. (2021) “Plaxis Monopile Designer CE V21 Manual”.

Petrasovits, G., and Award, A. 1972. “Ultimate lateral resistance of a rigid pile in cohesionless soil.” Proc., 5th European Conf. on SMFE 3, The Spanish Society for Soil Mechanics and Foundation, 407–412.

Prasad, Y. V. S. N., and Chari, T. R. 1999. “Lateral capacity of model rigid piles in cohesionless soils.” Soils Found., 392, 21–29.

Robertson, P. K., and Cabal, K. (2014). “Guide to Cone Penetration Testing for Geotechnical Engineering - 6th Edition”.

Schnaid, F., and Yu, H. S. (2007). “Interpretation of the seismic cone test in granular soils.” Géotechnique, 57(3), 265–272.

Suryasentana, S., and Lehane, B. M. (2014). “Numerical derivation of CPT-based p–y curves for piles in sand”, 64(3)

Wind Europe (2020). “Offshore wind in Europe: key trends and statistics.”

(intentionally left blank)

Appendix D

Lapastoure, L.-M., Diambra, A., Thusyanthan, I. Jalilvand, S. and Igoe, D. (2023). Overview of a new cyclic methodology for the geotechnical design of monopiles supporting offshore wind turbines in sand. 9th International SUT OSIG Conference, London, UK.

Overview of a new cyclic methodology for the geotechnical design of monopiles supporting offshore wind turbines in sand

L.-M. Lapastoure & D. Igoe
Department of Civil, Structural and Environmental Engineering, Trinity College Dublin, Dublin, Ireland

A. Diambra
Department of Civil Engineering, University of Bristol, Bristol, UK

I. Thusyanthan & S. Jalilvand
Gavin and Doherty Geosolutions, Dublin, Ireland

ABSTRACT: One of the key monopile design drivers is the requirement to limit the permanent rotation accumulated through the lifetime of the structure. DNV-ST-0126, which is one of the main standards used for the design of offshore wind turbines, suggests a limit of 0.5 degrees at mudline (including an allowance for 0.25 degrees inclination due to installation) to ensure turbine serviceability. However, no approach to estimate this accumulated rotation is recommended by DNV. EA-Pfahle (German recommendations on piling) and CFMS (French committee for soil mechanics and geotechnics) recommend the use of simple semi-empirical cyclic models. These models were developed based on laboratory-scale pile tests for very specific loading conditions and soil types. A new procedure to predict monopile lateral cyclic response relying on cyclic contour diagrams has recently been developed by Gavin and Doherty Geosolutions (GDG). This paper aims to present this approach highlighting the advantages of using site-specific cyclic data. The suitability of the proposed approach is shown using a case study in sand where the results are compared with models available in the literature.

1 Introduction

Offshore wind energy will be one of the key enablers in addressing climate change targets of a net-zero future by 2050. As the offshore wind industry matures, larger turbines are being installed in increasingly deeper waters resulting in larger loads applied to the foundations (Wind Europe, 2022). Therefore, the optimisation of the foundations for both safe and cost-effective design is becoming more important to ensure these ambitious targets can be achieved.

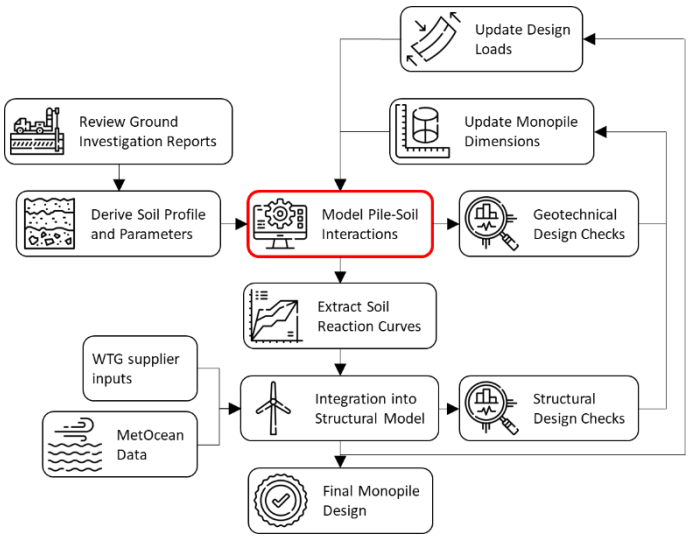

Figure 1. High level summary of monopile design process.

Monopiles are the most popular foundation type, supporting about 80% of the wind turbines installed to date (Wind Europe, 2022). Figure 1 presents a high-level summary of the monopile design process. It highlights that pile-soil interactions are central to the monopile design process, affecting both structural and geotechnical checks.

One of the key monopile design drivers is the requirement to limit the permanent rotation accumulated through the lifetime of the structure. DNV-ST-0126 (DNV, 2021), which is one of the main standards used for the design of offshore wind turbines, suggests a limit of 0.50 degrees at mudline to ensure turbine serviceability. However, no approach to estimate this accumulated rotation is recommended by DNV.

A new procedure to predict monopile lateral cyclic response relying on site specific cyclic contour diagrams has recently been developed by the authors. This paper aims to present this approach highlighting the advantages of using site-specific cyclic data. The suitability of the proposed approach is shown using a case study where the results are compared with models available in the literature.

2 Cyclic models from the literature

Abadie (2016) distinguishes three main categories of models used in practice to predict the monotonic re-

sponse of laterally loaded pile (see Figure 2). The same categorisation may be applied to cyclic loading. The models are classified depending on their complexity: (1) three-dimensional finite element analyses, (2) Winkler-type approaches, and (3) macro-element models.

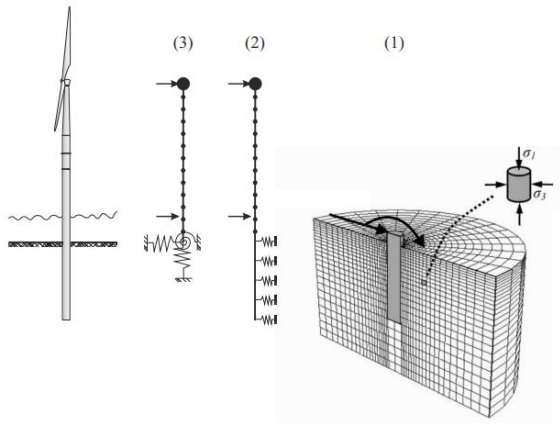

Figure 2. Monopile-soil interaction modelling methodologies after Abadie (2016).

2.1 *Three-dimensional finite-element analysis*

Three-dimensional finite element analyses (FEA) model the soil surrounding the pile as a continuum. It allows inspection of stress and strain distributions within the soil in addition to pile deflections and internal forces. Such approaches require advanced soil constitutive and numerous input parameters. Once, properly calibrated they are regarded as the most accurate approaches but require large computation time. The soil cyclic response is directly captured by advanced constitutive models (e.g. SANISAND-MS (Liu et al., 2021), HCA (Niemunis, 2015)) or by downgrading the input soil properties (e.g. UD-CAM/PDCAM; Page et al. 2013). Due to their complexity, these models are typically only used for research purposes.

2.2 *1D FEA Winkler-type approaches*

1D FEA Winkler-type approaches are often regarded as satisfactory compromise between accuracy and computation time. They involve modelling the pile embedment by means of one-dimensional elastic beam elements. The pile-soil interactions are captured by nonlinear soil reaction curves such as 'p-y' curves, predicting the soil reaction, p, as a function of the pile lateral displacement, y. Winkler-type approaches allow inspection of deflection and internal forces along the entire pile embedment but give no indication of the stress and strain distribution in the soil continuum surroundings the pile. The accuracy of such approaches relies on the calibration of the soil reaction curves considered. The PISA project has set out new state of the art approach to develop monotonic soil reaction curves but no guidance on cyclic loading is provided (Burd et al. 2020; Byrne et al. 2020). The soil cyclic response is usually captured by downgrading the monotonic soil reaction curves (e.g. API (API, 2014), SOLCYP-L (Solcyp, 2017)). 1D FEA Winkler-type approach are commonly used in the industry at all design stages but applicability of API and SOLCYP-L cyclic degradations for monopile design is questioned.

2.3 *Macro-element models*

Macro-element models are the most simplistic approach, incorporating the interactions between the pile and the soil into surface springs. Hence, such models provide no information on structural forces nor deflections along pile embedded length. EA-Pfähle (DGGT, 2013), the German recommendations for piling, recommends the model developed by Hettler (1981) to predict the deflection accumulation of piles subjected to cyclic lateral loading. The French committee for soil mechanics and geotechnics (CFMS, 2020) also recommends Hettler's model as well as models developed by Solcyp (2017) and Leblanc et al. (2010). These three models are macro-element models. They are the most likely to be used by the industry, especially at early stages of design. Due to their simplicity, macro-element models allow for quick computation and require minimum design inputs. However, these models were developed based on laboratory-scale pile tests for very specific loading conditions and soil types, making it challenging to apply them directly to a real monopile design case.

2.3.1 *Macro-element model by Hettler (1981)*

The macro-element by Hettler (1981) estimates the pile lateral displacement after N cycles (y_N) from the monotonic displacement under the same load level (y_s) as per equation (1).

$$y_N = y_s(1 + t \ln N) \qquad (1)$$

where the parameter t accounts for the system (pile and soil) sensitivity to cyclic loading and represents the rate of accumulation. Although no basis to estimate t is proposed, reported values range between 0.16 and 0.22 (DGGT, 2013). It should be noted that the approach was originally developed for pile displacement, but it is common practice in the industry to apply the same formulation to rotation. Hettler (1981) formulation is based on tests undertaken on homogeneous sands.

2.3.2 *Macro-element model by Leblanc et al. (2010)*

Leblanc et al. (2010a) specifically investigated the effect of cyclic loading on monopiles by considering low slenderness ratio (L/D = 4.5), large load eccentricity (e=M/H=5.4D) and focusing on pile ro-

tation. Based on 21 laboratory 1-g pile cyclic lateral tests in dry sand up to 65,000 cycles, a power function was found to best match the experimental results. The following expression to predict accumulation of pile rotation (θ_N) under cyclic loading was proposed:

$$\theta_N = \theta_s(1 + T_b T_c N^a) \qquad (2)$$

where a is a model constant with a value equal to 0.3 while T_b and T_c are parameters found to vary with the cyclic loading characteristics ζ_b and ζ_c, respectively. N is the number of load cycles and θ_s the static rotation.

ζ_b accounts for the maximum load magnitude (M_{max}) with respect to some reference load level (M_R) as per equation (3). Leblanc et al. (2010a) defines the reference load level (M_R) for a normalised mudline rotation of 4 degrees. The normalisation accounts for the vertical effective stress at pile toe. At laboratory scale, this resulted in an actual rotation of about 0.6 degrees, however at the monopile scale, this would be over 6 degrees. ζ_c accounts for the minimum component (M_{min}) of the cyclic loading as per equation (4). For pure one-way loading, $\zeta_c = 0$ while $\zeta_c = -1$ for pure two-way loading. The evolution of T_b and T_c with ζ_b and ζ_c is reported in Figure 3 after Leblanc et al. (2010a).

$$\zeta_b = \frac{M_{max}}{M_R} \qquad (3)$$

$$\zeta_c = \frac{M_{min}}{M_{max}} \qquad (4)$$

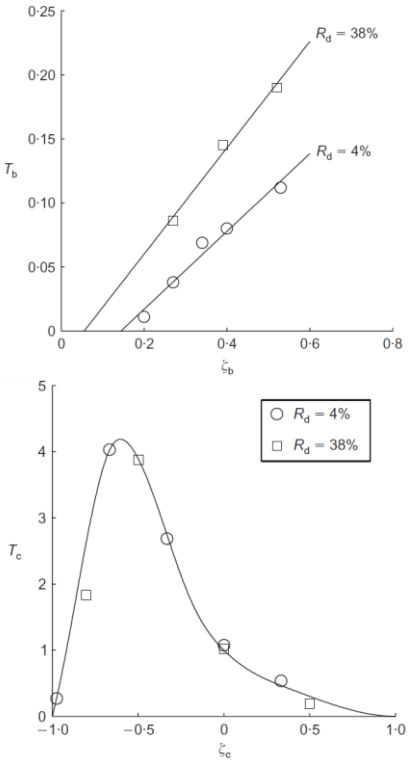

Figure 3. Evolution of Tb (top) and Tc (bottom) with the cyclic loading characteristics ζ_b and ζ_c (Leblanc et al., 2010a).

2.3.3 *Macro-element model by Solcyp (2017)*

Based upon a large centrifuge program, the Solcyp (2017) approach suggests a power relationship between accumulated pile displacement upon cyclic loading and the number of cycles for clay and a logarithmic function for sands. The relationship for sands, appropriate for the case study considered later in this paper, is presented in equation (5) where *CR* is a coefficient accounting for pile stiffness, H_{cyc} is cyclic moment amplitude and H_{max} is maximum cyclic moment.

$$y_N = y_1 \frac{0.235}{CR}\left(\frac{H_{cyc}}{H_{max}}\right)^{0.35} \log_{10} N \qquad (5)$$

The coefficient *CR* accounting for pile relative stiffness is calculated as per equation (6) where $(EI)_{ref}$ is the actual pile bending stiffness and $(EI)_{flexible}$ is the bending stiffness limit for flexible behaviour. The coefficient takes a minimum value of 1 for flexible pile and increase with pile stiffness. Hence, the rate of cyclic accumulation in equation (5) decreases when pile stiffness increases.

$$CR = \left(\frac{(EI)_{ref}}{(EI)_{flexible}}\right)^{\frac{1}{5}} \geq 1 \qquad (6)$$

Solcyp (2017) requires defining the limit for flexible behaviour $(EI)_{flexible}$ by plotting the pile mudline static displacement under conventional load limit, H_{lim}, as a function of pile bending stiffness EI. An example is provided in Figure 4. The conventional load limit, H_{lim}, is calculated as per equation (7) where $H(y = D)$ and $H(y = D/2)$ are the lateral loads leading to pile mudline static displacement of one pile diameter and one half of pile diameter, respectively (see example in Figure 4) H_{lim} is estimated for the actual pile bending stiffness, $(EI)_{ref}$.

$$H_{lim} = H(y = D) - 2H(y = D/2) \qquad (7)$$

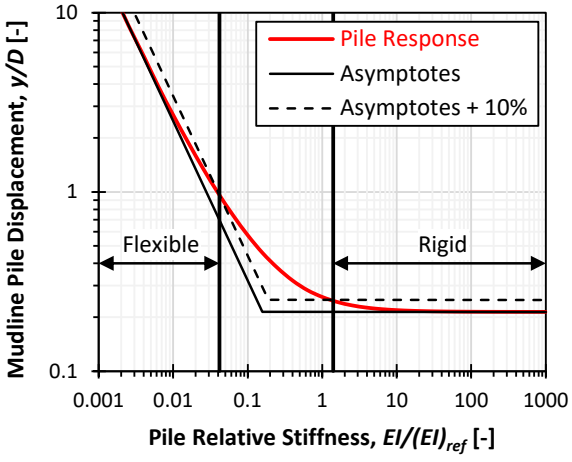

Figure 4. Example calculation of limit of flexible behaviour $(EI)_{flexible}$.

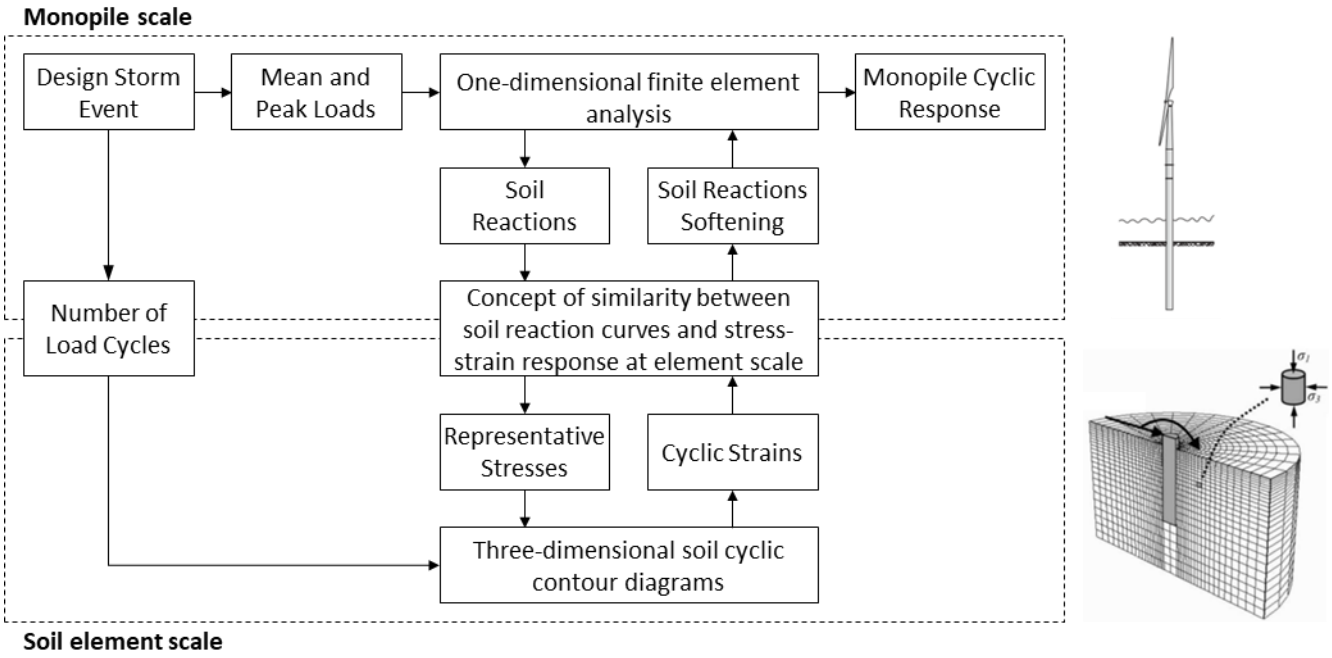

Figure 5. Overview of GDG cyclic model.

3 Overview GDG cyclic model

An in-house cyclic design methodology for sands and clays has been developed and implemented by the authors. Through the different load packets of the design cyclic load history, monotonic soil reaction curves are softened in a 1D FE solver, as presented in Figure 5. This Winkler-type approach benefits from the direct use of site-specific cyclic soil degradation data. In comparison to the recommended macro-element models, any soil conditions can be considered as long as cyclic contour diagrams are available for each different unit. The model runs in few seconds thanks to the computational efficiency of 1D FEA.

The approach relies on the concept of similarity between the soil reaction curves (at monopile scale) and the soil stress-strain behaviour (at element scale). The soil response to cyclic loading at element scale is identified by means of three-dimensional cyclic contour diagrams, which are key input to the approach. If no site-specific data are available, contour diagrams from the literature for similar soil conditions can be considered. For example, the NGI database can be scaled as per the approach proposed by Andersen et al. (2023).

The theory of the "concept of similarity" was presented by Zhang et al. (2020) for clays; the concept of similarity used in this approach is illustrated in Figure 6. The ratio of soil lateral reaction p to ultimate reaction p_u at the p-y level is considered equivalent to the ratio of mobilised shear stress τ to shear strength τ_u from a DSS test. Similarly, the pile displacement y is normalised over y_{50} (displacement at which 50% of the capacity is mobilised) and is considered equivalent to the ratio of the shear strain γ to γ_{50}.

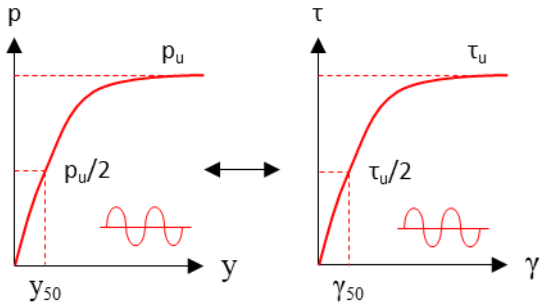

Figure 6. Similarity between soil reaction curves and stress-strain response at element scale.

Figure 7 summarises the process of soil reaction curves softening. The monotonic soil reaction curves are soften by shifting the curves by $y_{shift,i}$. The shift is applied at p_i, the soil reaction mobilised under lateral load H_i, and represent the ratcheting. The magnitude of the shift is directly scaled from the cyclic contour diagrams based on the number of cycles and the soil mobilisation (p_i/p_u). Cyclic degradation generally decreases with depth with no cyclic degradation experienced close to the point of rotation (about 2/3L for monopiles). The process is repeated for each load package in the cyclic load history.

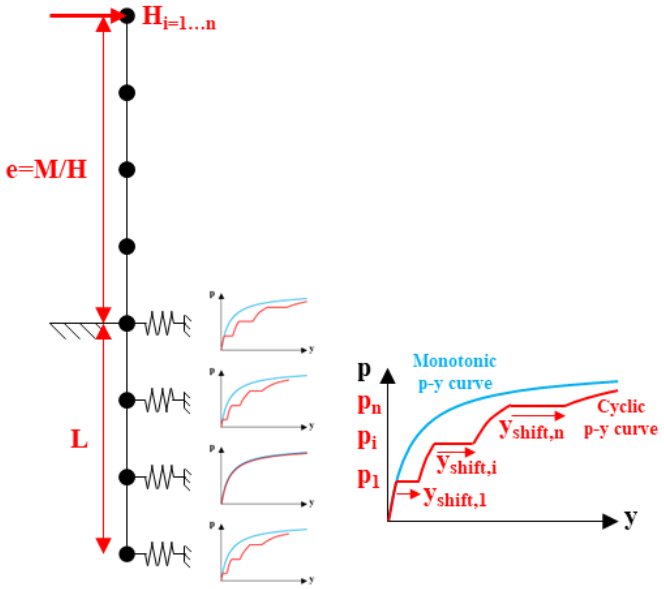

Figure 7: Example of soil reaction softening.

The main difference between the sand and clay model is how the drainage conditions are accounted for. In sand, the approach accounts for the generation of excess pore pressure and partial drainage upon cyclic loading. Sand permeability and rate of loading highly influences the drainage conditions. Only the sand model has been applied in the following case study because cohesive soils were not encountered at this specific location.

4 Case study

The new cyclic model has recently been applied for a sensitivity study during detailed foundation design of large capacity WTG installed in about 30 m water depth in the North Sea. Some outcomes of this project will be presented in the following. Given the level of confidentiality of the project, only limited data can be shared. As shown on Figure 8, the soil profile was relatively homogeneous with dense sand ($D_R \approx 70\%$, $G_0 \approx 60$ MPa) for the top 10 m followed by very dense sand ($D_R \approx 90\%$, $G_0 \approx 120$ MPa).

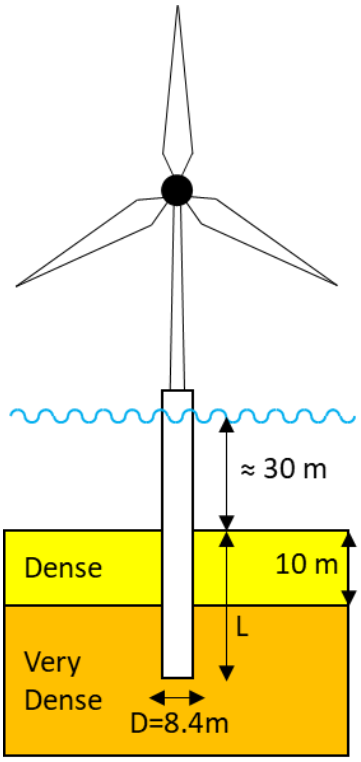

Figure 8. Site conditions.

The monopile monotonic response was computed using the PISA numerical based approach whereby the monotonic soil reaction curves were calibrated from a suit of 3D FEA for a range of monopile geometries (implementation presented in Lapastoure & Igoe, 2022). The HS-small soil model was used to model sand in Plaxis 3D using the CPT based approach presented in Igoe and Jalilvand (2022).

The accumulated permanent rotation was calculated considering a 36h storm build up event. The 3 macro-element models presented above and recommended by EA-Pfahle (DGGT, 2012) and CFMS (2022) were considered. Figure 9 presents an example superposition procedure used to calculate the accumulation of pile mudline rotation through the different load packages. For Hettler, predictions are based on t = 0.22 (UB) and t = 0.16 (LB). For Leblanc, UB and LB predictions are presented using the two T_b functions reported in Leblanc et al. (2010). For Solcyp, both the SOLCYP-G model (macro-element model presented in section 2.3.3) and SOLCYP-L model (winkler-type approach presented in Solcyp, 2017) are considered.

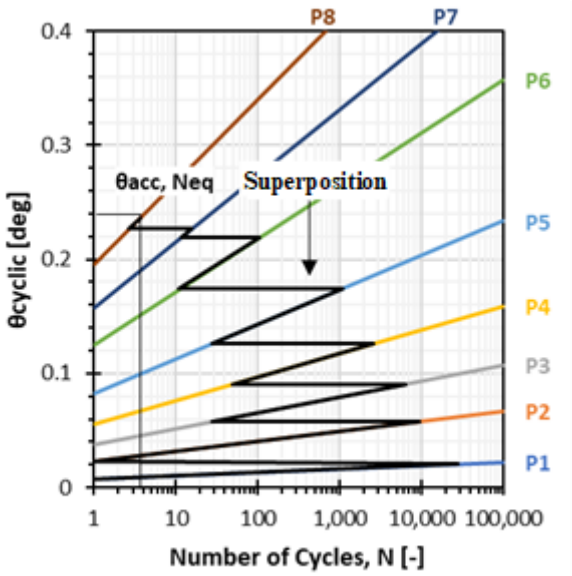

Figure 9. Example superposition procedure for the macro-element models.

The GDG cyclic model was also applied using site-specific cyclic contour diagrams. An example plot showing the development of cyclic strain as a function of the stress level and number of cycles in presented in Figure 10. Cyclic contour diagrams and other inputs parameters were inferred from a series of direct simple shear and triaxial laboratory tests.

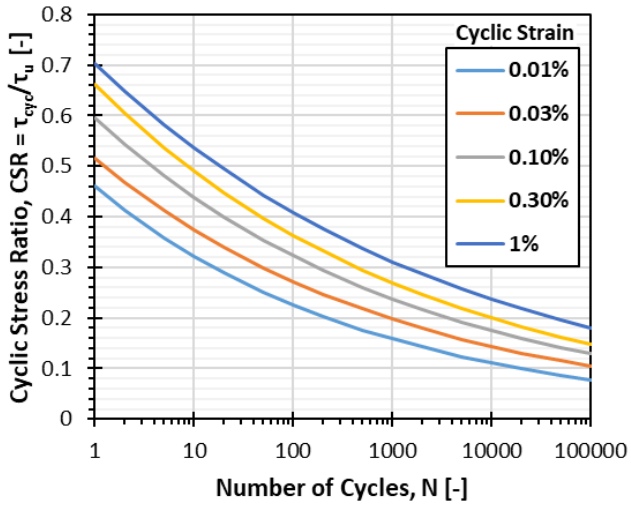

Figure 10. Example contour diagram showing development of cyclic strain as a function of stress level and number of cycles.

The results of the different models are compared on Figure 11 in terms of accumulated permanent rotation, $\theta_{acc,perm}$, versus pile embedded length, L (note that the pile diameter was fixed at 8.4 m and average wall thickness at 80 mm). This plot is used to optimise the pile embedded length and ensure compliance with DNV requirements.

One can notice the significant differences between the different models on Figure 11. SOLCYP-G generally leads to little accumulation of rotation. This is due to the high rigidity (CR) of monopiles lowering the rate of accumulation in equation (5). Hettler generally leads to larger accumulated rotation with a constant rate of accumulation (t = 0.16 or 0.22). Leblanc initially leads to little accumulated rotation for large pile penetration because the monopile ultimate capacity is much larger than the cyclic loads, reducing T_b in equation (2); however, the predicted accumulated permanent rotation sharply increases as the pile decreases.

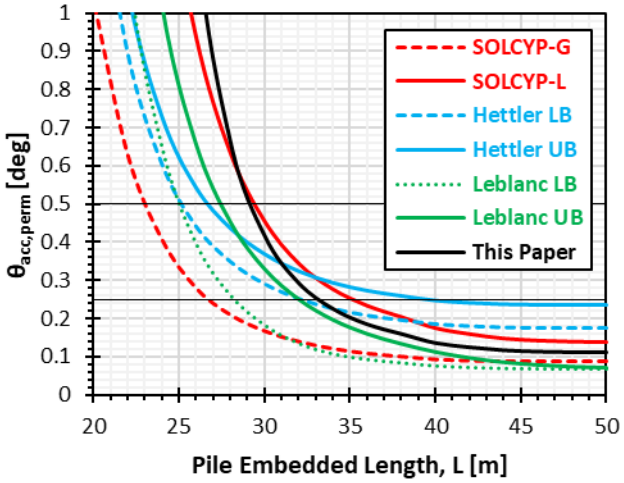

Figure 11. Comparison of accumulated permanent rotation calculated with GDG cyclic model and other cyclic models recommended in the literature.

Table 1 summarises the design embedded pile lengths based on the different models for two design criteria: 0.25 deg and 0.50 deg. Different design criteria are used depending on the turbine manufacturer requirements. The cyclic model presented in this paper compare relatively well with the literature range for the 0.25 deg criterion but generally leads to larger pile penetration for the 0.50 deg criterion.

Table 1. Comparison of design embedded pile length based on different criteria and cyclic models.

Model	Design Embedded Length, L [m]			
	0.25 deg criterion		0.50 deg criterion	
	min	max	min	max
Solcyp	26.9	35.2	23.2	29.5
Hettler	32.2	39.4	25.3	26.8
Leblanc	28.3	32.0	25.2	27.5
This paper	33.2		29.3	

5 Conclusion

DNV-ST-0126 suggests to limit the permanent rotation accumulated during the lifespan of wind turbine is often found a crucial monopile design driver. Given the shortcomings of the basic macro-element models recommended by EA-Pfahle (DGGT, 2013) and CFMS (2022), a new in-house cyclic model based on site-specific soil cyclic contour diagrams has been developed. The model is presented, and suitability of the proposed approach is shown through a case study in sand-dominated soils where

the results are compared with models available in the literature. The model benefits from the direct use of site-specific soil cyclic contour diagrams and computational efficiency of 1-dimensional finite-element analysis. Any soil conditions can be considered and the model runs in only few seconds allowing for optimisation of monopile design.

To further develop and validate the cyclic approach, 6 piles with outside diameter of 427 mm were driven in sands to 1 m, 1.5 and 2 m embedment at the Blessington test site in Ireland and are currently being tested. This new set of cyclic field tests will extend existing literature with smaller slenderness ratios (L/D in the range of 2.2 to 4.4) which are more representative of actual monopile designs. The result of the tests and further validation of the model will be disseminated in future publications.

Acknowledgement

The research conducted in this publication was funded by the Irish Research Council Postgraduate Employment-based Programme under grant number EBPPG/2019/4. The collaboration with University of Bristol was supported by the Royal Academy of Engineering Industrial Fellowship scheme, grant number IF2021/64.

References

API (2014). ANSI/API Recommended Practice 2GEO. First edition, April 2011 + addendum 2014.

Abadie C. (2016). Cyclic lateral loading of monopile foundations in cohesionless soils. PhD thesis. University of Oxford.

Andersen, K. H., Engin, H.K., D'Ignazio, M. & Yang, S. (2023). Determination of cyclic soil parameters for offshore foundation design from an existing data base. Ocean Engineering, vol. 267, 113180.

Burd, H.J., Taborda, D.M., Zdravković, L., Abadie, C.N., Byrne, B.W., Houlsby, G.T., Gavin, K.G., Igoe, D.J., Jardine, R.J., Martin, C.M. and McAdam, R.A. (2020). PISA design model for monopiles for offshore wind turbines: application to a marine sand. Géotechnique, 70(11), 1048-1066.

Byron W. Byrne, Guy T. Houlsby, Harvey J. Burd, Kenneth G. Gavin, David J. P. Igoe, Richard J. Jardine, Christopher M. Martin, Ross A. McAdam, David M. Potts, David M. G. Taborda, and Lidija Zdravković (2020). PISA design model for monopiles for offshore wind turbines: application to a stiff glacial clay till. Géotechnique 2020 70:11, 1030-1047. DOI: 10.1680/jgeot.18.P.255

CFMS (2020). Recommendations for planning and designing foundations of offshore wind turbines. Version 2.1.

DGGT (2013). Recommendations on pilling (EA-Pfähle).

DNV (2021). DNV-ST-0126: Support structure for wind turbines.

Igoe, D. & Jalilvand, S. (2022). 3D Finite Element Modelling of Monopiles in Sand Validated Against Large Scale Field Tests. Proceedings to ISFOG 2022.

Lapastoure, L.-M. & Igoe, D. (2022). Implementation of PISA numerical framework for offshore wind foundation design. Proceedings to the Civil Engineering Research Association of Ireland 2022 conference.

LeBlanc, C., Houlsby, G. T. & Byrne, B.W. (2010). Response of stiff piles in sand to long-term cyclic lateral loading. Géotechnique 60, No. 2, 79–90.

Liu, H., Kementzetzidis, E., Abell, J. A., & Pisanò, F. (2021). From cyclic sand ratcheting to tilt accumulation of offshore monopiles: 3D FE modelling using SANISAND-MS. Géotechnique.

Niemunis, A, Wichtmann, T, Triantafyllidis, T. (2005). A high-cycle accumulation model for sand. Computers and Geotechnics; 32. No. 4, 245–263.

Page, A., Jostad, H. P. & Saue, M. (2013). Application of an undrained and a partially drained cyclic accumulation model for monopile design. 5th International Young Geotechnical Engineers' Conference

Solcyp (2017). Design of piles under cyclic loading: SOLCYP recommendations. John Wiley & Sons.

Wind Europe (2022). Offshore wind in Europe - key trends and statistics 2021.

Zhang, Y., Andersen K. H. & Jeanjean, P. (2020). Verification of a framework for cyclic p-y curves in clay by hindcast of Sabine River, SOLCYP and centrifuge laterally loaded pile tests. Applied Ocean Research, vol. 97, 102085.

Appendix E

Lapastoure, L.-M. and Igoe, D. (2023). Exploring the use of machine learning for the geotechnical design of monopiles supporting offshore wind turbines, ISMLG conference, Cork, Ireland.

ISMLG 2023
4th International Symposium on Machine Learning and Big Data in Geoscience
University College Cork, 29th August – 1st September 2023

Exploring the use of machine learning for the geotechnical design of monopiles supporting offshore wind turbines

Louis-Marin Lapastoure[*1,2], and David Igoe[1]

[1]Department of Civil, Structural and Environmental Engineering, Trinity College Dublin, College Green, Dublin 2, Ireland

[2]Gavin and Doherty Geosolutions, Unit A2, Nutgrove Office Park, Dublin 14, Ireland

[*]presenting author (email: lapastol@tcd.ie)

Keywords: Offshore wind, Geotechnical engineering, Monopile, Machine learning

1 INTRODUCTION

The Offshore Renewable Energy Strategy published by the European Commission has set ambitious targets of developing 300 GW of offshore wind by 2050 [1]. Monopiles are the most popular foundation type, supporting about 80% of the offshore wind turbines installed to date in Europe [2]. The design of monopiles is primarily governed by lateral loading, as they sustain large wind, waves, and current loads. The industry state-of-the-art approach currently consists in computing the monopile lateral response using advanced 3-dimensional finite element analysis. Once calibrated such analyses are considered as the most accurate but require large computation time. This research investigates the use of machine learning for preliminary design. A database of 3D FEA computed monopile lateral response has been created for a separate project and is now used to train number of machine learning algorithms. It is shown that one should be careful when using machine learning algorithm made readily available in packages such as MATLAB machine learning toolbox. Even a model that seems to be perfectly trained may be completely wrong. It is also shown how one can simply add some knowledge of the physics of the problem to lead to better results.

METHODOLOGY

A database of monopile response to lateral loading was created using advanced 3-dimensional finite element analysis. The details of the calculations are presented in [3] with an overview presented on Figure 1. The database includes a range of sand relative density (RD from 30% to 90%), pile diameter (D from 6 m to 12 m) and ratio of pile embedment to diameter (L/D from 2 to 6). The lateral load is applied 60 m above mudline and the diameter to wall thickness ratio is fixed at 110. Although the database currently only considered homogeneous soil conditions, it is still deemed representative of realistic design scenarios and is considered for the exploring the use of machine learning.

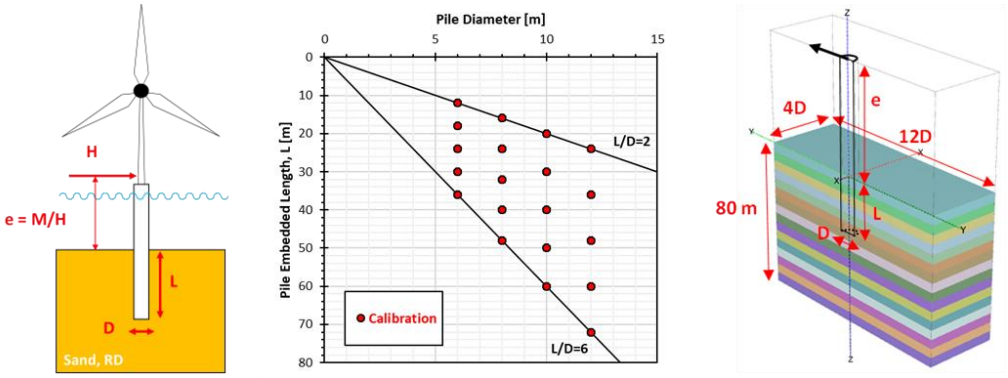

Figure 1. Overview of the database of 3D FEA.

The MATLAB machine learning toolbox offers numerous algorithms readily available (neural networks, gaussian processes, support vector machines, decisions tress, etc.). All these models can be automatically trained to any dataset with very inputs required by the user regarding the machine learning algorithms meta parameters. All these models were trained against the database presented previously in order to predict the mudline pile rotation as a function of the pile embedded length, pile diameter, relative density and lateral load. This would constitute a quick tool for preliminary monopile design.

RESULTS & DISCUSSIONS

MATLAB automatically ranked the models based on accuracy metrics such as R^2 comparing the true to predicted output. Model 5.4 “Exponential Gaussian Process Regression”, Model 5.1 “Rational Quadratic Gaussian Process Regression” and Model 8.5 “Trilayered neural networks” appear to be the best three models with $R^2 > 0.99$ as shown on Figure 2. It should be noted that although the authors have limited knowledge of the various models, they were all automatically trained by MATLAB.

Once trained, the performance of the top 3 models was compared to 3D FEA for a verification case taken within the calibration space. Figure 3 shows how the pile mudline moment-rotation responses compare. Although the predicted responses are within the right order of magnitude, all three models show significant shortcomings. Model 8.5 may seem the most accurate but the stiffness increase between 4 and 5 degrees is aphysical. Models 5.1 and 5.4 exhibit smoother response but do no intercept at (0,0). One would expect no rotation when no loads applied and vice versa.

Model 5.4 “Exponential Gaussian Process Regression” was retrained with the dataset but to predict foundation rotational stiffness rather than the pile rotation. It essentially leads to the same thing for a geotechnical engineer but adding some physical knowledge of the problem was found to greatly improve the predictions as shown on Figure 4.

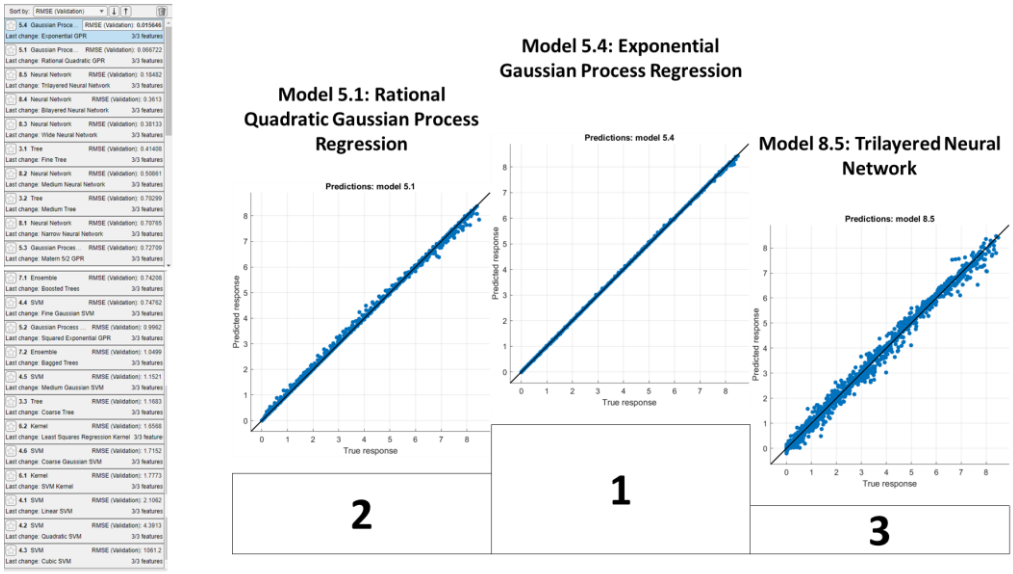

Figure 2. Ranking various machine learning algorithm automatically trained by MATLAB.

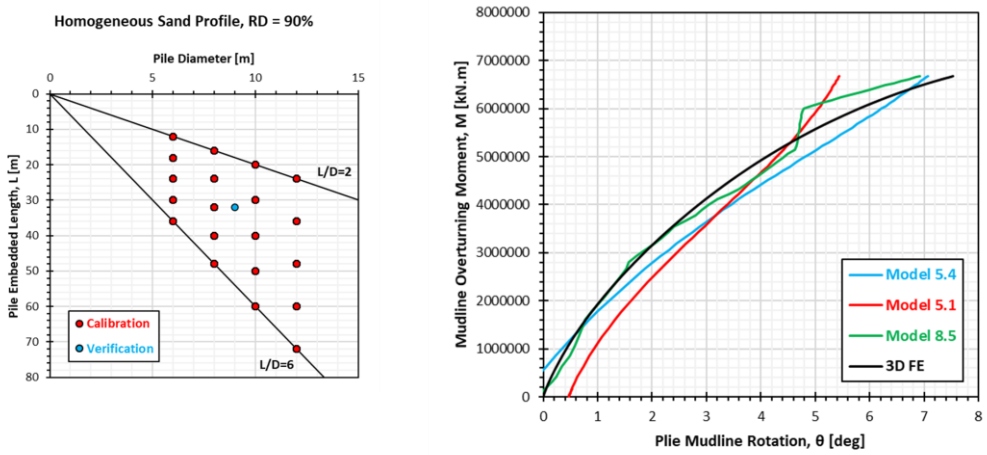

Figure 3. Verification of models performance based on pile mudline moment-rotation response.

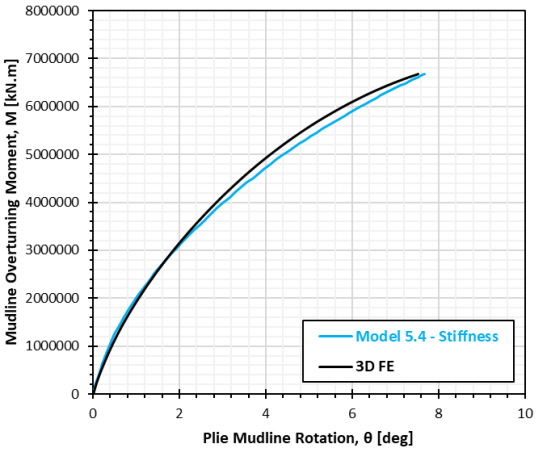

Figure 4. Same verification as Figure 3 but with prediction of stiffness rather than rotation.

2 CONCLUSIONS

The aim of this presentation is to investigate the use of machine learning in offshore geotechnical engineering. This is done by using a database of monopile response to lateral loading using advanced 3-dimensional finite element analysis. The database was used to train several machine learning algorithms. Through this experimentation, the authors would like to warn about the apparent simplicity of some package such MATLAB machine learning toolbox. Such packages are making a number of machine learning algorithms readily available although the user may have no knowledge of their specificities nor understanding of the meta parameters. Even when the models seem to be perfectly trained (R^2~1), their predictions can be off. This might be due to overfitting which can easily happened when the meta parameters of the machine learning algorithm are not selected carefully. The presentation will also discuss how the addition of some physical knowledge of the problem might help the training to the different machine learning algorithms.

ACKOWLEDGEMENTS

The research conducted in this publication was funded by the Irish Research Council Postgraduate Employment-based Programme under grant number EBPPG/2019/4.

REFERENCES

[1] European Commission (2020). An EU Strategy to harness the potential of offshore renewable energy for a climate neutral future.

[2] Wind Europe (2022). Offshore wind in Europe - key trends and statistics 2021.

[3] Lapastoure, L. M., & Igoe, D. (2022). 3D FE derivation of CPT based soil reaction curves for monopile lateral static design in sand. In Cone Penetration Testing 2022 (pp. 991-997). CRC Press.

(intentionally left blank)

Appendix F

Prediction of short piles response to lateral monotonic load in dense sand at Blessington. XVIII European Conference on Soil Mechanics and Geotechnical Engineering, Lisbon, Portugal.

Proceedings of the XVIII ECSMGE 2024
GEOTECHNICAL ENGINEERING CHALLENGES
TO MEET CURRENT AND EMERGING NEEDS OF SOCIETY

ISBN 978-1-032-54816-6

ECSMGE 24
XVIII EUROPEAN CONFERENCE ON SOIL MECHANICS AND GEOTECHNICAL ENGINEERING

Prediction of short piles response to lateral monotonic load in dense sand at Blessington

Prédictions de la réponse de pieux courts sous charge monotonique latérale dans le sable dense de Blessington

L.-M. Lapastoure*
Department of Civil, Structural and Environmental Engineering, Trinity College Dublin, Dublin, Ireland
Gavin and Doherty Geosolutions, Dublin, Ireland

D. Igoe
Department of Civil, Structural and Environmental Engineering, Trinity College Dublin, Dublin, Ireland

**lapastol@tcd.ie (corresponding author)*

ABSTRACT: This paper presents some initial results of an experimental campaign aimed at extending the existing database of pile lateral field tests. Monopiles with low slenderness ratios (L/D, ratio of pile embedment to pile diameter) less than 4.5 are deemed to be representative of current and future monopile foundation designs for the offshore wind industry. The monopile field testing consisted of both monotonic and cyclic tests with slenderness ranging from 2.2 to 4.4. A total of 6 piles with an outer diameter of 457 mm were driven and tested in dense sand at the Blessington test site, located south to Dublin in Ireland. Three different approaches were used to predict the monotonic pile responses. Traditional approaches (API and PISA rule) were found to significantly underestimate both piles stiffness and ultimate capacity. A novel set of CPT based correlations of HS-small parameters for three-dimensional finite-element analyses recently developed by Trinity College Dublin was found to provide very accurate predictions of both stiffness and ultimate reaction.

RÉSUMÉ : Cet article présente les premiers résultats d'une campagne expérimentale visant à étendre la base de données existante d'essais in-situ de pieux chargés latéralement. Des rapports d'élancement (L/D, rapport entre la profondeur et le diamètre du pieu) plus faibles sont plus représentatifs des dimensions des foundations monopieux supportant actuellement les éoliennes en mer. Des pieux avec des rapports d'élancement allant de 2.2 à 4.4 ont été testés sous charges monotoniques et cycliques. Au total, 6 pieux d'un diamètre extérieur de 457 mm ont été battues et testés dans du sable dense sur le site d'essai de Blessington, situé au sud de Dublin en Irlande. Trois approches différentes ont été utilisées pour prédire la réponse des pieux sous chargement monétique. Les approches traditionnelles (API et PISA rule) ont sous-estimé de manière significative la rigidité et la capacité ultime des pieux. Trinity College Dublin a récemment développé un jeu de corrélations bases sur le CPT pour les paramètres du model de soil constitutif HS-small, populaire pour les analyses éléments finis 3D. Cette approche s'est avérée fournir des prédictions très précises de la rigidité et de la réaction ultime des pieux.

Keywords: Offshore Wind; Geotechnical Engineering; Monopiles; Field Tests

1 INTRODUCTION

This paper outlines the preliminary findings from an experimental initiative aimed at expanding the current repository of lateral field tests for low L/D monopiles. Monopiles are large diameter open ended steel pipe piles which are typically impact driven into the seabed and are the most commonly used foundation for offshore wind turbines. As the offshore wind industry matures, larger wind turbines are being design which require monopiles with diameters in excess of 10 m. These XL monopiles typically have slenderness ratios (L/D, where L is the embedded length and D the diameter) less than 4.5. In this paper, the results from one of the monotonic field test piles with L/D=3.3 is compared to three different approaches for predicting the lateral responses of the piles. The paper shows that current rule-based beam-spring approaches such as API (2011) and PISA-rule based method (Burd et al. 2020) both significantly underestimate the stiffness and ultimate capacity of these small scale piles. In contrast, a 3D Finite Element approach developed at Trinity College Dublin, using CPT-based correlations, provides highly accurate predictions for the entire load-displacement response.

2 METHOOLOGIES

This section presents 3 different approaches to predict the response of piles subjected to monotonic lateral loading in sands.

2.1 API

The traditional industry practice used to follow the oil and gas industry design standard (API, 2014). The 'p-y approach' involves modelling the pile by means of one-dimensional elastic beam elements. At each depth, a 'p-y curve' defines the non-linear relationship between the soil resistance, p, mobilised as a result of the pile lateral displacement, y. The soil layers are assumed to behave independently therefore the curves are uncoupled. API RP 2GEO (API, 2014) provides basis for the formulation of the non-linear p-y curves in sands, soft clays and stiff clays. In sands, it takes the form of a hyperbolic tangent as shown by equation (1):

$$p = Ap_u \tanh\left(\frac{kz}{Ap_u}y\right) \quad (1)$$

Where:

- $A = \left(3 - 0.8\frac{z}{D}\right) \geq 0.9$ for monotonic loading
- p_u is the ultimate lateral resistance at depth z.
- k is the rate of increase with depth of initial modulus of subgrade reaction at depth z.
- y is the lateral pile deflection at depth z.
- z is the depth below ground level.

The interested reader is invited to refer to API (2014) section 8.5.6 for additional information, including basis for calculation of p_u and k.

2.2 PISA rule

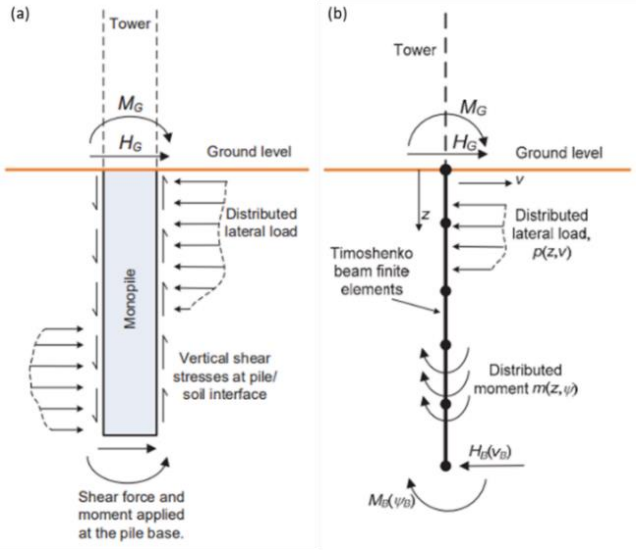

Figure 1. PISA design model: (a) soil reaction components acting on the pile; (b) implementation in 1D FE (after Burd et al., 2019).

The PISA design model (Burd et al., 2020) represents the state-of-the-art design methodology for monopiles and is now used globally in the industry. Like API, the PISA approach rely on one-dimensional finite-element analyses. However, PISA considers three other soil reaction components in addition to the distributed lateral load: the distributed moment, the base shear and the base moment (see Figure 2). The soil reaction curves can be constructed from a set of equations referred to as 'depth variation functions' (DVFs). The DVFs provide basis to generate nornalised soil reaction curves. The normalisation in sand of each components in summarised in Table 1. Following the PISA rule-based approach, the DVFs from the Generalised Dunkirk Sand Model (GDSM) developed by Burd et al. (2020) is considered in this study. The main soil inputs for this approach are the soil realtive density, small strain shear modulus, G_0, and unit weight.

Table 1. Soil reaction curves normalisation (after Burd et al., 2019).

Normalised variable	Dimensionless form in sand
Lateral displacement, $\bar{y}$	$\frac{yG_0}{D\sigma'_v}$
Pile cross-section rotation, $\bar{\psi}$	$\frac{\psi G_0}{\sigma'_v}$
Distributed lateral load, $\bar{p}$	$\frac{p}{D\sigma'_v}$
Distributed moment, $\bar{m}$	$\frac{m}{D\lvert p\rvert}$
Base horizontal load, $\bar{H}_B$	$\frac{H_B}{D^2\sigma'_V}$
Base moment, $\bar{M}_B$	$\frac{M_B}{D^3\sigma'_v}$

2.3 3D FEA

With the development of computational power, it is now standard practice to use three-dimensional finite element analyses for monopile design.

In this study, the piles were modelled at full scale and half-space in Plaxis 3D. The pile structure is modelled using linear-elastic isotropic plate elements with standard steel properties (Young's modulus of 210 GPa and Poisson's ratio of 0.3). The pile is weightless since the focus is on lateral loading. Interfaces at the outside and inside of the pile capture the soil-structure interactions.

The sand is modelled with the Hardening soil model with small strain stiffness (HS-small) assuming drained conditions. All the inputs required for the constitutive models were calibrated from site specific CPTs following the approach recently developed in Trinity College Dublin and presented in Igoe and Jalilvand (2020). The approach has already been validated against a large database of lateral pile field tests, including the PISA test in Dunkirk.

3 EXPERIMENTAL CAMPAIGN

The test site is located in Blessington, in an active quarry approximately 25 km south-west of Dublin, Ireland. Prior to pile installation, cone penetration testing (CPT) was undertaken at each desired pile location. Relevant CPT profiles are plotted on Figure 2 demonstrating minimum vertical or lateral soil variability. The site comprises of homogenous dense sand deposits.

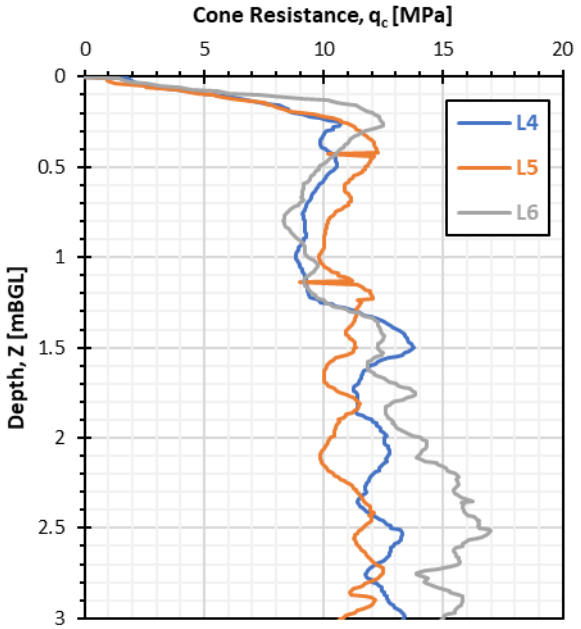

Figure 2. CPT profiles in terms of cone tip resistance (after Lapastoure and Igoe, 2024).

A total of 6 piles with an outer diameter (D) of 457 mm were driven at CPT locations. Pile embedded lengths (L) are ranging from 1 m to 2 m (L/D ranging from 2.2 to 4.4). The piles were installed in a 3x2 grid with the longer piles installed at the centre as shown on Figure 1. The longer piles were used as reaction piles to test the shorter piles. A stick-up length of 1.5 m was left out to ensure the lateral load could be applied with sufficient eccentricity to be representative of offshore conditions. The loads were applied at an eccentricity of 1.37 m (about 3*D).

During each test, both piles were instrumented with inclinometers and linear variable differential transducer at ground level. The lateral load was applied with a hydraulic jack and measured with a tension load cell. The experimental campaign consisted of 5 field tests:

- Test 1: Monotonic test between L6 (L/D=2.2) and L5 (L/D=4.4).
- Test 2: Monotonic test between L4 (L/D=3.3) and L5 (L/D=4.4).
- Test 3: Cyclic test (4000 cycles in total) followed by monotonic push over between L3 (L/D=3.3) and L2 (L/D=4.4).
- Test 4: Cyclic test (3670 cycles in total) followed by monotonic push over between L1 (L/D=2.2) and L2 (L/D=4.4).
- Test 5: Cyclic test (3160 cycles in total) between L2 (L/D=4.4) and L5 (L/D=4.4).

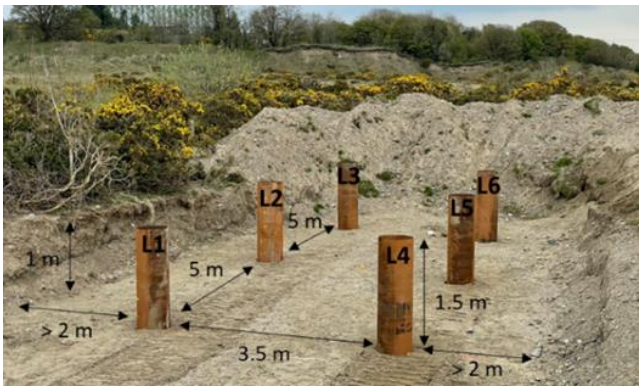

Figure 3. Piles arrangement (after Lapastoure and Igoe, 2024).

Only the results of the monotonic tests are considerd for this study (Test 1 and Test 2). The interested reader is invited to refer to Lapastoure and Igoe (2024) for more information.

4 PRELIMINARY RESULTS

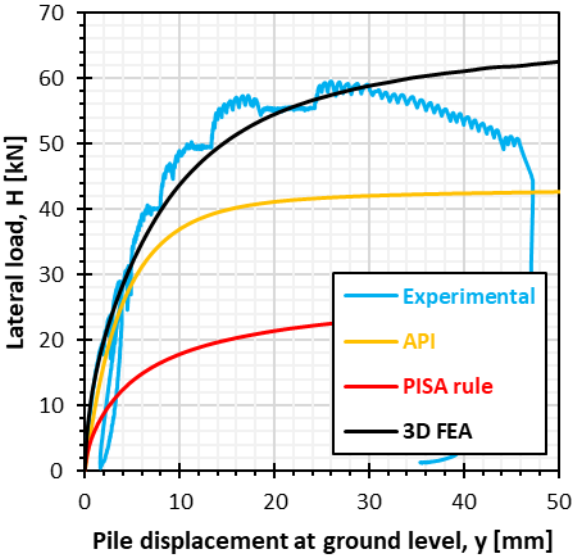

Figure 4. Comparison of experimental and predicted load-displacement response at ground level for pile L4 (L/D=3.3).

Figure 4 presents a comparison of experimental and predicted load-displacement response at ground level

for pile L4 (L/D=3.3). For consistency, all three approaches (API, PISA rule and 3D FEA) are based on the soil parameters correlated from the CPT based approach presented in section 2.3. The predictions based on the API and PISA rule approaches are found much softer than the actual pile response. The 3D FEA approach is found to provide a very good prediction.

Table 2 compares the blind predicitons to the experimental response for piles L4 (L/D=3.3), L5 (L/D=4.4) and L6 (L/D=2.2) in terms of initial stiffness and ultimate reaction.The initial stiffness is defined as the secant stiffness for a pile displacement of D/1000 at ground level, where D is the pile diameter. The ultimate reaction is defined for a pile displacement of D/10 at ground level for the numerical models, and as the maximum lateral load reached for the experimental tests. Ultimate reaction could not be reached during the test for L5 due to limitations with the loading system.

PISA rule is found to largely underestimate the stiffnesses and the ultimate reactions by more than 50%. This is because the depth variation functions from the General Dunkirk Sand Model (GDSM) are being used outside of their calibration space. Indeed, Burd et al. (2020) calibrated the GDSM against three-dimensional finite element analyses with pile diameters ranging from 5 m to 10 m. In this experimental study, piles have a diameter of 457 mm.

Although the API ‘p-y‘ approach was developed for long and flexible piles, it is found to perform slightly better than PISA rule for these short and rigid piles. However, it still significantly underestimates stiffnesses (37% to 53%) and ultimate reactions (about 30%).

3D FEA is found to provide very good matches with the experimental data, the average error being less than 5% accross the different pile penetrations. These results further validate the CPT based correlations of HS-small prameters developed by Igoe and Jalilvand (2020).

Table 2. Comparison of blind predictions to experimental piles response in terms of initial stiffness and ultimate capacity.

Approach	Initial stiffness relative error [%]			Ultimate capacity relative error [%]		
	L4	**L5**	**L6**	**L4**	**L5**	**L6**
Field test	-44.4	-36.9	-53.3	-28.6	-	-30.6
API	-50.9	-48.8	-57.9	-59.2	-	-57.3
PISA rule	8.8	4.5	5.6	3.9	-	-2.0
3D FEA	-44.4	-36.9	-53.3	-28.6	-	-30.6

5 CONCLUSION

This paper presents the initial results of a recent campaign of pile lateral field tests. 6 piles with diameter of 457 mm and penetration ranging from 1 m to 2 m were driven into dense sands at the Blessington test site in Ireland and subjected to monotonic and cyclic loading.

The piles response to monotonic loading were predicted ahead of testing using three approaches: API ‘p-y curve’ approach, PISA rule-based approach and three-dimensional finite-element analysis with a novel set of CPT based correlations for all the input parameters to the soil constitutive model. The API and the PISA rule approaches were found to largely underestimates both initial stiffness and ultimate reaction for all piles. The 3D FEA prediction with CPT based input parameters were found to match very well with the experimental monotonic response for all piles.

These results further validate the CPT based correlations developed by Igoe and Jalilvand (2020) and suggest that the approach can be used for monopile foundations design supporting offshore wind turbines which are characterised by low slenderness ratios (L/D). The full list of correlations and parameters used in the 3DFE modelling is provided in Igoe and Lapastoure (2024).

ACKNOWLEDGMENT

The research conducted in this publication was funded by the Irish Research Council employment-based postgraduate programme under grant number EBPPG/2019/4.

REFERENCES

API (2014). ANSI/API Recommended Practice 2GEO. First edition, April 2011 + addendum 2014.

Burd, H.J., Taborda, D.M., Zdravković, L., Abadie, C.N., Byrne, B.W., Houlsby, G.T., Gavin, K.G., Igoe, D.J., Jardine, R.J., Martin, C.M. and McAdam, R.A. (2020). PISA design model for monopiles for offshore wind turbines: application to a marine sand. Géotechnique, 70(11), 1048-1066.

Igoe, D. and Lapastoure, L.-M. (2024). Field lateral load tests on monopiles in dense sand at Blessington – Part 1 – Monotonic loading. Submitted to Geotechnique.